Queen's University Belfast

Library Form

To be completed by Student

DEGREE	Doctor of Philosophy
FULL NAME	Simon Thomas Murray
THESIS TITLE	Applications of Membrane Aerated Biofilm Reactors for Wastewater Treatment

SUMMARY: (max. 300 words)

Despite being the subject of peer reviewed research since the mid-1980s, the conservative nature of the wastewater treatment industry means that the commercial application of membrane aerated biofilm reactors has not realized the potential that the published research demonstrates.

The early research demonstrated the ability of membrane aerated biofilm reactors to achieve good levels of pollutant removal from various types of wastewater, but also exposed several weaknesses of the technology (i.e. cost of membranes, control of biofilm thickness) which have prevented the concept of MABfRs being developed in viable wastewater treatment technologies.

However, as membrane technology has developed, the cost of suitable membranes has fallen, prompting the research community to revisit the concept. This later batch of research has identified several niche applications where membrane supported biofilms can be used for effective removal of pollutants from water.

Using the MABfR for the treatment of secondary effluent as a polishing step is another niche application which has been identified and is examined in this work; leading to the development of a patented treatment technology – the BioSettler.

I give permission for my thesis to be made available *(a) forthwith
*(*Please complete/delete as appropriate)* (b) after a period of ____ (maximum 5 years)

For inclusion in the University Library, consultation by readers in the School, to be sent on temporary loan to other institutions, photocopied, electronically reproduced and/or published in whole or in part, under regulations determined by the University.

Signature of Student: **Date:**

NB: Authors of theses should note that giving this permission does not in any way prejudice their rights.

To be completed by Examiner

CERTIFICATION OF SUBMITTED WORK

I hereby certify that this is the final accepted copy of the submitted work and that any required amendments have been completed and submitted within the deadline.

Signature of Examiner: **Date:**

Applications of Membrane Aerated Biofilm Reactors for Wastewater Treatment

Simon Thomas Murray MEng

A thesis submitted for the Degree of Doctor of Philosophy

The School of Chemistry and Chemical Engineering

Queen's University Belfast

2016

Acknowledgements

I would like to thank those who have been involved in the supervision of my project at the various times during its duration: Dr Wendy McLoone (née McMinn), Professor Stephen Allen, Professor Ronnie Magee, Professor David Rooney, Dr Elaine Groom, and Mr Joel Ferguson. Their guidance, inspiration and most of all patience have been instrumental in the completion of this project.

Without the funding provided through the QUESTOR research programme and the guidance provided by the members of the QUESTOR Industrial Advisory Board this project would not have been possible. In particular, I would like to thank Sam Irwin and Karen McDowell of NI Water, John Toner of Williams Industrial Services and Paddy McGuinness of Colloide Engineering who have supported the BioSettler project from the beginning.

I am also indebted to the staff of the QUESTOR ATU for their assistance with various aspects of this work; Dr Julie-Anne Hanna, Ciarán Prunty, David Parker, Patricia McCrory, Kathyrn Rogers, Kerry Kelly and Dr Nick Johnston. A special mention must go to the late Alex Marshall, whose unique brand of genius was essential to the completion of this project.

I am also grateful to final year students who have assisted me in some of the experimental work presented here – Ciarán Doyle, Barry McQuaid and Niall Moroney – and to some of the technical staff of the School of Chemistry and Chemical Engineering who have assisted in the construction and maintenance of the equipment used in this work, especially Jackie O'Connor, Suzanne Evans, Martin Catney and Kirin Hill.

Summary

Despite being the subject of peer reviewed research since the mid-1980s, the conservative nature of the wastewater treatment industry means that the commercial application of membrane aerated biofilm reactors has not realized the potential that the published research demonstrates.

The early research demonstrated the ability of membrane aerated biofilm reactors to achieve good levels of pollutant removal from various types of wastewater, but also exposed several weaknesses of the technology (i.e. cost of membranes, control of biofilm thickness) which have prevented the concept of MABfRs being developed in viable wastewater treatment technologies.

However, as membrane technology has developed, the cost of suitable membranes has fallen, prompting the research community to revisit the concept. This later batch of research has identified several niche applications where membrane supported biofilms can be used for effective removal of pollutants from water.

Using the MABfR for the treatment of secondary effluent as a polishing step is another niche application which has been identified and is examined in this work; leading to the development of a patented treatment technology – the BioSettler.

Table of Contents

Acknowledgements i

Summary ii

Table of Contents iii

List of Figures x

List of Tables xiv

Abbreviations and Symbols xvi

List of Abbreviations xvi

List of Symbols xvii

1 Introduction 1

1.1 General Introduction 1

1.2 Wastewater treatment 2

1.2.1 Wastewater treatment in Northern Ireland 4

1.3 Drivers for upgrade of wastewater treatment works 5

1.3.1 Legislative drivers 5

1.3.2 Other drivers for wastewater treatment upgrade 8

1.4 Proposed technology – The BioSettler™ 8

1.5 Aims and Objectives 11

1.6 Conclusions 12

2 Review of wastewater sources, composition and treatment options 13

2.1 Wastewater and wastewater treatment 13

2.1.1 Sources of wastewater 13

2.1.2 Wastewater characterisation 17

2.1.3 Current wastewater treatment technologies 20

2.1.4 Biofilms 24
2.2 Biology of wastewater treatment 26
2.2.1 Aerobic heterotrophy 27
2.2.2 Nitrification 28
2.2.3 Denitrification 30
2.2.4 Stoichiometry of wastewater biology 31
2.3 Bubbleless Aeration 32
2.3.1 Historical Context 33
2.3.2 Mass transfer mechanism 34
2.3.3 Modes of operation 35
2.3.4 Evaluation of Oxygen Mass Transfer Coefficient 36
2.3.5 Calculation of oxygen flux 38
2.3.6 Bubble formation 38
2.3.7 Effect of attached biomass on oxygen transfer 39
2.3.8 Design of hollow fibre membrane contactors 40
2.4 Membrane Attached Biofilm Processes 41
2.4.1 Pollutant removal 42
2.4.2 Control of biofilm thickness 45
2.5 Biological azo dye wastewater treatment 45
2.6 Inclined Plate Settlers 48
2.6.1 Design Considerations 49
2.6.2 Operational Issues 50
2.6.3 Modelling 50
2.7 Conclusion 52
3 Materials and Methods 53

3.1 Mass Transfer Studies 53
3.1.1 Membrane Materials 53
3.1.2 Membrane Modules 54
3.1.3 Parameter measurement 55
3.1.4 Nitrogen diffusion 56
3.1.5 Stirring equipment 56
3.1.6 Pumping equipment 56
3.1.7 Datalogging 57
3.1.8 Experimental Set-up 57
3.1.9 Experimental procedure 58
3.2 Membrane Aerated Biofilm Reactor Studies 60
3.2.1 Reactor Set-ups 61
3.2.2 Synthetic media 63
3.2.3 Seeding of reactors 66
3.3 Effluent characterisation 67
3.3.1 pH 68
3.3.2 Ammoniacal Nitrogen 68
3.3.3 Chemical Oxygen Demand 68
3.3.4 Nitrate 69
3.3.5 Nitrite 70
3.3.6 Turbidity 70
3.3.7 Colour 70
3.3.8 Biochemical Oxygen Demand (BOD_5) 71
3.4 Effluent disposal 72
4 Mass Transfer Studies 73

4.1 Saturation concentration 73
4.1.1 Effect of membrane type 74
4.1.2 Effect of inlet pressure 76
4.2 Oxygen Transfer 77
4.2.1 General observations 77
4.2.2 Calculation of average oxygen flux 79
4.2.3 Calculation of mass transfer coefficient 79
4.3 Effect of air side flowrate 80
4.4 Effect of inlet air pressure 83
4.5 Effect of water side flowrate 86
4.6 Conclusions 94
5 Membrane Aerated Biofilm Reactor Studies – Part 1 95
5.1 Reactor start-up 95
5.2 General observations 96
5.2.1 pH 96
5.2.2 Nitrite concentration 98
5.3 Stoichiometric model development 99
5.4 Pollutant removal 104
5.4.1 Removal Efficiency 104
5.4.2 Removal rates 106
5.4.3 Total Nitrogen Removal 107
5.5 Response to increased inlet pressure 110
5.6 Apparent oxygen flux 112
5.6.1 Assumptions 112
5.6.2 Reaction scheme 114

5.6.3 Effect of inlet pressure 115
5.6.4 Mass transfer coefficient 118
5.7 Conclusions 122
6 Membrane Aerated Biofilm Reactor Studies – Part 2 123
6.1 Pollutant removal 123
6.1.1 Chemical Oxygen Demand 124
6.1.2 Ammoniacal nitrogen 126
6.1.3 Total nitrogen 128
6.2 Removal rates 129
6.2.1 Oxygen consumption 130
6.2.2 Relative oxygen consumption 132
6.2.3 Denitrification 136
6.3 Model development 139
6.3.1 Assumptions 140
6.3.2 Model inputs 142
6.4 Model validity 145
6.4.1 Normalised standard deviation method 145
6.4.2 Sensitivity analysis 149
6.5 Conclusions 154
7 Design and operation of a pilot-scale BioSettler™ 155
7.1 Pilot scale design 155
7.1.1 Justification of design 157
7.1.2 Membranes 161
7.1.3 Auxillary equipment 164
7.2 Trial locations 165

7.2.1 Site 1 165
7.2.2 Site 2 165
7.3 Trial results 166
7.3.1 Site 1 166
7.3.2 Trial 2 169
7.3.3 Solids Removal 170
7.3.4 Biochemical Oxygen Demand 171
7.3.5 Ammoniacal Nitrogen 173
7.4 Potential performance of scaled up system 174
7.4.1 Pollutant removal 174
7.4.2 Energy consumption 176
7.4.3 Energy consumption of unit pollutant removal 177
7.5 Conclusions 178
8 Treatment of azo dye waste in the Membrane Aerated Biofilm Reactor – a feasibility study 179
8.1 Experimental conditions 179
8.2 General observations 180
8.2.1 Biofilm establishment 180
8.2.2 Method of colour removal 181
8.2.3 pH 182
8.2.4 Ammoniacal nitrogen concentration 183
8.2.5 Nitrate concentration 184
8.2.6 UV/vis spectrometry 185
8.3 Colour removal 190
8.3.1 AO7 Removal rate 191

8.4 COD removal 193
8.4.1 COD removal rate 194
8.5 Worked example 196
8.6 Conclusions 197
9 Conclusions and Further Work 199
9.1 Summary of conclusions 199
9.2 Recommendations of further work 200
References 202

List of Figures

Figure 1-1: Simplified schematic of Activated Sludge Process (adapted from Gray, 2004) 3
Figure 1-2: Trickling filter at NIW Parkgate WwTW 3
Figure 1-3: Rotating Biological Contactor (WIS Ltd) 4
Figure 1-4: Aerial view of Belfast WwTW, highlighting the relative sizes of aerobic treatment and settlement tanks (Adapted from GoogleMaps) 8
Figure 1-5: Inclined plate showing projected settling area and footprint (adapted from Metso Minerals, 2006) 9
Figure 1-6: Structure of membrane aerated biofilms 10
Figure 1-7: Membrane location in the BioSettler 11
Figure 2-1: Diurnal variations in wastewater flowrate and strength for a typical WwTW (Tchobanoglous & Burton, 1991b) 15
Figure 2-2: Structure of Acid Orange 7 16
Figure 2-3: Schematic Inclined Plate Settler (Parkson, 2010) 21
Figure 2-4: Inclined Plates 21
Figure 2-5: Molecular transport in dense membranes (left) by differences in permeation and microporous membranes by molecular filtration 22
Figure 2-6: Membrane classification (Radcliff & Zarnadze, 2004) 23
Figure 2-7: General structure of Membrane Aerated Biofilms 26
Figure 2-8: Steps in the reduction of nitrate (adapted from Madigan & Martinko, 2006) 30
Figure 2-9: Examples of microbial respiration and associated redox potentials (adapted from Madigan & Martinko, 2006) 31
Figure 2-10: Anaerobic and aerobic degradation pathways of azo dyes 46
Figure 3-1: Structure of silicone rubber (left) and polyethersulphone polymers 53
Figure 3-2: Silicone rubber membrane module 54
Figure 3-3: Schematic diagram of experimental set-up 57
Figure 3-4: Water reservoir tank, magnetic stirrer and Hach-Lange LDO Meter 58
Figure 3-5: Schematic diagram of MABfR A Set-up 61

Figure 3-6: Schematic diagram of MABfR B set-up 62
Figure 3-7: Spent (left) and unused COD vials 69
Figure 3-8: Fresh (left) and used nitrate vials 69
Figure 3-9: Spectrophotometer cuvettes 71
Figure 4-1: Temperature-saturation correlations (0.5 bar) 75
Figure 4-2: Effect of inlet pressure on saturation oxygen concentration (20 °C) 76
Figure 4-3: Change in dissolved oxygen over duration of mass transfer experiments (Silicone Rubber, 0.5 bar inlet pressure, 2 lpm gas side flowrate, 550 ml min^{-1} water side flowrate). 77
Figure 4-4: Bubble formation on membrane surface (Silicone Rubber, 0.5 bar inlet pressure, 2 lpm gas side flowrate, 550 ml min^{-1} water side flowrate) 78
Figure 4-5: Plot of $\boldsymbol{lnC*-CtC*}$ versus t (Silicone Rubber, 0.5 bar inlet pressure, 2 lpm gas side flowrate, 550 ml min^{-1} water side flowrate) 80
Figure 4-6: Effect of air side flowrate on average oxygen flux (0.5 bar inlet pressure, 550 ml min^{-1} water flowrate – minimum and maximum value error bar) 81
Figure 4-7: Effect of air flowrate on overall mass transfer coefficient (0.5 bar inlet air pressure, 550 ml min^{-1} water flowrate – minimum and maximum value error bars) 83
Figure 4-8: Effect of inlet pressure on average oxygen flux (2 lpm air flowrate, 550 ml min^{-1} water flowrate, minimum and maximum value error bars) 84
Figure 4-9: Effect of inlet air pressure on mass transfer coefficient (2 lpm air flowrate, 550 ml/min water flowrate, minimum and maximum value error bars) 85
Figure 4-10: Effect of water flowrate on average oxygen flux (0.5 bar air pressure, 2 lpm air flowrate, minimum and maximum value error bars) 86
Figure 4-11: Effect of water flowrate on overall mass transfer coefficient (0.5 bar inlet air pressure, 2 lpm air flowrate, minimum and maximum value error bars) 87
Figure 4-12: 'Wilson plot', minimum and maximum value error bars 89
Figure 4-13: Sherwood number versus Reynolds number (0.5 bar, 2 lpm inlet flow, minimum and maximum value error bars) 91
Figure 5-1: Influent and effluent pH 97
Figure 5-2: Bulk nitrite concentration (days 1-190) 98
Figure 5-3: f_s/sludge age relationships 101

Figure 5-4: Pollutant removal efficiency in Runs 1-7 (standard error bars) 104
Figure 5-5: Effect of inlet pressure on pollutant removal rates (standard error bars) 106
Figure 5-6: total nitrogen removal in Runs 1-7 (standard error bars) 108
Figure 5-7: Effect of inlet pressure on denitrification rate 109
Figure 5-8: Variation in COD and Ammoniacal nitrogen concentrations in response to changes in inlet air pressure. 111
Figure 5-9: Simplified reaction scheme 114
Figure 5-10: Effect of inlet pressure on apparent oxygen flux (standard error bars) 115
Figure 5-11: Effect of inlet pressure on overall oxygen mass transfer coefficient 120
Figure 6-1: Influent and Effluent COD concentrations in Runs 8-12 124
Figure 6-2: Average COD concentrations and percentage COD removal (standard error bars) 125
Figure 6-3: Influent and effluent ammoniacal nitrogen concentrations during Runs 8-12 126
Figure 6-4: Average ammoniacal nitrogen concentrations and percentage ammoniacal nitrogen removal in Runs 8 - 12(standard error bars) 127
Figure 6-5: Influent and effluent Total-N concentrations in Runs 8-12 128
Figure 6-6: Apparent oxygen flux during Runs 8-12 131
Figure 6-7: fraction of supplied oxygen utilized by aerobic heterotrophs at different COD:Amm-N ratios 134
Figure 6-8: Variation of denitrification rates with nitrate availability (standard error bars) 138
Figure 6-9: Sensitivity analysis for inlet pressure 150
Figure 6-10: Sensitivity analysis for influent ammoniacal nitrogen concentration 151
Figure 6-11: Sensitivity analysis for influent COD concentration 152
Figure 6-12: Sensitivity analysis for nitrate nitrogen 153
Figure 7-1: CAD diagrams – cross sectional (left) and bird's eye view 156
Figure 7-2: BioSettler prototype tank 156
Figure 7-3: Inlet flow patterns 158
Figure 7-4: Membrane arrangement in BioSettler 159
Figure 7-5: BioSettler plate spacing 159

Figure 7-6: V-notch weirs in BioSettler tank....160
Figure 7-7: Cross flow operation....162
Figure 7-8: Daicen Membrane Module....162
Figure 7-9: Membrane module construction....163
Figure 7-10: Membrane sealing with epoxy resin....163
Figure 7-11: Membrane modules in BioSettler unit....164
Figure 7-12: Layout of Newtownbreda WwTW (Googlemaps).....166
Figure 7-13: Second influent intake point used at Site 1.....167
Figure 7-14: Sludge buildup on membranes....168
Figure 7-15: Damage to membranes....168
Figure 7-16: Sample location at Site 2....170
Figure 7-17: Solids concentrations during BioSettler trial 2....171
Figure 7-18: BOD concentrations during BioSettler trial 2....172
Figure 7-19: Ammoniacal nitrogen concentrations during BioSettler Trial 2....173
Figure 7-20: Zena membrane module....175
Figure 8-1: Biofilm development after 12 days of operation....180
Figure 8-2: Removed biomass initially (left) and during greatest colour removal....182
Figure 8-3: Influent and effluent pH during Run 2....182
Figure 8-4: Ammoniacal concentrations throughout dye investigation....184
Figure 8-5: Absorbance spectra for standard AO7 solutions....186
Figure 8-6: Calibration curve for AO7 concentration....187
Figure 8-7: Solutions of Acid Orange 7 (left), Fe (III) Chloride and Riboflavin (right) at the concentration used in the influent media....188
Figure 8-8: Cumulative absorbance effects....189
Figure 8-9: Colour removal in Runs 1-3....190
Figure 8-10: Influent and effluent COD concentrations during Runs 1 - 3....194

List of Tables

Table 1-1: Level of Treatment mandated by the UWwTD (adapted from DEFRA, 2002) 6
Table 2-1 : Typical composition of untreated municipal wastewater 14
Table 2-2: Typical analysis of Dye house wastewater (Wilkinson 2007) 16
Table 2-3: Typical distribution of Aerobic Heterotrophic Bacteria in Activated Sludge (Bitton, 2005) 28
Table 2-4: Comparison of pollutant removal rates achieved in selected MABfR studies 43
Table 2-5: Denitrification rates of various MABfR studies 44
Table 3-1: Synthetic waste composition 64
Table 3-2: Composition of stock solutions used with MABfR A 65
Table 3-3: Composition of synthetic dye waste used in MABfR B 66
Table 3-4: Wastewater analyses 67
Table 4-1: Comparison of saturation constants 74
Table 4-2: Saturation coefficients for 0.5 barg inlet pressure 74
Table 4-3: Pressure flowrate pairs used in inlet air pressure investigation 84
Table 4-4: Experimental and calculated membrane mass transfer coefficients 89
Table 4-5: Comparison of membrane mass transfer coefficients 90
Table 4-6: Obtained Sherwood number/ Reynolds number relationships 91
Table 4-7: Mass transfer correlations for hollow fibre modules 92
Table 5-1: Conditions during start-up period 95
Table 5-2: Conditions throughout inlet pressure investigation 96
Table 5-3: Average and standard deviation pH 98
Table 5-4: Values of a_e used in model development (McCarty, 1975) 100
Table 5-5: Cell decay rates (Manser *et al.*, 2006) 100
Table 5-6: Mass ratios of substrates involved in microbial reactions in the MABfR 103
Table 5-7: Comparison of pollutant removal efficiencies 105
Table 5-8: Comparison of pollutant removal rates 106
Table 5-9: Values used in calculation of gas side oxygen concentration 120
Table 5-10: Mass transfer coefficients at different experimental conditions 121

Table 6-1: Pollutant loadings in Run 8-12 124
Table 6-2: COD and ammoniacal nitrogen removal rates in Runs 8-12 (standard errors) 129
Table 6-3: Comparison of pollutant removal rates (standard errors where shown) 130
Table 6-4: Obtained and predicted average oxygen fluxes 131
Table 6-5: Average oxygen fluxes in runs 8-12 132
Table 6-6: Rates of microbial processes and oxygen uptake (mean values, standard errors) 133
Table 6-7: Oxygen usage in Runs 8-12 (mean values) 134
Table 6-8: Denitrification rates in runs 8-12 (mean values, standard errors shown) 136
Table 6-9: Comparison of denitrification rates 136
Table 6-10: Relationships used to calculate reaction rates in MABfR model 144
Table 6-11: Experimental and calculated COD concentrations for Runs 1-12 146
Table 6-12: Experimental and calculated Amm-N concentrations for Runs 1-12 147
Table 6-13: Experimental and calculated Tot-N concentrations for Runs 1-12 148
Table 6-14: Adjusted NSD (%) 149
Table 7-1: Summary of prototype dimensions 157
Table 7-2: Pollutant removal obtained during Trial 1 (Standard errors shown) 169
Table 7-3: Average pollutant removal rates 175
Table 7-4: Potential removal rates 175
Table 8-1: Component concentrations varied during dye degradation studies 180
Table 8-2: Average calculated AO7 concentrations in Runs 1-3 (standard errors shown) 187
Table 8-3: AO7 removal rates in Runs 1-3 191
Table 8-4: Comparison of AO7 removal rates in literature 193
Table 8-5: COD removal rates in Runs 1 - 3 194

Abbreviations and Symbols

List of Abbreviations

abs	absolute
Amm-N	Ammoniacal Nitrogen
AnAOB	Anaerobic Ammonia Oxidising Bacteria
AO7	Acid Orange 7
AOB	Ammonia oxidising bacteria
AOD	Ammoniacal Oxygen Demand
AU	Absorbance units
BOD	Biochemical Oxygen Demand
CFD	Computational Fluid Dynamics
CSTR	Continuous Stirred Tank Reactor
COD	Chemical Oxygen Demand
DO	Dissolved Oxygen
EMBR	Extractive membrane biofilm reactor
FISH	Fluorescent In-Situ Hybridization
HRT	Hydraulic Retention Time
IPS	Inclined Plate Settler
lpm	litres per minute
MABfR	Membrane Aerated Biofilm Reactor
Nit-N	Nitrate nitrogen
NIW	Northern Ireland Water
NOB	Nitrite oxidising bacteria
NTU	Nephelometric Turbidity Units
p.e.	Population equivalent
PES	Polyethersulphone
RBC	Rotating Biological Contactor
rpm	Revolutions per minute
SBR	Sequential Batch Reactor
SR	Silicone Rubber

Tot-N	Total nitrogen
TOD	Total Oxygen Demand
UWwTD	Urban Wastewater Treatment Directive
VOC	Volatile Organic Compound
WFD	Water Framework Directive
WwT	Wastewater Treatment
WwTW	Wastewater Treatment Works

List of Symbols

a	Specific membrane surface area
a_e	Cell yield coefficient
A	Absorbance
A_λ	Absorbance at wavelength λ
A_m	Membrane area
$A_{m,req}$	Required membrane area
$A_{m,req,T}$	Total required membrane area
b	Bacterial cell decay rate
ΔC	Concentration difference across membrane
C_{AO7}	Acid Orange 7 concentration
$C_{AO7,inf}$	Influent Acid Orange 7 concentration
$C_{AO7,\ eff}$	Effluent Acid Orange 7 concentration
C_{con}	Consent concentration
C_{eff}	Effluent concentration
$C_{j,exp,i}$	Effluent concentration of component j determined experimentally for experimental run i
$C_{j,calc,i}$	Effluent concentration of component j calculated using the model for experimental run i
C_{inf}	Influent concentration

d_e	external diameter of membrane fibre
d_i	internal diameter of membrane fibre
D_M	diffusivity of oxygen in membrane material
D_w	diffusivity of oxygen in water
ε	membrane porosity
f_{AH}	Fraction of oxygen used for aerobic heterotrophy
f_d	Biodegradable fraction of microorganisms
f_e	fraction of electron donor used for energy
f_{nit}	Fraction of oxygen used for nitrification
f_s	fraction of electron donor used for cell formation
G	Mass velocity
h	hour
J	Oxygen Flux
J_a	Apparent oxygen flux
$\bar{J}$	Average oxygen flux
K	Overall mass transfer coefficient
K_L	Liquid side mass transfer coefficient
K_G	Gas side mass transfer coefficient
K_M	Membrane mass transfer coefficient
L	Loading
$L_{AO7,req}$	Required AO7 removal (loading basis)
L_{eff}	Effluent loading
L_{COD}	COD loading
L_{Amm-N}	Ammoniacal nitrogen loading
L_{Nit-N}	Nitrate nitrogen loading
$\dot{m}$	Mass flowrate
M	Molar mass
M_{O2}	Molar mass of oxygen
NO_3^--$N_{available}$	Total available nitrate nitrogen
OUR	Oxygen uptake rate
OUR_{AH}	Aerobic heterotrophs oxygen uptake rate

OUR_{nit}	Nitrifiers oxygen uptake rate
Q	flowrate
r	Rate
r_{AO7}	Acid Orange 7 removal rate
r_{AH}	Aerobic heterotrophy rate
$r_{amm\text{-}N}$	Ammoniacal nitrogen removal rate
r_{COD}	COD removal rate
r_{den}	Denitrification rate
r_{nit}	Nitrification rate
$r_{tot\text{-}N}$	Total nitrogen removal rate
P_R	Pressure at reference conditions
S_M	Solubility of oxygen in polymer
T	Temperature
T_R	Temperature at reference conditions
t_s	Sludge age
τ	membrane tortuosity
V	Volume
v_c	critical velocity
wk	week
X	Biomass density

1 Introduction

This thesis is concerned with the use of membrane aerated biofilms as a means for treatment of wastewater streams. In particular, it investigates the feasibility of using such a method as a pre-treatment or polishing step in order to upgrade existing works – helping meet the demands placed by changing populations and legislation.

This introduction will explain the need for upgrading existing works – justifying the development of technologies such as that proposed by this project.

1.1 General Introduction

Wastewater is defined as any water which has been tainted by human activity. It is the combination of liquid and water carried wastes generated by residences, commercial and industrial buildings; along with stormwater and groundwater which enter the sewerage system (Metcalf & Eddy, 2003).

Wastewater treatment was first introduced during the second half of the 19th Century, as early hygienists made the link between outbreaks of cholera in Paris and London and the open sewers that primarily collected waste. In response, city planners such as Haussmann and Bazalgette incorporated subterranean sewers into the modernization plans of Paris and London respectively, although their system served little purpose other than to divert wastewater away from areas where drinking water was obtained.

Since these early attempts, introduced to protect the health of the rapidly growing urban populations, the focus of wastewater treatment has changed: the primary objective of wastewater treatment is now to minimize the effect of mankind's use of water on the environment, and to protect it for future generations.

1.2 Wastewater treatment

Wastewater treatment consists of a series of physical, chemical and biological operations, by which solid contaminants are removed and dissolved contaminants are converted by chemical and/or biological action to immiscible gaseous or solid phases which are then easily removed.

The majority of dissolved contaminants are easily oxidised by the action of bacteria. Larger works typically utilise the activated sludge process, whilst smaller facilities use either trickling filters or rotating biological contactors (RBCs).

The activated sludge process is a suspended growth process, first introduced into the U.K. at the beginning of the 20th Century. In the process, after primary treatments (mainly solids removal), the wastewater is mixed with the return activated sludge to form the mixed liquor – a suspension with typically 1500 – 3500 mg l^{-1} of biomass as suspended solids.

After aeration, the mixed liquor flows into settlement tanks, where the velocity is slowed to an extent where the solid particles drop to the bottom of the tank. The defining characteristic of the activated sludge process is that a large portion of this biomass is recycled back to the aeration tank (Figure 1-1); meaning that the mean cell residence time (average time spent by biomass in the treatment system) is much greater than the hydraulic retention time (average time spent by liquid in the treatment system) – allowing the biological activity to be maintained at the level required to achieve full treatment.

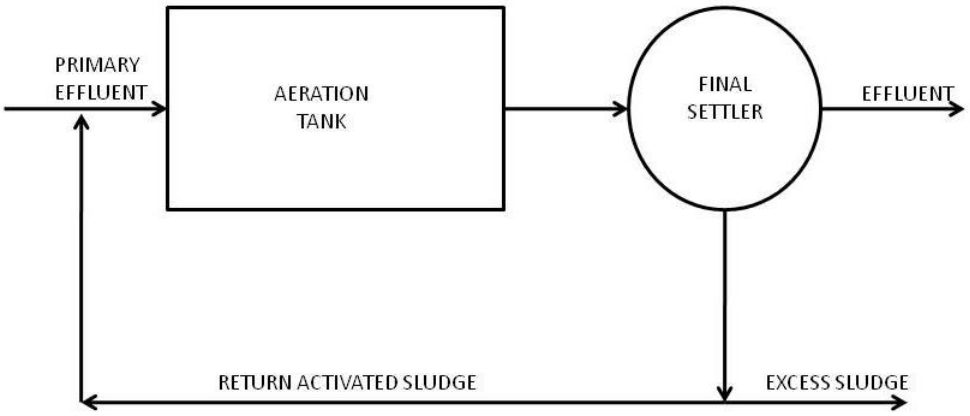

Figure 1-1: Simplified schematic of Activated Sludge Process (adapted from Gray, 2004)

Trickling, or percolating, filters were first introduced in 1893 (Tchobanoglous & Burton, 1991a), and consisted of a bed of porous rock over which wastewater is percolated or trickled, giving the name (Figure 1-2). An ecosystem develops on the surface of the rock, consisting of a mixture of heterotrophic and autotrophic bacteria, fungi, algae and larger organisms such as snails and worms. A modern trickling filter utilizes plastic packing material in order to maximise the contact area and area available for biofilm support. The system is passively aerated, with oxygen being transferred into the wastewater through the voids in the packing material.

Figure 1-2: Trickling filter at NIW Parkgate WwTW

Rotating biological contactors (RBCs) were first developed in the 1920s and became commercially available in 1965 (Gray, 2004). The basic design of an RBC consists of discs of biofilm support such as PVC, polyethylene or a similar material, which are mounted on a rotating horizontal shaft, positioned in such a way so as to be approximately 40% submerged in the liquid. Passive aeration takes place when the biofilm is above the level of the wastewater.

Figure 1-3: Rotating Biological Contactor (WIS Ltd)

A common feature of the activated sludge process, trickling filters and RBCs is a final settler in which biomass is removed by the physical process of settling from the effluent before discharge. Little or no biological treatment takes place in a standard settler, with the biological treatment limited by the amount of oxygen which can be transferred during the previous treatment steps.

1.2.1 Wastewater treatment in Northern Ireland

Northern Ireland Water (NIW), which operates as both a government owned company and non-departmental public body, is responsible for provision of municipal wastewater treatment. NIW treat approximately 120 million m^3 of wastewater each year in 656 WwTW (NI Water, 2013). Due to the non-urban nature of Northern Ireland, the majority of these works are small, serving a population equivalent (p.e) of less than 250, whilst

254 of these works are larger works, serving more than 250 p.e. (Fivelman, 2010). Population equivalent is the theoretical amount of pollution produced by one person in a day and is defined by British Water (2013) as 150 litres, containing 60 g of BOD and 8 g of Ammoniacal Nitrogen.

The larger works mainly achieve treatment through the application of the activated sludge process, whilst smaller works mainly use either trickling filters or rotating biological contactors.

1.3 Drivers for upgrade of wastewater treatment works

Northern Ireland has suffered from a historical underinvestment in the wastewater treatment infrastructure. As a result, at its formation in April 2007, NIW inherited a treatment works infrastructure which was significantly underperforming in comparison to those in other parts of the UK. In response to this, NIW launched a £290 million spending plan on plant upgrade (Fivelman, 2010). There were several drivers for this upgrade, as described in Sections 1.3.1 and 1.3.2.

1.3.1 Legislative drivers

In Northern Ireland, the discharge of wastewater effluent to any waterway or underground strata is regulated in accordance with the Water (Northern Ireland) Order 1999 (HMG, 1999). Under these regulations, persons wishing to discharge water must apply to the Northern Ireland Environment Agency (NIEA) for permission to do so.

A successful applicant will be issued a 'Consent to Discharge', which includes conditions relating to the quality and quantity of effluent which can be discharged. Similar systems operate in other parts of the U.K.

Three pieces of European legislation have had an effect on the values of these discharge consents:

a) The Urban Wastewater Treatment Directive
b) The Water Framework Directive
c) The Nitrates Directive

a) Urban Waste Water Treatment Directive

The Urban Waste Water Treatment Directive (UWwTD) (European Council, 1991a) aimed to protect the environment from the adverse effects of wastewater discharges; effectively by mandating the introduction of wastewater collection and setting a minimum standard for the treatment of this wastewater.

The minimum standards set are a function of both the population equivalent (p.e.) of the wastewater source and the status of the receiving waters, as summarised in Table 1-1. The terms population equivalent and the various levels of wastewater treatment are discussed more fully in Chapter 2.

Table 1-1: Level of Treatment mandated by the UWwTD (adapted from DEFRA, 2002)

Treatment	Process	Discharge Area
Preliminary	Screening of large solids	Fresh waters <2,000 p.e.
	Grit removal	Coastal waster <10,000 p.e.
Primary	Settlement of Suspended Solids	Coastal waters >10,000 p.e. in less Sensitive Areas
Secondary	Biological Treatment	Fresh waters >2,000 p.e.
		Coastal waters >10,000 p.e.
Tertiary	Various Methods	>10,000 p.e. to Sensitive areas

In Northern Ireland, the requirements of the UWwTD were transposed into The Urban Waste Water Treatment Regulations (Northern Ireland) 1995 (HMG, 1995). These regulations placed tighter numerical consents upon Northern Ireland Water (and their

predecessor DRD Water Service) and also provided a framework for measurement of compliance (NIEA, 2014).

b) Water Framework Directive

The Water Framework Direction (WFD) (European Council, 2000), due to be fully implemented by 2015, places the demand that all inland, coastal and maritime water courses achieve 'good' ecological status. Good status is assessed using a combination of biological, hydrological, physical parameters.

Transposed into The Water Environment (Water Framework Directive) Regulations (Northern Ireland) (HMG, 2003), the WFD has led to a series of plans for river basin management, taking a holistic view of all activities which affect the aquatic environment (NIEA, 2009).

c) Nitrates Directive

Concern over the widespread eutrophication of water bodies throughout Europe lead to the publication of the Nitrates Directive (European Council, 1991b). Eutrophication is the over fertilisation of lakes and rivers, from sources such as farming, sewage and industry, causing an accelerated growth of algae and other plants (DOE NI & DARD NI, 2004). This growth can form a barrier to oxygen transfer on the surface of waters, and lead to detrimental effects on biodiversity.

Locally, implementation of the Nitrates Directive has focussed on agriculture (DARD & DOE, 2010), but has also had an effect on wastewater, with the introduction of numerical consents on the total nitrogen and total phosphorous concentrations of wastewater effluents.

1.3.2 Other drivers for wastewater treatment upgrade

Wastewater treatment infrastructure is a significant consumer of electrical energy through aeration and pumping equipment (Kadar & Siboni, 1998). As this leads to sizeable operating costs and associated operational carbon emissions, wastewater treatment companies are now pursuing more efficient water and wastewater treatment technologies (Smyth *et al.*, 2013).

1.4 Proposed technology – The BioSettler™

As previously discussed, pressures caused by the tightening of discharge consents due to legislative changes and increased loading due to population growth mean that many WwTW struggle to meet consents.

In a wastewater treatment works using the activated sludge process, the area used by tanks providing biological treatment is relatively small to the area required by the tanks providing final settlement. Figure 1-4 shows an aerial of Belfast WwTW; the main treatment works for the city of Belfast designed to serve a population equivalent of 400,000. The footprint of the settlement tanks (red box) is approximately 3 times that of the aeration lanes (green box). As previously discussed, settling tanks are also included in WwTW operating using either trickling filters or RBCs.

Figure 1-4: Aerial view of Belfast WwTW, highlighting the relative sizes of aerobic treatment and settlement tanks (Adapted from GoogleMaps)

The solids removal potential of final settlers can be boosted by the installation of an array of inclined plates. These inclined plates reduce the vertical distance a solid particle

needs to fall to be removed from suspension and increases the available settling area, boosting solids removal rates (Figure 1-5). The concept and history of inclined plate settlers is discussed more fully in Chapter 2.

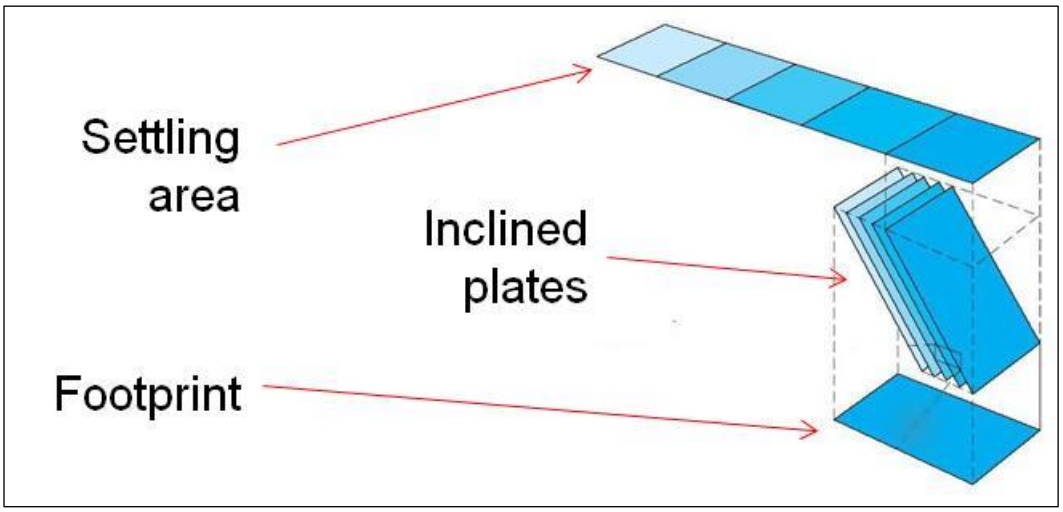

Figure 1-5: Inclined plate showing projected settling area and footprint (adapted from Metso Minerals, 2006)

However, in order for the area occupied by the final settling tanks to be utilised for biological treatment, oxygen must be introduced without bubbles as in the aeration tanks, as the turbulence associated with bubbles interferes with the settlement process.

One possible way in which oxygen can be introduced without bubbles is through the use of membranes. If a suitable tubular membrane is placed in a liquid stream and filled with compressed air; oxygen will diffuse from the inside of the membrane (where it is in high concentration), through the structure of the membrane material and into the liquid stream (where it is in low concentration). If the air pressure is maintained below a critical point, this process will occur without bubble formation.

If such a membrane is placed in a wastewater stream, a biofilm quickly forms upon the membrane surface (Figure 1-6). A biofilm is simply a group of microorganism cells grouped together on a surface like mould in a shower or plaque on teeth.

This biofilm consists of a mixture of heterotrophic bacteria, which utilise oxygen to remove organic carbon compounds, and nitrifying bacteria, which utilise oxygen to convert ammonia to nitrate. If the wastewater is of a significant strength, the biofilm will consume all of the oxygen supplied to it and an anoxic layer will form in the area closest to the bulk liquid. Denitrifying bacteria will occupy this area, meaning that such a system can provide additional BOD, ammoniacal and total nitrogen removal.

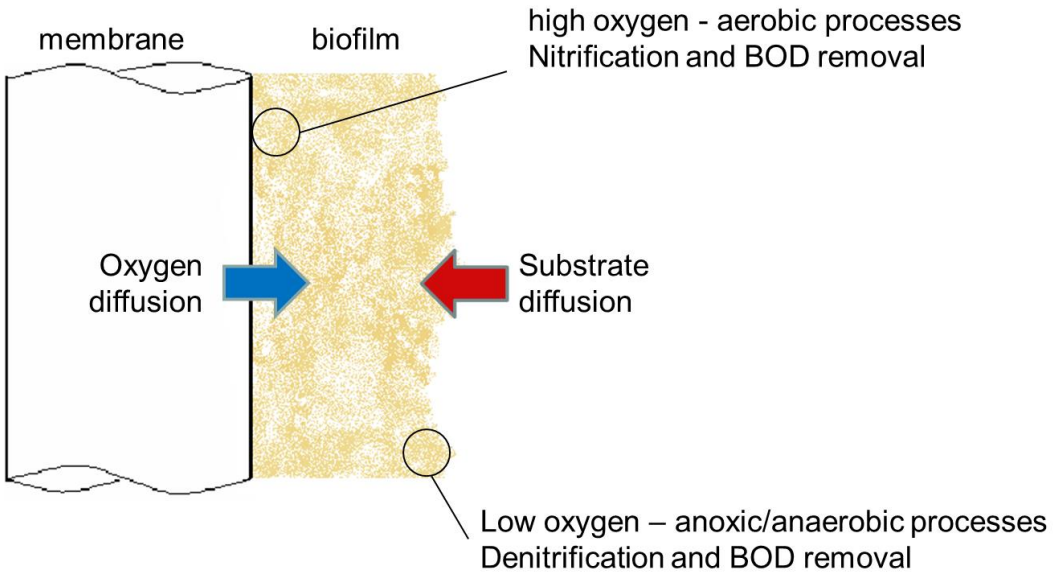

Figure 1-6: Structure of membrane aerated biofilms

This thesis introduces the BioSettler^{TM}, a novel for wastewater treatment which has been developed as described here, and has been patented (Groom *et al.*, 2009). The BioSettler combines the two existing technologies of membrane aerated biofilms and inclined plate settlers, by incorporating membrane aeration (with associated biofilm) on the underside of an inclined plate (Figure 1-7).

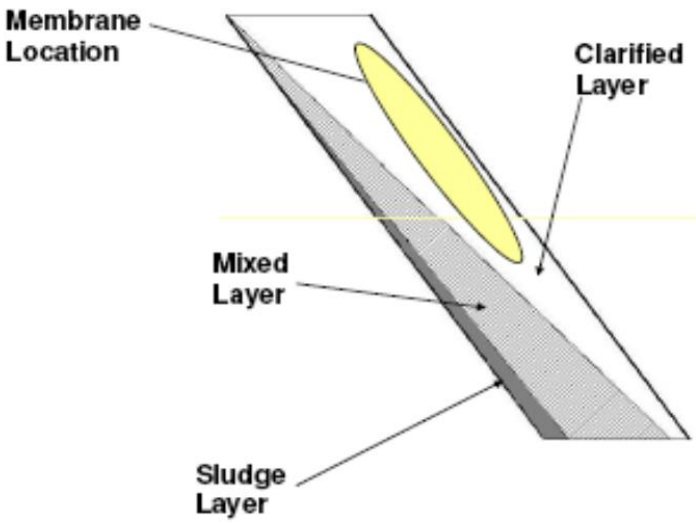

Figure 1-7: Membrane location in the BioSettler

Although established in their own right, this project is believed to be unique in combining the two systems into a single technology.

Employing such a system in wastewater treatments would yield two major advantages: the technology would lead to increases in the potential of final settling tank to remove solids and provide additional BOD, ammoniacal and total nitrogen removal.

Also, as the technology would be available as a retrofit package, it would be a significantly less expensive option for upgrade of wastewater treatment (Rubino, 1996). Additionally, this upgrade would be achieved without additional tanks being needed, making the technology suitable for use in situations where footprint is limited.

1.5 Aims and Objectives

This work aims to:

- Investigate the various factors that affect the bubbleless transfer of oxygen to water, specifically:
    - Membrane type;
    - Inlet air pressure;

    - Air flowrate;
    - Water side turbulence.
- Develop an understanding of the treatment of municipal wastewater in the MABfR, particularly of wastewater containing pollutant concentrations found in non-consent meeting secondary effluent. This will involve:
    - Investigation of the effect of inlet air pressure on pollutant removal;
    - Investigation of the effect of variation in wastewater composition on pollutant removal;
    - Model development to allow prediction of MABfR performance.
- Explore the use of the membrane aerated biofilm for the treatment of industrial wastewater, especially those originating from dye houses and containing azo dyes.
- Demonstrate the BioSettler concept with a pilot scale plant at a municipal WwTW.

1.6 Conclusions

Increasingly more demanding legislation governing the discharge of wastewater effluent, coupled with pressures from increasing and transient populations mean that upgrade of existing wastewater treatment infrastructure is required throughout the developed world.

Additionally, increasing environmental awareness and energy costs necessitate the development of wastewater treatment technologies which are more energy efficient that the current state of the art they will replace whilst matching or even exceeding the effectiveness of the treatment that they provide.

The use of Membrane Aerated Biofilms is one approach that is worthy of exploration in an attempt to meet these goals. When utilised as part of the BioSettler technology, membrane aerated biofilms can provide aerobic and anoxic conditions simultaneously and in the same tank, allowing a variety of wastewater pollutants to be mineralised. This thesis will explore the practicableness of this technology for wastewater treatment.

2 Review of wastewater sources, composition and treatment options

2.1 Wastewater and wastewater treatment

Wastewater is defined as any water which has been tainted by human activity. It is the combination of liquid and water carried wastes generated by residences, commercial and industrial buildings; along with stormwater and groundwater which enter the sewerage system (Tchobanoglous & Burton, 1991b).

If allowed to accumulate without treatment, several problems are caused. The organic molecules contained in this tainted water (such as sugars, fats, proteins) will be acted upon by microorganisms, consuming all available dissolved oxygen so that it is no longer available for fish and other aquatic organisms and producing unpleasant odours (e.g. hydrogen sulphide).

Additionally, wastewater may contain nutrients, which cause the excess growth of aquatic plants; mutagenic and carcinogen compounds and pathogenic microorganisms that originate in the digestion systems of humans and other domestic animals.

In order to protect human health and the environment from these threats, the discipline of wastewater engineering has developed. The discipline, which involves chemistry, biology, civil and chemical engineering, concerns itself with all aspects of the wastewater infrastructure, from collection at domestic dwellings and industrial premises where it is generated to its treatment and subsequent disposal or reuse.

2.1.1 Sources of wastewater

Almost every form of human activity generates wastewater. The composition and flowrate will vary greatly over time and as a function of the activity that produces it.

This thesis focuses on a solution for the need for upgrade of current wastewater treatment techniques and facilities, with an emphasis on two particular types of waste:

(i) Municipal wastewater;

(ii) Dye house wastewater.

2.1.1.1 Municipal wastewater

The term municipal wastewater refers to that wastewater which is produced from domestic residences and commercial properties (such as restaurants, shops and offices). Along with breakdown products of faecal matter and urine, municipal wastewater will contain residues of food and other solid materials, laundry detergents and other cleaning chemicals.

A typical analysis of untreated municipal wastewater is given in Table 2-1 (adapted from Tchobanoglous & Burton, 1991b). The various parameters used for characterisation of wastewater are discussed in more detail in Section 2.1.2.

Table 2-1 : Typical composition of untreated municipal wastewater

	Concentration (mg l^{-1})		
Contaminant	Weak	Medium	Strong
Solids (total)	350	720	1200
BOD_5	110	220	400
COD	250	500	1000
Nitrogen (Total as N)	20	40	85
Phosphorous (Total as P)	4	8	15
Grease	50	100	150

Municipal wastewater typically follows a diurnal pattern, with small volumes of wastewater reaching the treatment works at night and large flows in the morning and early evening (Healy & O'Flynn, 2011). Similar variations are seen in the daily variation of wastewater strength, as illustrated in Figure 2-1. In times of heavy rainfall, especially in areas where stormwater is also carried by the foul sewer, volume of wastewater

entering wastewater treatment units increases significantly, with an associated dilution effect which reduces wastewater strength.

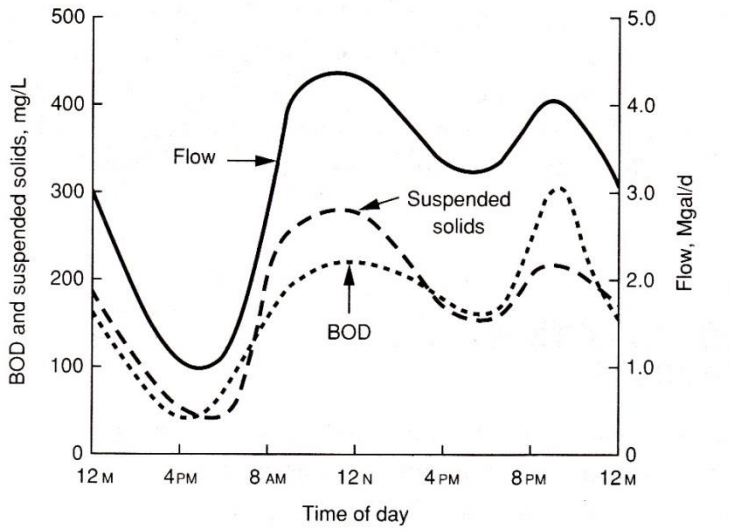

Figure 2-1: Diurnal variations in wastewater flowrate and strength for a typical WwTW (Tchobanoglous & Burton, 1991b)

To aid with the design of wastewater treatment facilities, the strength and volumes of wastewater produced by different activities are grouped into a notional unit called population equivalent (p.e.). This corresponds to the average volume and strength of wastewater produced per person at a typical domestic dwelling and currently is defined at 150 litres of wastewater, containing 60 g of Biochemical Oxygen Demand and 8 g of ammoniacal nitrogen as N (British Water, 2013).

2.1.1.2 Dye house wastewater

The process by which natural fibres are coloured is inherently inefficient, with 4 -12% of dyes lost to wastewater during textile processing (Coughlin *et al.*, 2002). In addition to unused dye molecules, dye house effluent will also contain dissolved metallic species, residues of adhesives chemicals used to adhere carpet to backing material and chemicals protect which the product from attack by microorganisms and insects (Wilkinson 2007).

Table 2-2: Typical analysis of Dye house wastewater (Wilkinson 2007)

Parameter	Value
Chemical Oxygen Demand	1500 – 2000 mg l^{-1}
Unused Dye	20 – 50 mg l^{-1}
pH	3.5 – 7.0
Suspended Solids	5 - 20 mg l^{-1}

Azo dyes; characterized by the presence of one or more azo bridges, nitrogen-nitrogen double bonds ($-N = N-$) (Van der Zee *et al.* 2003a), are the class of dye used most commonly industrially, accounting for approximately 70% of all dyestuffs used (Coughlin *et al.*, 2002). Although not widely used by commercial dye houses (Wilkinson 2007), the azo dye most commonly used in degradation studies in the literature is 1-Phenylazo-2-naphthol-4'-sulfonic acid, commonly known as Acid Orange 7 (AO7) or Orange II. The structure of AO7 is shown in Figure 2-2 (Fernandes *et al.*, 2004) .

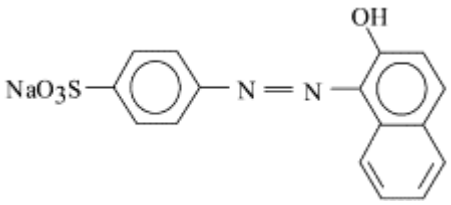

Figure 2-2: Structure of Acid Orange 7

In 2007, the world production of azo dyes was estimated at 500,000 tonnes (Pandey *et al.*, 2007). The production and dying processes are inherently inefficient, meaning at least 4% of the produced dyes are wasted, and ends up in domestic and industrial wastewater streams (Coughlin *et al.*, 2002). Although this results in significantly less volumes of wastewater than that produced by municipalities, the coloured nature gives azo dye effluent a significant impact on the general public.

The molecular structure of azo dyes makes them resistant to fading by exposure to sweat, soap, water, light and oxidizing agents (Davies *et al.*, 2006). Whilst this makes

them ideal for use as a dye, it makes them resistant to aerobic degradation in the activated sludge process – dye removal (if any) takes place via adsorption of azo dye molecules onto the settled activated sludge (Coughlin *et al.*, 2003).

2.1.2 Wastewater characterisation

Wastewater is characterised by the type and concentration of pollutants that it contains. The pollutants of interest in this study are listed and described in Sections 2.1.2.1 - 2.1.2.4 below. The methods by which they are obtained are detailed in Chapter 3.

2.1.2.1 Biochemical oxygen demand

Wastewater typically contains a mixture of organic compounds which are oxidised by the action of microorganisms. Identification and quantification of each individual organic compound is a very onerous task, and is therefore of little use to the wastewater industry.

Biochemical Oxygen Demand (BOD) is a parameter which, instead of quantifying the concentration of individual pollutants present, measures the amount of oxygen which is required by bacteria to oxidise them in a defined time period. A 5 day time period is most commonly used; but longer time periods are sometimes employed for practical reasons (e.g. laboratory schedules) or in wastewaters containing compounds which undergo very slow hydrolysis processes (Tchobanoglous & Burton, 1991b).

2.1.2.2 Chemical Oxygen Demand

Chemical Oxygen Demand (COD) is another measure of organic matter in wastewater that can be oxidised. Rather than a time consuming biological determination, the COD test chemically oxidises the wastewater using a reagent such as an acidic dichromate solution, as described by Equation 2-1:

$$C_nH_aO_bN_c + dCr_2O_7^{2-} + (8d + c)H^+ \rightarrow nCO_2 + \frac{a + 8d - 3c}{2}H_2O + cNH_4^+ + 2dCr^{3+}$$

Equation 2-1

The amount of COD present can then be related to the amount of chromate ion reduced to Cr(III), as ascertained by spectroscopic measurement of colour change from orange to green.

The value of COD is typically higher than that of BOD, as wastewaters commonly contain organic substances which can be oxidised chemically but not biologically (e.g. large molecules such as protein chains or lignin); inorganic substances are also oxidised by chromate and certain organic substances can be toxic to the microorganisms used in the BOD test.

Despite these drawbacks, the COD test takes considerably less time than the BOD test (approximately 2 hours versus 5 days), and as such is used. Oftentimes, where the composition of wastewater is relatively consistent, a steady ratio of BOD:COD can be established, and COD used as an estimator for BOD.

2.1.2.3 Ammoniacal nitrogen

Ammoniacal nitrogen (a term that describes nitrogen in both the NH_3 and NH_4^+ forms) is a characteristic breakdown product of organic matter and urea. It is the most common nitrogenous pollutant contained in wastewater, with an estimated 100,000 tonnes of ammoniacal nitrogen being discharged to inland waters in the UK each year (DEFRA 2002).

The presence of ammoniacal nitrogen in wastewater presents a number of problems. At high levels (~35 mg l^{-1} and greater) the distinctive strong unpleasant odour is detectable by the human nose. The un-ionised form, NH_3, can cause pH shifts and changes in the solubility of toxic substances, adversely affected receiving waters. Ammoniacal nitrogen

will also undergo nitrification (biological conversion to nitrate), causing depletion of dissolved oxygen in receiving water.

Exposures of 24 hours to ammoniacal nitrogen concentrations of as low as 0.2 mg l^{-1} have been reported as being toxic to fish (Woods 2003). As a result environmental protection agencies such as the Northern Ireland Environmental Agency, who are responsible the regulation of wastewater discharges, place stringent limits on those discharges in areas which serve as habitat for fish (Stewart 2014).

2.1.2.4 Nitrate

Nitrate (NO_3^-) is the product of the biological oxidation of ammonia, is therefore commonly found in wastewater. Although it is preferable to discharge nitrate nitrogen rather than ammoniacal nitrogen to receiving waters as nitrate does not deplete the dissolved oxygen, nitrate is still a pollutant (Grady *et al.* 1999).

Nitrate nitrogen can be converted by plants and algae into organic matter. When nitrate is present in high concentrations, this can lead to the growth of 'algal blooms', which form a blanket on the surface of the receiving water, which, in addition to appearing unnatural and unsightly, can alter the temperature, light levels and oxygen availability, leading to adverse effects on the aquatic ecosystem.

High nitrate nitrogen concentration in drinking water has been linked to 'blue-baby syndrome', where nitrate interferes with the oxygen carrying capacity of haemoglobin in the blood, potentially leading to death (US EPA, 2012).

2.1.2.5 Total Suspended solids

Wastewater contains a variety of solid materials ranging from large inorganic material such as stones and rags to microscopic bacterial cells, which must all be removed from the wastewater stream before discharge. Larger particles can cause blocking of channels

of water courses with associated flooding; whilst smaller particles can reduce the sunlight availability for aquatic plants and affect the temperature of water courses.

Solid materials are removed from wastewater based on physical size and difference in density. For example, wastewater is typically passed through a 6 mm screen on arrival at a treatment works, whilst solid particle such as activated sludge flocs are removed by providing quiescent conditions are sufficient residence time for them to settle to the bottom of clarifier tanks.

2.1.3 Current wastewater treatment technologies

Wastewater treatment falls into three categories: physical, chemical and biological, with the majority of wastewater treatment processes being a combination of the three different categories used in sequence.

For example, a typical municipal wastewater treatment works may consist of the following steps: screening (physical); grit removal (physical); coagulation and flocculation (chemical and physical); primary settling (physical); activated sludge (biological) and final setting (physical).

In addition to the biological processes explained in Sections 2.2.1 - 2.2.3, knowledge of two physical unit operation technologies is essential for understanding of this thesis. These technologies are (i) inclined plate settlers and (ii) membranes.

2.1.3.1 Inclined plate settlers

Analysis of the mechanisms by which settling occurs in both primary and secondary settling tanks in wastewater treatment plants reveals that the flowrate of wastewater through the settling tank that can be settled is proportional to its area and a critical velocity, v_c, as shown in Equation 2-2.

$$Q = Av_c$$ **Equation 2-2**

This equation implies that the greatest volume of wastewater could theoretically be settled by a tank approaching infinite surface area. Although correct theoretically, this approach is impractical, as the demand on plant footprint would be too great (Tchobanoglous *et al.*, 2004). A practical solution to increasing available settling surface is to fit settling tanks with an array of overlapping inclined plates as shown in Figure 2-3 and Figure 2-4.

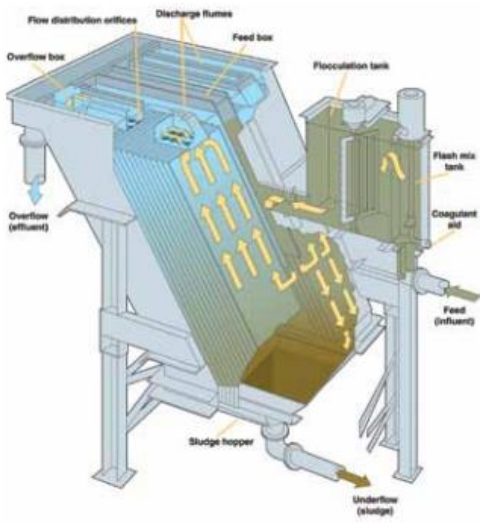

Figure 2-3: Schematic Inclined Plate Settler (Parkson, 2010)

Figure 2-4: Inclined Plates

These systems are called inclined plates settlers and can provide up to 10 m^2 for every m^2 of footprint (Parkson, 2010). Influent enters the plates through the side, with settled solids sliding down the upper plate surface to be collected at the bottom, whilst clarified effluent rises up the back of the inclined plate and is collected through an overflow weir at the top in the same way as in a standard settling tank.

2.1.3.2 Membranes in wastewater treatment

The word membrane is used to describe a thin interface that acts as a selective barrier which can be used to control the permeation rate of chemical species which come into contact with it (Baker *et al.*, 1991). Membranes affect separation through differences in

solubility and diffusivity or molecular size. Membranes occur in nature in biological cells, and artificial membranes mimicking this phenomenon are commonly used for a variety of purposes including controlled drug release, gas separations, electronic applications and wastewater treatment.

Membranes are characterised by their composition and structure. The membranes of interest in this thesis are categorised as being either nonporous dense membranes or microporous membranes.

Dense membranes consist of dense, uniform, structures, through which permeants are transported by diffusion under the driving force of a pressure, concentration or electrical potential gradient. The separation of components by the membrane is related to their transport rate in the membrane material, which is a function of their diffusivity and solubility in the membrane material. Dense materials are commonly used in gas separation applications and are formed from materials such as silicone rubber and polytetrafluoroethylene.

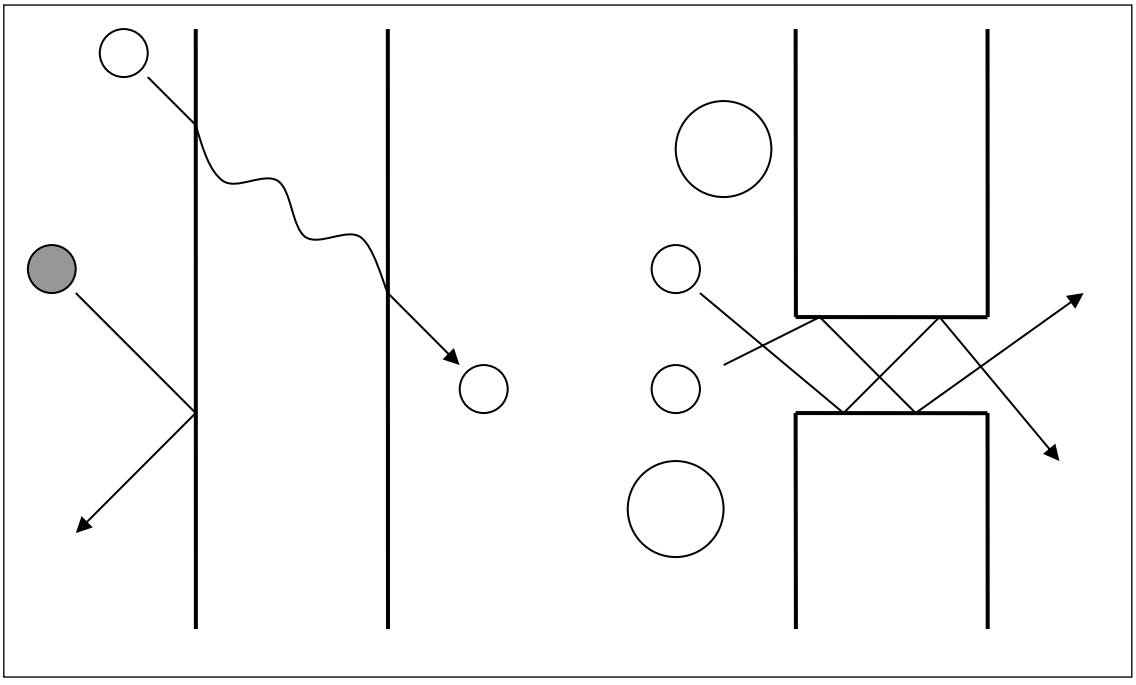

Figure 2-5: Molecular transport in dense membranes (left) by differences in permeation and microporous membranes by molecular filtration

Microporous membranes have structures which are similar to conventional filters, having a rigid, highly voided structure with a random distribution of interconnected pores (Baker *et al.*, 1991). The pores are smaller than in conventional filters, ranging from approximately 0.01 to 10 µm in diameter. Microporous membranes are further differentiated from each other based on the size of particles or molecules they retain, as illustrated in Figure 2-6.

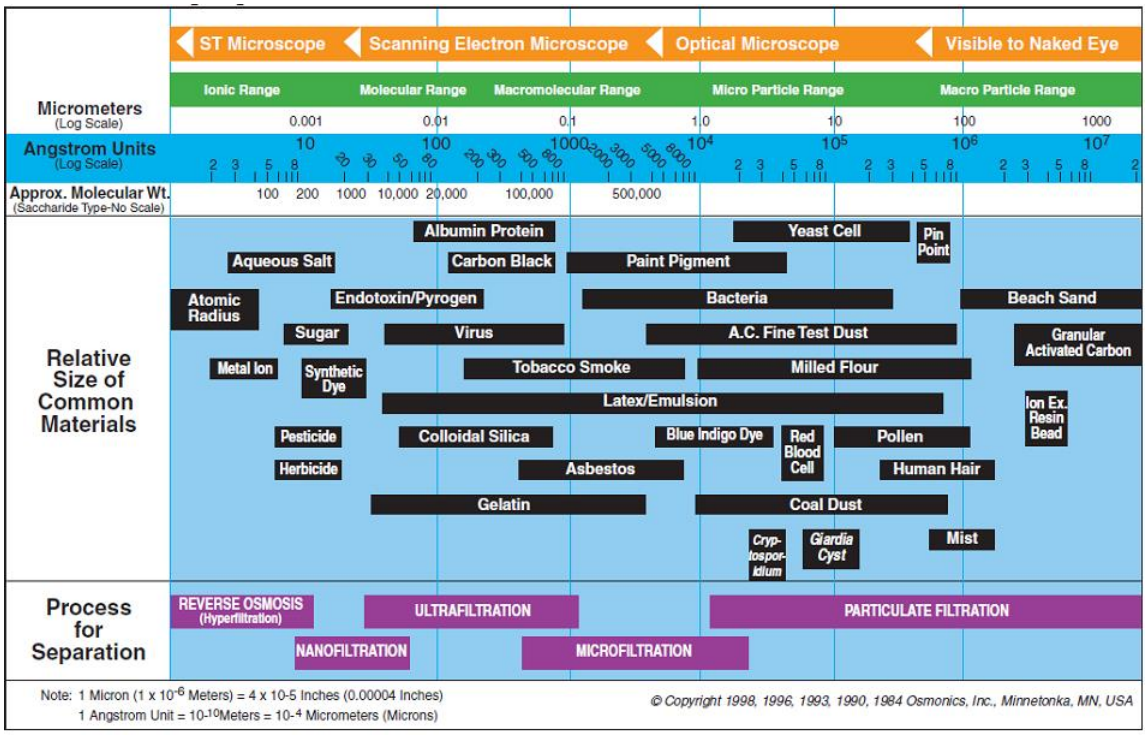

Figure 2-6: Membrane classification (Radcliff & Zarnadze, 2004)

Molecules larger than the larger pores will be completely rejected by the membrane. Molecules smaller than the largest pores, but larger than the smallest pores will be partially rejected in relation to the pore size distribution. In general, only particles with significant difference in molecular size can be separated using membranes.

Additionally, microporous membranes can be either hydrophobic or hydrophilic. In hydrophilic membranes, the membrane pores fill with liquid whilst in hydrophobic membranes; the pores remain gas-filled during operation. Hydrophilic membranes are generally preferable for liquid-phase filtrations, whilst hydrophobic are more suited to

gas transfer operations due to the higher diffusivities of gases through other gases compared to liquids.

2.1.4 Biofilms

The term biofilm is used to describe a colony of bacterial cells, held together in a matrix of extra-cellular polymeric material, produced by the organisms themselves (Madigan & Martinko, 2006). Biofilms were traditionally thought of as being associated with a surface, but recently the term biofilm has been expanded to include granular sludge, with the defining characteristic being the existence of substrate gradients (Morgenroth, 2008).

Biofilm is the most common form of bacterial life with mould grown in showers, plaque on teeth being common examples (Madigan & Martinko, 2006). Four reasons have been identified as to why biofilms form:

(a) Safety in numbers;
(b) Allows cells to remain in a favourable niche (e.g. close to a source of substrate);
(c) Allows bacterial cells to exist close together, facilitating intercellular communication;
(d) It is the default way in which bacterial cells grow (Madigan & Martinko, 2006).

Significant volumes of research are concerned with the prevention of biofilm formation, especially in medical applications, where biofilm formation can lead to the spread of infection (Monroe, 2007), or in membrane separation processes, where biofilm formation can lead to reduction in permeate flux (Dreszer *et al.*, 2014).

2.1.4.1 Biofilms in wastewater

Due to their high biomass retention, biofilm systems are very suitable for bacterial processes with involve slow growth rates (e.g. those for ammonia removal), and have been in use since the early wastewater systems developed by Victorian engineers.

Nowadays, alongside the two well established wastewater treatment technologies introduced in Chapter 1, there are two novel biofilm technologies which have yet to be adopted by the wastewater treatment industry, but have been the subject of significant published research, namely Extractive Membrane Biofilm Reactors (EMBRs) (e.g. Livingston *et al.*, 1998) and Membrane Aerated Biofilm Reactors (MABfRs) (e.g. Stephenson *et al.*, 2000).

Extractive membrane biofilm reactors are a relatively novel wastewater technology which combines aspects of the trickling filter and separation membranes, and is used in wastewater treatment as a replacement for settling (Stephenson *et al.*, 2000). In an EMBR, the biofilm acts as part of the separation membrane, adding biological treatment as wastewater moves through it (Livingston *et al.*, 1998).

This is particularly useful in the treatment of those wastewaters containing volatile organic compounds (VOCs), as the biofilm separates the VOCs from the aerated compartment of the bioreactor, preventing air stripping of VOCs to the atmosphere (Pavasant *et al.*, 1996).

2.1.4.2 Membrane attached biofilms

Membrane aerated biofilm reactors (MABfRs) are those systems in which dense or microporous gas transfer membranes are used to transfer oxygen to bacteria present on the membrane surface without the formation of bubbles (Stephenson *et al.*, 2000). The biofilm is attached to the membrane surface and wastewater is present on the outer surface of the biofilm so that counter diffusion of oxygen and substrate occurs into the biofilm.

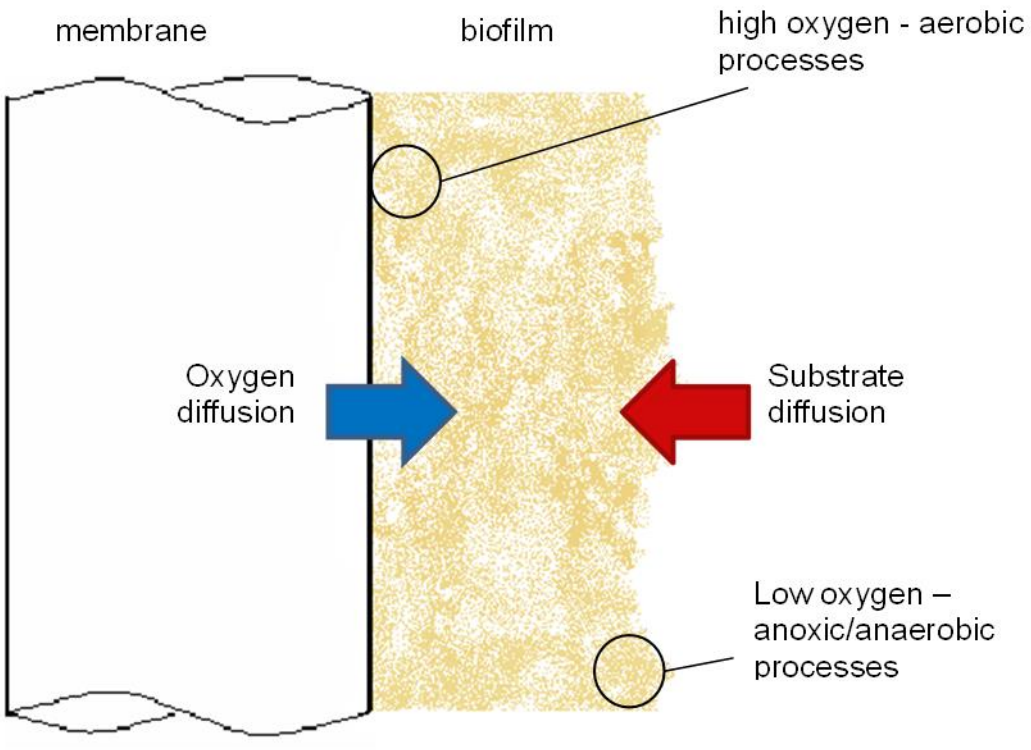

Figure 2-7: General structure of Membrane Aerated Biofilms

MABfRs can be operated with either pure oxygen or compressed air as the aeration gas, with the economics of the system favouring compressed air due to the high cost of pure oxygen production. Various different membrane types and arrangements are used as discussed further in Section 2.4.

2.2 Biology of wastewater treatment

Aerobic (in the presence of elemental oxygen), anoxic (without elemental oxygen) and anaerobic (in absence of oxygen) biological processes have historically been used for wastewater treatment.

Due to their low energy usage and the possibility of generating biogas, anaerobic processes are of increasing interest. This biogas can then undergo a combustion process and be used to generate renewable heat and electricity.

However, the types of wastewater streams which are of sufficient strength to generate significant volumes of biogas are limited – especially in Northern Ireland where sewers typically carry both sewage and storm water. Additionally, there are associated problems with odour nuisance caused by the co-production of hydrogen sulphide gas, with associated opposition from those living in the areas surrounding treatment works.

In Scotland, for example, legislation has been introduced preventing the release of odours from wastewater treatment works and other industrial sources. In response to this, water companies had been forced to place covers on some wastewater treatment units to prevent foul odours being released into the air.

Three biological processes are of interesting in this study

(i) Aerobic heterotrophy;
(ii) Nitrification;
(iii) Denitrification.

Aerobic heterotrophy and nitrification are aerobic processes, whilst the process of denitrification takes place in anoxic conditions. These three processes are summarized in Sections 2.2.1 - 2.2.3 below.

2.2.1 Aerobic heterotrophy

Heterotroph is the name given to those microorganisms who obtain their energy through the oxidation of organic matter (Bitton, 2005). The process is described as aerobic when the oxidation utilises elemental oxygen and can be described by the half reaction shown as Equation 2-3, where organic matter is represented by $\{CH_2O\}$, a theoretical molecule of COD (McCarty, 1975).

$$\{CH_2O\} + O_2 \rightarrow CO_2 + H_2O \qquad \textbf{Equation 2-3}$$

In addition to obtaining energy, heterotrophs use also organic carbon for cell synthesis, and as organic matter is the most common dissolved pollutant in wastewater, heterotrophs dominate wastewater treatment systems (Grady *et al.*, 1999). *Pseudomonas*, an extensively studied genus of bacteria due to their prevalence as an opportunistic pathogen in humans, is the most commonly found in wastewater (Bitton, 2005). A typical analysis of activated sludge is shown in Table 2-3.

Table 2-3: Typical distribution of Aerobic Heterotrophic Bacteria in Activated Sludge (Bitton, 2005)

Genus or Group	% Total Isolates
Comamonas-Psuedomonas	50.0
Alcaligenes	5.8
Pseudomonas (fluorescent)	1.9
Paracoccus	11.5
Unidentified (gram-negative rods)	1.9
Aeromonas	1.9
Flavobacterium-Cytophaga	13.5
Bacillus	1.9
Micrococcus	1.9
Coryneform	5.8
Arthrobacter	1.9
Aureobacterium-Microbacterium	1.9

2.2.2 Nitrification

Nitrification is a two stage process by which ammoniacal nitrogen is converted to nitrate-nitrogen by the action of autotrophic bacteria, and is the most common method for the removal of ammoniacal nitrogen in traditional wastewater treatment.

It is a two stage process, with the two separate stages being carried out by different groups of bacteria. Both stages are carried out by autotrophic bacteria, meaning than no organic carbon is involved in the process; carbon dioxide is instead used as a carbon source for cell synthesis.

First ammonia is converted to nitrite – a process carried out by bacteria known as nitrosofyers or ammonia oxidizing bacteria (AOB). *Nitrosomonas* is the most common AOB found in WwTW, but many other genera have been identified as being able to carry out this stage including *Nitrosococcus*, *Nitrosospira* and *Nitrosocystis*.

The conversion proceeds via two steps as shown by the half equations below:

$$NH_3 + O_2 + 2e^- \rightarrow NH_2OH + H_2O$$ **Equation 2-4**

$$NH_2OH + H_2O + \tfrac{1}{2}O_2 \rightarrow NO_2^- + 2H_2O + H^+$$ **Equation 2-5**

The second stage involves the conversion of the produced nitrite to nitrate. This step is known as 'true' nitrification and the bacteria that carry it out are known as nitrifiers (nitrate producers). *Nitrobacter* is the most common nitrifier found in WwTW, though *Nitrococcus*, *Nitrospira* and *Nitrocystis* have also been isolated.

The conversion occurs in accordance with the half equation given in Equation 2-6:

$$NO_2^- + \tfrac{1}{2}O_2 \rightarrow NO_3^-$$ **Equation 2-6**

Under steady state conditions, nitrite is not accumulated. As such, it is an accepted assumption to condition the action of AOB as the rate determining step (Gray, 2004). The detection of significant amounts of nitrite is evidential to inhibition of the second 'true' nitrification step.

Nitrification is highly dependent on wastewater temperature, with a drop in temperature from 20°C to 15°C resulting in a drop in nitrification effectiveness of 35% (Komorowska-Kaufman *et al.*, 2006).

2.2.3 Denitrification

Denitrification is the biological process by which microorganisms convert nitrite and nitrate to elemental nitrogen. It is an anoxic process, meaning that it takes place in the absence of elemental oxygen; and heterotrophic processes, requiring organic carbon for cell synthesis and energy generation (Dincer & Kargi, 2000).

The process proceeds via the pathway shown in Figure 2-8 below, with both nitrate and nitrite being acceptable starter species.

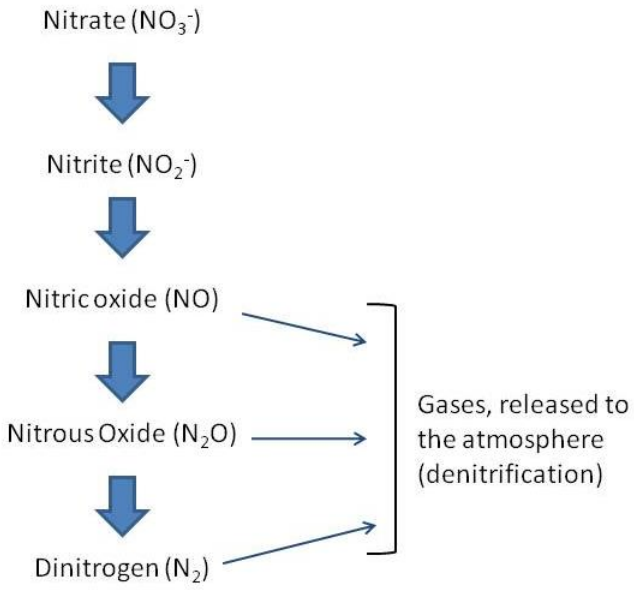

Figure 2-8: Steps in the reduction of nitrate (adapted from Madigan & Martinko, 2006)

Denitrification is carried out by a large range of microorganisms including *Escherichia coli* and *Pseudomonas sp*. These microorganisms are facultative aerobes; they carry out aerobic respiration when oxygen is present as an electron donor, and utilise other chemical species (such as nitrate) when it is not. Use of oxygen as an electron donor is preferable, as in this way the microorganisms gain most energy (Madigan & Martinko, 2006).

Reduction potential (redox potential) is a useful parameter for predicting which chemical species are used as an electron donor in biological processes. The redox potentials most

suited to different biological processes are illustrated in Figure 2-9. Anoxic processes, such as denitrification, take place at a redox potential of approximately +400 mV. Aerobic processes take place at higher redox potentials, with anaerobic processes taking place at negative redox potentials.

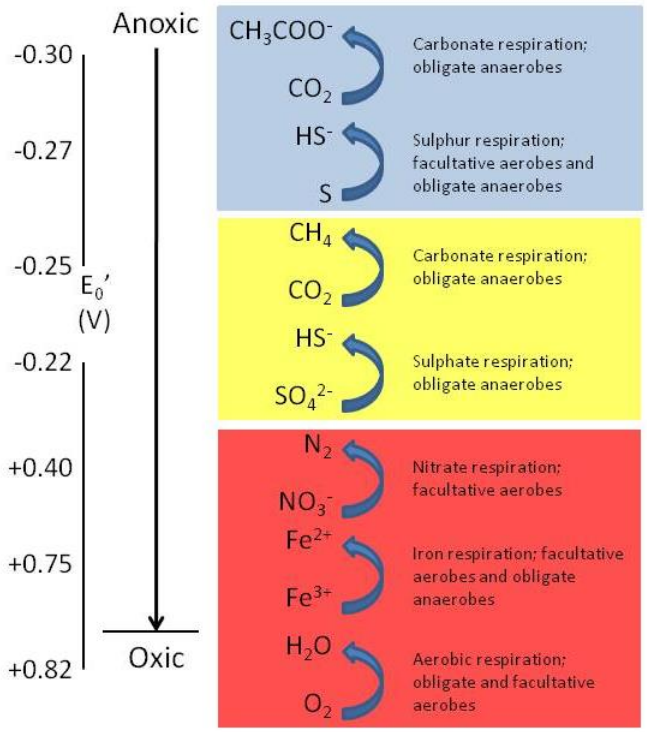

Figure 2-9: Examples of microbial respiration and associated redox potentials (adapted from Madigan & Martinko, 2006)

2.2.4 Stoichiometry of wastewater biology

McCarty (1975) published a method for developing a stoichiometric equation for reactions mediated by bacteria in wastewater. The method involves the combination of three half reactions: one for the oxidation of the electron donor (R_d); one for the reduction of the electron acceptor (R_a); one for the assimilation of new bacterial cells (R_c). The overall R is obtained as described in Equation 2-7.

$$R = R_d - f_e R_a - f_s R_c$$ **Equation 2-7**

Where: f_e = fraction of electron donor used for energy

f_s = fraction of electron donor used for cell formation

In order to achieve a balanced equation:

$$f_e + f_s = 1$$ **Equation 2-8**

f_s and f_e are functions of cell yield coefficient, cell decay rate, solids retention time (sludge age) and the biodegradable fraction of microorganisms as described by the relationship in Equation 5-3.

$$f_s = a_e\left(1 - \frac{f_d b t_s}{1 + b t_s}\right)$$ **Equation 2-9**

Where: a_e = cell yield coefficient

f_d = biodegradable fraction of active microorganism

b = cell decay rate (day^{-1})

t_s = solid retention time (days)

The method also presents the half equations for a variety of different nitrogen sources, electron acceptors and electron donors which can be combined as required. Values for a_e for a selection of common electron donor/electron acceptor pairs are also reported.

The construction of such stoichiometric equations for the various microbial reactions taking place in wastewater is extremely useful as it allows the establishment of a mass balance of the various inputs to the system. As such, this approach has been employed in many modelling studies, including those that investigated pollutant removal with membrane attached biofilms (Ergas & Reuss, 2001, Shanahan & Semmens, 2004).

2.3 Bubbleless Aeration

Bubbleless or bubble-free aeration is achieved by placing a thin film of synthetic membrane between the gas and liquid phases. Oxygen is transported through the

membrane material by virtue of a concentration gradient, and dissolves directly from the surface of the membrane into the liquid phase (Côté *et al.*, 1989).

2.3.1 Historical Context

One of the earliest examples of relevant published research is that conducted by Robb (1968), in which the transfer of oxygen to water, through various polymer membranes, was investigated. In a study of 27 polymeric materials, including polystyrene, polyethylene, polyvinylchloride and polyamide-6, silicone rubber was found to perform best. The study also suggests possible uses for a silicone rubber membrane based on the permeability: as a membrane oxygen enricher, as an air regenerator for possible use in a nuclear fallout situation and to extract oxygen from fresh water; but did not suggest any uses of silicone membranes which have come into common use.

A later study by Yasuda & Lamaze (1972) found, that with hydrophobic porous membranes, the rate of oxygen transfer into water was controlled by the liquid boundary layer – the resistance of which can be greatly reduced by operation in the turbulent regime.

Recent works have utilised a variety of materials for gas transfer into water-based solutions/mixtures, for a variety of purposes. Most commonly, these materials have been polyethylene (PE) (Brindle *et al.*, 1998), polypropylene (PP) (Ahmed *et al.*, 1996) and polytetrafluoroethylene (PTFE) (Schneider *et al.*, 1995), but less common materials such as silicone rubber (Coté *et al.*, 1989) and Gore-Tex® (Timberlake *et al.*, 1988) have also been utilised. In some studies, composite membranes have been used (e.g. Ahmed *et al.*, 2004) – combining gas transfer properties of one material with the robustness of another – allowing higher pressures to be used and therefore larger gas fluxes to be achieved.

With microporous membranes, i.e. those constructed from materials such as PP and PE, the formation of bubbles restricts operation to low pressures. As transmembrane

concentration difference (a function of transmembrane pressure) is the driving force for mass transfer through the membrane, the rate of mass transfer is therefore limited. Dense membranes, constructed of materials such as silicone rubber, can be operated at higher pressures without bubble formation occurring, leading to greater oxygen fluxes.

2.3.2 Mass transfer mechanism

Membrane materials are categorised into microporous and dense membranes based on the mechanism of gas transfer. In dense membranes, oxygen is transported from the gas side to the water side via a solution-diffusion mechanism; oxygen is absorbed into the polymer on the gas and is transported by diffusion through the membrane wall to the interface with the liquid. There it then dissolves into the liquid phase and is transported away from the membrane surface via diffusion.

When calculating the total mass transfer resistance (*1/K*), the gas mass transfer resistance can be considered to be negligible, meaning it can be expressed as the sum of the liquid film resistance ($1/K_L$) and the membrane resistance ($1/K_M$):

$$\frac{1}{K} = \frac{1}{K_M} + \frac{1}{K_L}$$ **Equation 2-10**

where: K = overall mass transfer coefficient (ms^{-1});

K_M = membrane mass transfer coefficient (ms^{-1});

K_L = liquid side mass transfer coefficient (ms^{-1}).

The liquid film mass transfer resistance is a function of hydrodynamic variables and can be estimated for a given design through empirical mass transfer correlations.

The estimation of the membrane resistance is different for dense and porous membranes. For the case of a dense polymer membrane, when the gas solubility in the polymer can be represented by a linear isotherm and the diffusion coefficient in the membrane is constant, the mass transfer resistance through the membrane can be expressed as Equation 2-11

$$\frac{1}{K_M} = \frac{l}{S_M D_M} \qquad \textbf{Equation 2-11}$$

where: l = membrane thickness (m);

S_M = solubility coefficient of the gas in the polymer (m^3m^{-2});

D_M = diffusion coefficient of the gas in the polymer (m^2s^{-1}).

Much more complex mechanisms exist for the transfer of gas through a porous membrane. If the total gas pressure is maintained below the bubble point of the porous membrane, there should be essentially no total pressure difference across the membrane and transport should take place via diffusion through membrane pores- especially true for low solubility gases such as oxygen, nitrogen and carbon dioxide (Yang & Cussler, 1986). If the membrane is made from a hydrophobic material, the pores remain gas filled, and the oxygen transfer occurs via a gas-gas diffusion or Knudsen flow mechanism, depending upon parameters such as membrane morphology, the nature of the gas mixture, and the total gas pressure. The mass transfer resistance of the membrane ($1/K_M$) in this situation is normally considered negligibly small compared to the liquid film resistance ($1/K_L$), as first suggested by Yasuda & Lamaze (1972).

2.3.3 Modes of operation

Literature contains details of two different modes of membrane operation – either in the form of a flat sheet or hollow fibre tube. Tubular membranes have the advantage in the amount of surface area they can provide for mass transfer, especially when combined

with others in the form of a fibre bundle. Additionally, hollow fibre membranes can be operated either in dead end mode, where each individual fibre is sealed, or in flow through mode (Fang *et al.*, 2004).

Flow-through operation holds two major disadvantages: oxygen transfer efficiencies of 100% can never be achieved and Volatile Organic Compounds (VOCs) will be stripped to the atmosphere. Dead-end operation can avoid these, but Côté *et al.* (1989) recommended avoiding its use as it was compromised by water condensation on the gas side of the membrane fibre. This was not found with flow-through mode, as any water vapour entering the fibre was swept away instead of being allowed to accumulate.

More recent work by Fang *et al.* (2004), reported that condensation is unavoidable regardless of whether flow-through or dead-end operation is utilised. Due to higher mass transfer coefficients for water compared to gas, the gas stream will quickly become saturated with water vapour and condensation will occur. Several solutions were suggested to overcome this problem, including incorporation of sections of hydrophilic microporous material at the effluent end of the fibres. This will allow condensate to return to the external solution, provided internal gas pressure exceeds external water pressure.

2.3.4 Evaluation of Oxygen Mass Transfer Coefficient

An accepted procedure determining the overall oxygen transfer coefficient is presented by the American Society of Civil Engineers (ASCE, 1992). The method involves the removal of dissolved oxygen (DO) from a known volume of water and reoxygenation to a value near saturation. Measuring the DO concentrations at various times, t, during the reaeration period allows the oxygen transfer coefficient to be found using Equation 2-12, which can be linearised to find a value of K_L at each determination point.

$$e^{-K_L at} = \left[\frac{C_s - C_t}{C_s - C_0} \right]$$ **Equation 2-12**

Where: K_L = liquid side mass transfer coefficient (ms^{-1})
a = specific surface area (m^2m^{-3})
C_t = oxygen concentration in bulk liquid at time t ($mg\ l^{-1}$)
C_s = oxygen concentration in equilibrium with gas as given by Henry's Law
C_0 = initial concentration (C_t at t = 0)

A modified form of this method is employed by Côté *et al.* (1989), in their study involving the use of silicone rubber membranes for oxygenation of water. Due to the different solubilities of oxygen and nitrogen in membrane materials, the value of the Henry's Law constant for this system cannot be easily determined. To avoid this problem, the gas side oxygen concentration is used, allowing the overall mass transfer coefficient to be obtained instead, as detailed in Equation 2-10

$$e^{-Kat} = \left[\frac{C_g - C_t}{C_g - C_0} \right]$$ **Equation 2-13**

where: K = overall mass transfer coefficient, m/s
C_g = oxygen concentration in gas phase

Although use of this method eliminates the difficulties involved in calculation of interfacial concentration required by the ASCE method, errors are introduced due to the uncertainty of gas phase concentrations caused by pressure drop and changes in gas composition along the length of the membrane as a result of diffusion and back diffusion through the membrane material.

An alternative method, based purely on bulk liquid side concentrations, is presented by Cussler (1997). The method requires knowledge of the saturation concentration at the experimental conditions and obtains an average value of the overall mass transfer coefficient according to Equation 2-14:

$$C_t = C^*(1 - e^{-Kat}) \qquad \textbf{Equation 2-14}$$

Where: C^* = saturation oxygen concentration in bulk liquid at experimental conditions

2.3.5 Calculation of oxygen flux

Average oxygen flux can be obtained by calculation from the obtained mass transfer coefficient as introduced by Côté (1989) as shown in Equation 2-15.

$$\overline{J} = K\Delta C \qquad \textbf{Equation 2-15}$$

Where: $\overline{J}$ = average oxygen flux
K = overall mass transfer coefficient
ΔC = concentration difference across membrane

The use of Equation 2-15 requires knowledge of the oxygen concentration on the air side of the membrane, which can be difficult to obtain for the reasons outlined in Section 2.3.2. An alternative method is the calculation of oxygen flux directly from experimental data using Equation 2-16:

$$\overline{J} = \frac{(C_t - C_0)}{a(t_t - t_0)} \qquad \textbf{Equation 2-16}$$

2.3.6 Bubble formation

Equation 2-15 is valid only below a critical value of transmembrane pressure, which is a function of the membrane geometries (Coté *et al.*, 1989). Above this critical value, several researchers have reported the formation of a layer of bubbles which act as an additional mass transfer resistance and reduce oxygen flux (Casey *et al.*, 1999, Coté *et al.*, 1989, Ahmed & Semmens, 1996). In order to avoid this during operation, any increase in gas pressure should be accompanied by an increase in liquid side fluid pressure.

Literature contains details of two possible causes of bubble formation. In investigations where deoxygenation was achieved by the use of nitrogen gas, the water becomes saturated with nitrogen, meaning any nitrogen that diffused through the membrane at the beginning of the aeration period (where air was used on the gas side) would be unable to enter the bulk liquid, leading to the formation of bubbles (Coté *et al.*, 1989).

Alternatively, bubble formation has also been attributed to higher than saturation values of gas concentration at the membrane/gas interface, with oxygen concentrations of up to 100 mg l^{-1} being reported (Casey *et al.*, 1999).

However, in a MABfR, although bubbles were observed during startup with pressures exceeded 0.5 bar, they were not seen once the biofilm had reached a thickness of 100µm, allowing higher pressures to be used (Casey *et al.*, 1999).

2.3.7 Effect of attached biomass on oxygen transfer

The presence of a biofilm on the surface of an aeration membrane affects the mass transfer through the membrane in number of different ways. Results from experimental (e.g. dos Santos & Livingston, 1995) and modelling studies (Essila *et al.*, 2000) suggest that respiration of biomass near the membrane surface leads to an increase in the rate of oxygen transfer through the membrane. This can attributed to the maintaining of a near-maximum concentration difference across the membrane, giving higher fluxes as suggested by Equation 2-15.

Additional studies by Casey *et al.* (2000a, 2000b) suggest that this 'respiring effect' is applicable only to young, thin biofilms. In thicker biofilms, the accumulation of biomass leads to an increase in the resistance of mass transfer, reducing the oxygen transfer rate. This has consequences for pollutant removal as the biofilm mass transfer resistance slows the diffusion of substrate to the oxygen rich areas of the biofilm and of oxygen to substrate rich areas of the biofilm.

Côté *et al.* (1989), suggest that the presence of a biofilm on the membrane surface will have a negative effect on the rate of oxygen transfer. The researchers did not carry out investigations with active biomass, but postulate that adsorption into the membrane of CO_2 and other respiration products will decrease the oxygen diffusion coefficient in the membrane material, slowing the oxygen transfer rate.

Shanahan & Semmens (2006) carried out one of the few investigations where the mass transfer characteristics of the clean membrane in a MABfR were established prior to establishment of a biofilm. Using a flat sheet membrane, local oxygen fluxes of the clean flat sheet membrane was calculated from a correlation similar of the form in Equation 2-15, developed in the work with a clean membrane, and compared to fluxes calculated from conversion of ammoniacal nitrogen to nitrate. The researchers observed reduction in fluxes in upstream sections of the membrane, where the presence of a biofilm reduced turbulence, and increases in downstream areas where the biofilm reduced the boundary layer. The implication of this work for tubular membranes, where the boundary is known to be of less significance, is that oxygen transfer is reduced by the presence of the biofilm.

2.3.8 Design of hollow fibre membrane contactors

When designing a hollow fibre membrane contactor for gas transfer, there are two elements that must be considered in order to maximise mass transfer:

(i) Maintenance of as high as possible concentration difference

(ii) Obtaining high mass transfer coefficients through good design.

The factors for consideration in design of hollow fibre contactors are analogous to those involved in the design of heat exchangers (Coulson *et al.*, 1999b). Mass transfer coefficients, like heat transfer coefficients, cannot be accurately calculated theoretically.

In the absence of theoretically derived design equations, empirical relations of the form of Equation 2-17 are used. Ascertained through lab scale experiments, they can be used for scale-up provided geometric similarity is maintained.

$$Sh = a\,\mathrm{Re}^{b}\,Sc^{c} \qquad \textbf{Equation 2-17}$$

$$Sh = \frac{K_L d}{D} \qquad \textbf{Equation 2-18}$$

$$Re = \frac{dv\rho}{\mu} \qquad \textbf{Equation 2-19}$$

$$Sc = \frac{\mu}{\rho D} \qquad \textbf{Equation 2-20}$$

Where: *Sh* = Sherwood number (dimensionless form of mass transfer coefficient)
Re = Reynolds number (dimensionless)
Sc = Schmidt number(dimensionless)
a,b,c = constants (dimensionless)
K = mass transfer coefficient (ms^{-1})
d = characteristic length (m)
D = diffusivity (m^2s^{-1})
V = velocity (ms^{-1})
P = density (kgm^{-3})
μ = viscosity (Pa.s)

The Schmidt number, found by divided the kinematic viscosity by the diffusivity of oxygen in water, is constant for all water-oxygen systems. A value of 0.33 is widely accepted for oxygen/water systems in the literature (e.g, Yang & Cussler, 1986, Coté *et al.*, 1989, Ahmed & Semmens, 1996, Vladisavljevic, 1999).

2.4 Membrane Attached Biofilm Processes

Many researchers have investigated the use of membrane aeration for wastewater treatment. Timberlake *et al.* (1988) conducted one of the first such studies and achieved significant nitrification of wastewater. Later studies by Brindle & Stephenson (1996) and Yamagiwa *et al*. (1994), who used a "fibrous woven support" in proximity to the membrane in order to increase the surface area available for biofilm attachment, obtained excellent BOD removal, nitrification and denitrification. These studies have

displayed that these three key processes of wastewater treatment can successfully be carried out simultaneously if correct process conditions can be maintained.

2.4.1 Pollutant removal

Membrane aerated biofilm reactors have been used to treat a variety of wastewaters including domestic wastewater (e.g. Pankhania *et al.*, 1999), artificial swine wastewater (Terada *et al.*, 2003), effluent containing acetonitrile (Li *et al.*, 2008) and effluent containing pharmaceuticals (Peng *et al.*, 2015).

The studies most relevant to this work are those which investigated the use of MABfRs in situations where aerobic heterotrophy and nitrification processes occurred simultaneously, with or without denitrification also taking place. A selection of these studies is discussed in Sections 2.4.1.1 and 2.4.1.2.

2.4.1.1 Aerobic processes

Timberlake *et al.* (1988) authored an early study on the use of MABfRs for wastewater treatment. Using a Gore-Tex membrane and modest lumen pressures, up to 55% organic carbon removal was achieved at rates up to 4.2 gTOC $m^{-2}day^{-1}$. Nitrification was also obtained concurrently at rates up to 0.6 gN $m^{-2}day^{-1}$, with simultaneous denitrification proceeding at the same rate.

Yamagiwa *et al*. (1994), using their "fibrous woven support" achieved simultaneous organic carbon removal and nitrification from a wastewater with a composition similar to that of secondary effluent (20 mg l-1, 4 mgN l-1 as ammonia). Conversation rates of 6.3 gTOC $m^{-2}day^{-1}$ and 2.2 gN $m^{-2}day^{-1}$ was obtained using lumen pressures between 19.6 and 29.4 kPa (gauge). The researchers also reported a limited effect of air pressure on reaction rates.

Downing & Nerenberg (2008a) investigated the nitrification rate of a membrane aerated biofilm in the presence and absence of BOD. The researchers obtained a nitrification rate of 1.5 gN $m^{-2}day^{-1}$ in the absence of BOD in the bulk liquid. This decreased to 1.3 gN $m^{-2}day^{-1}$ in the presence of 1 gBOD m^{-3} in the bulk, and to 0.4 gN $m^{-2}day^{-1}$ when the bulk BOD concentration was 10 g m^{-3}. The observed decrease in nitrification rate was attributed to increased competition for oxygen from heterotrophic bacteria. The researchers also noted that nitrification in the MABfR was less inhibited by BOD than in convention biofilms.

Satoh *et al.* (2004) carried out a microprobe study of nitrification in a MABfR. The researchers obtained nitrification rates of approximately 0.5 gN $m^{-2}day^{-1}$, whilst confirming through the use of the microprobes that the majority of nitrification took place close the membrane surface. The location of nitrifiers on the membrane surface, where oxygen concentrations are highest and BOD concentrations lowest, explains the reduced inhibition observed by Downing & Nerenberg (2008a).

COD and ammoniacal nitrogen removal rates obtained in the most relevant MABfR studies to this work are summarised in Table 2-4.

Table 2-4: Comparison of pollutant removal rates achieved in selected MABfR studies

Author	r_{COD} (gCOD $m^{-2}day^{-1}$)	$r_{amm\text{-}N}$ (gN $m^{-2}day^{-1}$)
Timberlake (1988)	0.19	0.04
Pankhania *et al*. (1994, 1999)	15.08	n/a
Yamagiwa *et al.* (1994)	6.3	2.2
Semmens et al. (2003)	10.0	2.0

2.4.1.2 Denitrification

Denitrification has not been studied to the same extent as aerobic processes. It is considered the more reliable of the two total nitrogen removal processes - consistently high denitrification rates are achieved in wastewater treatment plants under high COD

loadings. Nitrification is the less reliable of the two processes, and therefore requires more optimisation for effective nitrogen removal. As such it is the more studied process (Yamagiwa & Ohkawa, 1994).

Several studies have reported denitrification rates in MABfRs where denitrification was not the focus of the work. The achieved removal rates are summarised in Table 2-5.

Table 2-5: Denitrification rates of various MABfR studies

Author	Denitrification rates gN $m^{-2}day^{-1}$
Timberlake *et al.* (1988)	0.1 – 0.6
Semmens *et al.*	2.0
Satoh *et al.* (2004)	0.12 – 0.33
Downing & Nerenberg (2008a)	0.23 – 0.32

In a study using a membrane bioreactor (standard MBR - no aeration supplied by membrane), He *et al.* (2009) investigated the effect of C:N ratio on simultaneous nitrification and denitrification. The researchers found the highest rates of total nitrogen removal occurred at the highest C:N ratios, which was attributed to the availability of sufficient COD for complete denitrification to take place.

The most comprehensive study of total nitrogen removal using a MABfR was carried out by Walter *et al.* (2005). Using a synthetic feed which did not contain nitrate nitrogen, the researchers measured nitrogen removal rates at various C:N ratios. Nitrogen removal rates of up to 2 kg $m^{-3}day^{-1}$ were achieved with the highest rates obtained at the lowest C:N ratio – a result which is contrary to He *et al.* (2009).

Although not considered by the researchers, a likely explanation for this is that the higher C:N ratios led to less oxygen being utilised for nitrification; effectively meaning that the rate of nitrogen removal by denitrification was limited by nitrate availability. Matsumoto *et al.* (2007) carried out a modelling study based on a plug flow MABfR and

found the minimum C:N ratio for complete denitrification to occur can be calculated from stoichiometry to be 2.86.

In the previously mentioned microprobes study, Satoh *et al.* (2004) found denitrification to occur just above the nitrification zone (i.e. further away from the membrane surface), and obtained denitrification rates in the range 0.12 – 0.33 gN $m^{-2}day^{-1}$, when an organic carbon loading rate of 1.0 gCOD $m^{-2}day^{-1}$ was used.

2.4.2 Control of biofilm thickness

Several authors have commented on the negative effect thick biofilms can have on the rate of pollutant removal, as the excess biomass represents a substantial resistance to diffusion of substrate into the biofilm.

Hwang *et al.* (2010) operated a two-stage membrane biofilm reactor, where the first stage used pure oxygen as the lumen gas with the second stage using hydrogen; in a similar way to the Rittmann group (e.g. Lee & Rittmann, 2002). The system utilised periodic sparging of nitrogen gas, to maintain to steady biofilm thickness for optimal nitrification and denitrification. Whilst limited effect was seen on the nitrification performance, a 25% increase in denitrification rate was observed.

2.5 Biological azo dye wastewater treatment

A variety of treatment options, including adsorption (Walker *et al.*, 2003); chemical oxidation (Aleboyeh *et al.*, 2009); enzymatic catalysis (Cristovao *et al.*, 2009); constructed wetlands (Davies *et al.*, 2006) and various biological processes have been considered for dye house wastewater treatment.

There is a general agreement in the literature that the cleavage of the azo bond takes place under anaerobic or anoxic conditions, with the general reaction mechanism being that which is described by Figure 2-10.

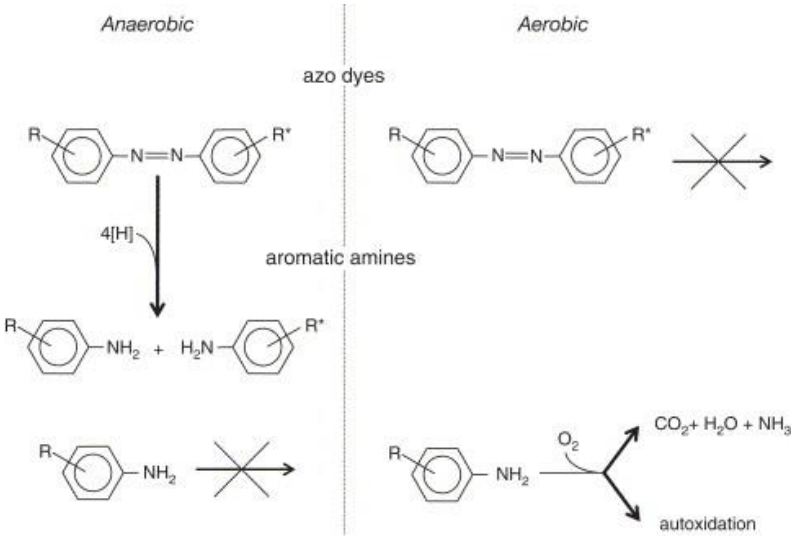

Figure 2-10: Anaerobic and aerobic degradation pathways of azo dyes (Van Der Zee & Villaverde, 2005)

As shown, azo dyes readily degrade in anaerobic conditions to form colourless aromatic amines which are resistant to further anaerobic degradation (Ong *et al.*, 2005) and have been reported as being or potentially being mutagenic agents (Shaw *et al.*, 2002). These aromatic amines breakdown further under aerobic conditions (Van Der Zee & Villaverde, 2005), meaning that azo dye waste requires a combination of aerobic and anaerobic/anoxic conditions in order to achieve complete removal.

The decolourisation and degradation of azo dye waste has been extensively studied by various researchers. Decolourisation, which involved the cleavage of the –N=N- azo bond, has been achieved under anaerobic, anoxic and aerobic conditions by different groups of bacteria (Pandey *et al.*, 2007). To date, there are no published studies on the use of membrane aerated biofilms for decolorisation of azo dye waste.

The first stage of the mechanism is the anaerobic reduction of the azo bond. Gingell & Walker (1971) proposed a two-stage mechanism for this reduction as described by Equation 2-21 and Equation 2-22.

$$2e^- + 2H^+ + (R - N = N - R') \rightarrow (R - NH - NH - R') \quad \textbf{Equation 2-21}$$

$$2e^- + 2H^+ + (R - NH - NH - R') \rightarrow (R - NH_2) + (R' - NH_2) \quad \textbf{Equation 2-22}$$

In the reduction, the azo compounds (the 'R' groups) are used as terminal electron acceptors, forming the R groups into amine compounds. This action breaks the azo bond, which is the dye's chromophore, removing the colour of the wastewater (Sponza & Isik, 2002).

Many of the amine compounds formed by this degradation are readily degraded under aerobic conditions (Brown & Labouruer, 1983). Complete degradation of sulphonated azo dyes may prove problematic as sulphonated aromatic amines are difficult to degrade (Tan *et al.*, 2000), but is possible in the presence of properly adapted consortium of microorganisms (Thumheer *et al.*, 1986).

The exact mechanism by which azo bond cleavage occurs is unknown. Due to their large molecular weight and polar nature, azo dyes are unlikely to pass through the cell membrane into bacteria cells (Levine, 1991). Pearce *et al.* (2006), amongst other researchers, suggest it is due to the action of the enzyme *azo reductase*, which is secreted by *Shewanella sp.* and other bacteria.

Alternatively, some authors suggest the azo bond reduction takes place outside of bacterial cells through chemical reactions with substrates such as sulphide, which are typically present in dye house effluent as it is a common additive to dye baths (Van Der Zee *et al.*, 2003a).

Additionally, chemical and biological reaction mechanisms have been shown to be accelerated by the addition of redox mediating compounds, which donate electrons to facilitate azo bond cleavage and are later regenerated. Van Der Zee *et al.* (2003a) demonstrated decolourisation of AO7 was significantly accelerated in the presence of the redox mediator riboflavin at a sub-stoichiometric level.

As previously stated, there are no published studies detailing the use of membrane aerated biofilms for decolourisation and degradation of azo dyes, but studies of biological processes utilising combined or sequential anoxic and aerobic conditions are contained in the literature.

Coughlin *et al*. (2002) investigated the use of a laboratory scale rotating biological contactor (RBC) and found the process capable of decolourising AO7 from a concentration of approximately 55 mg l^{-1} to below detection limits. A synthetic wastewater was used in which AO7 was the only possible source of COD. A consistently low effluent COD was obtained, which the researchers attributed to the complete mineralization of the azo dye.

To date, there has been only one example of azo dye decolourisation involving a MABfR. Wang *et al.* (2012) also used *Shewanella sp.* and achieved removal of up to 98% of AO7 with influent concentrations of between 50 – 200 mg l^{-1}. However, the MABfR was operated in sequential batch mode, and the researchers reported the biofilm attached to the membrane surface was "not competent for AO7 decolourisation". Additionally, the best removal efficiencies were achieved during a period when biomass from an activated sludge plant was mixed with the influent, and it may be speculated that adsorption of azo dye onto this biomass made a significant contribution to the dye removal.

2.6 Inclined Plate Settlers

The development of lamella settlers can be traced to two seemingly unrelated origins. Hazen (1904), in his seminal paper on wastewater settling, explained how settling rate was dependent upon settling area rather than tank volume, and suggested settling tanks therefore be split via a stack of horizontal plates in order to increase available settling area. It would have been normal practice at this time to periodically remove solids with a series of moving chains rather than self-cleaning with inclined tank floors. This is

acknowledged by Masschelein (1992) as the first description of the use of lamella plates in solids removal processes.

Boycott (1920) observed that blood corpuscles settled faster in inclined tubes compared to those that are vertical. This phenomena has become known as the Boycott Effect (Acrivos & Herbolzheimer, 1979) and has led to the use of multiple inclined tubes or plates for settling processes in wastewater treatment (Mace & Laks, 1978), the mining industry (Cook & Childress, 1978), fertilizer production (Wenk, 1990) and in cell separation processes (Janelt *et al.*, 1997).

In addition to the greater settlement efficiency, lamella settlers are also very low in energy costs, command low capital costs, offer large savings in space occupied and can settle fine suspensions at a high rate (Saleh & Hamoda, 1999, Humpal & Chiesa, 1990). A disadvantage of lamella settlers is that, given certain process conditions, the flow channels can become blocked; this can be overcome by fine screening of the influent upstream of the settler (Grady *et al.*, 1999).

Historically, there has been very little interest in the research of inclined plate or lamella settlers, reflected in paucity of published research on the topic.

2.6.1 Design Considerations

Despite being in use since the 1960s, there are no definitive equations governing the design of a lamella or inclined plate settler (IPS). Designs are based on experience and established industry procedures, and quite often compromises have to be made in order to produce an economically viable and practicable solution.

Instead, the design process involves following best practice established through existing installations, and it is recommended that bench and/or pilot scale testing is carried out prior to commissioning of a full scale unit (Humpal & Chiesa, 1990).

2.6.2 Operational Issues

The inclined plates are typically spaced 2 inches apart and inclined at angles between 45° and 60° to the horizontal. With angles below 45°, operation can be compromised by plugging of flow channels by settled material, whilst at angles greater than 60°, long flow channels must be employed to achieve desired settlement.

When determining the optimum angle and selecting a plate material, the wastewater characteristics such as flow rate, influent suspended solids, type of solids and whether or not the waste stream is corrosive, are of importance – the density, size distribution, abrasiveness and 'stickiness' (whether they will adhere to the plates) of the solids must also be considered (Saleh & Hamoda, 1999). Materials such as polyethylene, polyvinylchloride, cement and wood are commonly used (Probstein & Hicks, 1978).

More recently, de Hoxar (2000) introduced a settler in which moving plates, with a spiral arrangement, are used. These spiral settlers offer improved solid removal efficiency and produce thicker sludge than traditional lamella settlers, and additionally can remove particles that are lighter than water, as well as those that are heavier.

2.6.3 Modelling

The hydrodynamic flow in lamella settlers is very complex (Demir, 1995). Early attempts to characterise the flow (e.g. (Ponder, 1925)) based on kinematic arguments, were unsuccessful; with predicted settling rates consistently higher than experimentally measured values.

Probstein *et al.* (1978) introduced a model based on the existence of three stratified layers: clarified layer, feed suspension layer and sludge layer. The researchers also identified the existence of two modes of operation ('subcritical' and 'supercritical' modes) depending on the ratio of the thickness of the clarified layer to channel height. The supercritical mode was shown to be more stable, and lead to the design of a new type of settler, where influent was introduced approximately one third of the distance

from the bottom of the plate, thus minimizing mixing between influent and settled material.

Recently, an attempt has been made to use dimensional analysis in order to find the optimum parameter values for solids removal with an inclined plate settler (Sarkar *et al.*, 2007) . The researchers obtained relationships which described the experimental results for three different zones of operation (based on the ratio of Reynolds number to Froude number), with good correlation fit coefficients (>0.93). However, there is lack of consistency of units throughout the researchers' calculations, which brings into question the validity of their results. Additionally, the study used a monodisperse suspension of sand and did not consider particle size.

A more recent Computational Fluid Dynamics (CFD) analysis by Salem *et al*. (2011) investigated the impact of feeding inclined plate settlers using a nozzle system. The researchers found this new inlet configuration led to better flow distribution over the inclined plates with an associated improvement in separation efficiency; especially at higher flowrates. Good agreement between the CFD model and experiment results was also achieved. However, the work was based on the separation of crushed walnut suspensions of uniform particle size, and is therefore of limited use in wastewater treatment applications, where particle sizes vary greatly allow with other parameters such as viscosity and density.

The studies have successfully produced models which adequately explain the produced results. The studies have, however, generally dealt with model systems using discrete particle sizes and little or no variation in the 'stickiness' or floc forming ability of the solids. Therefore, these studies have not resulted in a comprehensive collection of design equations, and design of inclined plate settlers remains based on experience from industry.

2.7 Conclusion

The majority of the work carried out on the use of membrane aerated biofilms for municipal wastewater treatment has focussed on the treatment of primary effluent. This work builds on the existing body of research by investigating the treatment of secondary effluent; additionally combining membrane aerated biofilms with inclined plate settlers to create a new wastewater treatment technology.

This work will also explore the decolourisation of azo dye waste; something that has not been reported previously using membrane aerated biofilms, but has been achieved with other various biological processes.

3 Materials and Methods

The laboratory experimental work carried out during this project falls into two categories: mass transfer experiments, where the oxygen transfer from air to water through polymer membranes was characterised and compared for different membrane materials, and membrane aerated bioreactor studies, where biofilms were grown on the surface of polymer membranes and used for pollutant removal from wastewater.

The experimental set-ups and methods used for these laboratory studies are described here in this Chapter. Pilot scale studies were also undertaken at municipal WwTWs; the set-ups and methods for this work are described in Chapter 7.

3.1 Mass Transfer Studies

3.1.1 Membrane Materials

In this study, the oxygen transfer characteristics of two different membrane types are investigated and compared: silicone rubber (polydimethylsiloxane), an example of a dense membrane, and polyethersulphone (PES), an example of a microporous membrane. The repeating structures of these two polymers are shown in Figure 3-1.

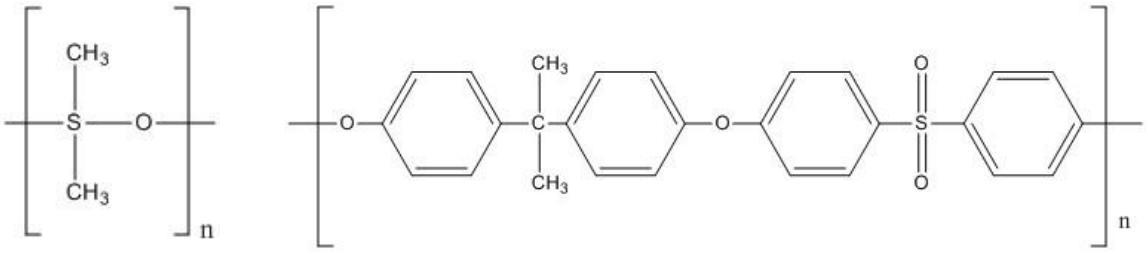

Figure 3-1: Structure of silicone rubber (left) and polyethersulphone polymers

The silicone rubber used was peristaltic pump tubing (Watson-Marlow Pumps, U.K.) with an average tube bore of 1 mm and a wall thickness of 0.35 mm.

The PES membranes used were 0.2 µm (nominal pore size) microfiltration membranes (A/G Technology Corporation, U.S.A.), with an external diameter of 1.5 mm, an average wall thickness of 50 µm and a porosity of 30%.

3.1.2 Membrane Modules

In order to characterise the oxygen transfer properties of the membrane materials, it was necessary to construct a membrane module. The modules were designed and constructed using the same principles associated with that of a shell and tube heat exchanger – the design of which allows high velocity of flow to be obtained, even at low levels of volumetric liquid throughput, and therefore a good mixing regime is maintained (Coulson *et al.*, 1999b). This set-up is similar to that used in studies by Doig *et al.* (1999) investigating diffusion rates of solutes in a liquid-liquid extraction operation with silicone rubber membranes and by Yang and Cussler (1986) in an investigation into the gas-liquid transfer characteristics of polypropylene hollow fibre membranes.

Figure 3-2: Silicone rubber membrane module

A cylindrical polycarbonate tube with an internal diameter of 25 mm was used to form the shell, with the membrane fibres forming the tubes. The desired number (12) of fibres were fed through a polycarbonate end plate, fitted inside the tube and secured and sealed using an epoxy resin potting compound (RS Components, U.K.). The fibres were evenly spaced around a central stainless steel support, which maintained a constant distance between the two polycarbonate end plates during module construction.

The unit was made water and air tight by the use of modified George Fischer plumbing fittings (RS Components, U.K.), allowing the module to be connected to compressed air and water supply as required. This set-up essentially is that of a shell and tube mass exchanger, with one shell pass and one tube pass. The unit was operated in counter-current flow, as this mode of operation gives a higher mean transfer difference compared to co-current flow (Coulson *et al.*, 1999b).

3.1.3 Parameter measurement

3.1.3.1 Dissolved oxygen

Dissolved oxygen (DO) concentration and temperature were measured during each experimental run using a Hach-Lange LDO dissolved oxygen meter (Isis Environmental, U.K.) connected to a Hach-Lange sc100 Controller (Isis Environmental, U.K.).

The probe uses a membrane material whose response to incident laser light changes with changing dissolved oxygen concentration; allowing DO concentration measuring without any oxygen consumption, therefore giving more accurate measurements of DO especially at low DO levels.

The probe is capable of measuring DO concentrations from 0-20 mg l^{-1} to a resolution of ±0.01 mg l^{-1} and temperatures of 0-50ºC to an accuracy of ±0.2ºC.

3.1.3.2 Air flowrate

Air flowrate was measured on a volumetric basis by use of two air flow control meters (Key Instruments, U.S.A.), on the inlet and exhaust sides of the membrane module. The exhaust side flow control meter controlled the flow of air through the membrane module, whilst the inlet side was purely for measurement purposes. Two different ranges of meters were used: capable of measuring 0 - 1.2 lpm or 0 - 5 lpm as required by experimental conditions.

3.1.3.3 Air pressure

Inlet air pressure was controlled by a IMI Norgren (RS Components, U.K.) pressure regular on the inlet side and measured by pressure gauges (RS Components, U.K.), capable of measuring between 0 and 2.5 bar. A similar pressure gauge was used to measure air pressure on the exhaust side. Compressed air was available from a service line at a maximum pressure of approximately 6 barg.

3.1.4 Nitrogen diffusion

Prior to the start of each experimental run, dissolved oxygen was stripped from tap water by sparging with nitrogen gas. Nitrogen gas (BOC, U.K.) was bubbled through the tank using two Pyrex Grade 1 (pore index 90 – 150 μm) glass spargers (SciLabWare, U.K.).

3.1.5 Stirring equipment

To ensure the water in the sampling tank was well mixed, an IKA-Combimag Reo magnetic stirrer (IKA Labortechnik, Germany) was employed in combination with a 25 mm x 5 mm x 5 mm triangular prism magnetic flea (Sigma Aldrich, U.K.). A rotational speed of approximately 500 rpm was used, giving good mixing without any vortexing or significant surface aeration occurring.

3.1.6 Pumping equipment

During each experimental run, the known volume of water was circulated from the measurement tank, through the membrane module and returned to the measurement tank by the action of a peristaltic pump.

The pump used was a Watson-Marlow 302S (Watson-Marlow, U.K.) capable of operating at speeds between 0 and 65 rpm. The pump was used with an 8 mm internal diameter tube, giving flowrates up to 550 ml min^{-1}.

3.1.7 Datalogging

The sc100 controller is supplied with 2 analog (4-20 mA) outputs. Designed for use as a control loop, these outputs were connected to a PC via an ADC-11 Data logger (Pico Technology Limited, U.K.), and used for logging the DO and temperature data.

The 4-20 mA signal output is proportional to the DO concentration and temperature reading detected by the probe, and can be converted back to original values using calibration factors via the software provided with the datalogger.

During the mass transfer experiments, a data logging period of 10 seconds was used. For the saturation concentration experiments, and when bulk dissolved oxygen in the MABfR was monitored, a data logging period of 10 minutes was used – as in these experiments the rate of change of oxygen concentration was much slower.

3.1.8 Experimental Set-up

The equipment described above was set-up up as shown in Figure 3-3 and Figure 3-4.

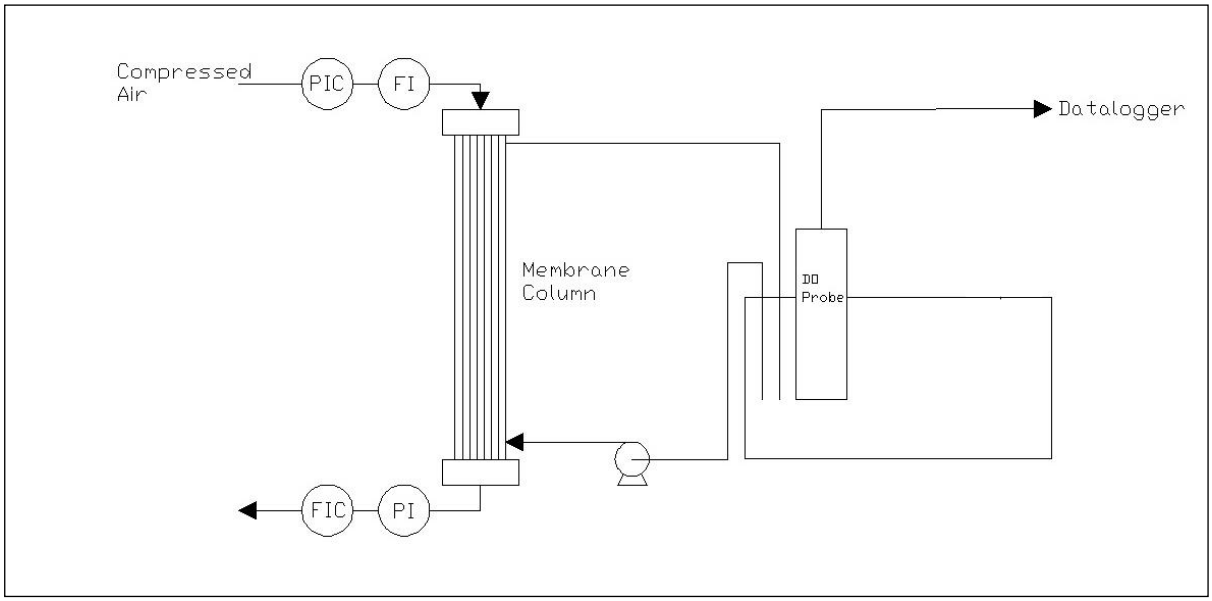

Figure 3-3: Schematic diagram of experimental set-up

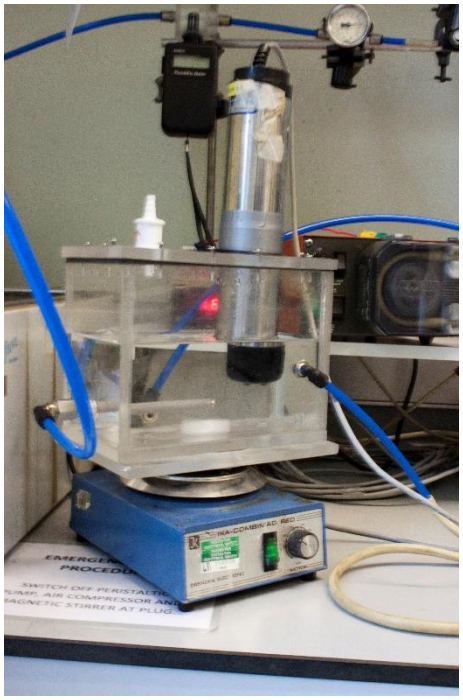

Figure 3-4: Water reservoir tank, magnetic stirrer and Hach-Lange LDO Meter

3.1.9 Experimental procedure

3.1.9.1 Aeration experiments

The oxygen mass transfer was investigated using a modified form of the method described by the ASCE Standard (ASCE, 1992), and analysed using the method detailed by Cussler (1997).

Two litres of tap water was placed in the holding tank, the lid fitted and the DO probe, nitrogen gas spargers and inlet and outlet tubes put in position. The water was then deoxygenated by bubbling nitrogen through the mixture under intense mixing until the dissolved oxygen concentration dropped below 0.20 mg l^{-1}.

Once this DO value was obtained the following procedures were carried out to conduct the experiment:

- Impeller speed was reduced to the minimum value (~100 rpm)

- Compressed air was circulated through the tubes of the membrane module by setting the inlet air pressure and exhaust air flowrate to the desired values
- Water was circulated through the membrane module shell by operating the pump at the desired setting
- Data was recorded by switching on the datalogger

The experiment then continued until a DO concentration of 6 mg l^{-1} was achieved.

3.1.9.2 Saturation Concentration Experiments

In order to use the analysis technique detailed by Cussler (1997) for ascertaining mass transfer coefficients, saturation concentrations at experimental conditions must be known.

To obtain the required saturation values, a modified form of the procedure previously used for determining the temperature-saturation concentration relationship for surface aeration – intended for calculating oxygen concentrations in water courses (Hendrickson *et al.*, 1960) – was used.

The work of Hendrickson *et al*. (1960) found that saturation concentration displays a third order polynomial dependence on liquid temperature, giving a relationship of the form:

$$[DO]^* = a + b_1 T + b_2 T^2 + b_3 T^3 \qquad \textbf{Equation 3-1}$$

Where: $[DO]^*$ = saturation oxygen concentration at temperature T (mg l^{-1})
a = saturation oxygen concentration at 0 °C (mg l^{-1})
b_1 = empirical coefficient (mg l^{-1}°C^{-1})
b_2 = empirical coefficient (mg l^{-1}°C^{-2})
b_3 = empirical coefficient (mg l^{-1}°C^{-3})
T = temperature (°C)

As the enriching action of the membranes is dependent upon oxygen permeation rates in the membrane material and gas side oxygen concentration, the saturation point must be established for each of the membrane materials used in the study at each of the values of inlet pressure used in experimental runs.

Ascertaining the constants for use in Equation 3-1 used a modified form of the set-up described in Section 3.1.9. As much as was practicable of the experimental equipment was placed in a Grant Instruments JB5 water bath (Grant Instruments, U.K.) and the water bath temperature set for the desired value. In order to achieve temperatures below ambient, copper coils through which coolant was circulated were placed in the water bath. The coolant was circulated by Büchi CH 9230 recirculation chiller (Büchi, Switzerland), capable of temperatures in the range -10 °C - +10 °C.

The membrane module was then operated with maximum water side flowrate until no change in oxygen concentration was observed (typically after 24 hours). Due to heat losses thermal equilibrium between the heating/cooling water and aeration water was not achievable, but a stable approach temperature was obtained.

3.2 Membrane Aerated Biofilm Reactor Studies

Two MABfRs were operated in this study – both reactors used the same silicone rubber as used in the aeration experiments as the membrane material. MABfR A was operated with effluent designed to replicate ammoniacal nitrogen and organic carbon concentrations in a non-consent compliant settler effluent in a munipical WwTW and MABfR B used effluent designed to replicate effluent from the textile industry.

3.2.1 Reactor Set-ups

3.2.1.1 MABfR A

The equipment set-up used with MABfR A is shown in Figure 3-5.

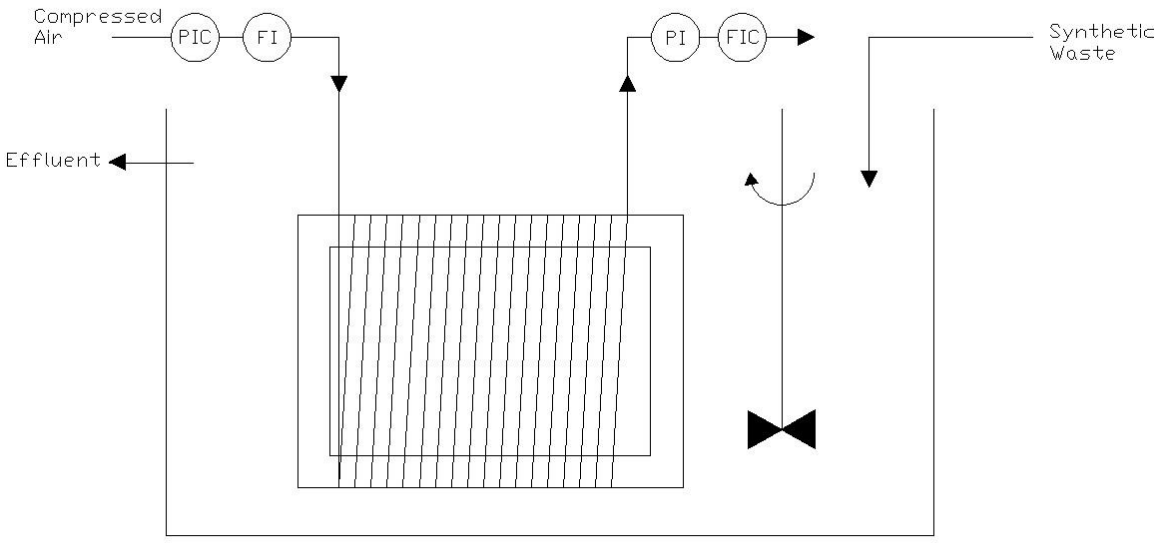

Figure 3-5: Schematic diagram of MABfR A Set-up

The membrane module consisted of 5.0 m of silicone rubber membrane, split into two approximately equal lengths wrapped around a PVC tube frame to give an effective total membrane surface area of 0.024 m^2, estimating that 10% of the available membrane area is lost due to contact with the PVC frame.

The active volume (total volume minus volume of the membrane module) of the reactor tank was 4.35 l, giving a specific surface area of 5.52 m^2m^{-3}.

Synthetic waste was delivered to the reactor by a Watson Marlow 101U/R peristaltic pump (Watson Marlow, U.K.). The pump is capable of speeds between 2 and 32 rpm

and when fitted with a 3.2 mm internal diameter tube can deliver between 3.25 and 52 ml min^{-1}. Effluent was allowed to overflow and collected for analysis.

The reactor was operated at ambient conditions with no temperature control employed. Temperature was recorded during sample collection however, and was found to lie in the range 17.1 – 21.8 °C during reactor operation.

3.2.1.2 MABfR B

The equipment set-up used with MABfR B is shown in Figure 3-6.

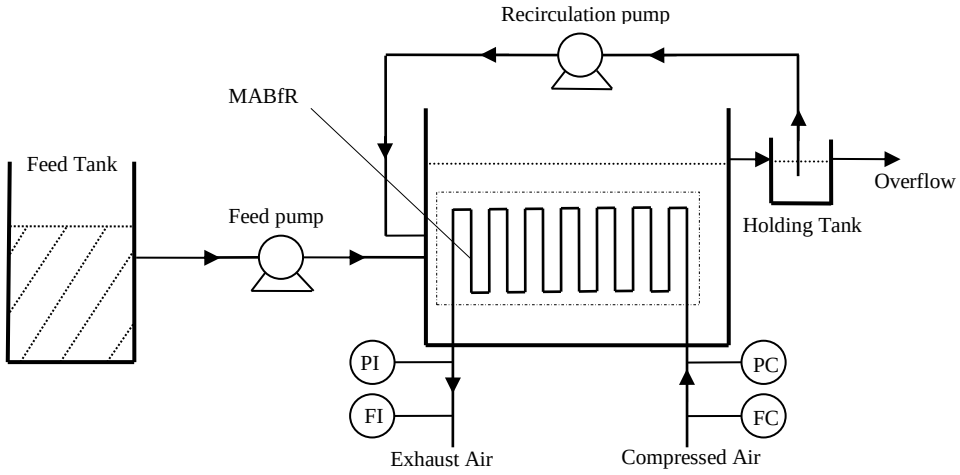

Figure 3-6: Schematic diagram of MABfR B set-up

The membrane module consisted of lengths of silicone rubber wrapped around a PVC frame. One fibre, 1.58 m in length was wrapped in the horizontal plain and a shorter, 0.68 m length was arranged in the vertical plain. Again allowing for a 10% loss of membrane surface area due to contact with the frame, this gave an effective membrane surface area of 0.00374 m^2.

The active volume of the reactor, including the holding tank was 0.91 l, giving a specific membrane surface area of 4.11 m^2m^{-3}. As with MABfR A, no temperature control was employed.

Synthetic waste was delivered by a Watson Marlow 101U/R peristaltic pump (Watson Marlow, U.K.), identical to that used in MABfR A. To prevent shortcutting and force contact between influent and the membranes, the influent was introduced to the bottom of the tank via a feed tube.

A recirulation pump provided mixing by returning liquor from the holding tank to the feed tube of the reactor. Recirculation was carried out by a Watson Marlow 501U peristaltic pump (Watson Marlow, U.K.), at a flowrate of 4.3 l h^{-1}.

Effluent was allowed to overflow from the holding tank and collected for analysis.

3.2.2 Synthetic media

The composition of the synthetic wastewaters used in MABfR A and MABfR B are detailed in Sections 3.2.2.1 and 3.2.2.2 respectively. All components were of analytical grade.

3.2.2.1 MABfR A

The concentrations of the various components used in the synthetic waste used in the MABfR A are given in Table 3-1:

Table 3-1: Synthetic waste composition

Component	Concentration
Soluble Starch	50 mg l^{-1}
NH_4Cl	30 mg l^{-1}
$CaCl_2.2H_2O$	5 mg l^{-1}
$MgSO_4.7H_2O$	4 mg l^{-1}
NaCl	7 mg l^{-1}
K_2HPO_4	28 mg l^{-1}
Na_2CO_3	10 mg l^{-1}
$NaHCO_3$	20 mg l^{-1}
Fe(III)-citrate	1 mg l^{-1}
Trace elements	

The media used in the MABfR was designed to replicate the ammonia and organic carbon concentrations in non-compliant settler effluent (Irwin 21st April 2006, personal correspondence). The recipe is based on that contained in OCED Guidelines (OECD, 1984), though for use in this project peptone and meat extract have been replaced by soluble starch as the sole carbon source (so that soluble COD concentration can be related to starch concentration) and ammonium chloride is used as the source of ammonia as opposed to urea contained in the OCED guidelines.

Trace elements, required in order to ensure proper microbial growth, were supplied based on a recipe included in Alef (1995).

To prepare the media detailed in Table 3-1, 50 mg l^{-1} of soluble starch was added to an appropriate amount of distilled water. This solution was then autoclaved at 121 °C for 20 minutes in order to improve the stability of the media (Alef, 1995).

After sterilisation, 1 ml of each of three stock solutions was added to each litre of the synthetic waste to give the media the composition detailed in Table 3-1. The composition of the stock solutions is detailed in Table 3-2.

Table 3-2: Composition of stock solutions used with MABfR A

Stock Solution 1 – Salts + Trace elements					
NH_4Cl	30 g l^{-1}	$MnCl_2$	0.01 g l^{-1}	Na_2MoO_4	0.01 g l^{-1}
$CaCl_2$	4 g l^{-1}	$ZnCl_2$	0.01 g l^{-1}	$CoCl_2$	0.01 g l^{-1}
$MgSO_4$	2 g l^{-1}	KBr	0.01 g l^{-1}	$Al_2(SO_4)_3$	0.01 g l^{-1}
NaCl	7 g l^{-1}	KI	0.01 g l^{-1}	HBO_3	0.01 g l^{-1}
Fe(III)-citrate	1 g l^{-1}	$CuSO_4$	0.01 g l^{-1}	EDTA	0.01 g l^{-1}

Stock Solution 2 - Carbonate		**Stock Solution 3 - Phosphate**	
$NaHCO_3$	20 g l^{-1}	K_2HPO_4	28 g l^{-1}
Na_2CO_3	10 g l^{-1}		

In the period where the effect of pollutant loading on the performance of the MABfR was investigated, changes were made to the influent synthetic media. These changes are discussed in the relevant section in Chapter 6.

3.2.2.2 MABfR B

The concentrations of the various components of the synthetic media used with MABfR B during Run 1 are given in Table 3-3. The synthetic media was designed to replicate the COD and azo dye concentrations present in effluent from a local carpet factory (Wilkinson 2007).

Table 3-3: Composition of synthetic dye waste used in MABfR B

Component	Concentration
Acid Orange 7	20 mg l^{-1}
Peptone	200 mg l^{-1}
Sucrose	550 mg l^{-1}
NH_4Cl	350 mg l^{-1}
$MgSO_4$	50 mg l^{-1}
$Fe(III)Cl_3$	10 mg l^{-1}
K_2HPO_4	30 mg l^{-1}
$NaHCO_3$	30 mg l^{-1}
Trace elements	

Trace elements, required for healthy microbial growth, were used in the same concentration as with MABfR A and detailed in Table 3-2.

Changes were made to the composition of the synthetic media used with MABfR B for runs 2 and 3. These changes are discussed in the relevant section of Chapter 8.

3.2.3 Seeding of reactors

The biomass used in this study were unknown mixed populations, obtained from three sources:

a. Garden soil, in a way similar to that used by Lees (1951) for the first successful isolation of nitrifying bacteria.
b. Activated sludge from a local municipal wastewater treatment works (Newtownbreda WwTW, NI Water, U.K.). The wastewater treatment works was achieving simultaneous organic carbon removal and nitrification at the time of sludge sampling.
c. An experimental lab scale unit achieving azo dye decolourisation using *Shewanella sp.* (Lipscomb *et al.*, 2008).

Several grams of garden soil/activated sludge/dye degrading biofilm was collected and added to 200 ml of the synthetic media detailed in Table 3-1 in a conical flask. The flask was then placed in a water bath overnight at 37 °C and allowed to settle. The supernatant was then used to seed the reactor.

3.3 Effluent characterisation

Samples of influent and effluent were regularly collected and immediately analysed for pH (which is temperature dependant), and either analysed immediately, or stored in accordance with Standard Methods until analysis was carried out (ASCE, 1992).

If analysis was to take place within 48 hours, the samples were refrigerated at 4 °C until analysis took place; otherwise they were frozen at –17 °C, and defrosted overnight in a refrigerator before analysis was carried out. Freezing of samples was only employed at times when analysis could not be carried out (for example during lab holidays).

The analyses carried out on the influent and effluent from the MABfRs are summarized in Table 3-4.

Table 3-4: Wastewater analyses

	Reactor A		Reactor B	
	Influent	Effluent	Influent	Effluent
pH	X	X	X	X
COD	X	X	X	X
Ammoniacal Nitrogen	X	X	X	X
Nitrite		X		
Nitrate	X	X		
Turbidity		X		X
Colour			X	X

3.3.1 pH

pH was measured with a Hanna Instruments 8424 pH meter (Hanna Instruments, U.K.) at ambient temperature. The meter has a measurement range of -2.00 to 16.00, a resolution of 0.01 pH units and an accuracy of ±0.01 pH units.

Accuracy of the meter was checked periodically by comparison with a pH 7.00 buffer solution, and calibrations with pH 4.00, 7.00, 9.04 buffer solutions were carried out if required.

3.3.2 Ammoniacal Nitrogen

Ammoniacal Nitrogen concentration was ascertained through use of Hach-Lange sensION^{TM}2 fitted with Ammonia Ion Selective Electrode (Isis Environmental, U.K.), capable of measuring NH_4^+-N concentrations between 0.05 and 14,000 mg l^{-1} over a temperature range of 0 – 50 °C.

25 ml of sample was adjusted to high pH through the addition of one Hach-Lange Ammonia Ionic Strength Adjustor (ISA) powder pillow (Isis Environmental, U.K.). The ISA converts all ammoniacal nitrogen to free ammonia gas. The gas diffuses through the electrode membrane and causes a pH change in the electrode solution. The magnitude of the pH is proportional to the ammonia concentration in the solution being measured (Hach Company, 2001). The probe was calibrated before each use with 10 mg l^{-1} and 100 mg l^{-1} NH_4^+-N standards.

3.3.3 Chemical Oxygen Demand

The Chemical Oxygen Demand (COD) was determined by a Hach-Lange DR2800 Spectrophotometer (Isis Environmental, U.K.) using the Reactor Digestion Method. Low range (3-150 mg l^{-1}) digestion vials were used with feed and effluent samples from Reactor A and high range (20-1500 mg l^{-1}) digestion vials used with feed and effluent samples from Reactor B. Any turbidity (which would give a false high reading) was

removed by centrifugation at approximately 13,000 rpm for 6 minutes in a 1.5 ml Eppendorf tubes (Premier Scientific Ltd., U.K.) with a MSE Micro Centaur centrifuge (Anachem Scotlab, U.K.)

The method involves the oxidation of the sample at 150 °C for 2 hours by potassium dichromate. As the oxidation progresses the orange dichromate ion ($Cr_2O_7^{2-}$) is itself reduced to the green chromic ion (Cr^{3+}) (Figure 3-7). Colorimetric determination of the amount of $Cr_2O_7^{2-}$ remaining or Cr^{3+} produced allows the COD of the sample to be ascertained (Hach Company, 2007).

For MABfR A, where soluble starch is the only source of organic carbon, the value of the COD can be directly related to starch concentration (dichromate does not oxidise ammonia to nitrate).

Figure 3-7: Spent (left) and unused COD vials

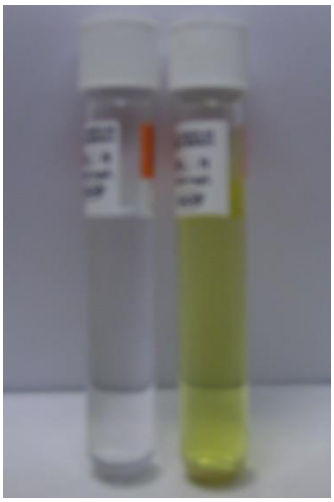

Figure 3-8: Fresh (left) and used nitrate vials

3.3.4 Nitrate

Nitrate concentration was established, again through use of a Hach-Lange DR 2800 Spectrophotometer (Isis Environmental, U.K.), using the chromotropic Acid Method with Test 'N Tube™ NitraVer® X Reagent Set. The method can accurately determine nitrate concentrations between 0.2 and 30.0 mg l^{-1}.

The method involves reaction of nitrate with chromotrophic acid under acid conditions to yield a yellow product (Figure 3-8). The amount of product is ascertained by absorbance at 410 nm and is directly related to nitrate concentration (Hach Company, 2007).

3.3.5 Nitrite

Nitrite concentration was determined by a Hach Lange DR 2800 Spectrophotometer (Isis Environmental, U.K.) using the Diazotization Method with Test 'N Tube™ NitriVer® Nitrite Reagent Vials. The method is capable of measuring NO_2^--N concentrations between 0.003 to 0.500 mg l^{-1}.

Nitrite concentration is determined by colorimetry at 507 nm following reaction of the sample with excess sulfanilic acid to form an intermediate diazonium salt which then couples with chromotropic acid to produce a pink coloured complex. The pink colour is directly proportional to the amount of nitrite present (Hach Company, 2007).

3.3.6 Turbidity

Turbidity, as a guide to the amount of suspended biomass present in an effluent sample, was obtained by a Hach-Lange 2100P Turbidimeter (Camlab, U.K.). The meter has a measurement range of 0 – 1000 Nephelometric Turbidity Units (NTU) and a resolution of 0.01 NTU and an accuracy of ±2 % of reading value.

3.3.7 Colour

Colour absorbance was determined using a Perkin-Elmer Lamba 9 UV-Visble spectrophotometer (Perkin-Elmer, U.K.). Samples, which were centrifuged at 13,000 rpm for 6 minutes to remove any turbidity, were placed in polycarbonate cuvettes (Premier Scientific, U.K.) and scanned from 700 nm to 300 nm, with the absorbance of the samples normalized against the absorbance of a blank; a cuvette containing distilled water (Figure 3-9).

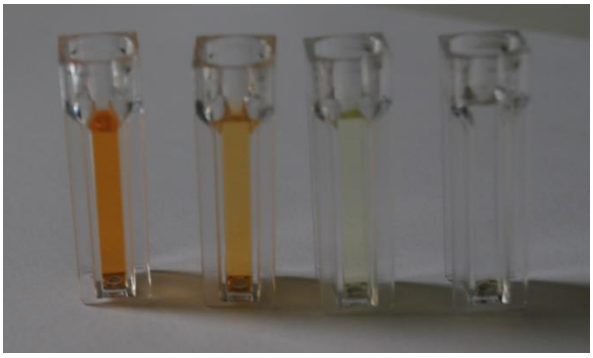

Figure 3-9: Spectrophotometer cuvettes

The concentration of coloured compounds contained in the samples can then be found by identification and quantification of the compounds λ_{max}, the wavelength at which maximum absorbance is observed. Concentration can then be related to the maximum absorbance via reference with a calibration curve, in accordance with Standard Methods (Clesceri *et al.*, 1998).

3.3.8 Biochemical Oxygen Demand (BOD_5)

Biochemical Oxygen Demand was carried out on selected samples from the pilot trails using the same method employed by Northern Ireland Water (Irwin 21st April 2006), a modified form of that contained in Standard Methods (Clesceri *et al.*, 1998).

In the method, a sample of wastewater is diluted with oxygen saturated water which has been seeded with microorganisms and contains nutrients. The dissolved oxygen concentration is measured and the sample is placed in a thermostatically controlled incubator at 20 °C for 5 days, after which the DO concentration is measured again. The BOD is determined from the change in sample DO in comparison to a blank sample prepared in the same way.

Allyl thiourea is added to the samples in order to suppress nitrification during the inhibition period. The result is therefore the BOD due to the presence of carbonaceous rather than ammoniacal compounds.

3.4 Effluent disposal

All microbial biomass has the potential to be, or to become, pathogenic. As such, all effluent was collected and treated with a disinfection solution (Virkon) before being flushed to drain with excess water.

4 Mass Transfer Studies

In order to maximize the treatment potential of the MABfR, it was first necessary to study the transfer of oxygen through polymer membranes. The data obtained through these studies allowed choices to be made regarding the membrane type, membrane arrangement and the various parameters (air flowrate, air inlet pressure, water flowrate) in order to maximize the oxygen flux and therefore the aerobic treatment potential of the MABfR.

4.1 Saturation concentration

In order to use the equations contained in Cussler (1997) for obtaining mass transfer coefficients from experimental data, knowledge of the saturation concentration at the experimental conditions is required.

Although temperature-concentration relationships for oxygen-water systems are contained in literature (e.g. Hendrickson *et al.*, 1960), they cannot be applied in this situation. The saturation concentration in this case is not only a function of temperature, but also of the oxygen concentration with which it is in equilibrium, which in turn changes with both air-side gas pressure and membrane type.

The temperature-saturation concentration relationships for each value of inlet pressure used in the investigation for both silicone rubber and polyethersulphone were therefore found experimentally; thereby allowing Equation 3-1 to be used to find the oxygen concentration at saturation.

$$[DO]^* = a + b_1 T + b_2 T^2 + b_3 T^3 \qquad \textbf{Equation 3-1}$$

The saturation constants (for use in Equation 3-2) found in this study (using tap water) for surface aeration were compared with those of Hendrickson *et al*. (1960), from a study using distilled water (Table 4-1). The values obtained in this study were slightly lower than those in the literature. This can be explained by the fact that gas solubility decreases with increased dissolved salts concentration. This has been long accepted as a cause of variation in oxygen levels in marine situations (Gerlach, 1994).

Table 4-1: Comparison of saturation constants

	Hendrickson et al. (1960)	This study
a	14.652	13.374
b_1	-0.4102	-0.2264
b_2	0.007910	0.002739
b_3	-0.00007777	-0.00002525
R^2	0.999	0.997

4.1.1 Effect of membrane type

The temperature-saturation concentration coefficients for use in Equation 3-1 for both silicone rubber and polyethersulphone using an inlet pressure of 0.5 barg are shown in Table 4-2.

Table 4-2: Saturation coefficients for 0.5 barg inlet pressure

	Silicone Rubber	Polyethersulphone
a	16.61	15.03
b_1	-0.37	-0.33
b_2	2.80×10^{-3}	1.53×10^{-3}
b_3	17.3×10^{-6}	24.0×10^{-6}
R^2	0.999	0.999

Values of the coefficients for all of the inlet pressures used in this study were all ascertained and are contained in Appendix 1.

The data from Table 4-1 and Table 4-2 have been used to plot Figure 4-1 to illustrate the effect of temperature on the saturation oxygen concentration for the experimental setup used in this study.

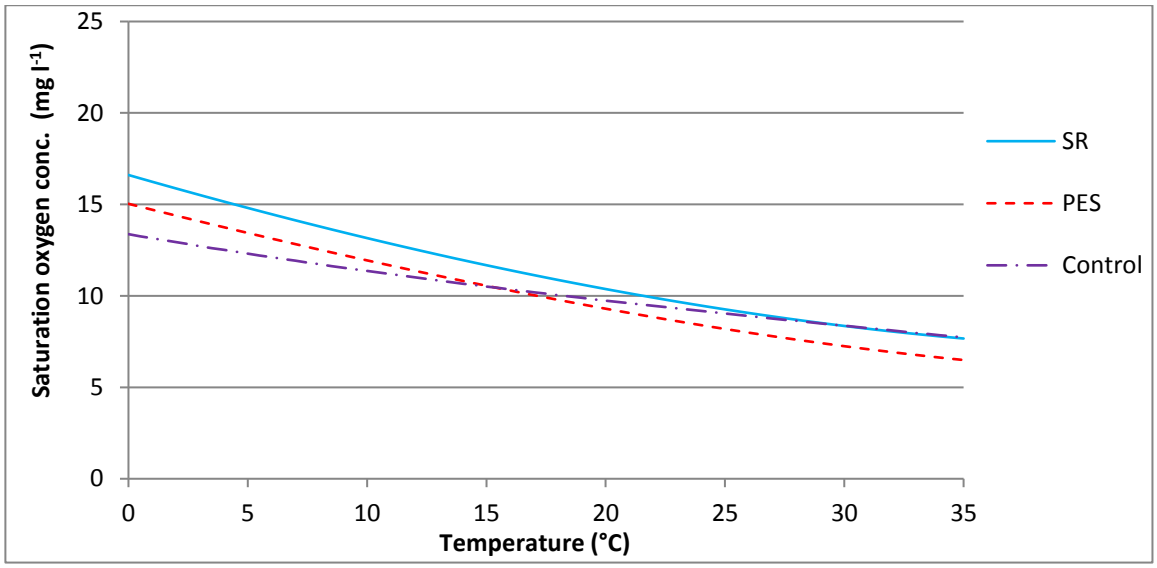

Figure 4-1: Temperature-saturation correlations (0.5 bar)

Figure 4-1 shows that the oxygen saturation concentration is greater when silicone rubber is used compared to polyethersulphone at all temperatures. This is the result of a higher interfacial concentration of oxygen due to higher oxygen permeability in silicone rubber compared to polyethersulphone (Robb, 1968). This enrichment effect has been previously noted as the cause of elevated saturation concentrations in work by Casey *et al*. (1999).

The plots for silicone rubber and polyethersulphone are similar in shape, but different to the control trace. The only factor affecting the saturation concentration in the control situation is the solubility of oxygen in water at the experimental conditions. This is not the case with diffusion through a membrane where temperature also effects the free volume of the polymer material and hence the solubility and diffusion constants of the system (Zhang & Cloud, 2006).

4.1.2 Effect of inlet pressure

The effect of inlet pressure on the saturation concentration at 20 °C is shown in Figure 4-2, using values calculated from the relationships obtained for each set of membrane material and pressures.

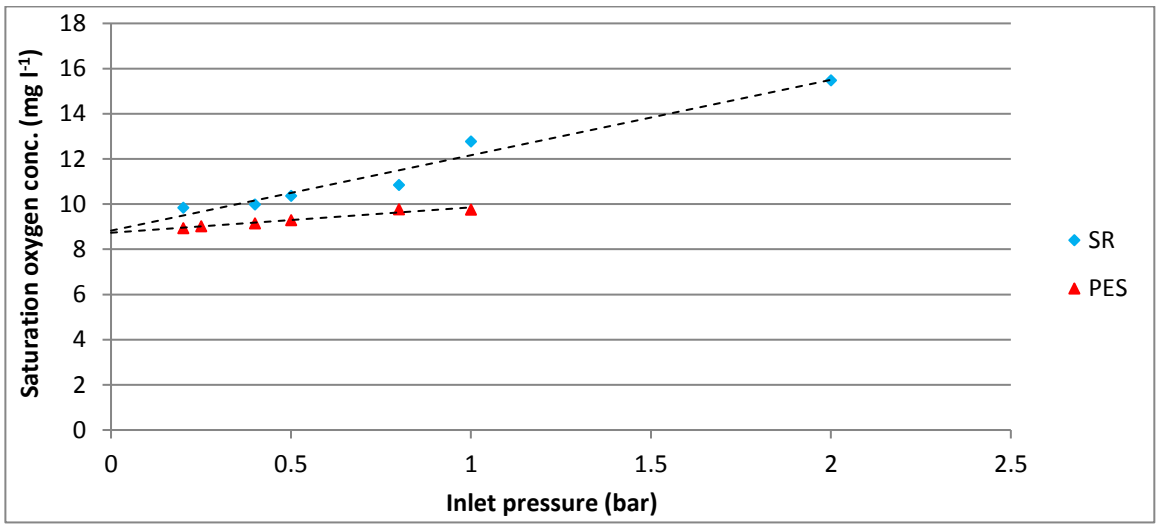

Figure 4-2: Effect of inlet pressure on saturation oxygen concentration (20 °C)

Linear regression of the information displayed in Figure 4-2 reveals proportionality between inlet pressure and saturation oxygen concentration with both the silicone rubber and polyethersulphone membrane modules. This result is expected as a linear increase in pressure is accompanied by a linear increase in oxygen partial pressure.

Both of the relationships have correlation coefficients in excess of 0.95 and an intercept of approximately 8.8 mg l^{-1}, which is close to the saturation concentration of 9.7 mg l^{-1} predicted by the coefficients in Table 4-1. The error between the theoretical saturation concentrations at zero inlet pressures and that obtained through surface aeration only is partially explained by the pressure losses experienced as air flows through the module. Use of an average pressure gives an intercept of approximately 9.1 mg l^{-1}, with the remainder of the error being attributed to error of experimentation.

4.2 Oxygen Transfer

4.2.1 General observations

4.2.1.1 Change of Dissolved Oxygen

The dissolved oxygen/time relationship for a typical aeration experiment is shown in Figure 4-3. Similar plots were obtained in all aeration experiments.

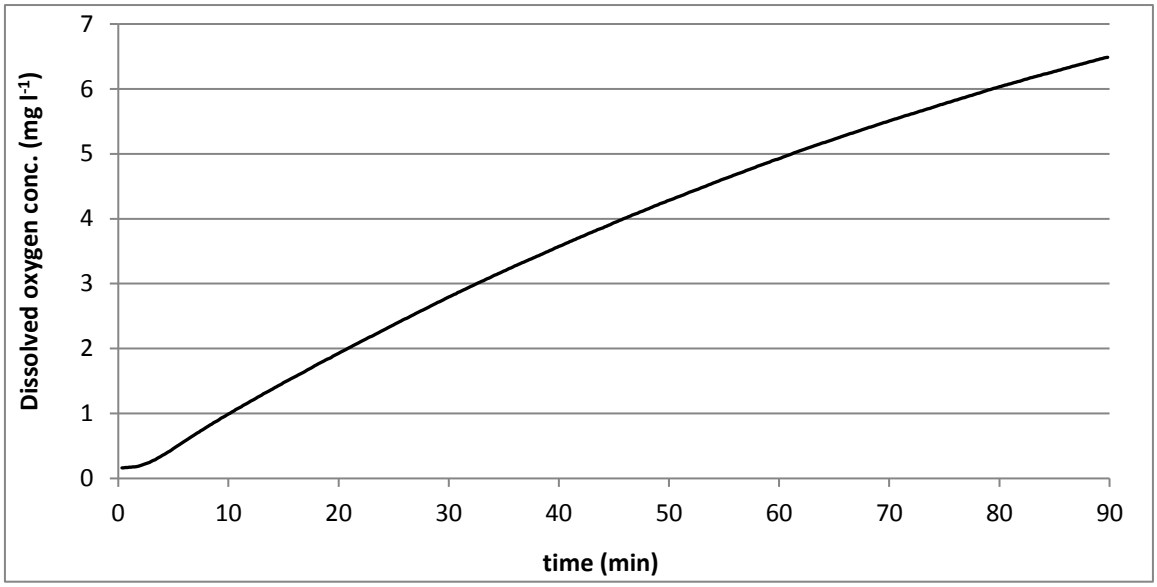

Figure 4-3: Change in dissolved oxygen over duration of mass transfer experiments (Silicone Rubber, 0.5 bar inlet pressure, 2 lpm gas side flowrate, 550 ml min^{-1} water side flowrate).

Initially, the increase in dissolved oxygen concentration was slow as mass transfer was limited by the oxygen concentration in the membrane material. Once membrane saturation was achieved, aeration was controlled by diffusion away from the membrane surface and slowed down as the water side concentration approached saturation.

4.1.1.1 Bubble formation

During the aeration experiments, a layer of bubbles formed on the membrane surface, as also observed by Côté *et al*. (1988) and Casey *et al.* (1999), and as shown in Figure 4-4. These bubbles gradually grew in size as the experiment progressed, until they reached a

critical size where the bubble was sufficiently buoyant to overcome surface tension forces and escaped into the bulk flow.

Figure 4-4: Bubble formation on membrane surface (Silicone Rubber, 0.5 bar inlet pressure, 2 lpm gas side flowrate, 550 ml min^{-1} water side flowrate)

Two possible explanations for the composition of these bubbles exist:

1. As part of the experimental procedure, oxygen was first stripped by passing a stream of nitrogen bubbles through the water layer. This formed a saturated solution of nitrogen and therefore any nitrogen passing through the membrane would be unable to enter the bulk phase and would instead form bubbles on the membrane surface.

2. The bubbles are composed of oxygen and form on the membrane water interface where oxygen concentrations exceed the saturation value – interface oxygen concentrations of up to 100 mg l^{-1} have been achieved using silicone rubber membranes (Casey *et al.*, 1999).

It is likely that a combination of these two explanations is valid, and the bubbles are composed of a mixture of oxygen and nitrogen gases.

Côté *et al*. (1989) attributed these nitrogen bubbles to an observed decrease in oxygen mass transfer coefficient when air is used as the aeration gas. The researchers suggested

that these bubbles were responsible for stripping of oxygen at the membrane surface, preventing diffused oxygen from entering the bulk fluid.

4.2.2 Calculation of average oxygen flux

Average oxygen flux was obtained from the experimental data using Equation 4-1:

$$\bar{J} = \frac{(DO_{DO=5} - DO_{DO=1})}{a(t_{DO=5} - t_{DO=1})} \qquad \textbf{Equation 4-1}$$

Where: $\bar{J}$ = average oxygen flux ($gO_2m^{-2}h^{-1}$)

$t_{DO=5}$ = time at which dissolved oxygen = 5 mg l^{-1} (h)

$t_{DO=1}$ = time at which dissolved oxygen = 1 mg l^{-1} (h)

a = specific surface area (m^2m^{-3})

The average flux reported in this study was calculated between dissolved oxygen concentrations of 1 mg l^{-1} and 5 mg l^{-1}, chosen to exclude any instability during the early stages of experimental runs and the effect of initial oxygen concentration, which varied from experiment to experiment for practical reasons.

4.2.3 Calculation of mass transfer coefficient

The overall mass transfer coefficient, K, was calculated from experimental data using a linearized form of Equation 2.5:

$$\ln\left(\frac{C^* - C_t}{C^*}\right) = -Kat \qquad \textbf{Equation 4-2}$$

Where: C^* = saturation oxygen concentration at experimental conditions (mg l^{-1})

C_t = oxygen concentration at time t (mg l^{-1})

a = specific surface area (m^2m^{-3})

t = time (s)

K = overall oxygen mass transfer coefficient (ms^{-1})

A plot of $\ln\left(\frac{C^*-C_t}{C^*}\right)$ versus t yields a straight line through the origin with a gradient of $-Ka$, as shown in Figure 4-5. This plot is typical of those obtained for all experiments carried out in the investigation. Again the interval between DO = 1 mg l^{-1} and DO = 5 mg l^{-1} was used for comparison purposes.

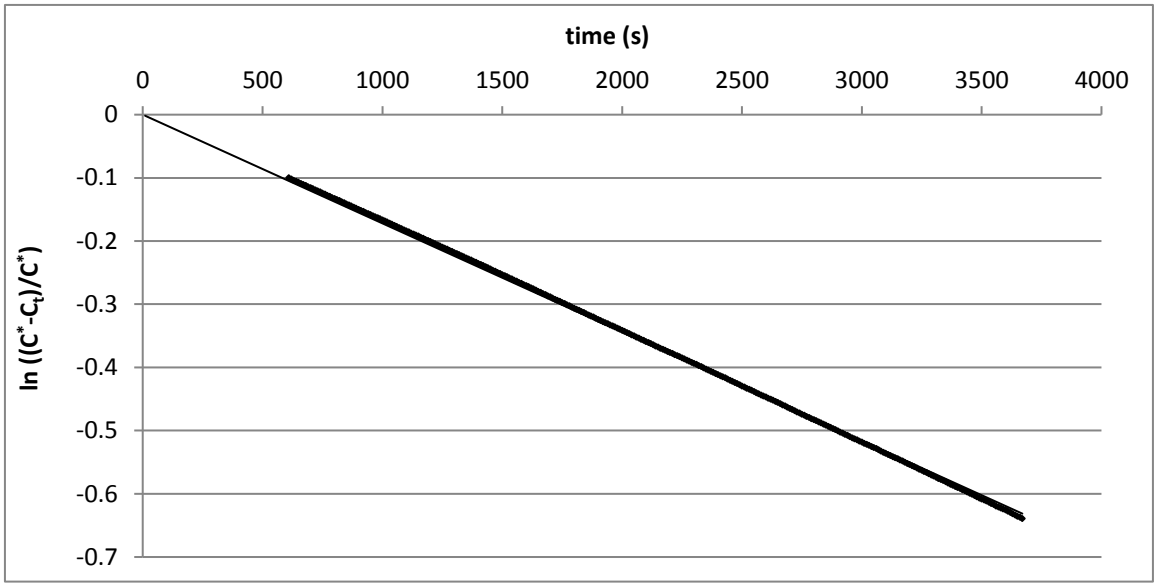

Figure 4-5: Plot of $ln\left(\frac{C^*-C_t}{C^*}\right)$ versus t (Silicone Rubber, 0.5 bar inlet pressure, 2 lpm gas side flowrate, 550 ml min^{-1} water side flowrate)

4.3 Effect of air side flowrate

The effect of the air side flowrate on the oxygen transfer through the two membrane materials was investigated at inlet flowrate values between 0.6 and 5 litres of air, an inlet pressure of 0.5 bar and a water side flowrate of 550 ml min^{-1}. Although not directly measured, mass velocity, G, is the true independent variable being investigated in this experimental work, as calculated by Equation 4-3 (Darby, 1996). Mass velocity is related to pressure drop as shown in Equation 4-4, also given by Darby. Different air flowrates were chosen for the two membrane modules in order to give a constant pressure drop for comparison purposes.

$$G = \frac{\dot{m}}{A} = \frac{\dot{V}\rho}{NA}$$ Equation 4-3

$$P_1^2 - P_2^2 \propto G^2$$ Equation 4-4

Where: $\dot{V}$ = Volumetric air flowrate (m^3s^{-1})

$\dot{m}$ = Mass flowrate of air (kgs^{-1})

ρ = Air density (kgm^{-3})

A = Cross section of tube (m^2)

N = Number of tubes

P_1 = Inlet pressure (kgm^{-2})

P_2 = Exhaust pressure (kgm^{-2})

a) Average Oxygen flux

The average fluxes obtained over the range of air side flowrates used in the investigation are shown in Figure 4-6.

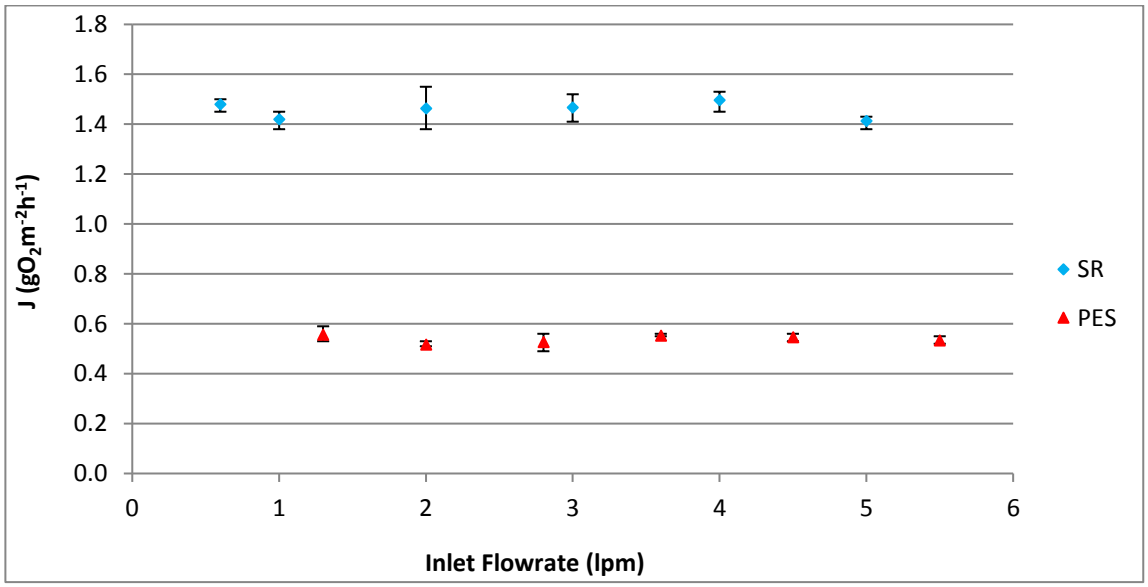

Figure 4-6: Effect of air side flowrate on average oxygen flux (0.5 bar inlet pressure, 550 ml min^{-1} water flowrate – minimum and maximum value error bar)

Figure 4-6 shows that air side flowrate had no significant effect on the oxygen flux through either the silicone rubber or polyestersulfone membranes used in this study. Gas flowrate is known to have a proportional effect on pressure drop (Darby, 1996), and therefore, it may have been expected that increasing the flowrate would have a negative effect on mass transfer, as, at higher flowrates, higher pressure losses would be experienced, leading to a drop in the driving force. However, in practice, the pressure drop along the length was negligible along the short length (0.19 m) of the polymer tubes, and the total pressure drop (difference between inlet and outlet) was constant at a level of approximately 0.05 bar throughout all experiments.

Additionally, Figure 4-6 does not reveal any evidence of inhibition of oxygen transfer due to condensation of back diffused water vapour on the inner surface of the membrane fibres. Fang et al. (2004), state that condensation is inevitable in hollow fibre membranes; the mass transfer coefficient will be greater for water vapour than for gases such as oxygen or nitrogen due to relative molecule sizes. They suggest however, that the effects of condensation can be minimised by operating with sufficient gas flow to enable condensate to be discharged from the module. The absence of condensation in this study indicates that the range of flowrates used was sufficient to act as aeration and sweep gas, preventing significant oxygen mass transfer inhibition.

b) Mass Transfer Coefficient

Figure 4-7 shows the effect of gas side inlet flowrate on overall mass transfer coefficient.

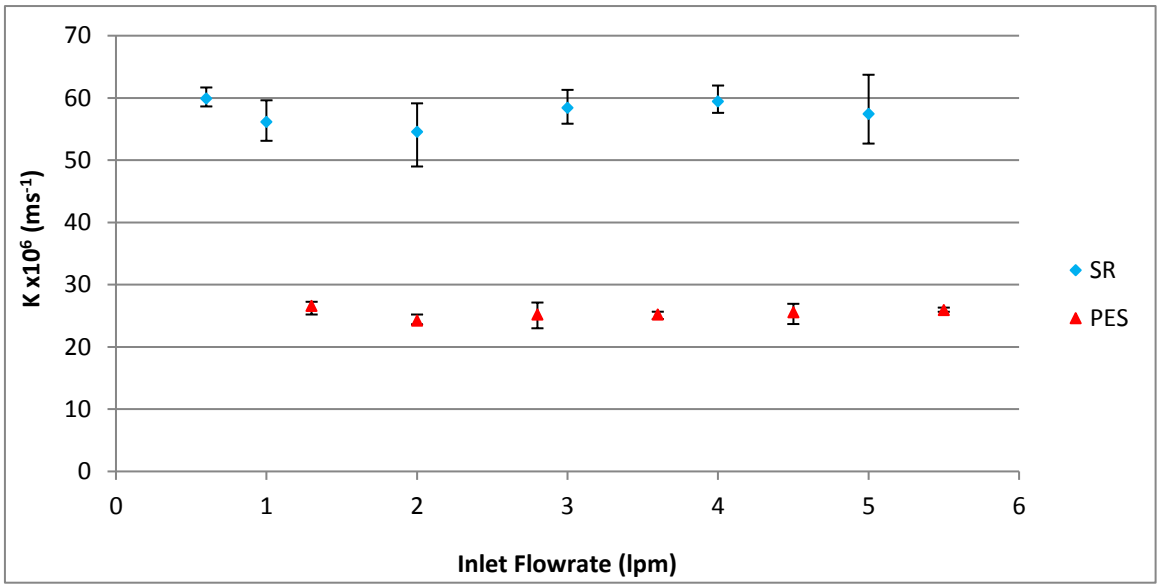

Figure 4-7: Effect of air flowrate on overall mass transfer coefficient (0.5 bar inlet air pressure, 550 ml min^{-1} water flowrate – minimum and maximum value error bars)

Variation in the air inlet flowrate caused no discernable trend over the ranges tested on the overall mass transfer coefficient of oxygen transfer to water through either silicone rubber or polyethersulphone hollow fibre membranes. The value of the mass transfer coefficient was constant at approximately $25x10^{-6}$ ms^{-1} for the polyethersulphone membrane module and $58x10^{-6}$ ms^{-1} for the silicone rubber membrane module. The lack of a significant effect on the overall mass transfer coefficient justified the omission of a term describing the mass transfer resistance of the gas side boundary layer in Equation 2-1.

4.4 Effect of inlet air pressure

The effect of inlet air pressure on the oxygen transfer through the two membrane materials was investigated using the pressure and air flowrate pairs shown in Table 4-3.

Volumetric air flowrate was varied in addition to inlet pressure to ensure the mass velocity was constant in all experiments.

Table 4-3: Pressure flowrate pairs used in inlet air pressure investigation

Inlet pressure (bar)	Inlet air flowrate (lpm)
0.20	5.0
0.25	4.0
0.40	2.5
0.50	2.0
0.80	1.25
1.0	1.0
2.0	0.5 (silicone rubber only)

a) Average Oxygen flux

The average oxygen obtained fluxes are shown in Figure 4-8.

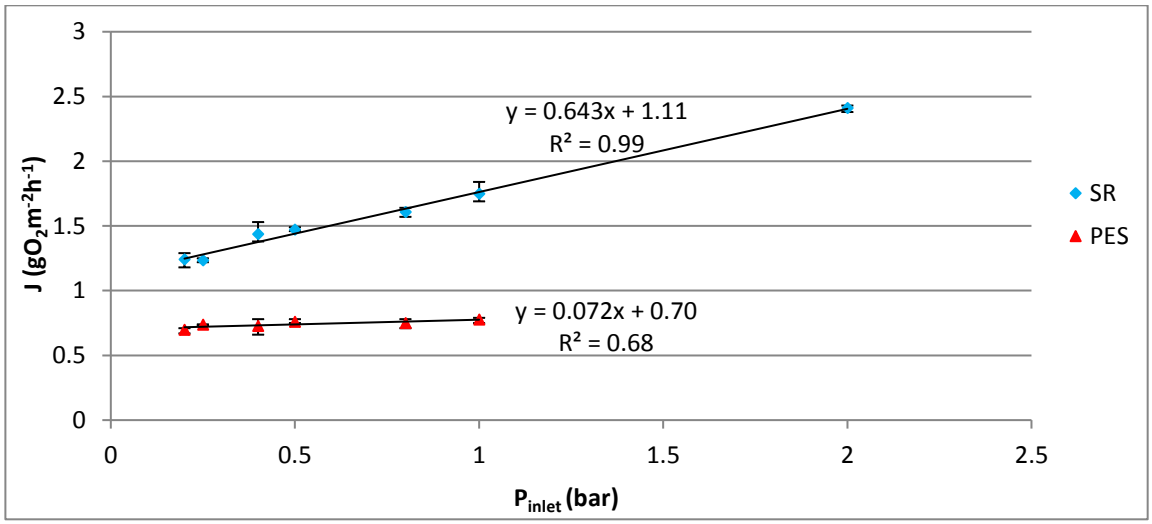

Figure 4-8: Effect of inlet pressure on average oxygen flux (2 lpm air flowrate, 550 ml min^{-1} water flowrate, minimum and maximum value error bars)

Figure 4-8 shows a directly proportional relationship between inlet pressure and obtained oxygen flux. This trend is expected as higher inlet pressure leads to a greater gas side oxygen concentration and hence a larger driving force. Higher oxygen fluxes are obtained with larger driving forces as shown by Equation 2-6.

The trace for polyethersulphone does not display as strong a relationship; the pressure coefficient is much lower and the correlation coefficient is very poor. This indicates that oxygen mass transfer is not limited by gas side oxygen concentration and instead is limited by the oxygen concentration in the membrane itself.

A possible explanation for this is that the membrane material is hydrophilic; the membrane pores are filled with water and limited by the diffusion rate of oxygen in the water filled pores. As the diffusivity of oxygen is much slower in water than it is in air, this results in slower mass transfer rates (Li *et al.*, 2010). This explanation is discussed further in Section 0c.

b) Mass Transfer Coefficient

The effect of inlet air pressure on calculated overall mass transfer coefficients is shown in Figure 4-9.

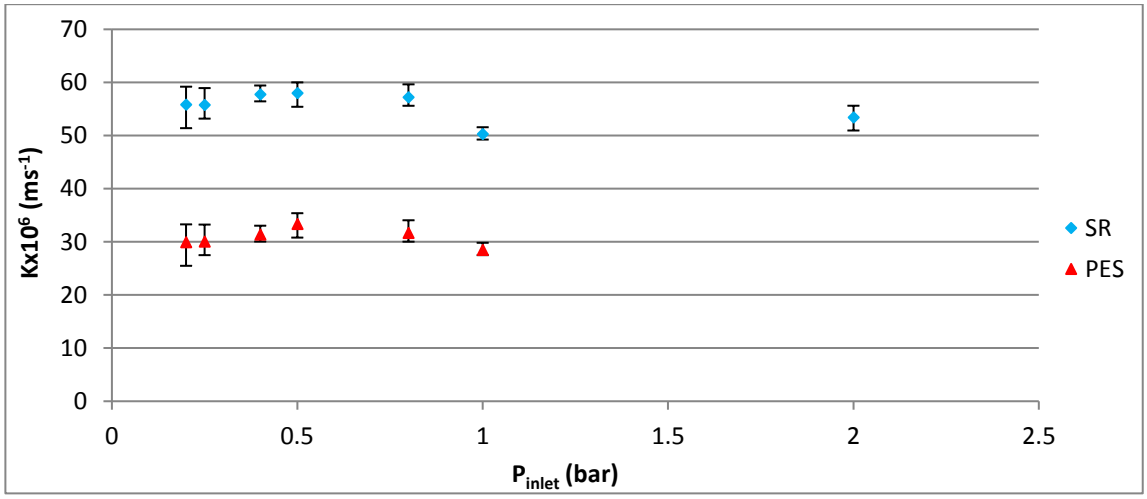

Figure 4-9: Effect of inlet air pressure on mass transfer coefficient (2 lpm air flowrate, 550 ml/min water flowrate, minimum and maximum value error bars)

No statistically significant effect of inlet air pressure on the mass transfer coefficient was observed. A similar result was obtained by Côté *et al.* (1989), although a decrease in mass transfer coefficient, attributed to increased significance of bubble formation, was observed at oxygen partial pressures above the range included in this study.

4.5 Effect of water side flowrate

The effect of water side flowrate on the oxygen mass transfer characteristics of the two membrane materials was investigated over the flowrate range 150-550 ml min^{-1}.

a) Average Oxygen Flux

The average oxygen fluxes obtained over the water flowrate range are shown inFigure 4-10.

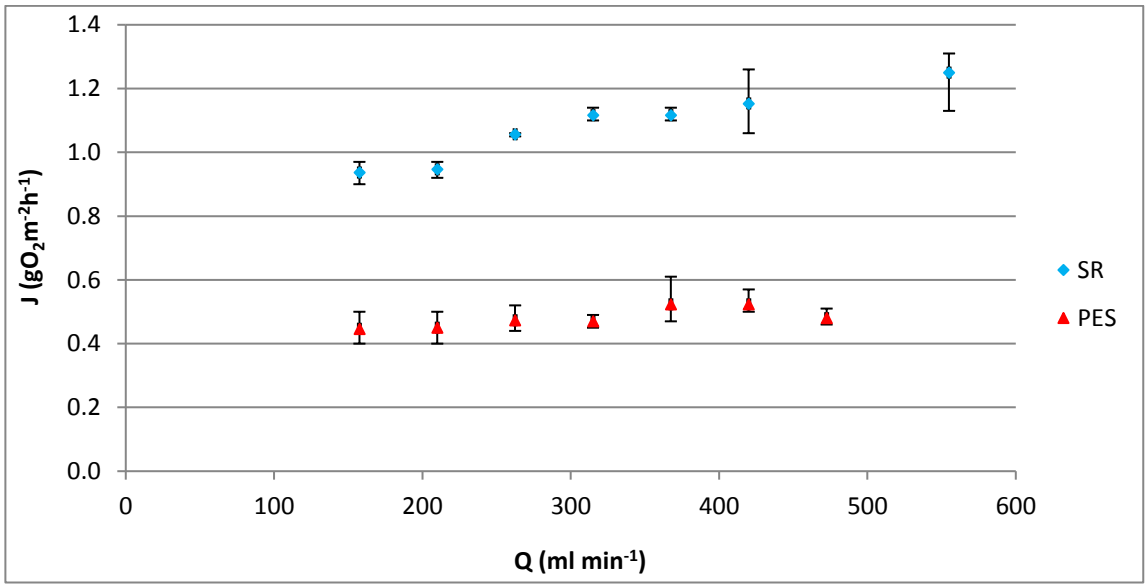

Figure 4-10: Effect of water flowrate on average oxygen flux (0.5 bar air pressure, 2 lpm air flowrate, minimum and maximum value error bars)

Higher oxygen fluxes were obtained at higher water flowrates. This result is to be expected as it is in accordance with the well-established theory that the size of the boundary layer, and hence the resistance to mass transfer, decreases with increasing water velocity.

b) Overall mass transfer coefficient

The effect of inlet air pressure on calculated overall mass transfer coefficients is shown in Figure 4-11.

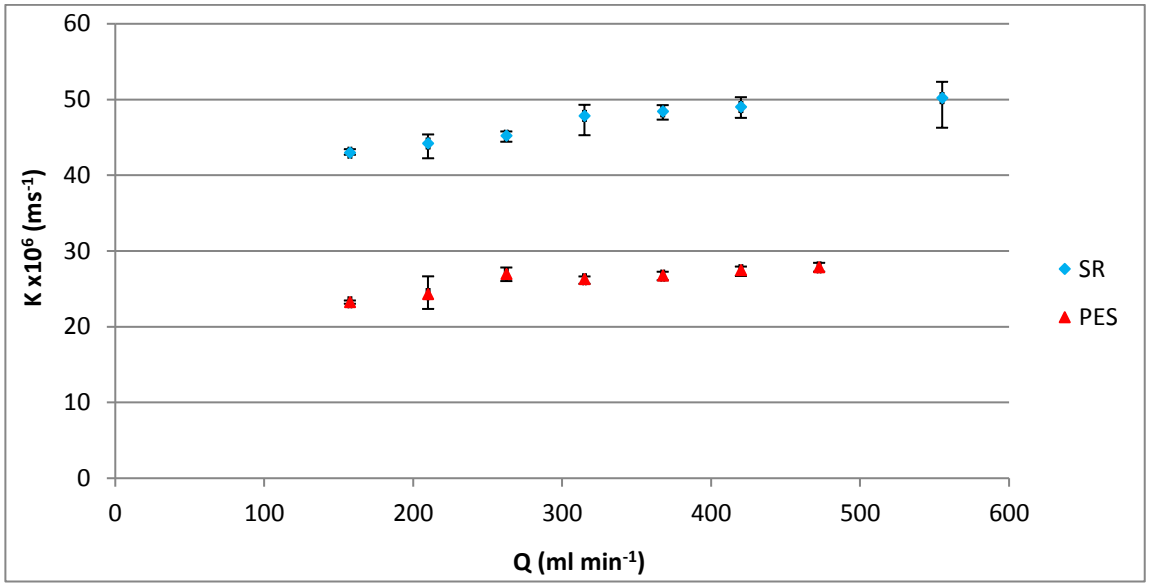

Figure 4-11: Effect of water flowrate on overall mass transfer coefficient (0.5 bar inlet air pressure, 2 lpm air flowrate, minimum and maximum value error bars)

Both membrane modules showed an increase in overall mass transfer coefficient with increased water side flowrate. Again this is related to the decrease in the size of the boundary layer on the shell side of the shell-and-tube mass exchanger.

c) Obtaining individual membrane mass transfer coefficients

The membrane mass transfer resistance can be calculated using Equation 4-5 for dense silicone rubber, adapted from Côté *et al*. (1989), and Equation 4-6 for hydrophilic microporous polyethersulphone (Vladisavljevic, 1999).

$$\frac{1}{K_M} = \frac{d_e \ln\left(\frac{d_e}{d_i}\right)}{2D_M} \qquad \textbf{Equation 4-5}$$

$$\frac{1}{K_M} = \frac{(d_e - d_i)\tau}{2D_w\varepsilon} \qquad \textbf{Equation 4-6}$$

Where: K_M = membrane mass transfer coefficient (ms^{-1})

D_M = diffusivity of oxygen in membrane material (m^2s^{-1})

D_w = diffusivity of oxygen in water (m^2s^{-1})

d_e = external diameter of membrane fibre (m)

d_i = internal diameter of membrane fibre (m)

ε = membrane porosity

τ = membrane tortuosity

For calculating membrane resistance of hydrophobic membranes, the term D_w is replaced with D_a, the diffusivity of oxygen in air.

Alternatively, having calculated overall oxygen mass transfer coefficients from the experimental data, a Wilson plot can be constructed in order to obtain the membrane mass transfer resistance. The Wilson plot, originally developed to obtain experimentally heat transfer coefficients in heat exchangers (Fernandez-Seara *et al.*, 2005), involves plotting the inverse of the water side flowrate versus the inverse of the overall mass transfer coefficient. This has been previously used in work by Vladisavljevic (1999) to determine individual resistances in hollow fibre membrane contactor systems.

The y-intercept of the plot represents a theoretical point of infinite water flowrate where the liquid film resistance, $1/K_L$, equals zero. The value of y-intercept is therefore equal to the value of the membrane resistance, $1/K_M$.

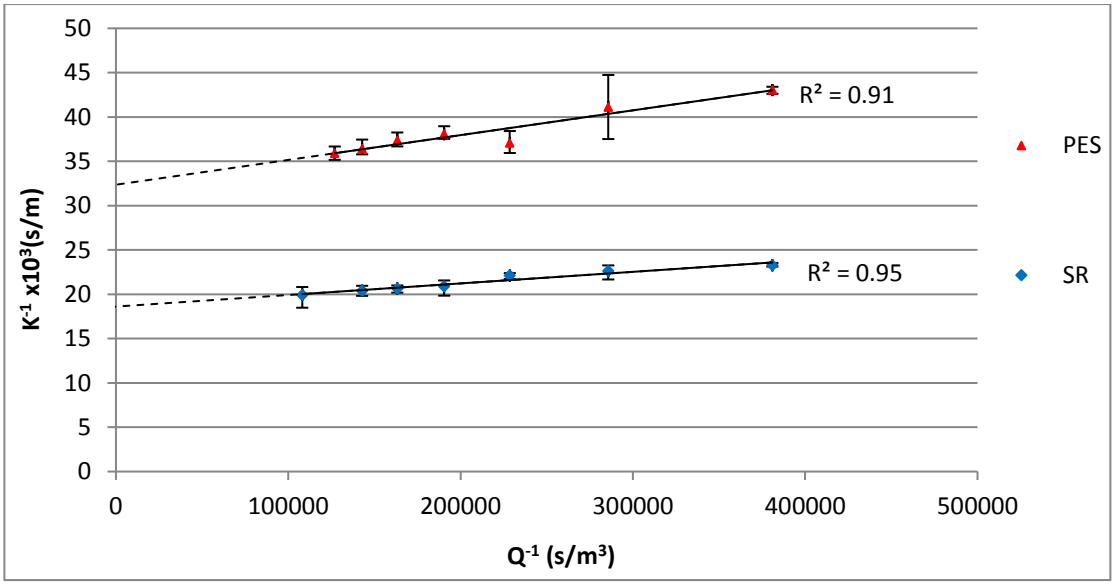

Figure 4-12: 'Wilson plot', minimum and maximum value error bars

The membrane mass transfer resistances obtained from the Wilson plot and calculated by Equation 4-5 and Equation 4-6 are presented in Table 4-4. The calculated values are displayed in the middle column and the graphically obtained values in the right hand column.

Table 4-4: Experimental and calculated membrane mass transfer coefficients

	$1/K_{M(calc)}$ ($m^{-1}s$)	$1/K_{M(exp)}$ ($m^{-1}s$)
SR	33950	18610
PES	27030	32540

The $1/K_M$ value for silicone rubber found experimentally is of the same order as the calculated value and relates very closely to the value of 52.6 $x10^{-6}$ $m^{-1}s$ calculated by Côté *et al.* (1989), for the mass transfer coefficient for silicone rubber membranes of similar thickness and oxygen permeability to that used in this study.

The value obtained for polyethersulphone is much higher than those obtained in literature for hydrophobic microporous membranes; indeed Yang and Cussler (1986) state that the membrane resistance of a hydrophobic material is negligible. This indicates

the membrane used in this study was hydrophilic, verifying the suggested explanation for the observed results with variations in inlet pressure obtained with the polyethersulphone membrane module. Table 4-5 compares the obtained values to those obtained in literature.

Table 4-5: Comparison of membrane mass transfer coefficients

	Membrane material	$1/K_M$ ($m^{-1}s$)
This study	PES	32540
Vladisavljevic (1999)	hydrophilic PES	21200

The membrane mass transfer resistance is very similar to that found by Vladisavljevic, with hydrophilic polyethersulphone membranes of similar dimensions to those used in this study, supporting the assertion that the polyethersulphone membranes used in this study were hydrophilic.

Using the information from the Wilson plot and the experimentally obtained values of K, the liquid side mass transfer coefficient, K_L, was obtained from Equation 4-7, a rearranged form of Equation 2-1:

$$K_L = \left(\frac{1}{K} - \frac{1}{K_M} \right)^{-1} \qquad \textbf{Equation 4-7}$$

The liquid film resistance can then be plotted in its dimensionless form, the Sherwood number, Sh, against the dimensionless Reynolds number, Re, on a logarithmic scale, with the dimensionless numbers being calculated using Equation 4-8 and Equation 4-9.

$$Sh = \frac{K_L d}{D} \qquad \textbf{Equation 4-8}$$

$$\mathrm{Re} = \frac{Qd\rho}{A(1-\phi)\mu}$$ **Equation 4-9**

Where: d = characteristic length (m)

A = flow area (m^2)

φ = membrane packing density

Q = volumetric flowrate of water (m^3s^{-1})

μ = water viscosity (Pa.s)

ρ = water density (kgm^{-3})

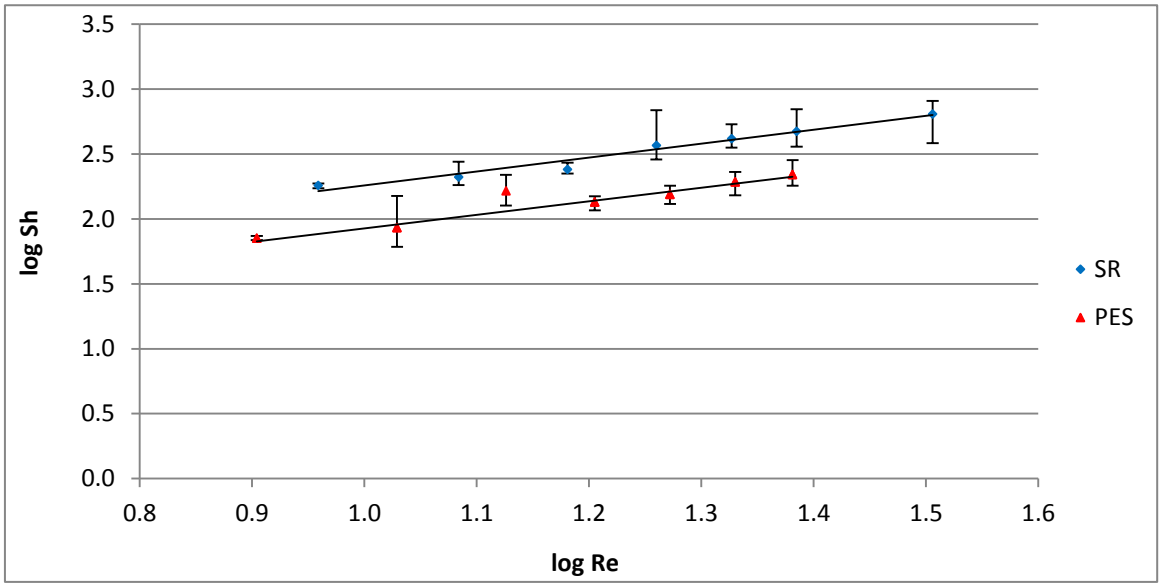

Figure 4-13: Sherwood number versus Reynolds number (0.5 bar, 2 lpm inlet flow, minimum and maximum value error bars)

A least squares regression of the data in Figure 4-13 gives the following correlations with correlation fit coefficients in excess of 0.97.

Table 4-6: Obtained Sherwood number/ Reynolds number relationships

	Correlation	Correlation coefficient	
SR:	$Sh = 543.3\,\mathrm{Re}^{1.07}$	0.97	Equation 4-10
PES:	$Sh = 106.9\,\mathrm{Re}^{1.05}$	0.99	Equation 4-11

The exponent on Reynolds number is approximately equal to 1.00 for both the silicone rubber and polyethersulphone membrane modules – explaining the pseudo-proportional nature of Figure 4-11.

In this study, the effect of the Schmidt number, Sc, was not evaluated. A power dependence of 0.33 is widely accepted in literature (Vladisavljevic, 1999, Yang & Cussler, 1986, Ahmed & Semmens, 1996, Coté *et al.*, 1989), and setting the exponent to this value allows the development of the following relationships incorporating Sc:

SR: $Sh = 1.99\,\mathrm{Re}^{1.07}\,Sc^{0.33}$ **Equation 4-12**

PES: $Sh = 0.96\,\mathrm{Re}^{1.05}\,Sc^{0.33}$ **Equation 4-13**

The exponent on the Reynolds number is similar in both cases, reflecting the geometric similarity of the two modules. The variation in the exponents may be related to the slight difference in the voidage fraction caused by differences in fibre diameters. Table 4-7 compares the obtained relationships to those contained in literature.

Table 4-7: Mass transfer correlations for hollow fibre modules

Study	Voidage Fraction	Relationship
Schöner *et al*. (1998)	0.51	$Sh = 1.76Re^{0.82}Sc^{0.33}$
This study	0.945	$Sh = 1.99Re^{1.07}Sc^{0.33}$
This study	0.957	$Sh = 0.96Re^{1.05}Sc^{0.33}$
Yang & Cussler (1986)	0.97	$Sh = 1.25\left(Re\frac{d}{l}\right)^{0.93}Sc^{0.33}$
Li et al. (2010)	0.994	$Sh = 0.20Re^{1.03}Sc^{0.33}$

The value of the coefficient is different for the two different membranes modules. Zheng *et al.* (2005), link this to membrane porosity, γ, arguing that mass transfer in microporous membranes takes place through the membrane pores only, and therefore the pore area only should be considered in calculation of the membrane specific surface area. Applying this analysis to the polyethersulphone membrane modules, using the

manufacturer's supplied porosity yields Equation 4-14; a modified form of Equation 4-13.

$$Sh = 3.20\gamma \,\mathrm{Re}^{1.05}\, Sc^{0.33}$$ **Equation 4-14**

The lack of agreement between this relationship and Equation 4-12 for the silicone rubber membrane module implies that the assertion by Zheng *et al.* (2005) that mass transfer takes place through the membrane pores only is not correct. A more likely explanation is that mass transfer is a combination of both diffusion through the water filled pores and a solution diffusion mechanism through the membrane wall (Vladisavljevic, 1999).

Further comparisons between this study and others are difficult. An observation previously made by Yang & Cussler (1986) - fluid flow through the shell of a shell-and-tube heat or mass exchanger is extremely complex and no fundamental mathematical description of its nature exists (Zheng *et al.*, 2005).

As a result of this, the literature contains multiple methods of developing the relationship involving different calculations of Reynolds number (i.e. different characteristic length), different Reynolds number ranges, use of different dimensionless groups, incorporating membrane fibre length (Yang & Cussler, 1986), incorporating membrane porosity (Zheng *et al.*, 2005), and incorporation of pressure (Ahmed *et al.*, 2004).

However, comparing the relationships obtained in this study to those contained in literature for other parallel flow, hollow fibre membrane modules serves the purpose of establishing the reliability of the data obtained. Although different relationships were found, the differences can be explained by the difference in the membrane materials and modules geometries used in the various investigations.

4.6 Conclusions

The oxygen mass transfer characteristics of silicone rubber and polyethersulphone membranes were ascertained and compared at different values of inlet pressure, air flowrate and water side flowrate.

Higher oxygen transfer rates were obtained at all parameter values with silicone rubber, attributed to the high permeation rates of oxygen in silicone rubber and the hydrophilic nature of the PES membranes used in this study.

Mass transfer coefficients and oxygen fluxes were found to increase with increasing inlet pressure and increasing liquid side flowrate. Airside flowrate was not found to have a statistically significant effect on mass transfer. These results were all corroborated by theory and previous research, and justified some of the assumptions used in the data analysis.

Relationships between the Sherwood number (dimensionless form of the liquid side mass transfer coefficient) and the Reynolds number (dimensionless form of the liquid side flowrate) were obtained, with good correlation coefficients, verifying the experimental approach used.

The values of the constants in the Sherwood number – Reynolds number relationships differed significantly from those contained in published research. These differences are explainable by differences in experimental setup, membrane materials studied and data analysis techniques.

5 Membrane Aerated Biofilm Reactor Studies – Part 1

Influence of inlet pressure on MABfR performance

In total, MABfR A was operated continuously and monitored for 18 months. This chapter describes the first 190 days of operation, when the inlet pressure was varied between 1.0 and 2.0 bar gauge and a hydraulic retention time (HRT) of 1 day was used. This section examines the results obtained during this period, and uses the obtained results to develop a method for obtaining oxygen flux from pollutant removal rates.

5.1 Reactor start-up

The reactor was filled with synthetic waste and inoculated with supernatant obtained from garden soil in accordance with the procedure outlined in Section 3.2.5. With an initial inlet pressure of 0.5 barg and HRT of 5 days, visible biomass was observed on the membrane, membrane support and the walls of the tank within 5 days.

The HRT was then decreased stepwise over a period of 76 days using the values detailed in Table 5-1, to avoid washout of biomass before membrane attachment occurred. Throughout this period, the bulk pH was monitored and adjusted if needed via dropwise addition of 0.1 mol l^{-1} NaOH solution to keep the pH in the range 6-7.5 and maintain ideal growth conditions for the bacteria of interest in this study (Semmens *et al.*, 2003).

Table 5-1: Conditions during start-up period

Day	Inlet pressure (bar)	Hydraulic retention time (days)
1-16	0.5	5
17-36	0.5	3.5
37-55	0.5	2
56-76	0.5	1.5

At the end of the start-up period, the membrane support rack was removed from the tank, all biomass removed from the walls of the tank, the membrane support rack replaced and the tank filled with fresh synthetic waste. The HRT was also reduced to 1 day and the inlet pressure increased to 1 bar. Bulk dissolved oxygen was monitored throughout this period and was observed to fall to below 0.20 mg l^{-1} after 8 days, after which the COD and ammoniacal nitrogen removal was considered to be oxygen limited.

5.2 General observations

The COD, ammoniacal nitrogen and total nitrogen removal throughout the 190 days of operation at 1 day hydraulic retention time are presented and discussed in sections below. The conditions throughout the 190 days in question are summarised in Table 5-2 below:

Table 5-2: Conditions throughout inlet pressure investigation

Day	Inlet pressure (bar)	HRT (days)
1-17	1.0	1.0
18-42	1.1	1.0
43-55	1.2	1.0
56-92	1.3	1.0
93-140	1.4	1.0
141-153	1.6	1.0
154-190	2.0	1.0

5.2.1 pH

Influent and effluent pH throughout the 190 days of operation at a HRT of 1 day are shown in Figure 5-1.

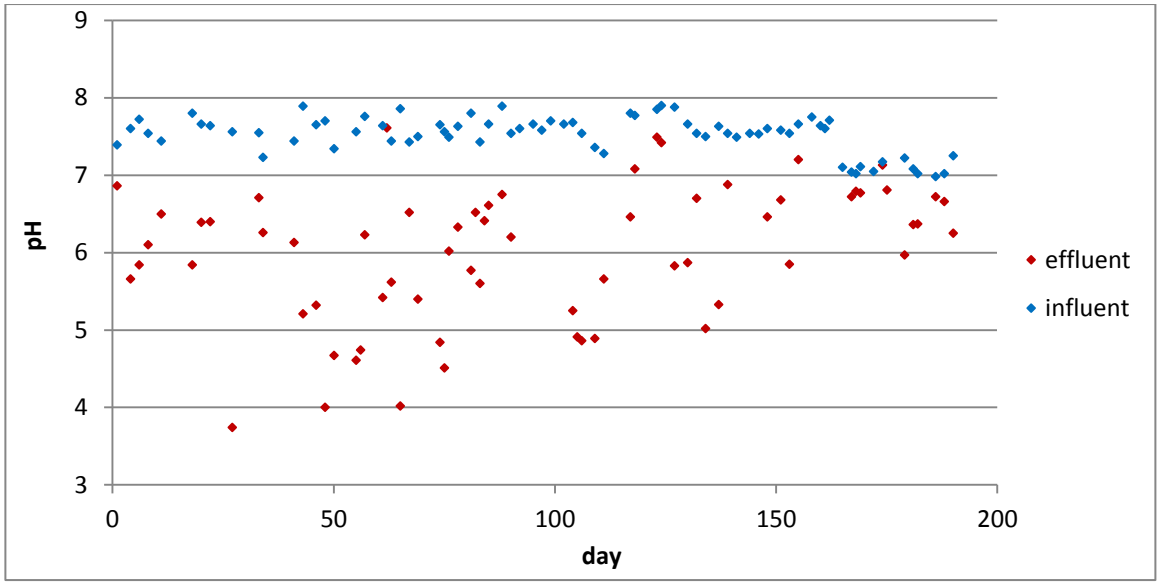

Figure 5-1: Influent and effluent pH

A drop in pH was observed through the action of the biofilm. As shown by the half equations for microbial processes in Chapter 1, consumption of basic carbonate and ammonia, and production of acidic carbon dioxide and nitrate, occurs in the biofilm leading to the change in pH. In order to maintain optimal conditions for biofilm growth, pH was manually adjusted through dropwise addition of 0.1 M sodium hydroxide solution if the value dropped below 5.0.

Variation in the pH of the influent media is caused by temperature, error in volume of stock solutions used in preparation of influent media and changes in stock solution concentration due to degradation etc.

The pH conditions throughout Runs 1-7 are summarized in Table 5-3.

Table 5-3: Average and standard deviation pH

	pH	
	Influent	Effluent
Average	7.52	6.00
Standard Deviation	0.24	0.88

5.2.2 Nitrite concentration

Figure 5-2 shows the bulk nitrite concentration throughout the duration of the pressure investigation.

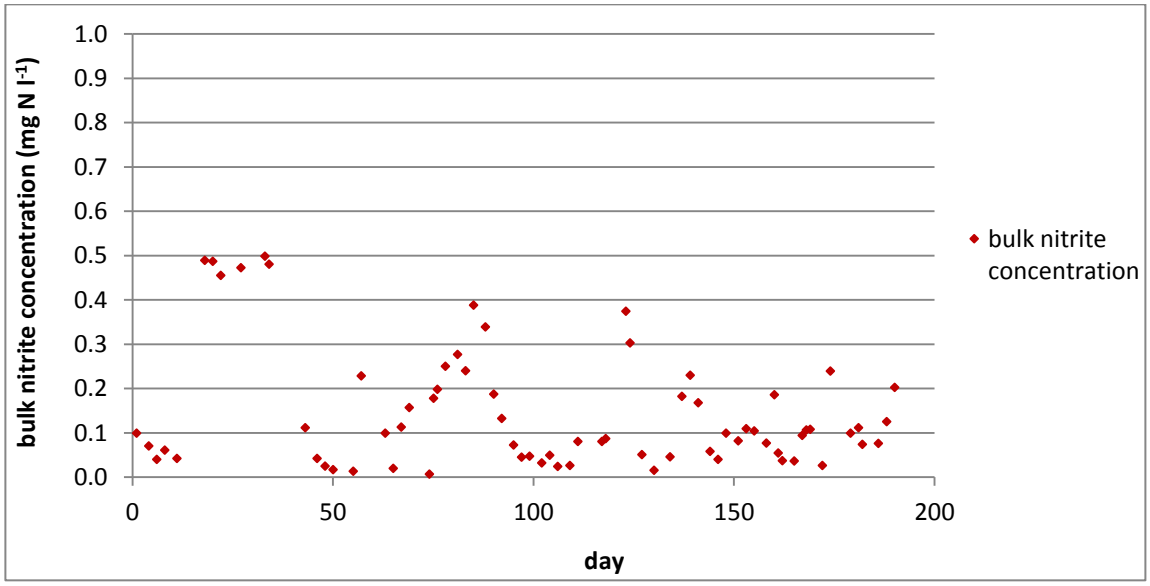

Figure 5-2: Bulk nitrite concentration (days 1-190)

The nitrite concentration was below the upper detection limit (0.500 mg l^{-1}) at all stages throughout the investigation, with an average concentration of 0.145 mg l^{-1} and a standard deviation of 0.135 mg l^{-1}.

The relatively low values obtained for bulk nitrite concentration (compared to influent NH_4^+-N concentrations of approximately 9.5 mg l^{-1}) implies that the majority of ammoniacal nitrogen in the influent media was completely oxidized to nitrate.

This result is not unexpected and can be explained by examining the growth rates of the two groups of bacteria responsible for nitrification. At ambient temperatures (at which the investigation was carried out), the growth rate for the most common nitrite oxidising bacteria, *Nitrobacter*, is significantly larger than the growth rate for the most common ammonia oxidizing bacteria, *Nitrosomonas* (Hellinga *et al.*, 1998). As such, it is generally the oxidiation of ammonia to nitrite which is the rate controlling step of the nitrification process, and nitrite accumulation is rare.

5.3 Stoichiometric model development

The half reactions for microbiological respiration given by McCarty (1975) can be combined to describe the reactions taking place in the MABfR. Constructing an overall stoichiometric reaction for a bacterial reaction involves combination of three oxidation half reactions: one for the electron donor (R_d); one for the electron acceptor (R_a); and one for bacterial cell assimilation (R_c). The overall reaction (R) is then obtained using Equation 5-1 (McCarty, 1975).

$$R = R_d - f_e R_a - f_s R_c \qquad \textbf{Equation 5-1}$$

Where: f_e = fraction of electron donor used for energy

f_s = fraction of electron donor used for cell formation

In order to achieve a balanced equation:

$$f_e + f_s = 1 \qquad \textbf{Equation 5-2}$$

f_s and f_e are functions of cell yield coefficient, cell decay rate, solids retention time (sludge age) and the biodegradable fraction of microorganisms as described by the relationship in Equation 5-3.

$$f_s = a_e\left(1-\frac{f_d b t_s}{1+bt_s}\right)$$ **Equation 5-3**

Where: a_e = cell yield coefficient

f_d = biodegradable fraction of active microorganism

b = cell decay rate (day^{-1})

t_s = solid retention time/sludge age (days)

The cell yield coefficient, a_e, is representative of the fraction of electron donor used for cell synthesis at zero sludge age, and can be calculated from thermodynamic considerations or determined experimentally. Values of a_e are available in literature, as shown in Table 5-4:

Table 5-4: Values of a_e used in model development (McCarty, 1975)

Reaction	Value of a_e
Aerobic heterotrophy	0.79
Nitrification	0.096
Denitrification	0.36

A value of 0.80 for the biodegradable fraction of biomass, f_d, is acceptable for both aerobic and anaerobic bacteria (McCarty, 1975). Cell decay rates are also available in literature, as shown in Table 5-5:

Table 5-5: Cell decay rates (Manser *et al.*, 2006)

Reaction	Value of b (day^{-1})
Aerobic heterotrophy	0.28
Nitrification	0.15
Denitrification	0.033

With the values in Table 5-4 and Table 5-5, it is possible to use Equation 5-3 to calculate the value of the fraction of electron donor, f_s, for various values of sludge age, t_s. The

obtained fs values are displayed in Figure 5-3. A logarithmic scale is used on the horizontal axis.

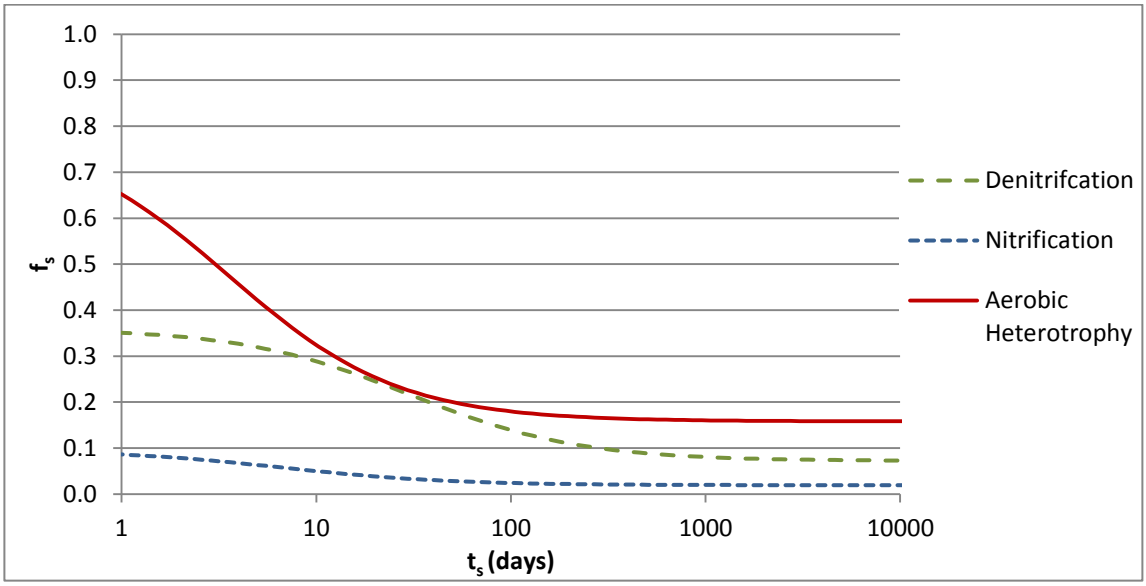

Figure 5-3: f_s/sludge age relationships

It can be seen from Figure 5-3 that the value of f_s reaches a steady value after a sludge age of approximately 1000 days. Sludge age is not a true measure of biomass residence time; rather it is the ratio of the mass of organisms in the reactor to the mass of organisms removed each day, as calculated by Equation 5-4 (Tchobanoglous & Burton, 1991a).

$$t_s = \frac{V_r X}{Q X_e} \qquad \textbf{Equation 5-4}$$

Where: V_r = Reactor volume (l)

X = biomass concentration in reactor (mg l^{-1})

Q = flowrate (l day^{-1})

X_e = biomass concentration in effluent (mg l^{-1})

One of the major advantages of the MABfR is the high biomass retention, with biomass concentrations of 14 gm^{-2} being observed by Brindle *et al*. (1998). In this study, the

biomass concentration in the effluent was very small, as evidenced by very low turbidity throughout reactor operation. As the value of X is much larger than X_e, it is appropriate to select the steady values for f_s, as sludge age cannot be accurately measured without the use of a destructive technique to obtain reactor biomass concentrations. A similar assumption was made in biofilm modeling work by Shanahan & Semmens (2004).

Using the steady values from Figure 5-3 in combination with the half equations contained in work by McCarty (1975); Equation 5-5, Equation 5-6 and Equation 5-7 can be developed to describe the stoichiometry of the relevant microbial processes taking place in Reactor A.

Aerobic Heterotrophy

$$\{CH_2O\} + 0.032HCO_3^- + 0.842O_2 + 0.032NH_4^+ \rightarrow 0.032C_5H_7O_2N + 0.874CO_2 + 0.968H_2O$$ **Equation 5-5**

Nitrification

$$NH_4^+ + 0.031CO_2 + 0.008HCO_3^- + 1.948O_2 \rightarrow 0.008C_5H_7O_2N + 0.992NO_3^- + 0.985H_2O + 1.985H^+$$ **Equation 5-6**

Denitrification

$$NO_3^- + 1.329\{CH_2O\} + H^+ \rightarrow 0.014C_5H_7O_2N + 0.493N_2 + 1.781H_2O + 1.260CO_2$$ **Equation 5-7**

Examination of Equation 5-6 and Equation 5-7 shows that, whilst nitrification produces acidity (1.985 moles of H^+ are produced per mole of NH_4^+ consumed), denitrification reduces acidity (1 mole of H^+ is consumed per mole of NO_3^- denitrified). This observation explains the pH regulatory effect of simultaneous nitrification and denitrification.

Conversion of the coefficients in Equation 5-5, Equation 5-6 and Equation 5-7 from a molar to mass basis leads to the following ratios:

Table 5-6: Mass ratios of substrates involved in microbial reactions in the MABfR

Nitrification			
NH_4^+-N	O_2	NO_3^--N	Biomass
1 g	4.45 g	0.99 g	0.113 g
Denitrification			
NO_3^--N	$\{CH_2O\}$	Biomass	
1 g	2.85 g	0.065 g	
Aerobic heterotrophy			
$\{CH_2O\}$	O_2	Biomass	
1 g	2.07 g	0.121 g	

The values in Table 5-6 are very similar to those published in the literature including the value of 4.54 gO_2 per gNH_4^+-N completely oxidised to nitrate contained in work by Brindle *et al*. (1998); and the value of 4.57 gO_2 per gNH_4^+-N used in a more recent study by Hasar *et al*. (2008) in which biomass synthesis was considered negligible. The ratio of 2.07 g of O_2 per g of COD for aerobic heterotrophy is comparable to the 2.11 g of oxygen per g of COD (presented by the authors as 0.473 g of COD per g of O_2) used by Shanahan & Semmens (2004), and the stoichiometric NO_3^--N:COD value for denitrification is very similar to the value of 2.86 used by in a modelling study by Matsumoto *et al*. (2007).

5.4 Pollutant removal

5.4.1 Removal Efficiency

The COD and ammoniacal nitrogen removal efficiencies throughout Runs 1-7 are shown in Figure 5-3.

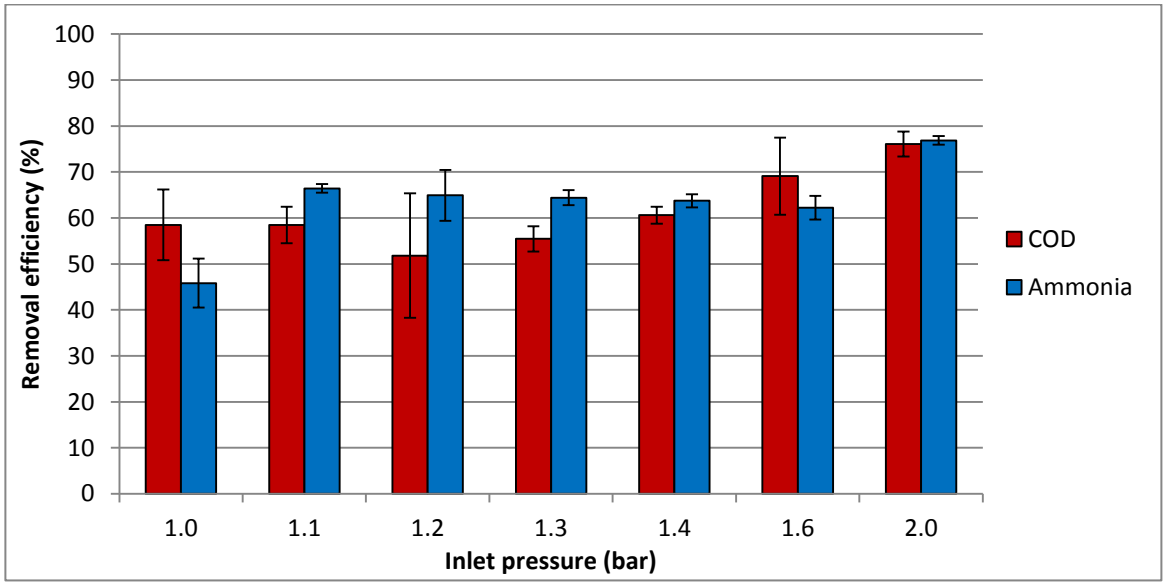

Figure 5-4: Pollutant removal efficiency in Runs 1-7 (standard error bars)

Figure 5-4 shows that, in general, higher pollutant removal efficiencies are achieved at higher inlet pressures, attributable to greater availabilities of oxygen achieved at higher pressures.

The absence of a discernible trend may be attributed to some of the experimental runs being long enough for bulk oxygen levels to approach zero (allowing oxygen flux to be calculated from pollutant removal), but not long enough for the biofilm to reach steady-state. Due to their location within the biofilm, the increase in oxygen availability is first exploited by nitrifying bacteria, leading to a disproportionately high ammoniacal nitrogen removal. The reasons for this occurring are discussed in greater detail in Section 5.5.

Additionally, the standard errors for COD removal are larger than those for ammoniacal nitrogen removal. There are two possible explanations for this observation. As growth rates for heterotrophic bacteria are larger than those for nitrifiers (Semmens *et al.*, 2003), respiration of any entrained biomass in the collected samples will have a greater effect on COD concentration than ammoniacal nitrogen concentration.

Table 5-7: Comparison of pollutant removal efficiencies

Author	**HRT (day)**	**a (m^2m^{-3})**	**% COD removal**	**% NH_4^+-N removal**
Timberlake (1988)	1.1	0.19	55.9	70.4
Pankhania *et al*. (1994, 1999)	0.042	510	89	44.4
Yamagiwa & Ohkawa (1994)	0.5	24.6	>95	90
Semmens *et al*. (2003)	0.25	422	>95	90
This study	1	5.52	76.1	76.9

The removal efficiencies obtained in this study do not compare favourably with those achieved in other studies where simultaneous COD and ammoniacal nitrogen removal was obtained (Table 5-7). Some studies report ammoniacal nitrogen and COD removal efficiencies of 90% and greater, but these studies used a different HRT, specific membrane area and pollutant loadings.

The ammonia removal levels in this study compare favourably with other studies treating wastewaters containing both COD and ammonia. Semmens *et al*. (2003), achieved approximately 90% removal, but the very high level of removal achieved by the researcher can be attributed to the very high specific membrane area used in their study.

Pollutant removal efficiency is a useful measure in comparing the effect of different parameter values within one pollutant treatment setup, but it is of limited use in making comparison between different setups. A better comparison between studies can be made by considering the pollutant removal rates on a specific membrane area basis.

5.4.2 Removal rates

The removal rates of COD and ammoniacal nitrogen on a specific membrane area basis are shown at the different inlet pressures used in Figure 5-5.

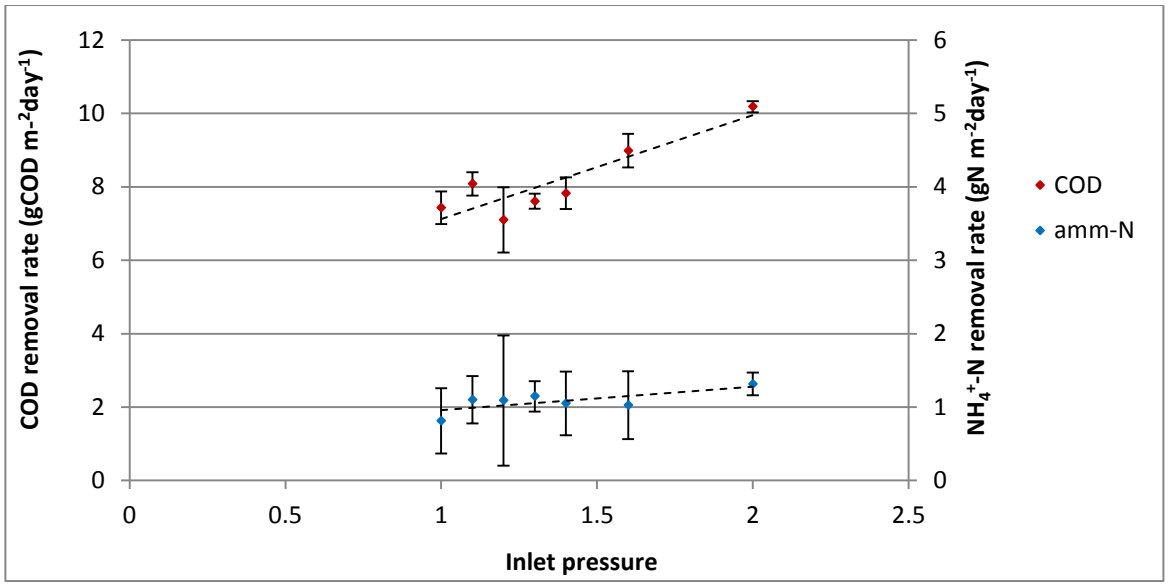

Figure 5-5: Effect of inlet pressure on pollutant removal rates (standard error bars)

Figure 5-5 shows a general upward trend, with the highest pollutant removal rates being achieved at the highest inlet pressure, where the availability of oxygen is greatest.

The removal rates achieved at 2.0 bar inlet pressure, are compared with those in published literature in Table 5-8.

Table 5-8: Comparison of pollutant removal rates

Author	HRT (day)	a (m^2m^{-3})	r_{COD} (gCOD $m^{-2}day^{-1}$)	r_{amm-N} (gN $m^{-2}day^{-1}$)
Timberlake (1988)	1.1	0.19	0.19	0.04
Pankhania *et al*. (1994, 1999)	0.042	510	15.08	n/a
Yamagiwa & Ohkawa (1994)	0.5	24.6	6.3	2.2
Semmens *et al*. (2003)	0.25	422	10	2
This study	1	5.52	10.2	1.32

When compared on a specific surface area reaction rate basis, the results obtained in this study relate well with those contained in previously published research. Using the same sample of publications as in Table 5-7, the COD and ammoniacal nitrogen removal rates range from 0.19 – 15.1 g $m^{-2}day^{-1}$ and 0.04 – 2.2 g $m^{-2}day^{-1}$ respectively compared to the 10.2 gCOD $m^{-2}day^{-1}$ and 1.32 gN $m^{-2}day^{-1}$ obtained in this study.

Pankhania *et al*. (1994, 1999) do not give details of the ammoniacal nitrogen removal rates in their study. The authors commented on the absence of nitrate being detected in the effluent and attributed this to the low pH of operation which is likely to have been inhibitory to nitrification. Additionally, the synthetic waste used in their study contained a high COD:Amm-N ratio (~20) and at these conditions aerobic heterotrophs significantly outcompete nitrifiers for available oxygen (discussed further in Chapter 6), explaining the relatively high COD removal rate achieved.

The poor performance of the Timberlake (1988) study can be attributed to the low pressure (0.2 barg) and hence low oxygen availability at the experimental conditions.

5.4.3 Total Nitrogen Removal

Nitrogen removal from wastewater is the result of two bacterial processes: assimilation by heterotrophs and denitrification (Yamagiwa & Ohkawa, 1994). The extent of total nitrogen removal achieved in Runs 1-7 is shown in Figure 5-6.

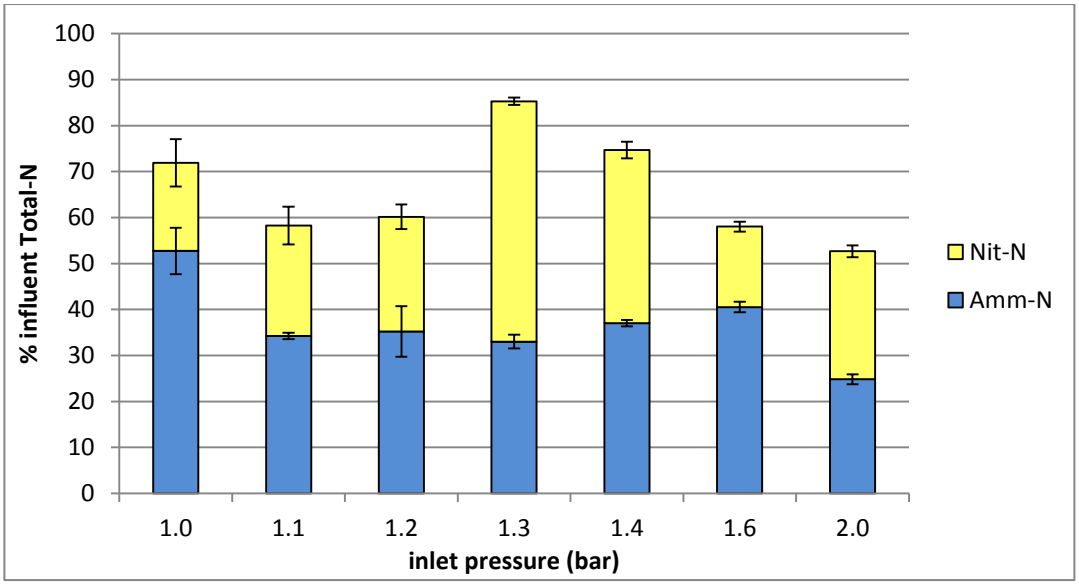

Figure 5-6: total nitrogen removal in Runs 1-7 (standard error bars)

The greatest extent of total nitrogen removal in Runs 1-7 was achieved in Run 7, where the inlet pressure was highest. The greater availability of oxygen due to greater inlet pressure leads to an increase in the nitrification rate. As a result, more nitrate was available for denitrifiers, hence the greater total nitrogen removal is achieved.

The rate of denitrification can be calculated using effluent nitrate concentrations and the relationship between ammoniacal nitrogen removal and nitrate production derived from stoichiometry (Table 5-6). The denitrification rate is obtained using
Equation 5-8.

$$r_{denitrification} = \frac{C_{nit-N(\text{inf})} + 0.99(C_{amm-N(\text{inf})} - C_{amm-N(eff)}) - C_{nit-N(eff)}}{a * HRT} \qquad \textbf{Equation 5-8}$$

Where: $C_{nit\text{-}N(inf)}$ = Influent nitrate concentration (mg N l^{-1})

$C_{nit\text{-}N(eff)}$ = Effluent nitrate concentration (mg N l^{-1})

$C_{amm\text{-}N(inf)}$ = Influent ammoniacal nitrogen concentration (mg N l^{-1})

$C_{amm\text{-}N(eff)}$ = Effluent ammoniacal nitrogen concentration (mg N l^{-1})

The denitrification rates at the different inlet pressures used in the investigation are shown in Figure 5-7.

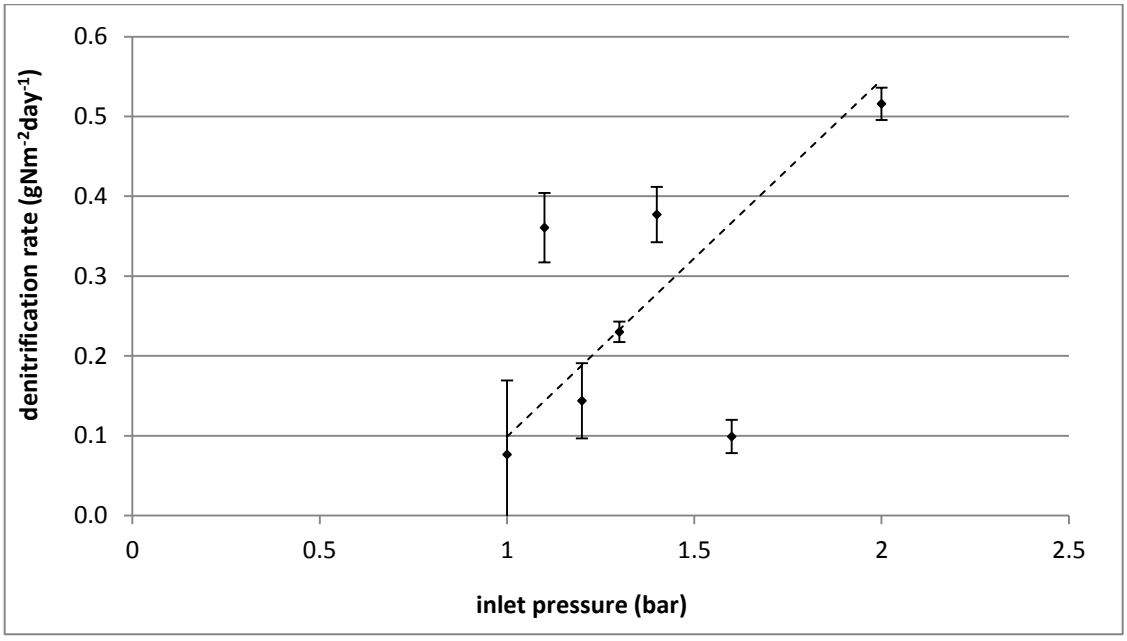

Figure 5-7: Effect of inlet pressure on denitrification rate

In general the rate of denitrification increases with increasing inlet pressure, as shown by the trend line, calculated ignoring rogue points at 1.1 and 1.6 bar inlet pressure. This trend mirrors that obtained between ammoniacal nitrogen removal and inlet pressure and implies that the denitrification rate is limited by nitrate availability in this situation.

The lower than expected denitrification rate obtained in Run 6 (1.6 bar inlet pressure) may be attributed to the short duration of this experimental run. As stated previously, the purpose of this series of experimental runs was to obtain an oxygen limited biofilm and enough data points to ascertain oxygen flux from pollutant removal – this was achieved in run 1.6 after only 10 days.

An increase in the inlet pressure leads to the extension of the aerobic zone closer to the biofilm/bulk interface (Casey *et al.*, 2000b). Any denitrifiers present before the inlet pressure increase are inhibited from performing denitrification by high oxygen concentrations, and this function of the biofilm is therefore lost. Due to the relatively slow growth rate of denitrifying bacteria, the reappearance of significant amount of

denitrifying bacteria takes longer than the duration of Run 6, accounting for the lower than expected denitrification rate observed in this period.

Denitrification rates in excess of those predicted by the trendline were also observed in run 2 (1.1 bar inlet pressure); again this discrepancy can be attributed to the short duration of the experimental run. As explained in Section 5.5, disproportionately large increases in nitrification are observed following an increase in inlet pressure. In run 2, the increase in inlet pressure did not lead to the loss of the denitrification function; instead it was boosted by the availability of greater amounts of nitrate, resulting in the high denitrification rate.

5.5 Response to increased inlet pressure

The bulk dissolved oxygen levels in the MABfR were monitored throughout periods in which the pressure was increased. Two different types of responses were observed; during the start-up period, increasing the inlet pressure would lead to an increase of the bulk dissolved oxygen concentration as oxygen limitation was removed from the biofilm.

Increasing the inlet pressure increases the availability of oxygen to the aerobic heterotrophic and nitrifying bacteria present in the biofilm. However, as the growth rates of aerobic heterotrophs are of the order of 7.3 day^{-1} compared to 0.6 day^{-1} for nitrifiers (Semmens *et al.*, 2003), it may be expected that it is aerobic heterotrophs that first exploit the greater availability of oxygen. This was not found to be the case in this investigation, as exemplified by Figure 5-8, which shows the COD and ammoniacal nitrogen concentrations from day 142 to day 170. The inlet pressure was increased from 1.6 to 2.0 bar on day 154, marked by a dashed line.

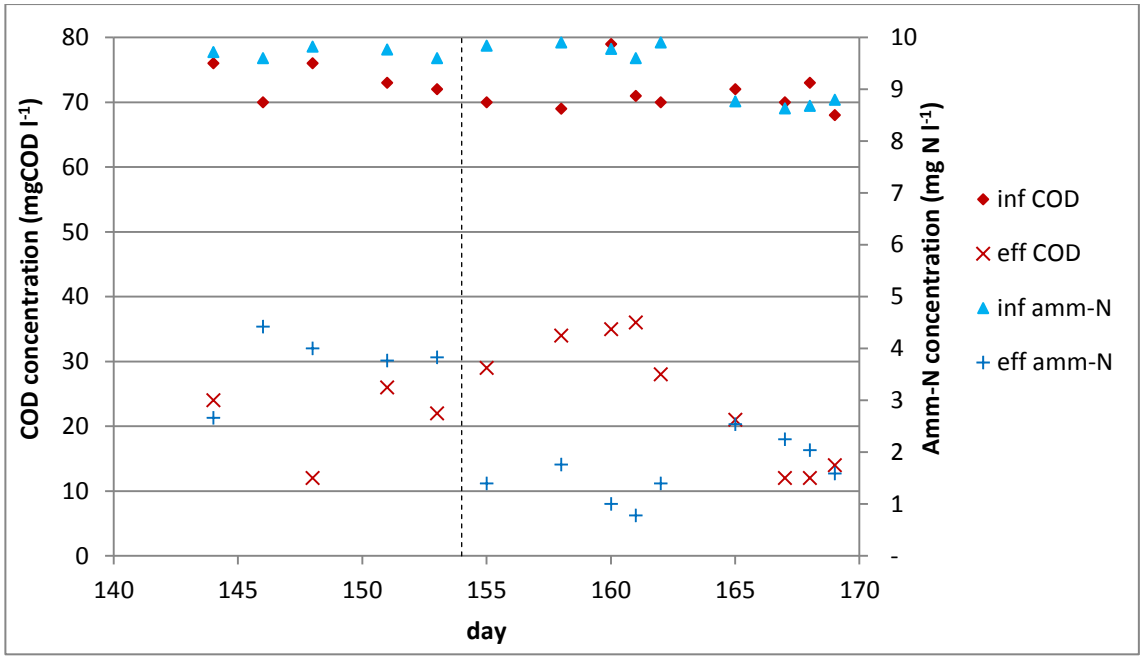

Figure 5-8: Variation in COD and Ammoniacal nitrogen concentrations in response to changes in inlet air pressure.

Effluent ammoniacal nitrogen concentrations show a significant decrease following the pressure increment, whilst effluent COD concentrations initially show an increase before gradually decreasing towards a steady state value.

This was also noted in work by Zhu (2008). Zhu carried out FISH analysis that verified modelling results by Shanahan & Semmens (2004) which predicted that the highest concentration of nitrifying bacteria is found at the membrane-biofilm interface.

As such, nitrifiers are ideally located to exploit the higher availability of oxygen and, in the short term, a disproportionate increase in the ammoniacal nitrogen removal is observed. The long term performance of the biofilm is controlled by influent concentrations, however, as discussed further in Chapter 6.

5.6 Apparent oxygen flux

The biofilm was operated under oxygen limited conditions from the end of the start-up period; all oxygen supplied from the membrane was consumed within the biofilm with none being transferred into the liquid phase.

Using the equations developed in Section 5.3, the oxygen uptake rate (OUR) can be calculated using the pollutant removal rates. The OUR can then be used to calculate the oxygen flux (Casey *et al.*, 1999).

5.6.1 Assumptions

In order to simplify the model the following assumptions are made:

1. **All oxygen is supplied from the membrane.**
   The tank was fitted with a PVC lid in order to reduce air flowrate over the surface of the water and minimise surface aeration. For the purposes of the analysis presented here, surface aeration is considered negligible.

2. **All oxygen supplied from the membrane is consumed within the biofilm.**
   The bulk oxygen concentration was periodically measured at values close to zero throughout the period of operation in question; implying no oxygen from the membrane reached the bulk fluid. Brindle *et al*. (1998) studied the oxygen utilisation efficiency (OUE) of a nitrifying biofilm, and achieved 100% OUE once the biofilm had reached maturity.

3. **All ammonia is utilised aerobically ie. no significant amount of Anaerobic ammonia oxidising bacteria (AnAOB) are present.**
   Although AnAOB have been successfully grown in biofilms (Tsushima *et al.*, 2007), they have extremely low growth rates and require highly specific conditions in order to obtain any significant amounts of the bacteria. Such conditions were not available in the reactor in this study. Additionally, work by Lackner *et al*. (2008) has shown that ANAMMOX bacteria are significantly

inhibited by the presence of heterotrophs, which predominate in the treatment of wastewater.

4. **All ammonia is completely oxidised to nitrate.**

   At ambient temperatures, the growth rate of ammonia oxidising bacteria (AOB) is less than that of nitrite oxidizing bacteria (NOB) (Hellinga *et al.*, 1998). Therefore, ammonia oxidation is considered the rate controlling step of the nitrification process. Throughout the experimental studies, the concentration of nitrite was monitored. At no time was any nitrite accumulation noted (Section 5.2.2), with detected concentrations typically being less than 0.100 mg l^{-1}. A similar assumption was made by Shanahan & Semmens (2004) in a modelling study of membrane aerated biofilms.

5. **Aerobic heterotrophy and denitrification are the only processes consuming soluble COD**

   Although it is possible that stratification can lead to the formation of anaerobic niches within the biofilm; no characteristic noxious odours and/or black ferrous sulfide deposits were observed during reactor operation, the absence of which was the basis of Timberlake *et al*. (1988) asserting anaerobic activity was negligible. This finding was supported in modelling work by Shanahan & Semmens (2004), of membrane aerated biofilms in contact with similar wastewaters.

6. **Complete denitrification takes place**

   Nitrate is reduced to elemental nitrogen with no loss from the system of NO or N_2O gases. The stoichiometric amount of COD is also removed from the system through the removal of nitrate. Again, this assumption was also made by Shanahan & Semmens (2004).

5.6.2 Reaction scheme

A simplified reaction scheme is presented in Figure 5-9 for clarity.

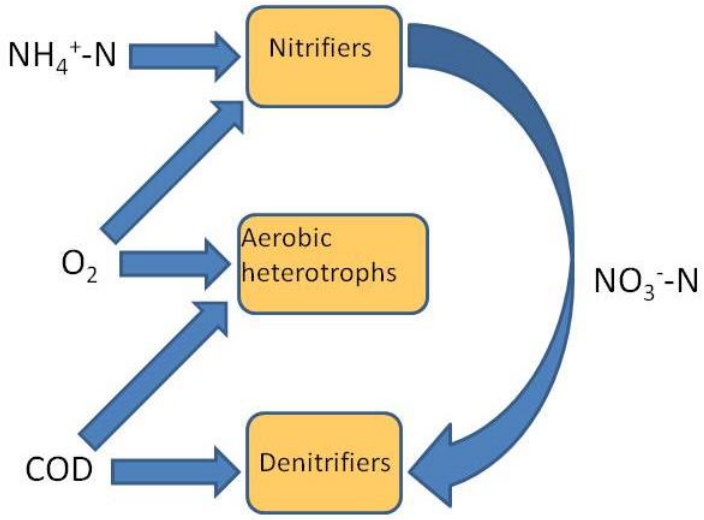

Figure 5-9: Simplified reaction scheme

Using the mass ratios from Table 5-6 and the assumptions detailed in Section 5.6.1, the following procedure is used in order to calculate the oxygen flux from pollutant removal:

oxygen consumed in nitrification:

$$OUR_N = 4.45 * (NH_4^+ - N_{(feed)} - NH_4^+ - N_{(eff)})$$

nitrate produced in nitrification:

$$NO_3^- - N_{(nitrification)} = 0.99 * (NH_4^+ - N_{(feed)} - NH_4^+ - N_{(eff)})$$

COD removed in denitrification:

$$COD_{(denitrification)} = 2.85 * (NO_3^- - N_{(feed)} + NO_3^- - N_{(nitrification)} - NO_3^- - N_{(eff)})$$

COD removed by aerobic heterotrophy:

$$COD_{AH} = COD_{feed} - COD_{denitrifiation} - COD_{eff}$$

oxygen consumed by aerobic heterotrophy:

$$OUR_{AH} = 2.07 * COD_{AH}$$

When the pollutant removal is calculated as a rate, as given by Equation 3-4, the apparent oxygen flux can then be obtained using Equation 5-9:

$$J_a = OUR_N + OUR_{AH} \qquad \textbf{Equation 5-9}$$

5.6.3 Effect of inlet pressure

Figure 5-10 illustrates the effect of inlet air pressure on apparent oxygen flux.

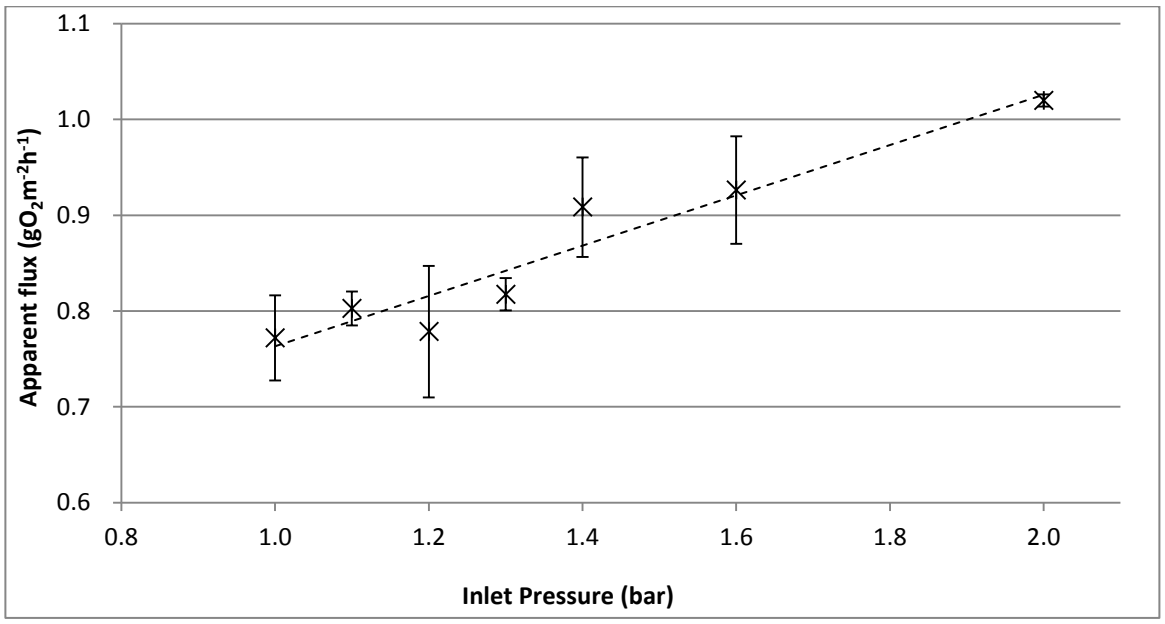

Figure 5-10: Effect of inlet pressure on apparent oxygen flux (standard error bars)

Figure 5-10 shows the existence of a statistically significant relationship between inlet pressure and apparent oxygen flux, albeit with a relatively poor correlation fit coefficient. The poor fit and errors in average apparent oxygen flux can be explained by the errors of analyses and the fact that a biofilm never truly reaches steady state (Casey *et al.*, 1999).

The maximum observed oxygen flux of approximately 1.0 $gO_2m^{-2}h^{-1}$ at 2.0 barg inlet pressure is much lower than the average values of approximately 2.4 $gO_2m^{-2}h^{-1}$, observed in mass transfer studies at similar inlet pressures with silicone rubber as the aeration material. This occurs despite the fact that the oxygen fluxes in the presence of the biofilm were obtained with a constant bulk dissolved oxygen concentration approaching zero, rather than being averaged over the range of 1 – 5 mg l^{-1} during the oxygenation experiments.

Comparisons between the obtained fluxes in the biofilm and the mass transfer experiments are difficult due to the difference in the geometries of the experimental setups, and the hydrodynamic conditions which result from this difference.

The arrangement of the membranes in the MABfR contained two relatively long tubes with several bends, giving increased pressure drop between inlet and exhaust (Coulson *et al.*, 1999a) – the average pressure within the membrane and mass transfer driving force was therefore lower.

The liquid side bulk turbulence was much lower – only moderate amounts of mixing were provided by the impeller, giving added significance of the liquid side mass transfer coefficient as described for low liquid side flowrates in Section 4.6.

Although the presence of a biofilm reduces the significance of the liquid side mass transfer resistance, it itself represents a mass transfer resistance so that Equation 2-1 has to be modified to allow for the presence of a biofilm:

$$\frac{1}{K} = \frac{1}{K_M} + \frac{1}{K_B} + \frac{1}{K_L}$$ **Equation 5-10**

Where: K_B = biofilm mass transfer coefficient (ms^{-1})

Although microbial respiration maintains the bulk oxygen concentration at values approaching zero, thus preserving a high concentration difference, the oxygen diffusivity in a biofilm is lower than in bulk solution (Ahmadi Motlagh *et al.*, 2006). This slow diffusion away from the membrane surface means that a biofilm will represent a greater barrier to mass transfer than a liquid boundary layer of the same thickness.

Additionally, the presence of a biofilm on the membrane surface may affect the mass transfer properties of the membrane material due to adsorption of CO_2 and other respiration products (Côté *et al.*, 1989), increasing the magnitude of the membrane mass transfer resistance.

Shanahan & Semmens (2006), carried out an investigation comparing oxygen transfer with and without biofilm present, and also found a reduction in oxygen flux in areas which experienced small boundary layers, as is expected in operation with hollow fibres, in accordance with the results presented here.

Although the results presented here display proportionality between inlet pressure and obtained oxygen flux in the presence of a biofilm, it is likely that this relationship does not hold for all values of inlet pressure. In operation with high pressure, the membrane will support a thicker, denser membrane. This thicker biofilm will represent a higher barrier to mass transfer and, in accordance with Equation 5-10, a lower value of the overall mass transfer coefficient.

Using linear regression, an empirical relationship (Equation 5-11) between apparent oxygen flux and inlet pressure can be obtained from Figure 5-10 with a correlation fit coefficient of 0.92:

$$\bar{J} = 0.26P_{inlet} + 0.50$$ **Equation 5-11**

The above relationship describes the situation in the reactor used in this study, but cannot be used to predict the oxygen flux in other MABfRs. Using the average absolute value for pressure in the membrane tubes yields the following relationship, with a similar fit coefficient to Equation 5-11.

$$J = 0.28P_{av(abs)} + 0.22$$ **Equation 5-12**

Where:
$$P_{av(abs)} = \left[\frac{\left(P_{inlet} + P_{outlet}\right)}{2}\right] + P_{atm}$$ **Equation 5-13**

P_{atm} = atmospheric pressure (bar)

5.6.4 Mass transfer coefficient

The overall mass transfer coefficient can be found from Equation 5-14, a rearranged form of Equation 2-6:

$$K = \frac{\bar{J}}{\Delta C}$$ **Equation 5-14**

where: $\bar{J}$ = Average oxygen flux ($gO_2\ m^{-2}h^{-1}$)

K = Overall mass transfer coefficient (mh^{-1})

ΔC = Concentration difference across membrane ($mg\ l^{-1}$)

Assuming that the dissolved oxygen concentration in the bulk phase of the reactor is zero, the concentration difference can be assumed to be equal to the oxygen concentration on the gas side of the membrane. As discussed in Section 2.1.1, this concentration is difficult to accurately determine as diffusion of oxygen and nitrogen from gas side to water side and back diffusion of water and respiration products (Côté *et*

al., 1988); combined with pressure losses due to friction (Darby, 1996) mean the concentration changes along the length of the membrane tube.

However, a useful approximation can be made by considering only the pressure losses in calculating the gas side oxygen concentration. During operation, the membrane fluxes were of the order of 1 $gO_2m^{-2}h^{-1}$ - small in comparison to the bulk gas mass flowrate which was approximately 150 g h^{-1}. Assuming, therefore, that the oxygen concentration can be assessed at the average absolute pressure of the system as given by Equation 5-13, the oxygen concentration can be found using the combined gas law. This also assumes the gas can be considered ideal as the conditions in question are not close to the critical conditions (Darby, 1996).

The concentration difference can then be calculated using Equation 5-15 and Equation 5-16 with the values contained in Table 5-9, allowing the overall mass transfer coefficient to be obtained from Equation 5-14.

$$V_{m(\exp)} = \frac{P_R T_{\exp} V_{m(R)}}{T_R P_{av(abs)}} \qquad \textbf{Equation 5-15}$$

$$\Delta C = \frac{f_{O2} M_{O2}}{V_{m(\exp)}} \qquad \textbf{Equation 5-16}$$

Table 5-9: Values used in calculation of gas side oxygen concentration

Parameter	Symbol	Value	Source
Molar volume at reference conditions	V_m	22.41 l mol^{-1}	Rogers & Mayhew (1994)
Pressure at reference conditions	P_R	1 atm (1.01325 bar)	Rogers & Mayhew (1994)
Temperature at reference conditions	T_R	273.15 K (0 °C)	Rogers & Mayhew (1994)
Fraction of oxygen in air	f_{O2}	0.2095	Rogers & Mayhew (1994)
Molar mass of oxygen	M_{O2}	32.00 g mol^{-1}	Green & Perry (2008)
Temperature at experimental conditions	T_{exp}	293.15 K (20 °C)	
Average absolute pressure	$P_{av(abs)}$		Equation 5-13

The effect of inlet pressure on the overall oxygen mass transfer coefficient is shown in Figure 5-11.

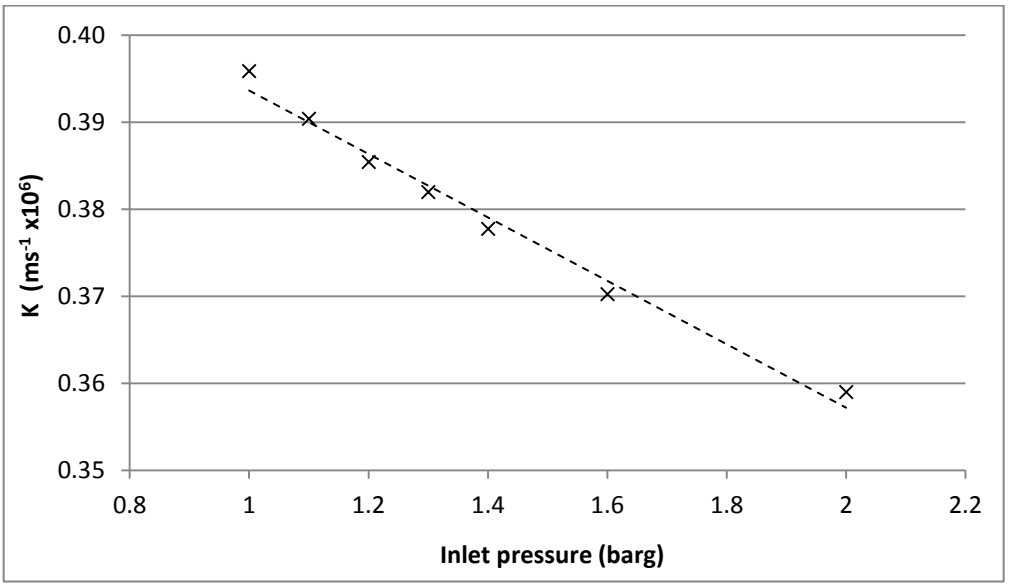

Figure 5-11: Effect of inlet pressure on overall oxygen mass transfer coefficient

Figure 5-11 displays the existence of an inversely proportional relationship between inlet pressure and overall oxygen mass transfer coefficient, with a correlation fit coefficient of

0.99. The proportionality is to be expected; it has already been shown that increased inlet pressure leads to an increase in oxygen flux (Figure 5-10). This increased availability oxygen means that more microbial biomass can be supported on the membrane surface, which increases the resistance to oxygen transfer.

The results obtained from experimental oxygen fluxes and Equation 5-14, Equation 5-15 and Equation 5-16 are displayed and compared to the membrane resistance found in Chapter 4 in Table 5-10. Units for mass transfer coefficients are given in hm^{-1} for agreement with those given previously for oxygen flux.

Table 5-10: Mass transfer coefficients at different experimental conditions

P_{in} (bar)	$P_{av(abs)}$ (bar)	ΔC (mg l^{-1})	K (ms^{-1} x10^{6})	$\frac{1}{K}$ (ms^{-1} x10^{-6})	$\frac{1}{K_M}$ (ms^{-1} x10^{-6})	$\frac{1}{K_L}+\frac{1}{K_B}$ (ms^{-1} x10^{-6})
1.0	1.96	540	39.6	2.53	0.0186	2.51
1.1	2.06	567	39.0	2.56	0.0186	2.54
1.2	2.16	595	38.5	2.59	0.0186	2.58
1.3	2.24	616	38.2	2.62	0.0186	2.60
1.4	2.34	643	37.8	2.65	0.0186	2.63
1.6	2.54	698	37.0	2.70	0.0186	2.68
2.0	2.91	801	35.9	2.79	0.0186	2.77

It can be seen that the combined resistance of the biofilm and liquid boundary layer is much greater than the membrane resistance, with less than 1% of the resistance being attributable to the presence of the membrane. This is in agreement with the work of Picard *et al.* (2012) with neon diffusion through membrane aerated biofilms and found the membrane contributed as little as 2% to the overall mass transfer resistance.

This finding has implications for the operation of an industrial MABfR; as the membrane does not significantly control the oxygen transfer in the presence of a biofilm, the oxygen permeability of a membrane material can be ignored during the membrane selection process.

5.7 Conclusions

The pollutant removal performance of a lab scale MABfR was monitored over a period of 190 days at various inlet air pressures. The pollutant removal rates were used to develop a stoichiometric model from which the apparent oxygen flux, and therefore mass transfer resistance of the biofilm, could be calculated.

The mass transfer resistance of the biofilm is much greater than that of the membrane ascertained in Chapter 4. The implication of this is that the oxygen permeability of a membrane material in a MABfR is not a major consideration in the design of a full scale MABfR, such as the BioSettler.

6 Membrane Aerated Biofilm Reactor Studies – Part 2 Effect of pollutant loading

Chapter 5 assessed the performance of the MABfR though Runs 1-7, where inlet air pressure was increased from 1.0 to 2.0 barg at a 1 day HRT, and developed a stoichiometric model allowing the oxygen flux to be estimated from pollutant removal. This chapter considers the effect of pollutant loading on the pollutant removal performance of the MABfR.

Examined in this chapter is a period of 230 days during which the MABfR was operated with a hydraulic retention time of 0.5 days and an inlet pressure of 3.0 barg. During this period, the COD, ammoniacal nitrogen and nitrate concentration of the influent synthetic wastewater was varied, and the effect of changing wastewater composition on reactor performance studied.

Linear regression of the generated data was then employed to produce a series of relationships which, when used in combination, describe the pollutant removal performance of the MABfR and can also be used to predict the performance at conditions outside of those employed in this study.

6.1 Pollutant removal

During the period in question, changes were made to the composition of the synthetic wastewater fed to the MABfR to achieve variation in the COD, NO_3^--N loadings and NH_4^+-N loadings. These changes were made in such a way as to produce five different experimental conditions, as summarised in Table 6-1.

Table 6-1: Pollutant loadings in Run 8-12

Run	Days	Influent COD loading ($gm^{-2}day^{-1}$)	Influent NH_4^+-N loading ($gm^{-2}day^{-1}$)	Influent NO_3^--N loading ($gm^{-2}day^{-1}$)	C:N ratio
8	1-71	23.8±0.6	4.25±0.08	0.04*	5.6
9	72 – 99	25.6±0.8	3.66±0.13	2.00±0.07	7.0
10	100 - 115	25.7±1.1	2.59±0.01	1.59±0.03	9.9
11	116 – 150	42.4±0.6	2.93±0.06	1.91±0.04	14.4
12	151 – 230	25.1±0.5	2.89±0.10	2.01±0.06	9.1

**no nitrate was added to the feed during Run 8; periodic analysis of influent found nitrate concentrations below the lower detection limit. For calculation purposes, the loading value quoted corresponds to the lower detection limit of 0.1 mg l^{-1}.*

6.1.1 Chemical Oxygen Demand

The observed influent and effluent COD concentrations during the experimental period in question are shown in Figure 6-1. For clarity, the vertical lines show the start of each experimental run (the same device is also used in Figure 6-3 and Figure 6-5).

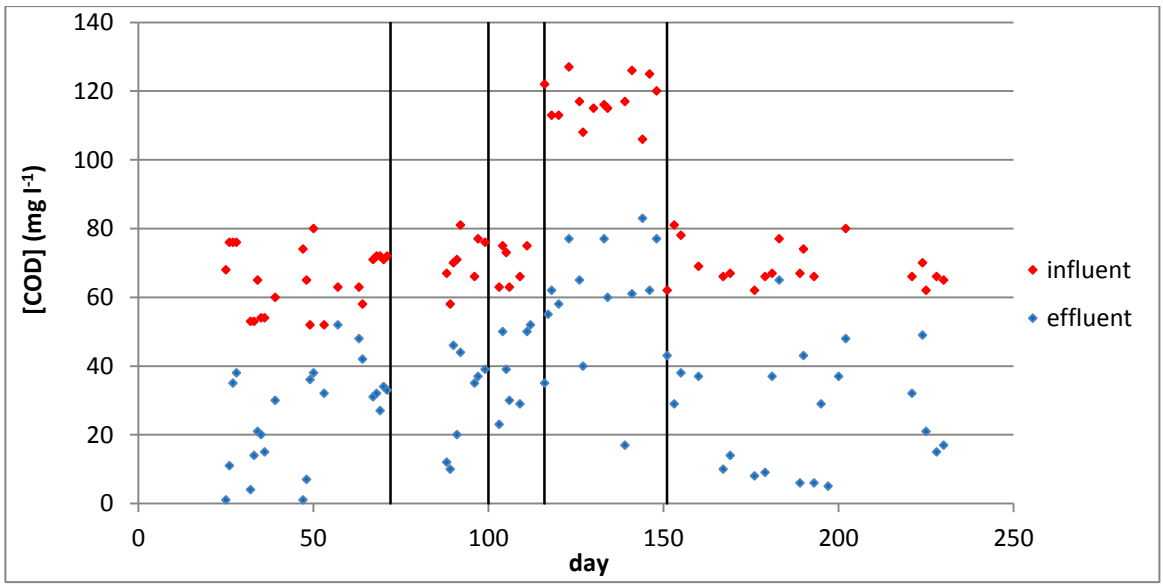

Figure 6-1: Influent and Effluent COD concentrations in Runs 8-12

The data displayed in Figure 6-1 illustrates that the effluent COD concentration was consistently lower than the influent concentration throughout the 230 days of operation

examined here. This indicates that successful treatment of this particular pollutant was achieved in the MABfR.

The data is somewhat scattered, with the effluent data points being more scattered than the influent data points, reflecting both the inherent inaccuracy of the COD analysis method (Hach Company, 2007) and the dynamic nature of a biofilm (Khoyi & Yaghmaei, 2005).

The average influent and effluent COD concentrations and percentage removals for Runs 8-12 are illustrated in Figure 6-2.

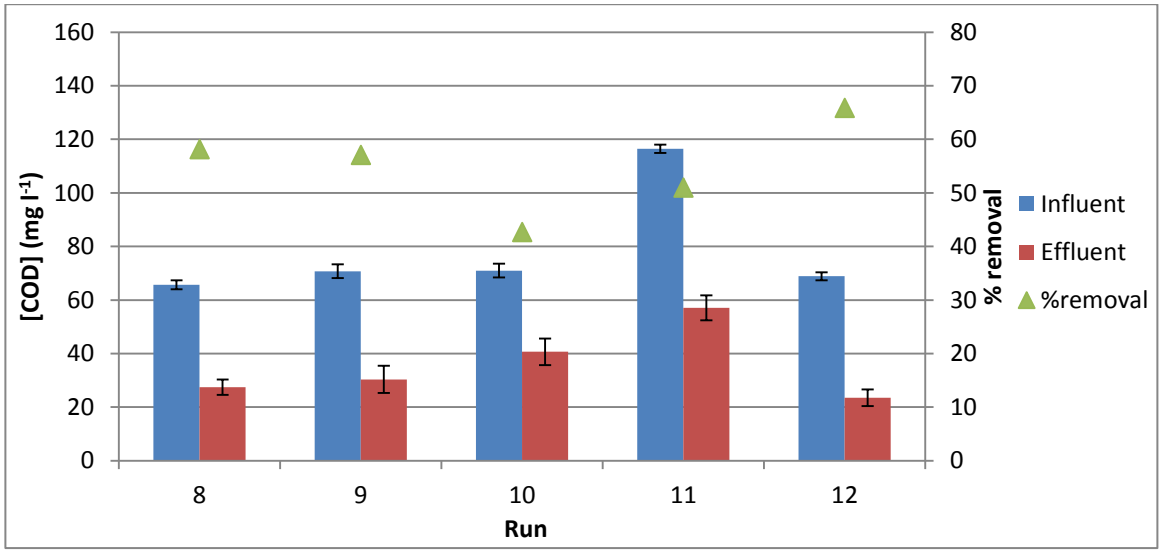

Figure 6-2: Average COD concentrations and percentage COD removal (standard error bars)

Figure 6-2 shows percentage removal in excess of 40% with the highest percentage removal achieved in Run 12, where 65.9% of influent COD was removed.

Comparisons between runs are difficult to make as COD is removed in the MABfR by two different microbial processes: aerobic heterotrophy and denitrification. In addition to limitations in the supply of oxygen, these processes both involve two substrates which can be rate limiting themselves, meaning that the higher COD consumption rates are not necessarily obtained at the highest COD loading rates. This is further discussed in Section 6.2.

6.1.2 Ammoniacal nitrogen

The observed influent and effluent ammoniacal nitrogen concentrations during the 230 of operation examined in this chapter are illustrated in Figure 6-3 below.

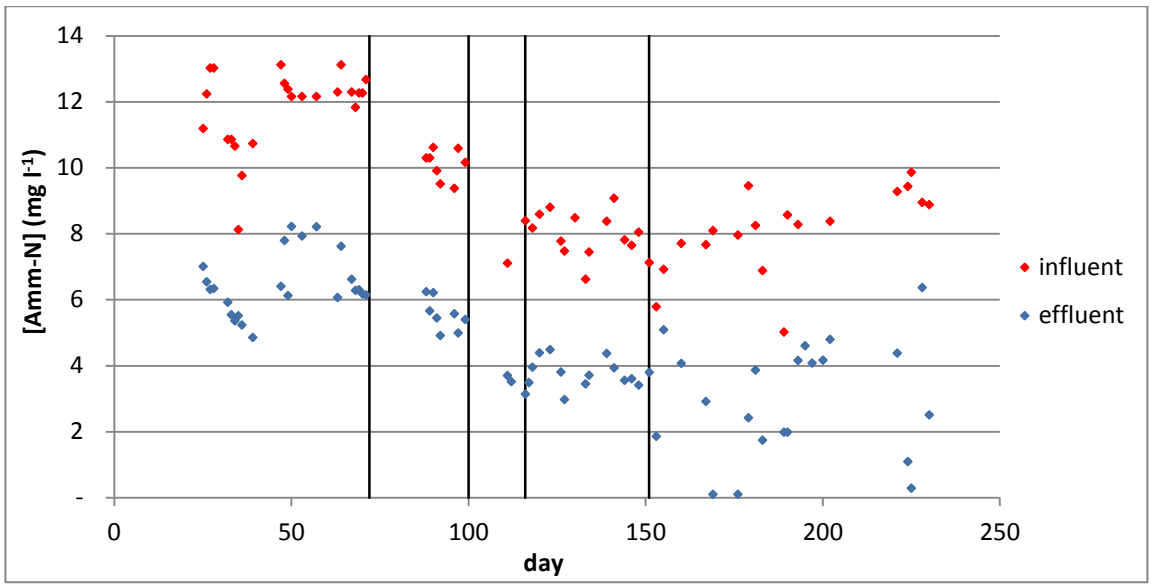

Figure 6-3: Influent and effluent ammoniacal nitrogen concentrations during Runs 8-12

The data displayed in Figure 6-3 indicate that ammoniacal nitrogen removal was consistently achieved throughout the 230 days of reactor operation. At all data points, the effluent concentration is lower than the influent concentration, implying that nitrification is taking place in the biofilm on the surface of the membrane.

In comparison to the COD data shown in Figure 6-1, the data are grouped closer together. This reflects both the higher accuracy of the method used for measuring ammoniacal nitrogen concentration (relative to the COD analytical method) and the structure of membrane aerated biofilms.

As previously discussed, nitrifying bacteria are predominately found at the membrane-biofilm interface (Shanahan & Semmens, 2004). In this location, they are able to take advantage of the 'safety in numbers' aspect of existing in a biofilm and are more

protected from the influence of instability in the bulk liquid than the aerobic heterotrophs which reside further from the membrane surface (Madigan & Martinko, 2006).

Figure 6-4 illustrates the average influent and effluent ammoniacal nitrogen concentrations and percentage removals achieved in Runs 8 – 12.

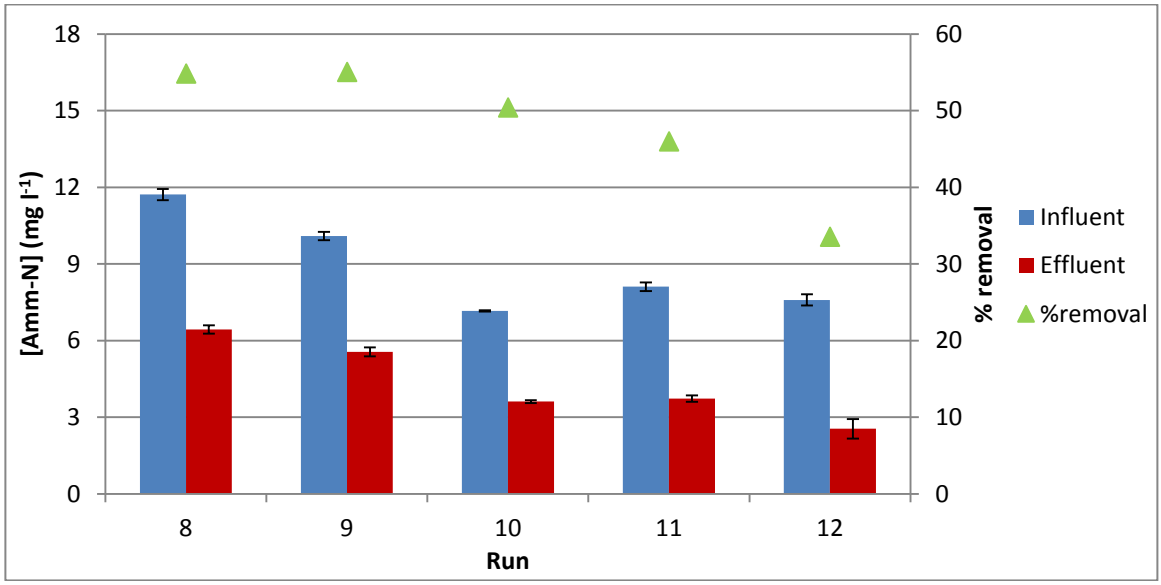

Figure 6-4: Average ammoniacal nitrogen concentrations and percentage ammoniacal nitrogen removal in Runs 8 - 12(standard error bars)

Figure 6-4 shows that the highest percentage removal was obtained in Runs 8 and 9, which are the runs with the highest ammoniacal nitrogen loading rate. Lower effluent concentration was obtained in Runs 10 – 12, with effluent concentrations in the range 2.5 – 3.7 mg l^{-1} being achieved.

The higher removal obtained at the higher loading rates is to be expected. Unlike COD, ammoniacal nitrogen is only consumed in significant quantities by one microbial process in the MABfR. As nitrifying bacteria are predominately found close to the membrane surface (Shanahan & Semmens, 2004), oxygen availability can be assumed not to be limiting to nitrification. It is well established that growth rates of nitrifying bacteria, and therefore ammoniacal nitrogen consumption rates, increase with increasing

ammoniacal nitrogen availability where ammoniacal nitrogen is the limiting substrate (Shah & Coulman, 1978).

Variation in percentage removal amongst the three runs with similar ammoniacal nitrogen loadings is due to competition for oxygen between nitrifiers and aerobic heterotrophs (Zhang *et al.*, 1995).

6.1.3 Total nitrogen

The observed total nitrogen concentrations throughout the 240 days examined in this section are illustrated in Figure 6-5 below

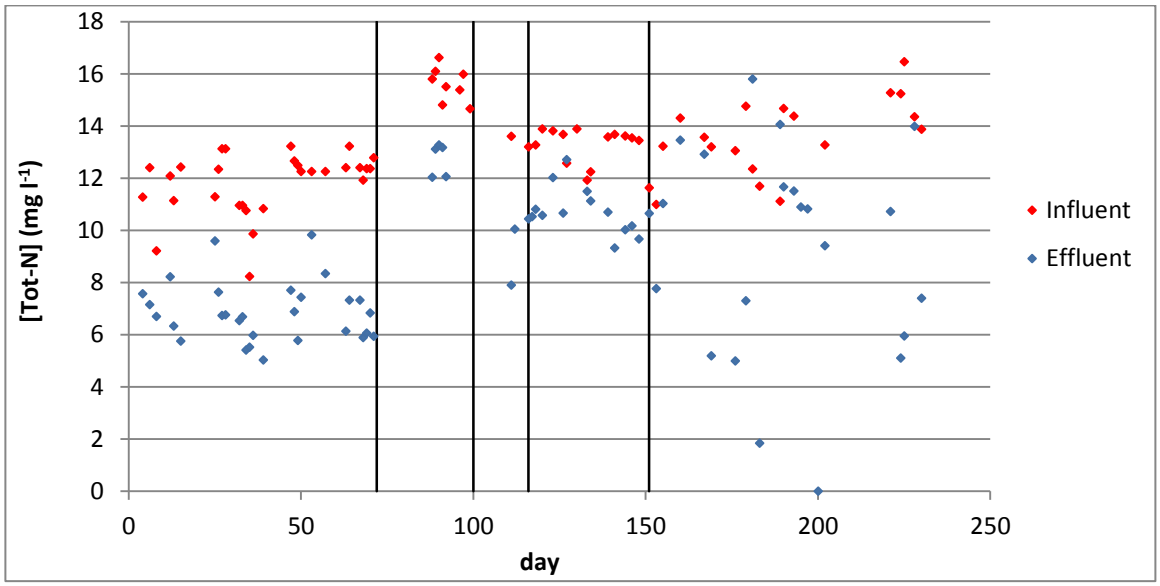

Figure 6-5: Influent and effluent Total-N concentrations in Runs 8-12

Figure 6-5 shows, that at the vast majority of data points, total nitrogen concentration was lower in the effluent compared to the influent, implying that total nitrogen removal was successfully and consistently achieved during the 230 days of operation of the MABfR. The handful of data points where effluent total nitrogen concentration was higher than influent concentration can be attributed to human errors which occurred during the sample collection and/or analysis.

The apparent instability in the total nitrogen removal can also be attributed to the stratified structure of membrane aerated biofilms. Nitrogen is converted to the gas phase, and therefore removed from the effluent via the process of denitrification. Previous research has shown that denitrification occurs in the anoxic area of the biofilm furthest from the membrane. In this location they are most likely to be sheared into the bulk phase and are not protected from inhibitory compounds (such as elemental oxygen) by the mass transfer resistance of the biofilm.

6.2 Removal rates

As discussed in Chapter 5, drawing comparisons with published research is difficult due to the range of inlet pressures, hydraulic retention times and specific surface areas used. Better comparisons are made using the removal rates. Table 6-2 gives the removal rates obtained during Runs 8-12.

Table 6-2: COD and ammoniacal nitrogen removal rates in Runs 8-12 (standard errors)

Run	COD:N ratio	r_{COD} (gCOD $m^{-2}day^{-1}$)	r_{amm-N} (gN $m^{-2}day^{-1}$)
8	5.6	13.8±1.0	1.92±0.08
9	7.0	14.6±1.8	1.64±0.06
10	9.9	11.0±1.8	1.29±0.02
11	14.4	21.5±1.7	1.59±0.06
12	9.1	16.9±1.1	1.83±0.14

Examination of the data in Table 6-2 reveals that the highest rate of COD removal was obtained in Run 11, the run with the highest COD:N ratio. This can be attributed to the higher growth rate, and therefore higher activity rate of bacteria which utilize COD for respiration, in line with Monod kinetics (Shah & Coulman, 1978).

The highest rates of ammoniacal nitrogen removal were obtained in Runs 8 and 12. These high rates can be attributed to the highest ammoniacal nitrogen loading in Run 8 (Shah & Coulman, 1978) and the low COD loading in Run 12 allowing aerobic nitrifiers to compete for oxygen more favourably (Zhang *et al.*, 1995).

Table 6-3 compares the results contained in literature to those generated by Run 8 of this study. Run 8 is chosen as no nitrate was added to the influent synthetic wastewater in this run, in common with the studies chosen for comparison.

Table 6-3: Comparison of pollutant removal rates (standard errors where shown)

Author	COD:N ratio	r_{COD} ($gCOD\ m^{-2}day^{-1}$)	$r_{amm\text{-}N}$ ($gN\ m^{-2}day^{-1}$)
Timberlake (1988)[a]	2.6 – 5.1	1.9 – 4.2	0.1 – 0.6
Pankhania *et al.* (1994, 1999)	14.0 – 21.3	15.1	n/a
Yamagiwa & Ohkawa (1994)	2.8	6.3	1.7 - 2.2
Semmens *et al.* (2003)	4.3 – 4.5	10	2
This study (Run 8)	5.6	13.8±1.0	1.92±0.08

[a]*The researcher used Total Organic Carbon as their measure rather than COD. TOC and COD removal rates are assumed here to be equal for comparative purposes.*

6.2.1 Oxygen consumption

The apparent oxygen flux was calculated from experimental pollutant removal rates, using the same method as described in Chapter 5. The apparent oxygen flux throughout the operational period in question is shown in Figure 6-6, alongside the predicted oxygen flux as given by Equation 5-11 developed in Chapter 5.

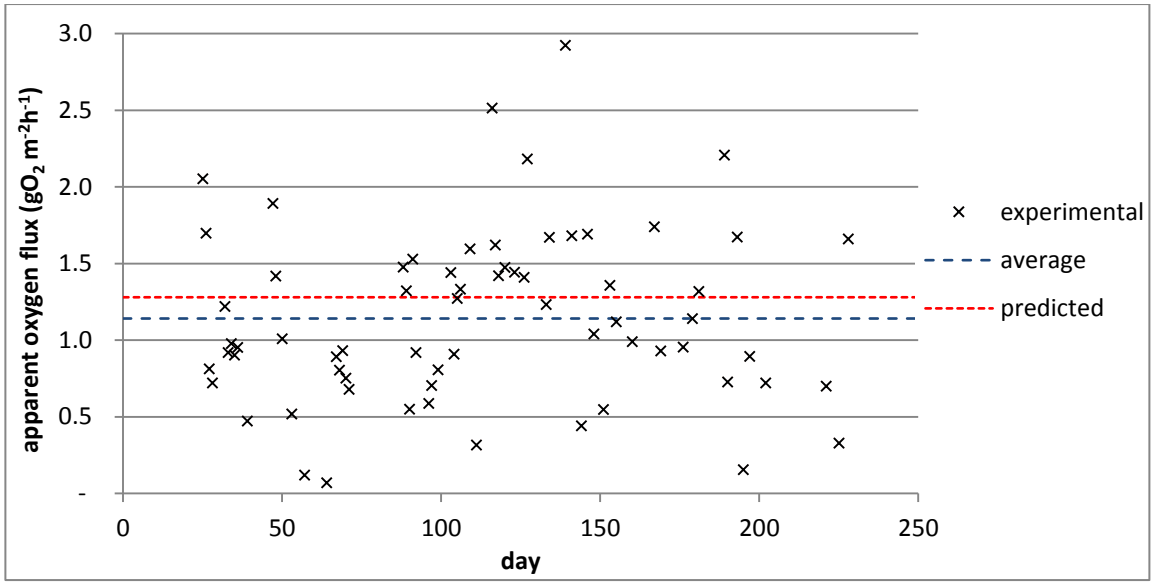

Figure 6-6: Apparent oxygen flux during Runs 8-12

In Figure 6-6 the red dashed line represents the oxygen flux as predicted by Equation 5-11 developed in the previous chapter. The average oxygen fluxes obtained experimentally and obtained through use of the previously developed relationships are summarised in Table 6-4.

Table 6-4: Obtained and predicted average oxygen fluxes

	Sample average	Equation 5-11	Equation 5-12
Oxygen flux ($gO_2\ m^{-2}h^{-1}$)	1.15	1.28	1.27

Various reasons exist as to why some of the experimentally obtained oxygen fluxes are higher than predicted, in addition to errors of analysis. Sloughing events, where areas of biofilm become detached from the membrane, occur periodically (Chambless & Stewart, 2007). These detachment events leave areas of the membrane temporarily exposed; greater oxygen transfer then occurs through the exposed membrane and is utilised by both the biofilm and free swimming bacteria, contributing to pollutant removal.

Several studies (e.g. Pankhania *et al.*, 1999) have reported a drop in performance associated with the development of thick biofilms, and as such prevention of excessive

biofilm growth in membrane attached biofilm reactors has become the focus of several researchers (e.g. Hwang *et al.*, 2010).

Figure 6-6 shows no evidence of the existence of a relationship between apparent oxygen flux changing influent composition over the duration of the 230 days in question. The absence of a discernible trend implies that influent concentration has negligible effect on the thickness and density of a biofilm associated with an aeration membrane over the range of wastewater compositions used in this study.

The average oxygen fluxes obtained during each of the experimental runs in question in this chapter are shown in Table 6-5 below. The average values were obtained using median analysis as in Chapter 5 to allow for uneven data sizes.

Table 6-5: Average oxygen fluxes in runs 8-12

Run	8	9	10	11	12
Oxygen flux ($gO_2\ m^{-2}h^{-1}$)	1.22	1.28	1.62	1.85	1.28

Performing an ANOVA on this data reveals that there is no statistically significant effect of wastewater composition on the obtained oxygen flux. This is important to the model development described in Section 6.3, as it justifies that oxygen flux can be related to intra membrane pressure (Casey *et al.*, 2000b), over the range of wastewater compositions used in this study.

6.2.2 Relative oxygen consumption

In the MABfR, oxygen is consumed as a result of aerobic heterotrophy and aerobic nitrification. Recent experimental (Meng *et al.*, 2008) and modelling studies (Matsumoto *et al.*, 2007) based on the operation of a MABfR in plug flow mode, have proposed that

the relative consumption of oxygen in an oxygen limited situation is controlled by the influent COD:N ratio.

Using the stoichiometric relationships developed in Chapter 5, the rates of aerobic heterotrophy and nitrification can be estimated in the same way that was previously used to obtain the oxygen uptake rate (OUR) and hence oxygen flux. This data is displayed in Table 6-6.

Table 6-6: Rates of microbial processes and oxygen uptake (mean values, standard errors)

	Run	8	9	10	11	12
$g\ m^{-2}day^{-1}$	r_{nit}	1.92±0.07	1.64±0.07	1.28±0.21	1.59±0.21	1.83±0.25
	OUR_{nit}	8.53±0.33	7.32±0.30	5.72±0.96	7.06±0.94	8.14±1.13
	r_{AH}	9.8±1.1	11.5±1.6	9.9±1.5	19.8±1.8	12.8±1.7
	OUR_{AH}	20.3±2.2	23.5±3.4	20.4±3.1	40.9±3.7	26.6±3.6

From the data displayed in Table 6-6, the fraction of oxygen supplied utilised by aerobic heterotrophs can be found using Equation 6-1.

$$f_{AH} = \frac{OUR_{AH}}{(OUR_{AH} + OUR_{nit})} \qquad \textbf{Equation 6-1}$$

Where: f_{AH} = Fraction of oxygen utilized by aerobic heterotrophs

Table 6-7 displays the fraction of supplied oxygen at the five different COD:ammoniacal nitrogen ratios used in this section of the investigation. The COD:ammoniacal nitrogen ratio is calculated using Equation 6-2.

$$COD/N_{ratio} = \frac{[COD_{inf}]}{[Amm - N_{inf}]}$$ **Equation 6-2**

Where: COD/N_{ratio} = COD:ammoniacal nitrogen ratio

$[COD_{inf}]$ = Influent COD concentration (mg l^{-1})

$[Amm\text{-}N_{inf}]$ = Influent Ammoniacal nitrogen concentration (mg l^{-1})

Table 6-7: Oxygen usage in Runs 8-12 (mean values)

Run	COD/N_{ratio}	f_{AH}	f_{nit}
8	5.6	0.70	0.30
9	7.0	0.76	0.24
10	9.9	0.78	0.22
11	14.4	0.85	0.15
12	9.1	0.77	0.23

The data presented in Table 6-7 and plotted in Figure 6-7, illustrates the relationship between the fraction of supplied oxygen utilised by aerobic heterotrophs and COD:N ratio.

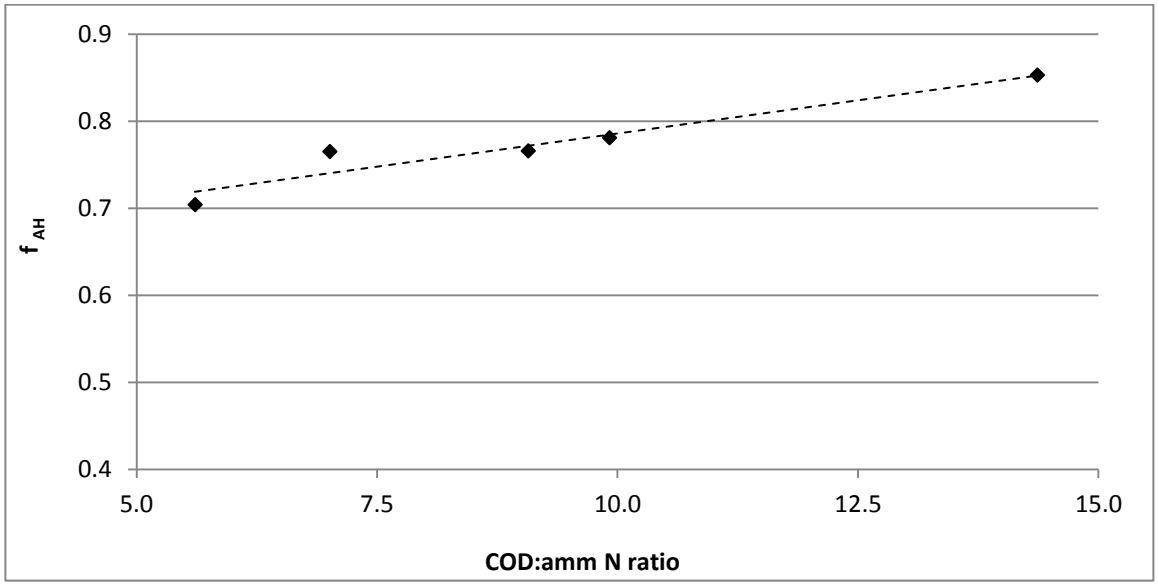

Figure 6-7: fraction of supplied oxygen utilized by aerobic heterotrophs at different COD:Amm-N ratios

The linear trend visible in Figure 6-7 suggests that the COD:N ratio also controls the relative consumption of oxygen in a mixed flow reactor, as used in this study. A higher fraction of oxygen is utilised by aerobic heterotrophs at higher COD:N, where their higher growth rates allow them to outcompete nitrifiers for oxygen and space in the biofilm structure (Zhang *et al.*, 1995).

Linear regression of the data in Figure 6-7 yields the empirical relationship Equation 6-3 with a correlation fit coefficient of 0.92.

$$f_{AH} = 0.016(COD/N_{ratio}) + 0.63$$ **Equation 6-3**

Where: f_{AH} = Fraction of supplied oxygen utilised by aerobic heterotrophs

COD/N ratio = gCOD per g Amm-N in influent media

Although the high correlation coefficient implies that Equation 6-3 describes well the fraction of oxygen used by the competing bacteria types over the range of COD/N ratios used in the investigation, it is only a linear approximation based on the data generated by this study. Microbial kinetics are complicated non-linear systems, and the relationship presented in Equation 6-3 is an estimation of the performance of the MABfR over the range of wastewaters used in this study.

With hindsight, the COD/N range used in the investigation should have been expanded in order to obtain the limits of applicability of the developed relationship, and to ascertain experimentally, if practicable, the loading ratio at which aerobic heterotrophs will completely outcompete nitrifiers for oxygen. This however, was not possible given the time constraints placed upon the project, and forms the basis of a section of suggested future work.

6.2.3 Denitrification

The denitrification rates obtained in Runs 8-12 are shown in Table 6-8.

Table 6-8: Denitrification rates in runs 8-12 (mean values, standard errors shown)

Run	8	9	10	11	12
Denitrification rate ($gN\ m^{-2}day^{-1}$)	1.42±0.10	1.10±0.20	0.40±0.19	0.61±0.12	1.26±0.33

Table 6-8 shows that the rate of denitrification rates achieved during stable operation falls in the range 0.40 – 1.42 $gN\ m^{-2}day^{-1}$. This compares favourably with the limited number of studies of denitrification in a MABfR contained in literature, as seen in Table 6-9.

Table 6-9: Comparison of denitrification rates

Author	Denitrification rate $gN\ m^{-2}day^{-1}$	Nitrification rate $gN\ m^{-2}day^{-1}$
Timberlake *et al*. (1988)	0.1 – 0.6	0.1 – 0.6
Semmens *et al*. (2003)	2.0	2.0
Satoh *et al*. (2004)	0.12 – 0.33	0.50
Downing & Nerenberg (2008a)	0.23 – 0.32	0.40 – 1.30
This study	0.40 – 1.42	1.28 – 1.92

In the majority of MABfR studies included in Table 6-9, including this study, the denitrification rate approaches the nitrification rate. Denitrification was reported to proceed at the same rate as nitrification by Timberlake *et al*. (1988) and Semmens *et al*. (2003), in reactors with effluent COD/TOC concentrations in the range 30-50 mg l^{-1}, implying that denitrification is controlled by nitrate availability.

The denitrification rates observed in this study are higher than those reported by Timberlake *et al*. (1988) and Downing & Nerenberg (2008a). Both studies reported that denitrification proceeded at the same rate at which nitrate was produced via nitrification.

A higher rate (~2.0 gN/m^{2}day) was reported by Semmens *et al*. (2003) in a reactor operated with higher strength wastewater than used in this study.

As stated previously, there has been limited research undertaken into the factors affecting denitrification in bacterial films. In addition to the studies discussed above, a kinetic study using sequential aerobic and anoxic reactors (for nitrification and denitrification, respectively), with denitrifying bacteria immobilised on support packing, found that the highest denitrification rates were obtained at the highest ammoniacal nitrogen loading rates (Dincer & Kargi, 2000). The authors attributed this to the greater availability of NO_x-N (nitrite and nitrate) to denitrifying bacteria in the anoxic reactor. Organic carbon loading has been found to only control the denitrification rate in situations when this pollutant loading was insufficient to obtain complete denitrification (Downing & Nerenberg, 2008b).

Figure 6-8 shows the effect of available nitrate on the denitrification rates obtained during runs 8-12 and runs 1-7, examined in the previous chapter. Available nitrate concentrations are calculated from influent nitrate loading and nitrification rate, as based on Equation 5-6 and shown below (Equation 6-4).

$$NO_3^- - N_{available} = L_{NO_3^- - N} + 0.992 r_{nit} \qquad \textbf{Equation 6-4}$$

Where: NO_3^--$N_{available}$ = Total available nitrate nitrogen (g m^{-2}day^{-1})

$L_{NO_3^- - N}$ = Nitrate nitrogen loading (g m^{-2}day^{-1})

r_{nit} = Nitrification rate (gN m^{-2}day^{-1})

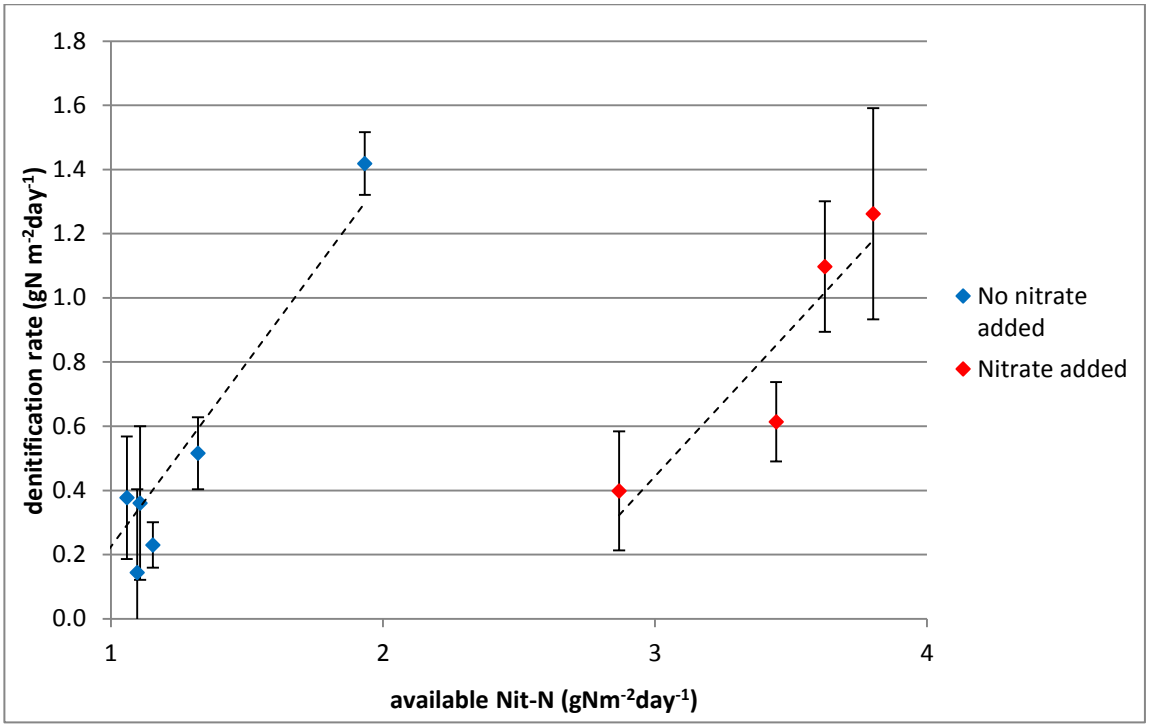

Figure 6-8: Variation of denitrification rates with nitrate availability (standard error bars)

Denitrification rates in the range 0.08 – 1.42 $gNm^{-2}day^{-1}$ were achieved. In general, the higher rates were obtained when nitrate was added to the feed mixture and nitrate availability was highest (Runs 9-12), but the highest rate was obtained in Run 8, when the reactor was operated at 12 hour HRT but with no nitrate in the feed.

The data displayed in Figure 6-8 is grouped in two separate groups; the group on the left corresponding to Runs 1-8, when no nitrate was added to the synthetic wastewater and the second group corresponding to Runs 9-12 when nitrate was added to the influent.

Linear regression was used on each of these groups and in turn yielded Equation 6-5 and Equation 6-6. This decision has neither basis in theory nor precedent in literature, but was taken to fit the data generated by the investigation. The empirical relationships have correlation coefficients of 0.91 and 0.85 respectively.

No nitrate added to feed: $$r_{den} = 1.15(NO_3^- - N_{available}) - 0.92$$ **Equation 6-5**

Nitrate added to feed: $$r_{den} = 0.92(NO_3^- - N_{available}) - 2.30$$ **Equation 6-6**

Where r_{den} = Denitrification rate (gN $m^{-2}day^{-1}$)

Despite the relatively poor fit coefficients, Equation 6-5 and Equation 6-6 adequately describes the data obtained from Runs 1-8 and 9-12 respectively. As with Equation 6-3, it cannot be suggested that these equations hold for all values of available nitrate loadings, but they are an adequate approximation of the system studied here.

The emergence of separate equations to describe the denitrification performance of the MABfR in the two different circumstances above implies that there is a difference in the availability of nitrate to denitrifiers between nitrate produced by nitrification and commercially produced nitrate as used in the synthetic wastewater used in this study.

This difference is without precedent in the literature and there is no evidence in the experimental results or in the literature to suggest that the addition of potassium ions (as KNO_3) has an inhibitory effect on denitrification. As removal of nutrients from WwTW effluents becomes of greater importance as the Water Framework Directive is fully implemented, further study of the factors controlling denitrification is likely to be required.

6.3 Model development

Modelling of biofilms and biofilm systems has been a major focus of recent biofilm research (e.g. Matsumoto *et al.*, 2007, Lackner *et al.*, 2008). Many of the models are extremely complex, require specialised software to be computed (e.g AQUASIM), and, although the modelling predictions are in very good agreement with experimental results, their complexity limits their applicability in 'real' applications.

The model presented here uses a 'black box' approach; compromising the accuracy of the model in favour of producing a model with applicability for a range of wastewater compositions.

6.3.1 Assumptions

1. **Oxygen transfer is controlled by gas side pressure.**
   Wastewater strength does have an effect on the structure and therefore oxygen permeability of biofilms (Bishop *et al.*, 1995). However, the effect is not significant over the range of wastewater compositions considered here, as shown by the results presented in Chapter 5. A similar conclusion was drawn by Casey *et al*. (2000b) from their work with Xylene degradation in a MABfR.

2. **Oxygen supplied by the membrane is completely consumed by the biofilm.**
   Dissolved oxygen concentrations of the bulk liquid were periodically measured and monitored during changes to the experimental setup. During steady operation, the bulk oxygen concentration showed little variation with values <0.1 mg l^{-1}.

3. **COD is consumed only by aerobic heterotrophy and denitrification.**
   Although it is possible for anaerobic niches to occur within the biofilm, no dark precipitates or distinctive odours were observed throughout the operation of the reactor, and, as such, any anaerobic activity can be considered negligible (Timberlake *et al.*, 1988).

4. **Ammoniacal nitrogen is consumed only by aerobic autotrophic respiration and cell synthesis in autotrophic respiration and aerobic heterotrophy.**
   Ammoniacal nitrogen removal by adsorption onto membrane tubing or the walls of the tank is negligible.

5. **Nitrogen for cell synthesis**

   Nitrogen required for cell synthesis is provided by ammoniacal nitrogen for both nitrifiers and aerobic heterotrophy (McCarty, 1975). Nitrate is used both as an oxygen source and nitrogen source by denitrifiers (Madigan & Martinko, 2006).

6. **Biomass washout is negligible.**

   Biomass does leave the reactor in the effluent, as evidenced by the slightly turbid nature of the effluent. However this turbidity was consistently low throughout the operation of the reactor (<10 NTU), and therefore is indicative of a low solids concentration in the effluent which can be considered negligible in comparison to the biomass concentration on the surface of the membrane.

7. **Biofilm is in a pseudo steady state**

   Although a biofilm is complex, dynamic system, with cell synthesis and death constantly occurring, in an oxygen limited biofilm the growth rates are limited by oxygen and substrate availability rather than biomass availability. As such, mature populations are in a pseudo steady state where the net growth and net death rates are equal.

8. **Dead biomass forms soluble COD, Amm-N and detritus.**

   For every gram of biomass that dies, 0.2 g of detritus is formed, with 0.8 g being made available in the liquid phase. This contributes a COD of 0.53 g and 0.12 g of ammoniacal nitrogen. A similar assumption was made in the modelling work of Shanahan & Semmens (2004).

6.3.2 Model inputs

Average oxygen flux:

$$\bar{J} = 0.28P_{av(abs)} + 0.22$$ **Equation 5-12**

Fraction of oxygen consumption:

$$f_{AH} = 0.016(COD/N_{ratio}) + 0.63$$ **Equation 6-3**

$$f_{nit} = 1 - f_{AH}$$ **Equation 6-7**

Oxygen uptake rates:

$$OUR_{AH} = f_{AH}\bar{J}$$ **Equation 6-8**

$$OUR_{nit} = f_{nit}\bar{J}$$ **Equation 6-9**

Denitrification rate:

No nitrate added to feed: $r_{den} = 1.15(NO_3^- - N_{available}) - 0.92$ **Equation 6-5**

Nitrate added to feed: $r_{den} = 0.92(NO_3^- - N_{available}) - 2.30$ **Equation 6-6**

Pollutant loading rates are used for dimensional consistency with oxygen flux and are calculated as detailed in Chapter 3 (Timberlake *et al.*, 1988).

$$L_s = \frac{C_{\inf}}{a(HRT)}$$ **Equation 3-4**

Reaction rates are then calculated from the equations above and mass ratios developed from the stoichiometric relationships derived in Chapter 5. The relationships between each reaction rate is shown in Table 6-10 (By convention, a species being consumed by a reaction is designated with a minus sign).

From the calculated reaction rates, the effluent concentrations of each of chemical species of interest can be calculated. These effluent ‘loadings’ can then be converted to effluent concentrations using Equation 6-10 , a rearranged form of Equation 3-4

$$C_{eff} = L_{eff}\, a(HRT)$$ **Equation 6-10**

Table 6-10: Relationships used to calculate reaction rates in MABfR model

Species / Process	O_2	$\{CH_2O\}$	NH_4^+-N	NO_3^--N	X (biomass)
Aerobic heterotrophy	$-OUR_{AH}$	$-0.483(OUR_{AH})$	$-0.0072(OUR_{AH})$		$0.0582(OUR_{AH})$
Nitrification	$-OUR_{nit}$		$-0.225(OUR_{nit})$	$0.223(OUR_{nit})$	$0.0254(OUR_{nit})$
Denitrification		$-2.85(r_{den})$		$-r_{den}$	$0.065(r_{den})$

6.4 Model validity

6.4.1 Normalised standard deviation method

The validity of the developed model was assessed by using a modified form of the normalised standard deviation (NSD) method introduced by O'Neill *et al*. (2009). The NSD for the removal of each relevant component (COD, Ammoniacal Nitrogen and Total Nitrogen) was calculated using Equation 6-11:

$$NSD(\%) = 100\frac{\sqrt{\left(\sum_{i=1}^{n}\left(\frac{\left(C_{j,\exp,i} - C_{j,calc,i}\right)}{C_{j,\exp,i}}\right)^2\right)}}{n-1} \qquad \textbf{Equation 6-11}$$

Where: n = number of experimental runs considered

$C_{j,exp,i}$ = effluent concentration of component j ascertained experimentally for experimental run i

$C_{j,calc,i}$ = effluent concentration of component j calculated using the model for experimental run i

The experimental and calculated effluent concentration values for COD, Ammoniacal Nitrogen and Total Nitrogen are given in Table 6-11, Table 6-12 and Table 6-13 respectively; alongside the influent concentration and percentage error for comparative purposes. The percentage errors are calculated using Equation 6-12:

$$error(\%) = \frac{\left|C_{j,\exp,i} - C_{j,calc,i}\right|}{C_{j,\inf,i}} \qquad \textbf{Equation 6-12}$$

$C_{j,inf,i}$ = influent concentration of component j for experimental run i

The influent, experimental effluent and calculated COD concentrations for Runs 1-12 are shown in Table 6-11.

Table 6-11: Experimental and calculated COD concentrations for Runs 1-12

Run	Average COD concentration			
	Influent ($mg\ l^{-1}$)	Experimental effluent ($mg\ l^{-1}$)	Calculated effluent ($mg\ l^{-1}$)	Error (%)
1	70	29	31	2.8
2	72	27	31	5.6
3	71	32	28	5.6
4	71	29	26	4.2
5	73	30	26	5.5
6	73	24	23	1.4
7	72	16	14	2.8
8	66	27	28	1.5
9	71	30	34	5.6
10	71	41	37	5.6
11	116	57	80	19.8
12	69	24	32	11.6

NSD (%) = 5.7

A significant error between the experimentally determined and calculated COD concentration can be seen for Run 11 (19.8%), with the experimental value being significantly lower than that which is predicted by the model. As seen in Table 6-4, the apparent oxygen flux for this experimental run was significantly larger than that predicted by Equation 5-12, which is used to obtain the oxygen flux as part of the model. The error between the calculated and experimental COD removal can therefore be attributed to this higher than normal oxygen availability. Considering the values for Run 11 as rogue and omitting them when calculating the NSD gives a reduced value of 4.8% for COD removal.

The influent, experimental effluent and calculated ammoniacal nitrogen concentrations for Runs 1-12 are shown in Table 6-12.

Table 6-12: Experimental and calculated Amm-N concentrations for Runs 1-12

Run	Average Ammoniacal nitrogen concentration			
	Influent ($mg\ l^{-1}$)	Experimental effluent ($mg\ l^{-1}$)	Calculated effluent ($mg\ l^{-1}$)	Error (%)
1	9.72	5.23	3.82	14.5
2	9.31	3.24	3.40	1.7
3	9.40	3.38	3.21	1.9
4	9.56	3.22	3.17	0.5
5	9.82	4.02	3.22	8.1
6	8.07	4.00	1.75	27.9
7	9.49	2.23	1.76	5.0
8	11.72	6.43	6.39	0.3
9	10.10	5.56	5.19	3.7
10	7.16	3.61	3.09	7.3
11	8.11	3.73	5.35	20.0
12	7.59	2.55	3.29	9.7

NSD (%) = 7.6

As with COD removal in Table 6-11, higher than predicted ammoniacal nitrogen removal was obtained in Run 11. Again this can be attributed to the higher than expected oxygen flux which was experienced during the duration of this experimental run. Omitting this run in calculation of the NSD yields a NSD of 6.2%.

In Chapter 5, it was discussed how the nitrification and denitrification rates observed during run 6 were not in accordance with the trend seen as inlet pressure was increased. Although the cause of this was not known, the same cause can be attributed to the significant error seen in Table 6-12 for Run 6. Also ignoring this run in calculation of the NSD gives a further reduction in the NSD value to 5.0%.

The influent, experimental effluent and calculated total nitrogen concentrations for Runs 1-12 are shown in Table 6-13.

Table 6-13: Experimental and calculated Tot-N concentrations for Runs 1-12

Run	Average Total Nitrogen concentration			
	Influent ($mg\ l^{-1}$)	Experimental effluent ($mg\ l^{-1}$)	Calculated effluent ($mg\ l^{-1}$)	Error (%)
1	9.8	9.4	8.0	13.5
2	9.4	7.4	7.6	2.5
3	9.5	8.6	7.4	13.0
4	9.7	8.3	7.3	10.9
5	9.9	7.8	7.3	4.6
6	8.2	7.6	5.9	21.2
7	9.6	6.7	5.7	10.6
8	11.8	7.8	8.2	3.0
9	15.6	12.6	12.4	1.1
10	11.6	10.4	10.1	2.8
11	13.3	11.5	12.4	6.2
12	13.1	9.6	10.4	6.4

NSD (%) = 5.0

It can be seen from Table 6-13 that there is better agreement between experimental and calculated total nitrogen concentrations for experimental runs 8-12 in comparison to runs 1-7. As discussed previously in Chapter 5, the duration of runs 1-7 was extended to obtain oxygen limitation, not to achieve steady pollutant removal. This is likely to be the cause of the greater error between calculated and experimental results.

As with ammoniacal nitrogen, considering the calculated results for Runs 6 and 10 to be rogue reduces the NSD to 3.3%.

Table 6-14 summarises the percentage NSDs obtained from the model for each of the experimental runs.

Table 6-14: Adjusted NSD (%)

Component	Adjusted NSD (%)
Chemical Oxygen Demand	4.8
Ammoniacal Nitrogen	5.0
Total Nitrogen	3.3

As seen above, removing results which are considered erroneous means than an NSD of 5.0% or lower is obtained for each of COD, Ammoniacal nitrogen and Total nitrogen. The authors that introduced this method considered an NSD of lower than or equal to 6.5% to be considered a good fit (O'Neill *et al.*, 2009), which indicates that the model presented here is a good description for the operation of the MABfR used in this study.

6.4.2 Sensitivity analysis

In addition to the use of the NSD method introduced by O'Neill *et al*. (2009), a sensitivity analysis was also carried out. This facilitated the examination of predicted effluent concentrations from the MABfR at conditions at which the unit was not operated during the experimental work.

These predicted concentrations could then be compared to models in other published work, allowing the model validity to be examined qualitatively in addition to the quantitative model fit measurement obtained from the NSD method.

The effect of changing inlet pressure, influent COD, ammoniacal nitrogen and nitrate nitrogen concentration was considered in the sensitivity analysis.

6.4.2.1 Effect of changing gas side pressure

The effect of changing inlet pressure (and hence oxygen flux) on effluent concentrations of COD, ammoniacal nitrogen and nitrate nitrogen is shown in Figure 6-9. The effluent

concentrations are calculated from the presented model based on an influent containing 60 mg l^{-1} COD, 10 mg l^{-1} (as N) Ammoniacal nitrogen and 5 mg l^{-1} (as N) nitrate nitrogen, and with the MABfR being operated using a 12 hour HRT.

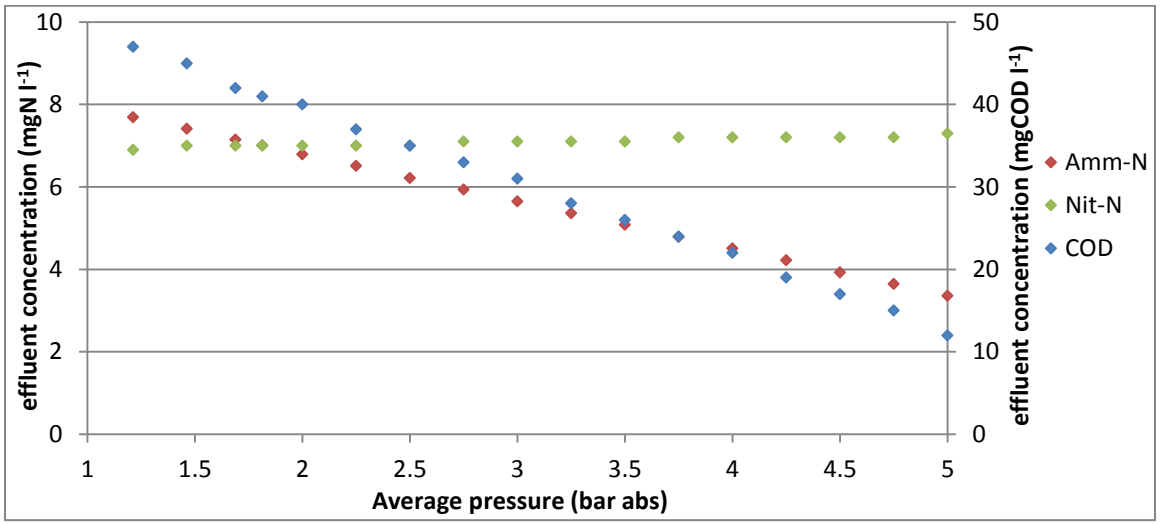

Figure 6-9: Sensitivity analysis for inlet pressure

As expected, increased inlet pressure leads to a decrease in the effluent concentration of COD and ammoniacal nitrogen – the wastewater components which require oxygen for removal. Effluent COD concentration decreases more strongly than effluent ammoniacal nitrogen concentration as it is removed by both aerobic heterotrophy and denitrification.

Effluent concentration of nitrate nitrogen is relatively insensitive with effluent concentrations varying only between 6.9 and 7.3 mg l^{-1}. At higher inlet pressures, more ammoniacal nitrogen is converted to nitrate nitrogen, but this higher availability of nitrate increases the rate of nitrate consumption by denitrification.

This is of interest for design of a full scale unit as total nitrogen consents are introduced in eutrophication sensitive areas as part of the full implementation of the Water Framework Directive.

6.4.2.2 Effect of changing influent ammoniacal concentration

Figure 6-10 shows the effect on changing influent ammoniacal nitrogen concentration on the calculated effluent concentrations of ammoniacal nitrogen, nitrate nitrogen and COD. The effluent concentrations are calculated based on an inlet pressure of 3 bar, with influent COD concentration of 60 mg l^{-1}, influent nitrate nitrogen 5 mg l^{-1} and a 12 hour HRT.

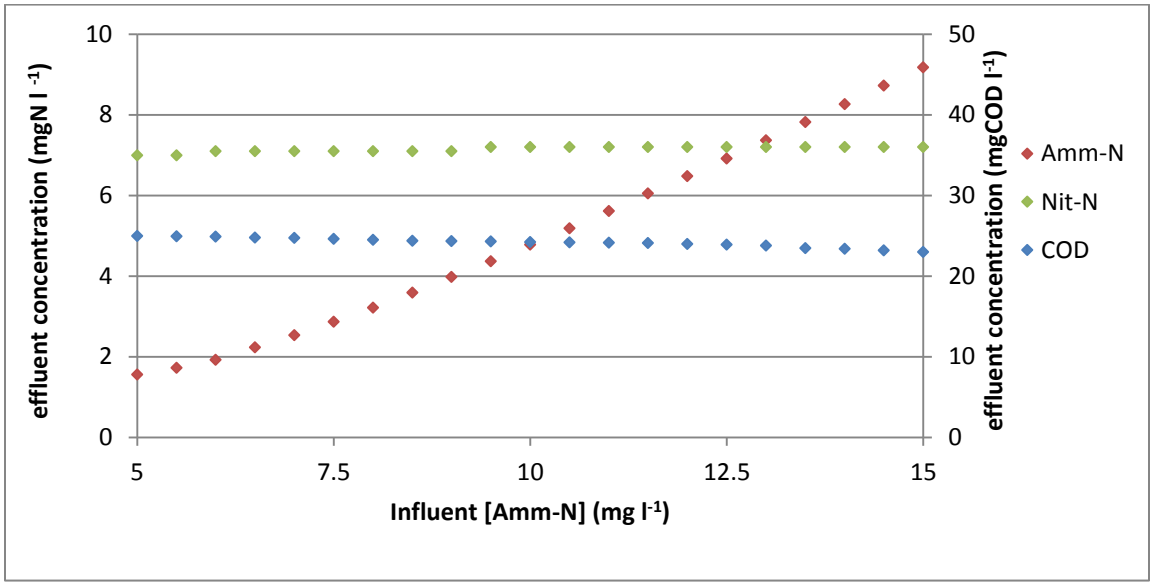

Figure 6-10: Sensitivity analysis for influent ammoniacal nitrogen concentration

Influent ammoniacal nitrogen concentration has little or no effect on the effluent concentration of COD or nitrate nitrogen, with effluent concentrations in the range 23 - 25 mgCOD l^{-1} and 7.0 – 7.2 mgN l^{-1}.

Under increasing ammoniacal nitrogen loading, the shift in the COD:N ratio means that more of the oxygen supplied by the membrane is consumed by nitrification (Equation 6-6 & Equation 6-7). This leads to an increase in the availability of nitrate nitrogen and an associated increase in the rate of denitrification, which has a regulatory effect on the effluent COD and nitrate nitrogen concentrations.

6.4.2.3 Effect of changing influent COD concentration

Figure 6-11 illustrates the effect of changing influent COD concentration on calculated effluent concentrations of ammoniacal nitrogen, nitrate nitrogen and COD. The effluent composition is calculated based on an inlet pressure of 3 bar, with influent concentrations of 10 mg l^{-1} ammoniacal nitrogen and 5 mg l^{-1} nitrate nitrogen and a HRT of 12 hours.

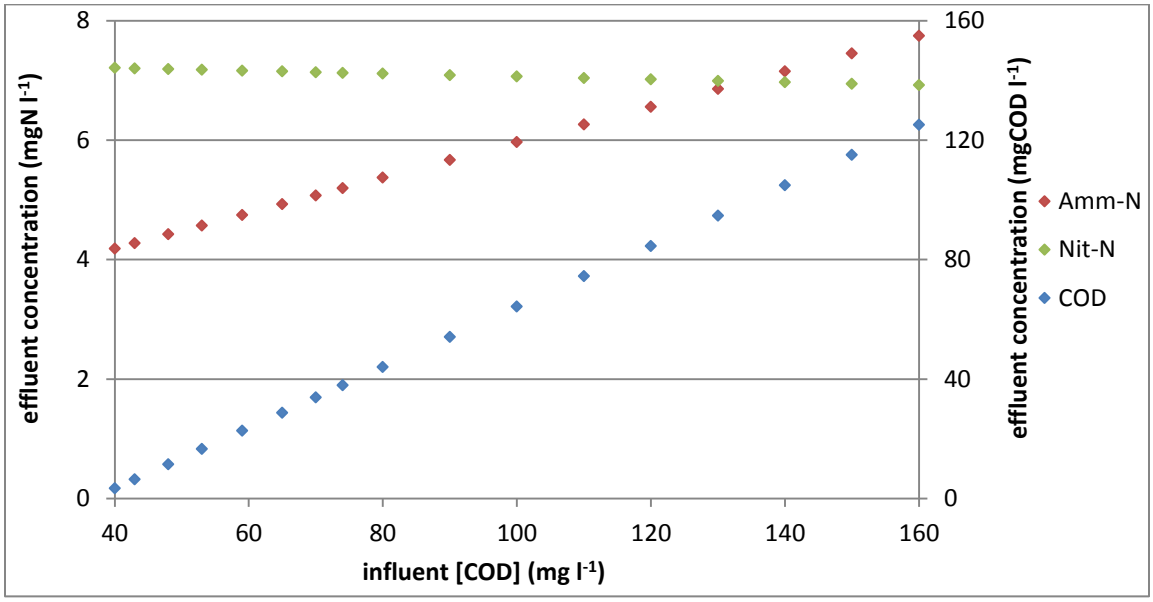

Figure 6-11: Sensitivity analysis for influent COD concentration

The effluent concentrations of both COD and ammoniacal nitrogen increase with increasing influent COD concentration. In the case of COD, this can be attributed to the increased influent concentration, and for ammoniacal nitrogen it is due to less oxygen being consumed by nitrifying bacteria in line with Equation 6-6 and Equation 6-7.

As with changing ammoniacal nitrogen, changing influent COD has little effect on the effluent nitrate nitrogen concentration with calculated values obtained in the range 6.9 – 7.2 mg l^{-1}. This is due to a combination of higher denitrification rates at low COD loadings and less nitrification at higher COD loadings.

6.4.2.4 Effect of changing influent nitrate concentration

The effect of influent nitrate-nitrogen on the calculated effluent pollutant concentrations is shown in Figure 6-12. The effluent concentrations are calculated based on an inlet pressure of 3 bar, with influent COD concentration of 60 mg l^{-1}, influent ammoniacal nitrogen concentration of 5 mg l^{-1} and a 12 hour HRT.

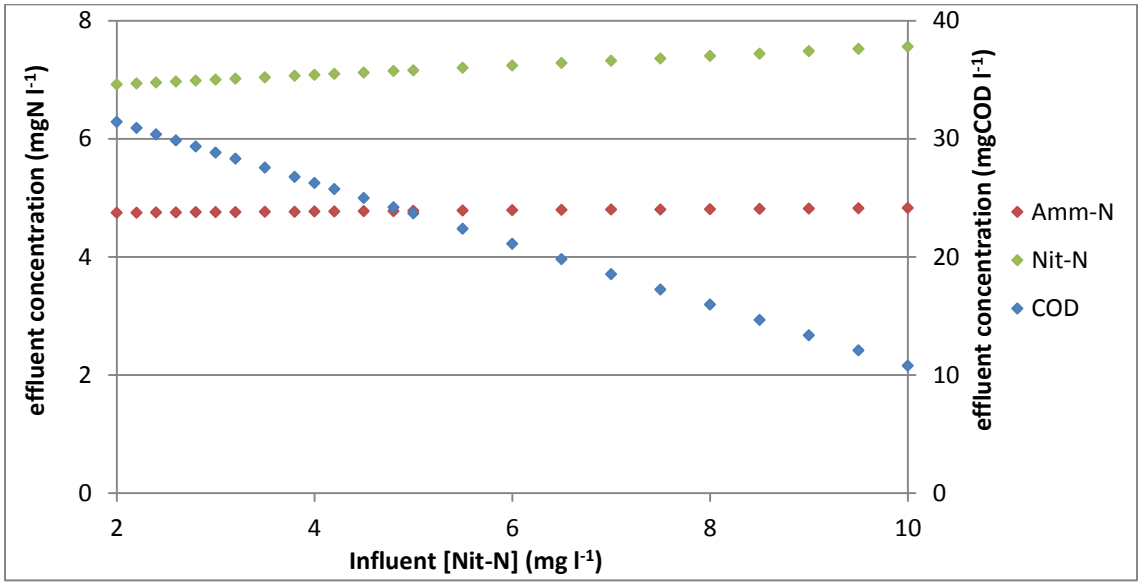

Figure 6-12: Sensitivity analysis for nitrate nitrogen

The effluent concentrations of both nitrate nitrogen and ammoniacal nitrogen are insensitive to influent nitrate nitrogen concentrations, with only small increases visible for both effluent concentrations. The fraction of available oxygen utilised by nitrification is independent of nitrate concentration (Equation 6-3), therefore ammoniacal nitrogen concentration is unaffected.

In accordance with Equation 6-8, the denitrification rate increases with increasing available nitrate concentration, with a proportionality of 0.92; accounting for the almost horizontal trend in effluent nitrate concentrations predicted by the model. A decrease in the effluent COD concentration is observed, as 2.85 g of COD is consumed by denitrification of each gram of nitrate nitrogen.

6.5 Conclusions

The MABfR was successfully operated for a period of 230 days at a HRT of 12 hours using a range of wastewater compositions to examine the effect of pollutant loadings on pollutant removal. The data generated allowed the formation of empirical equations which adequately described the results obtained with the range of pollutant loadings used here.

These empirical equations were utilised, in conjunction with established theory and other published research to develop a simple model which predicts the performance of the MABfR when operated over a range of inlet pressures and wastewater compositions.

However, the limit of operation over which the model is valid was not ascertained. Establishing these limits are a suggestion for further work in this area.

7 Design and operation of a pilot-scale BioSettler^{TM}

Chapter 5 and Chapter 6 have demonstrated the ability of a MABfR to provide treatment to wastewaters with compositions similar to those found entering a secondary settling tank.

Using the data generated in Chapters 5 and 6, and drawing on best practice found in industry, a 1.5 m^3 pilot scale BioSettler^{TM} was designed and constructed, and operated at two municipal WwTWs in Northern Ireland.

7.1 Pilot scale design

Inclined plate settlers were first mooted by Hazen in the early twentieth century (1904), were introduced by the Swedish Company, Parkson Corporation, in the 1960s (Hendricks, 2006) and have now entered widespread use. Despite this, the complexity of the interactions between fluid and particles flows, and the large number of parameters affecting these flows, mean that no definitive design equations are in existence.

In the absence of such design equations, the design presented here draws on the limited published academic, industrial best practice and marketing literature, intended to be compliant with the closest relevant design standard (BSi, 2002a).

Following consultation with local steel fabricators (Stoneyford Engineering, Lisburn, U.K.), the CAD drawings shown in Figure 7-1 were prepared.

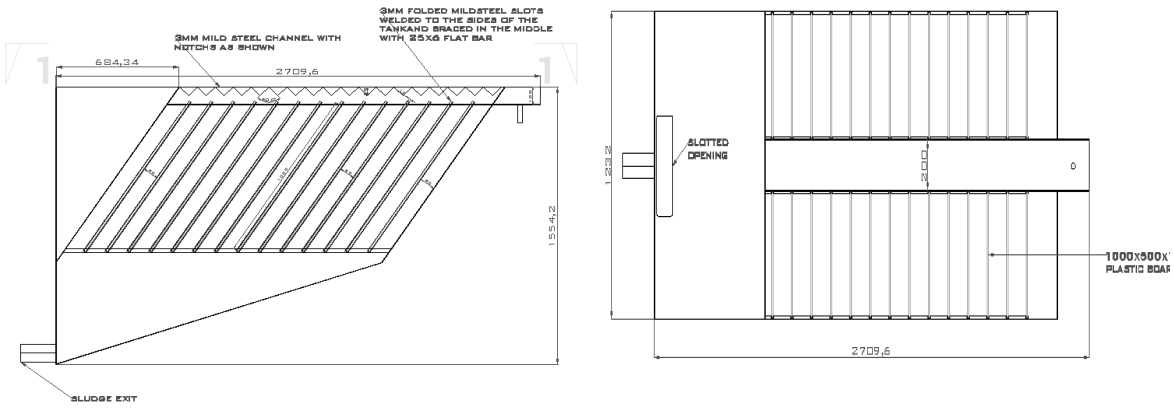

Figure 7-1: CAD diagrams – cross sectional (left) and bird's eye view

The prototype consists of three sections: an inlet zone, which acts in the same way as in a stilling box in conventional settler; a plate pack, where the settlement and treatment takes place; and a sludge collection zone, where settled sludge thickens and is removed from the unit by the action of a peristaltic pump.

The tank was constructed by Stoneyford Engineering (U.K.) in 6 mm mild steel, and protected by painting with suitable rust proof coating (Figure 7-2).

Figure 7-2: BioSettler prototype tank

Complete CAD diagrams and full details of the calculations are given in Appendix 3; a summary of the key dimensions is given in Table 7-1.

Table 7-1: Summary of prototype dimensions

Number of plate packs	2
Number of plates per pack	11
Area of plates	0.5 m^2
Plate angle	55° (above horizontal)
Settling volume	0.82 m^3
Inlet zone volume	0.35 m^3
Sludge collection volume	0.28 m^3
Angle of sludge collection zone	20° (above horizontal)
Total tank volume	1.45 m^3

7.1.1 Justification of design

7.1.1.1 Feed section

The purpose of the feed section in settling tanks is to dissipate the energy of the influent wastewater and evenly distribute the incoming flow over the two plate packs.

This is achieved in the BioSettler through a stilling section (the triangular section seen on the left hand side of the cross sectional CAD diagram in Figure 7-1), where the incoming flow is slowed. From there, it entered a channel between the two plate packs and was distributed between them, as illustrated in Figure 7-3.

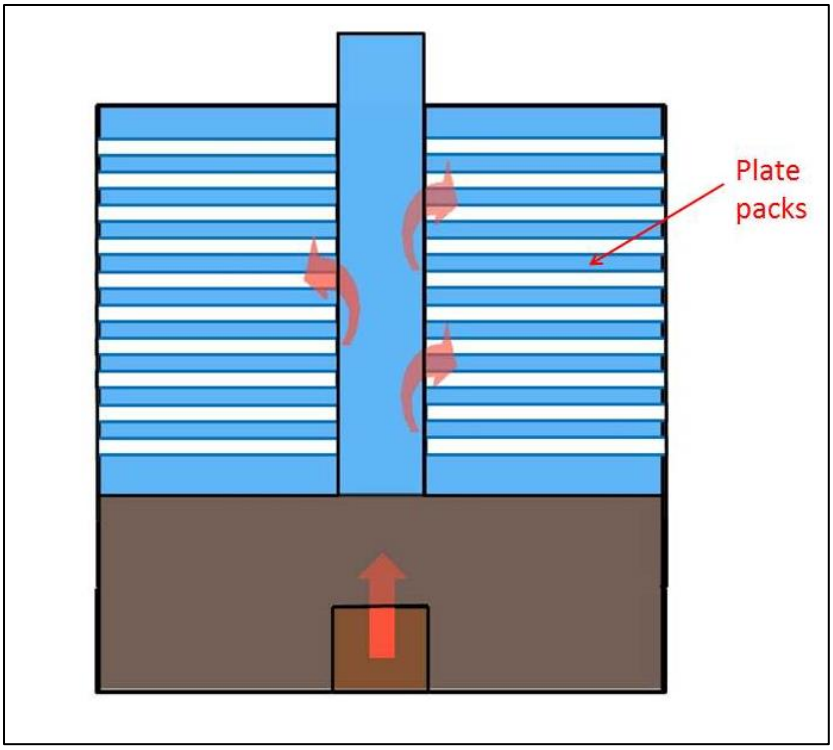

Figure 7-3: Inlet flow patterns

Pieces of PVC sheet were employed to force the influent to enter the plate in the lower 1/3 and prevent shortcutting.

7.1.1.2 Inclined plates

The selection of a plate spacing is a trade-off between solids removal and ease of operation; smaller plate spacings yield higher solid removal efficiencies (due to a reduction in the vertical distance a particle must fall to be removed from suspension), but also cause clogging of the flow channel between the two plates. As a compromise, a plate spacing of 1 - 3" (25 – 75 mm) is commonly employed (Metcalf & Eddy, 2003).

As illustrated in Figure 7-4, inclined plates lead to the formation of three discrete zones; a sludge layer, a mixed layer and a clarified layer. Although using a larger spacing means a longer residence time is required to achieve a specified degree of solids removal, this demand is compatible with the biological treatment supplied by the BioSettler, which improves with increasing HRT.

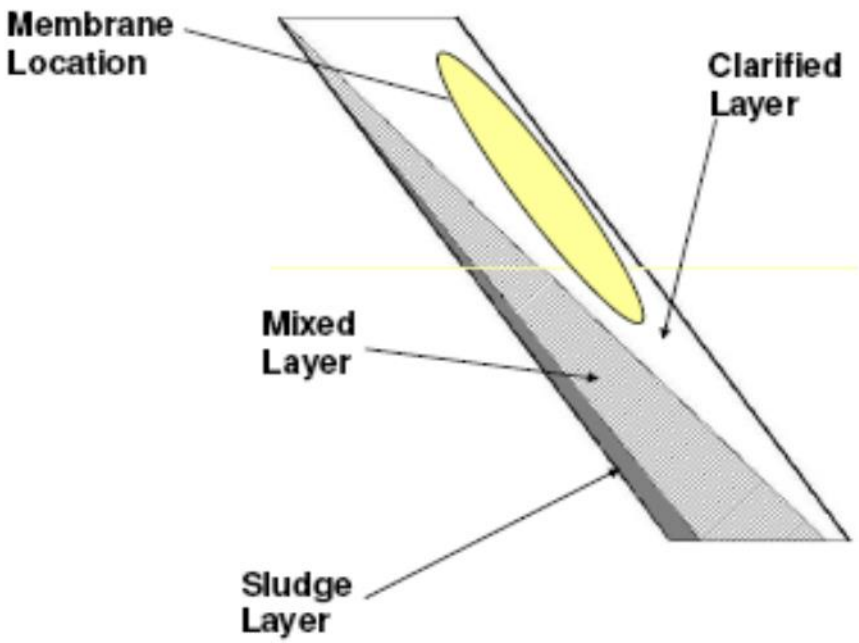

Figure 7-4: Membrane arrangement in BioSettler

In the BioSettler, a plate spacing of 90 mm, slighter higher than the industry standard, was used (Figure 7-5). This allowed the clarified layer to become large enough to accommodate the membrane module whilst reducing the likelihood of the membrane becoming fouled by solids.

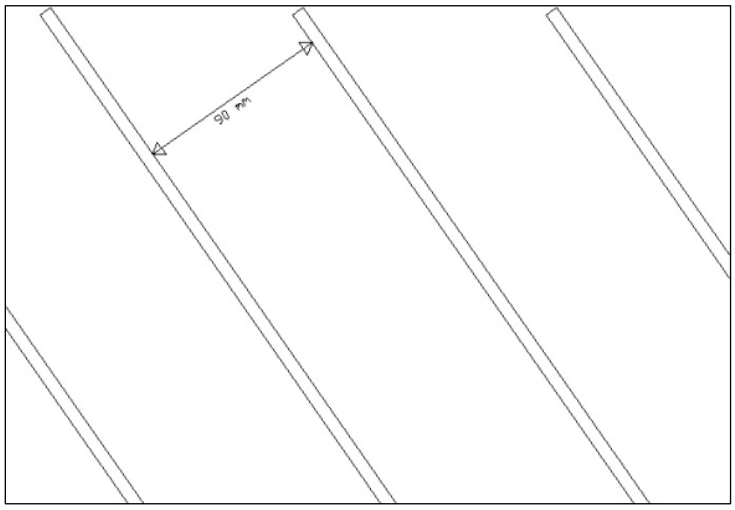

Figure 7-5: BioSettler plate spacing

7.1.1.3 Sludge collection section

In small settling tanks, where no scraper or suction mechanism is employed, it is standard industry practice to use tanks with floors angled at 50 - 60° above the horizontal (BSi, 2002a, BSi, 2002b). This allows sludge to thicken and effectively removed using gravity.

However, this was not possible in the design of the prototype BioSettler. Having a sludge collection zone angled at 50° above the horizontal would lead to a tank which was prohibitively high. Under health and safety regulations, a scaffold is required where work is to take place above head height (HMG, 2005). Provision of a scaffold was not possible within the project budget.

In order to meet the constraints of the budget, a tank with a floor sloped 20° above the horizontal was used. This gave a tank height of approximately 1.6 m, preventing the need for working above head height.

7.1.1.4 Effluent collection

Effluent was collected in a channel at the top of the tank, positioned between the two plate packs and fitted with v-notch weirs (Figure 7-6).

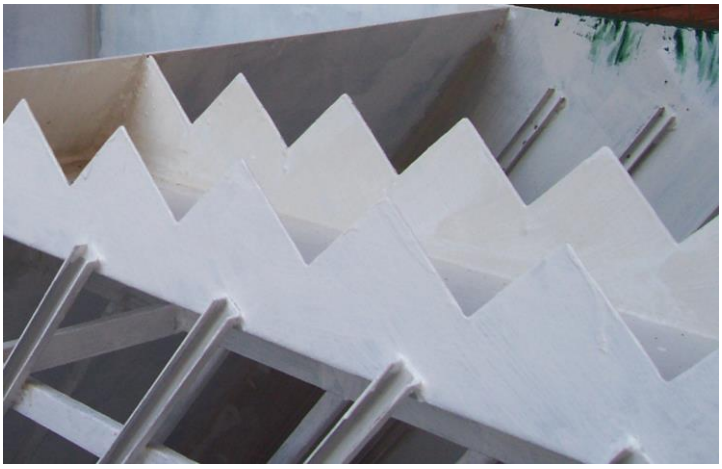

Figure 7-6: V-notch weirs in BioSettler tank

Once filled with liquid, the tank was levelled, ensuring that overflow was equal from all areas of the tank.

7.1.2 Membranes

In the experimental laboratory setups used in this project, long lengths of silicone rubber were wound around suitable frames to act as the membrane aerators. This arrangement was used due to simplicity of setups – only two hollow fibres had to be connected to the compressed air supply.

This setup, however, has two main drawbacks. Due the relatively large lengths of membranes required to obtain sufficient surface area to meet the oxygen transfer requirements and the number of bends required in order to wrap the tubing around their frame, the pressure drop was significant.

Additionally, using long lengths means that each individual hollow fibre has a greater surface area available for back diffusion of water vapour compared with shorter lengths, requiring greater air flowrate airflow to prevent condensation. This higher flowrate requirement and pressure drop mean that this arrangement is not practicable due to high operating costs.

Parallel flow, such as those used in the mass transfer experiments in this study, offers the highest average concentration driving force, and as such is preferable in situations where mass transfer is controlled by membrane mass transfer coefficient (Dindore *et al.*, 2005)
.
The work presented in Chapter 5 ascertained that, in the presence of a membrane attached biofilm, it is the biofilm which controls mass transfer. Cross-flow operation gives higher shell side mass transfer coefficients compared to parallel flow (Vladisavljevic, 1999), and therefore was chosen for this application to promote better substrate mixing between the biofilm and bulk liquid, as illustrated in Figure 7-7.

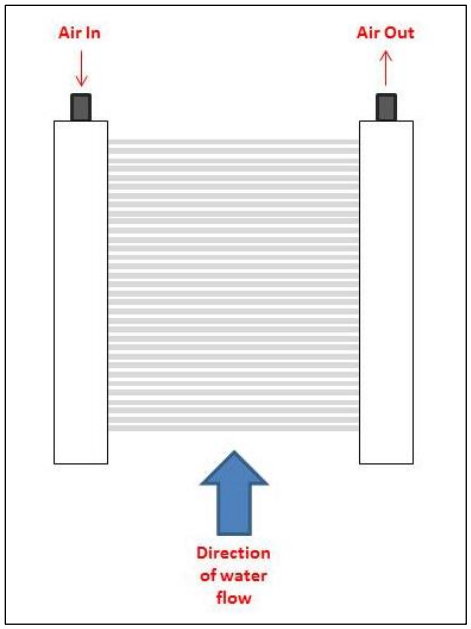

Figure 7-7: Cross flow operation

7.1.2.1 Membrane modules

Membranes were obtained from a hollow-fibre ultrafiltration membrane module (MWCO 150 kDa, Microdyn-Nadir GmbH, Wiesbaden, Germany) (Figure 7-8). The membrane fibres were rendered hydrophobic in line with instructions from the supplier by flushing out of the storage solution (1% aqueous formaldehyde solution) from the membranes and then drying by passing air through the membranes (Steube 2009). The module was then opened and the fibres used to form 20 membrane modules.

Figure 7-8: Daicen Membrane Module

To form each module, two lengths of 50 mm x 25 mm rigid PVC cable trunking (B&Q, U.K.) were cut and one side drilled with 78 holes. The holes were arranged in alternate rows of 3 and 2 in a staggered square arrangement with a nominal pitch of 10 mm.

The trunking was then secured 400 mm apart by 2 PVC struts and membrane fibres fed through each hole as shown in Figure 7-9. The membranes were then sealed and secured in position with an epoxy potting compound (R.S. Components, U.K.).

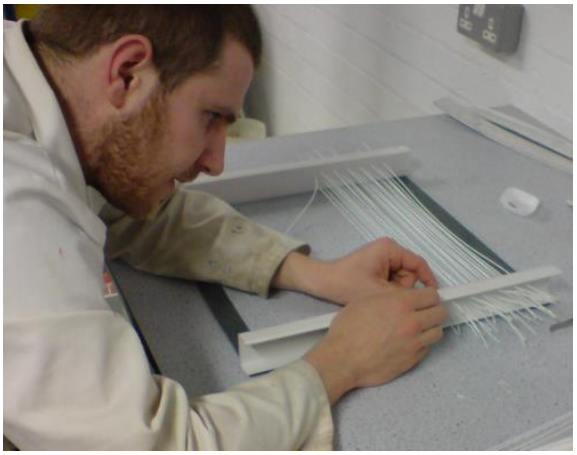

Figure 7-9: Membrane module construction

Figure 7-10: Membrane sealing with epoxy resin

The sections of cable trunking were then reformed and formed into boxes with two end pieces (B&Q, U.K.), one of which was fitted with a standard airline push fitting (R.S. Components, U.K.). These boxes were then sealed to make them air and water tight using a combination of heat and TEC7® sealant (Contech Building Products, Ireland).

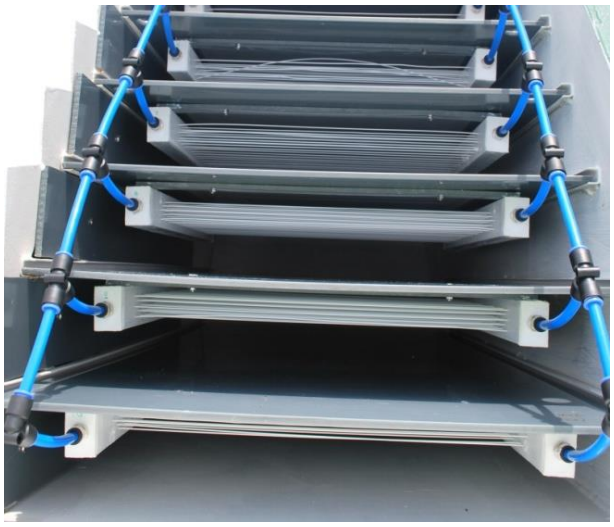

Figure 7-11: Membrane modules in BioSettler unit

The membranes supplied a total aeration area of 2.036 m^2. The membrane modules were attached to the underside of the inclined plates with the membrane fibres parallel to the plates as shown in Figure 7-11. This provided cross flow operation as the clarified effluent rose in the channels between the plates.

7.1.3 Auxillary equipment

7.1.3.1 Pumps

Influent wastewater was provided to the unit by use of a Watson-Marlow 604U peristaltic pump (Watson-Marlow Bredel, Falmouth, U.K.). Influent was drawn from the main works at a flowrate of 4 m^3day^{-1}, giving a hydraulic retention time of approximately 6 hours.

A similar pump also controlled underflow from the bottom of the tank to facilitate solids removal, with underflow rate determined by settled sludge volume.

7.1.3.2 Air blower

Air was provided to the lumen of the membranes by a Medo LA-120 Air Blower (Nitto-Kohki Europe Ltd, Watford, U.K.). Designed for aeration of fish ponds, the unit provides a constant air flowrate of 120 lpm of air at a pressure of 0.2 bar gauge.

7.1.3.3 Sampling equipment

Two ISCO 6700 automated water samplers were used to collect 24-hour composite samples of the wastewaters which were influent and effluent to the BioSettler unit. 125ml of both influent and effluent were collected at 90 minute intervals, giving a daily 2000 ml sample representative of each day's flow.

7.2 Trial locations

The unit was operated at two municipal WwTW owned and operated by Northern Ireland Water.

7.2.1 Site 1

The first site was Newtownbreda WwTW, a 40,000 p.e. activated sludge plant in South Belfast. The works produced fully nitrified and well settled effluent and was consent compliant in 2009. Significant urban growth has taken place since the plant was last upgraded in the 1980s and as such, the plant struggles with high hydraulic loading. Capital works were carried out after this demonstration was completed at the site to increase hydraulic capacity and add nutrient removal.

7.2.2 Site 2

The second site was a small works at Parkgate village, near Templepatrick in County Antrim. The treatment consisted of a primary settler, trickling filter and final settling tank. The works was borderline compliant with a 40:60 BOD:Suspended solids consent

and, as a result of these compliance issues, has now been decommissioned and replaced with a sewage pumping station which transfers wastewater to a larger works nearby.

7.3 Trial results

7.3.1 Site 1

Several problems were experienced during operation at the first site. At Newtownbreda WwTW, the aeration basins are split into three zones, with surface aerators and separated with baffles. On leaving the aeration basin, the MLSS is divided, with a fraction passing to the final settling tanks and the remainder being returned to the first of the three aeration zones via a recycle line.

It is from this recycle line (Figure 7-12) that influent to the BioSettler was initially drawn. However, in this location the feed intake became blocked with rags and other debris, and led to no flow reaching the unit. In the diagram, the position of the BioSettler is marked by the green rectangle, the first sample point by the red triangle and the second sample point by the yellow star.

Figure 7-12: Layout of Newtownbreda WwTW (Googlemaps).

To avoid this blocking from occurring, the intake point was moved to the third of the three aeration zones (Figure 7-13). The wastewater from this point has essentially the same composition as that in the recycle line, and the turbulence caused by the surface aerators helped clear any debris that built up on the influent intake pipe.

Figure 7-13: Second influent intake point used at Site 1.

7.3.1.1 Membrane damage

As discussed in Section 7.1.1.3, the slope of the prototype tank was less than ideal in order to comply with health and safety regulations. Whilst this did not interfere with the clarification of the influent wastewater, it did limit the rate at which solids could be removed from sludge collection section of the tank.

This complication led to long sludge retention times with the associated problem of rising sludge, caused by bubbles of nitrogen gas formed by denitrification. As pockets of settled sludge rose, they contacted the membrane modules and deposited large amounts of solids on the surface of the membranes Figure 7-14.

Figure 7-14: Sludge buildup on membranes

Figure 7-15: Damage to membranes

The weight of the sludge which built up on the membrane surface caused membranes breakages as shown in Figure 7-15. These membrane breakages led to the release of bubbles with associated turbulence causing solids to carry over the v-notch weir.

These breakages meant that only periodic operation was possible. In order to facilitate repairs, the plates were removed from the tank, broken membranes removed from the membrane module and the module made airtight again by patching the hole with TEC7® sealant.

7.3.1.2 Pollutant removal

Due to these problems, it was not possible to obtain a body of results. However, over the course of the trial, 32 days of data was collected when operation was not hindered by the issues described in Sections 7.3.1. This data is presented in average form in Table 7-2.

Table 7-2: Pollutant removal obtained during Trial 1 (Standard errors shown)

	Suspended Solids	COD	Ammoniacal Nitrogen
Average influent concentration (mg l^{-1})	3060±190	43.1±8.3	9.80±0.76
Average effluent concentration (mg l^{-1})	22.0±3.0	15.2±2.5	8.05±0.71
Removal (%)	99.3	64.7	17.9

Whilst limited inferences can be made from this data due to the periodic nature of operation during Trial 1, some conclusions can be drawn. Removal of COD and ammoniacal nitrogen was achieved; demonstrating that membrane aerated biofilms can obtain pollutant in 'real-life' situations.

Good solids removal was achieved with the BioSettler unit, with levels being reduced from the concentrations found in aeration tanks to levels which are consent compliant. This indicates that the process of bubblefree aeration does not interfere with the settling process.

7.3.2 Trial 2

The unit was operated at Parkgate WwTW for six weeks over the summer of 2010 at the same flowrates as at Newtownbreda WwTW. Removal of key pollutants was achieved, and the experience from Trial 1 meant that the unit was operated without interruption for 42 days. Longer operation was not possible as the treatment works was replaced with a sewage pumping station and flows were diverted.

To avoid operation being compromised by solids build-up in the BioSettler tank, as was the case during the Newtownbreda trial, the effluent from the final settling tank was used for BioSettler influent (Figure 7-16).

Figure 7-16: Sample location at Site 2

On day 36 of the trial, following a drop in performance, the liquid level in the unit was reduced to remove excessive biomass from the surface of the membranes and deposited solids from the surface of the inclined plates. In Figure 7-17, Figure 7-18 and Figure 7-19, this point where 'backwashing' took place is indicated by a vertical dashed line. For clarity, a seven day moving average was used.

7.3.3 Solids Removal

Figure 7-17 shows the influent and effluent suspended solids concentrations during Trial 2.

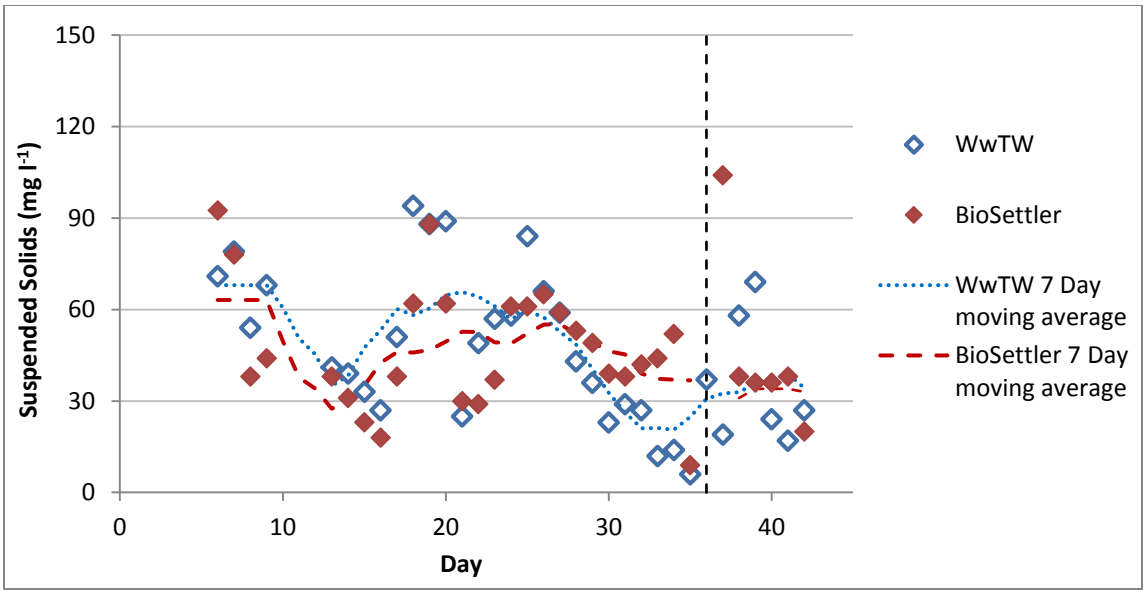

Figure 7-17: Solids concentrations during BioSettler trial 2

The effluent produced by the plant contained solids which were not settleable (verified by the use of Imhoff cones). The BioSettler was therefore not able to achieve significant additional solids removal in comparison to the plant. The data points where suspended solids concentration is higher in the BioSettler than plant effluent can be attributed to sloughing of biomass from the surface of the membranes into the bulk liquid.

7.3.4 Biochemical Oxygen Demand

Figure 7-18 shows the influent and effluent BOD concentrations obtained during Trial 2. Variations in wastewater composition are linked to rainfall.

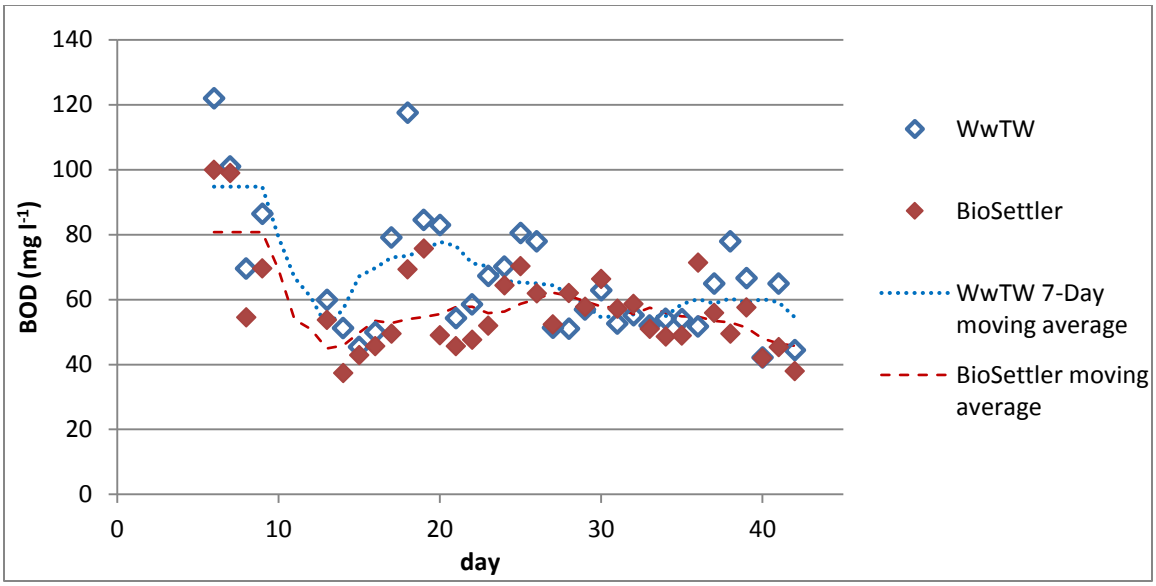

Figure 7-18: BOD concentrations during BioSettler trial 2

Following commissioning of the BioSettler, a biofilm was quickly established on the surface of the membranes and BOD removal was obtained. From Day 10 – 20 approximately 20% of the BOD contained in the influent wastewater was removed, at an average rate of 33.1 $gBODm^{-2}day^{-1}$. After day 20, a reduction in performance was seen; as biofilm maturity increases, so does the biofilm density. This denser biofilm slows the diffusion rate of both oxygen and substrate, reducing pollutant removal rates (Matsumoto *et al.*, 2007).

Prior to 'backwashing', from approximately Day 31 to Day 37, the BioSettler average BOD was higher than that of the plant effluent. This was limited by mass transfer due to biofilm density. A similar effect was noted by Pankhania *et al.* (1999) and can be attributed to a period when the rate of hydrolysis of wastewater constituents into a form where they are more readily available to microorganisms is faster than the rate at which they are utilised by the biofilm. Following backwashing, the BOD utilisation rate was boosted and BOD was once again removed by the BioSettler.

The BOD loading at Parkgate WwTW was much higher than was considered in the concept design; nonetheless, BOD removal rates of up to 96 $gBODm^{-2}day^{-1}$ were obtained. This figure is far in excess of those reported for similar investigations (e.g.

Pankhania *et al.*, 1999), and by previous laboratory work in this project. There are two possible explanations; either greater oxygen transfer rates are obtained with the membranes used in the pilot plant, or a significant amount of BOD removal is achieved through the removal of suspended biomass. It is likely that both mechanisms contribute to the high BOD removal rate.

7.3.5 Ammoniacal Nitrogen

The nitrification performance of the BioSettler was also detrimentally affected by the high BOD loading due to the competition between heterotrophic bacteria and nitrifiers for oxygen. Figure 7-19 shows the influent and effluent ammoniacal nitrogen concentrations during Trial 2.

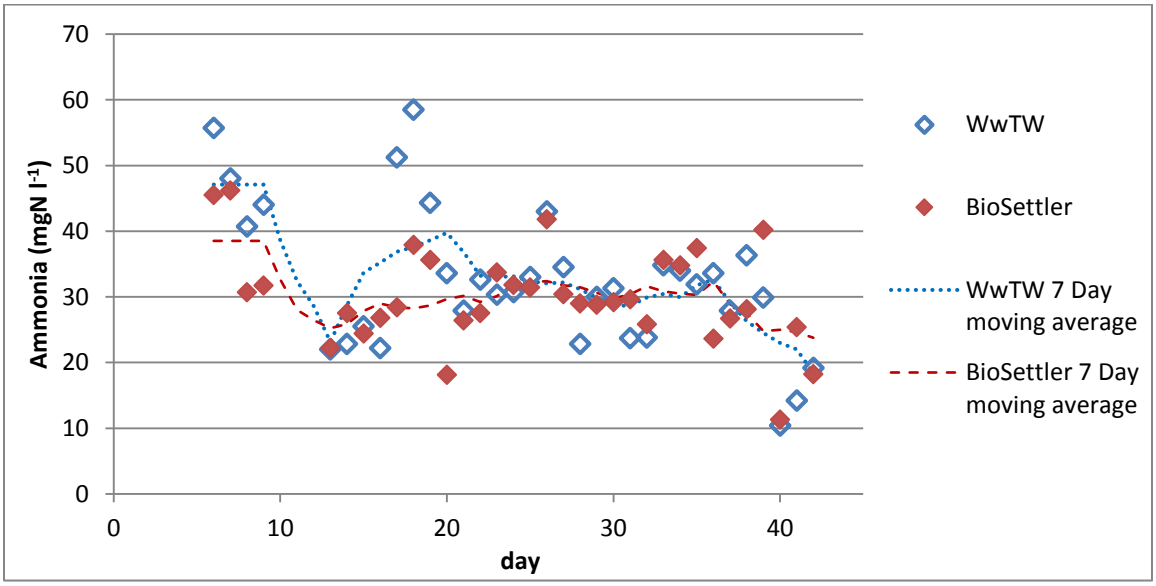

Figure 7-19: Ammoniacal nitrogen concentrations during BioSettler Trial 2

Stable nitrification was quickly established within the BioSettler and from Day 13 – 20 ammoniacal nitrogen was removed at an average rate of 13.4 $gNm^{-2}day^{-1}$ (giving approximately a 20% reduction in ammonia concentrations). This value is also higher than those contained in published research (e.g.Yamagiwa & Ohkawa, 1994), and, as with BOD removal, it is likely that suspended biomass contributes to ammoniacal nitrogen removal.

Ammoniacal nitrogen removal performance also declined after approximately Day 20 of the trial. Due to slower decay rates, nitrifying bacteria are predominately found on the membrane surface (Shanahan & Semmens, 2004). In this position they are starved of substrate in thick biofilms; therefore ammonia removal declined faster than BOD removal, which can occur in both aerobic and anoxic environments.

Heterotrophic bacteria have faster specific growth rates than nitrifying bacteria (Shanahan & Semmens, 2004). In situations where their growth is not limited by BOD availability, they can completely outcompete nitrifiers for space and oxygen in membrane aerated biofilms (Zhang *et al.*, 1995). For this reason, ammonia removal was not restored by backwashing on Day 36.

7.4 Potential performance of scaled up system

7.4.1 Pollutant removal

Using the data obtained between day 10 and day 20, at which time the biofilm on the membrane surface had reached maturity, but pollutant removal was not yet inhibited by excessive biofilm growth, the average pollutant removal rates shown in Table 7-3 can be calculated.

However, due to the poor settling characteristics of the wastewater at the Parkgate WwTW, suspended biomass was present in the BioSettler effluent. This suspended biomass had the potential to contribute towards pollutant removal. Allowing this contribution would likely be small due to the anoxic nature of the bulk liquid. To allow for this, only 50% of the obtained value is used for subsequent calculations. This leaves a conservative estimate of the removal achieved by the presence of the membrane attached biofilm.

Table 7-3: Average pollutant removal rates

	Obtained value	50% of obtained value
Average BOD removal rate ($gBODm^{-3}day^{-1}$)	33.1	16.5
Average NH_4-N removal rate ($gNm^{-3}day^{-1}$)	12.5	6.3

Practicalities of the manual manufacturing process using in the pilot scale BioSettler meant that the membrane specific surface area (SSA) was limited to 2.04 m^2m^{-3}. However, commercial membrane modules, such as those produced by Zena membranes (Czech Republic – shown in Figure 7-20), with dimensions which would fit onto the back of the BioSettler plates; contain 4 m^2 of membrane surface area.

Figure 7-20: Zena membrane module

The nature of these modules, consisting of bunches of membrane fibres, means that surface area will be lost as the membranes touch each other. Even if this means only 25% of this area could be utilised for membrane attachment, the SSA of the pilot-scale BioSettler would still be 20 m^2m^{-3} and the potential removal rates would increase by an order of magnitude, as shown in Table 7-4.

Table 7-4: Potential removal rates

	Potential value
BOD removal rate ($gBOD\ m^{-3}day^{-1}$)	161.8
NH_4-N removal rate ($gN\ m^{-3}day^{-1}$)	61.8

7.4.2 Energy consumption

Upgrade of a conventional settler to the BioSettler system will incur additional energy costs in the supply of air to the lumen of the membranes. At Parkgate WwTW, the unit was operated with excess air and specific energy consumption (estimated from the power rating of the blower unit) of 0.78 kWh m^{-3} compared with 0.5 kWh m^{-3} for traditional treatment systems (Kadar & Siboni, 1998).

However, air supply to the lumen provides both the required oxygen to the biofilm and acts as a sweep gas, removing water vapour which diffuses in the opposite direction – i.e. from the water side to the air side. It is likely that airflow used in the pilot unit was much greater than needed through the BioSettler system.

Work investigating the oxygen mass transfer in the same polyethersulphone membranes as in the pilot scale BioSettler without the presence of a biofilm has been carried out (Doyle, 2011). Operating at an air flowrate per fibre of 12 times lower than that in the BioSettler pilot unit, no inhibition in oxygen transfer by back diffusion of water vapour was observed.

This implies that the same blower unit could be used to supply air to 12 times as much membrane, and hence treat twelve times as much wastewater. If this flowrate could be realised, the specific energy consumption would be reduced to a much more favourable 0.065 kWh m^{-3}.

Additionally, as the presence of the biofilm acts as a barrier to mass transfer it may slow the transfer of water vapour into the lumen side of the membrane. The laboratory experiments discussed in Chapter 5 found the oxygen flux through the membrane in the presence of a biofilm (with bulk DO approximately equal to zero) to be only 44% of the average oxygen flux measured in Chapter 3 through clean membranes over the DO range 1 – 5 mg l^{-1}.

If a similar effect was observed for the rate of transfer of water vapour, it could be assumed that the same blower could be used for the aeration of another additional 2.25 times as much membrane and treat 2.25 as much wastewater, reducing the specific energy consumption still further to a figure of 0.028 kWh m^{-3}.

A better comparison is made between the aeration costs in a BioSettler and the energy costs involved in pumping wastewater from non-consent-meeting works to alternative locations for treatment. For example, following the closure of Parkgate WwTW, wastewater is now pumped from Parkgate Village to the new 78,000 p.e. Antrim WwTW via Templepatrick SPS – a distance of approximately 8.75 miles (14 km).

No data is available for the energy usage involved in pumping wastewater from Parkgate SPS to where it undergoes treatment (Smyth 2011). However, an estimate can be made from a study of the Oslo, Norway, wastewater treatment system (Venkatesh & Brattebo, 2011). Over the period 2000 – 2007, 46.34 GWh of energy were used in pumping of 1.01 Gm^3 of wastewater. Assuming wastewater was pumped a distance of 10 km on average, this gives a specific energy consumption of 0.46 kWh $m^{-3}km^{-1}$.

Applying this figure to the distance from pumping station to treatment works in the case of Parkgate gives an estimated specific energy consumption of 0.064 kWh m^{-3}. This is comparable with the energy cost of the BioSettler and implies that the BioSettler concept is energetically feasible, were upgrade possible with the installation of BioSettler system.

7.4.3 Energy consumption of unit pollutant removal

Assuming wastewater enters the treatment works at an average BOD of 200 mg l^{-1} and is treated to an effluent concentration of 10 mg l^{-1}, the specific BOD removal of the activated sludge can be calculated on an energy basis from the specific energy consumption on a volume basis. Using the figure reported by Kadar & Siboni (1998) – 0.5 kWh m^{-3} – yields a value of 0.38 gBOD kWh^{-1}.

The same parameter can be calculated for the BioSettler. Using the BOD removal rate reported in Table 7-3 (16.5 $gBODm^{-2}day^{-1}$), and a specific energy consumption of 0.028 kWh m^{-3} as calculated previously, a figure of 0.59 gBOD kWh^{-1} is obtained. This value is 55 % higher than that for activated sludge.

7.5 Conclusions

The performance of the BioSettler at two WwT sites has demonstrated the promise of the technology, despite operation with wastewaters of less than ideal characteristics. The two site trials have shown that the BioSettler concept is capable of simultaneous aerobic biological treatment (treating BOD and nitrifying ammonia), denitrification and solids removal.

During the initial trial (Site 1), improved suspended solids removal was demonstrated but the BOD and ammonia levels in the (MLSS) influent were too low to show a convincingly significant benefit due to treatment within the BioSettler.

At Site 2 the BOD and ammonia concentrations were very high, and, despite high specific removal rates achieved by the BioSettler, successful operation of the technology required control of biofilm growth. The variable performance of the BioSettler at Site 2 is adequately explained by competition between heterotrophs and nitrifiers and the limitations of mass transfer in the thick biofilm developed under high BOD loading. A weekly backwash is likely to be sufficient to control biomass overgrowth under conditions of high BOD loading.

The BioSettler technology is a simple and attractive option for upgrade of plants, promising minimal construction down time and reduced cost while maximising existing assets. Further demonstration of the technology is required to assess the full potential achievement of the promised benefits. This will allow optimisation of residence times and energy consumption as well as further assessment of performance.

8 Treatment of azo dye waste in the Membrane Aerated Biofilm Reactor – a feasibility study

The work reported in Chapters 4, 5 and 6 demonstrated the ability of membrane aeration to supply sufficient oxygen to maintain a biofilm where both aerobic and anoxic conditions exist.

Previous published research has demonstrated that these conditions are ideal for the treatment of dye house waste. This chapter investigates the possibility of using the MABfR to treat azo dye wastewater; which requires both aerobic and anoxic conditions for complete pollutant removal.

8.1 Experimental conditions

A MABfR was constructed as described in Chapter 3, again using silicone rubber as the aeration material. It was then operated for 121 days with a hydraulic retention time of 5 days, treating a synthetic dye house wastewater containing the azo dye Acid Orange 7 (AO7).

The investigation was carried out using three sets of experimental conditions. The aim of each of these three experimental runs is given below:

Run 1:	Establish AO7 reducing biofilm;
Run 2:	Investigate effect of riboflavin addition as redox mediator to the influent wastewater;
Run 3:	Investigate effect of 20% reduction in total oxygen demand (TOD) of influent wastewater.

The concentrations of those components of the synthetic wastewater, which varied in order to achieve each of the goals listed above, are given in Table 8-1.

Table 8-1: Component concentrations varied during dye degradation studies

Run	Duration (days)	Concentration (mg l^{-1}) Sucrose	Peptone	Ammonium Chloride	Riboflavin
1	1-58	550	200	350	-
2	58-75	550	200	350	10
3	75-121	440	160	280	10

8.2 General observations

8.2.1 Biofilm establishment

The reactor was seeded with a mixture of the supernatant from a soil suspension and the effluent from an anaerobic/microaerobic column treating azo dye waste (Lipscomb *et al.*, 2008). This column had previously been seeded with *Shrewanella sp.*, a bacteria shown to be capable of azo bond cleavage (Pearce *et al.*, 2006).

Figure 8-1 shows the presence of a thin biofilm on the surface of the membrane material, and the turbid nature of the bulk liquid, after 12 days of reactor operation. This relatively high turbidity can be attributed to the high COD of the influent media.

Figure 8-1: Biofilm development after 12 days of operation

8.2.2 Method of colour removal

Observations imply that removal of colour from the liquid bulk occurred in three ways:

(i) Adsorption onto tubing

(ii) Adsorption onto biomass

(iii) Azo bond cleavage

The adsorption of colour onto tubing and biomass was of greatest significance during early operation of the reactor. Tubing was observed to quickly (within 48 hours) take on an orange colour. Once this initial adsorption occurred, the adsorptive capacity of the tubing was exhausted, and adsorption onto the tubing is considered to have had negligible effect on colour removal.

During operation, biomass built up in the holding vessel, and was periodically removed by filtering the contents through laboratory filter paper. The filtrate was then returned to the system.

During early operation, biomass removed as the residue was orange in colour, implying that colour removal during this phase of operation was achieved through adsorption onto biomass. When the colour removal rates were at their greatest, the residue was grey in colour, implying that once the bacteria in the biofilm had become adapted to the system, colour removal was achieved through cleavage of the azo bond, rather than through adsorption onto biomass (Figure 8-2).

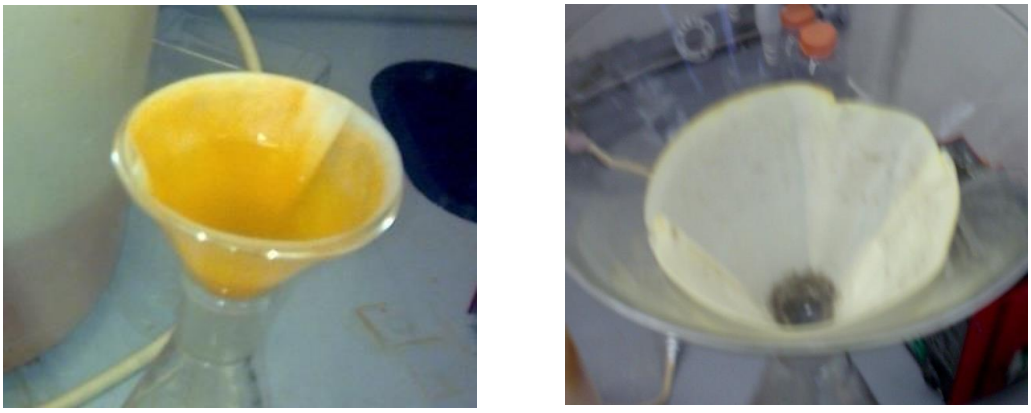

Figure 8-2: Removed biomass initially (left) and during greatest colour removal

8.2.3 pH

Similar changes to the influent and effluent pH were observed during the operation of the reactor, as exemplified by the data from Run 2 shown in Figure 8-3.

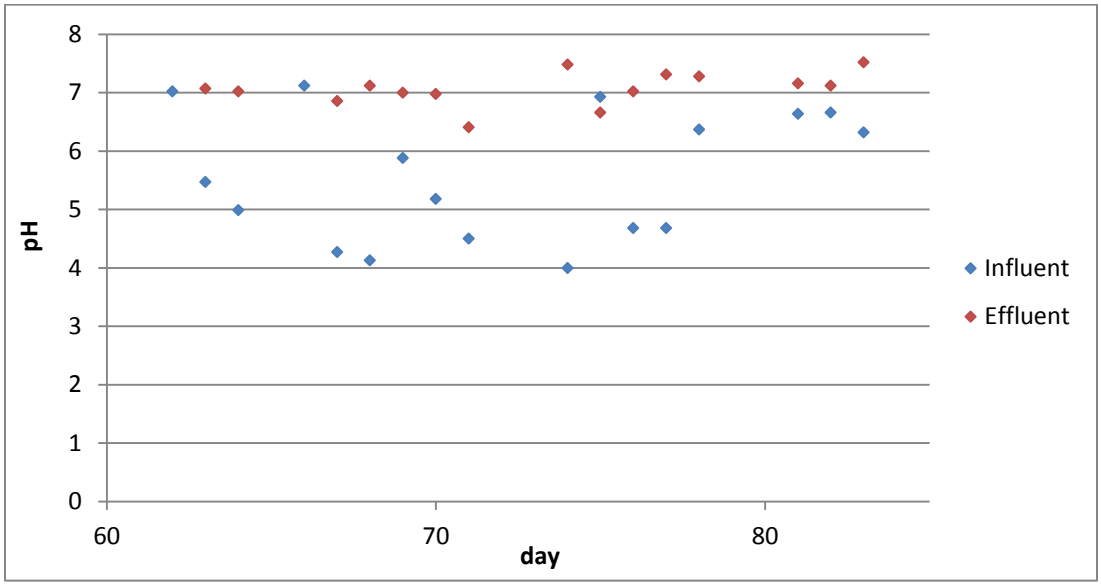

Figure 8-3: Influent and effluent pH during Run 2

The pH of the influent wastewater displays significant change during run 2, with values in the range 4.0 – 7.1 being observed during run 2. Furthermore, this variation can be seen to be cyclical, with the influent pH dropping over the course of 3-4 day periods which can be connected to the changing of the feed jar.

This drop in pH was accompanied by a sharp, pungent smell similar to that of acetic acid and can possibly be attributed to acidity produced by fermentation taking place in the feed jar. When compared with work in MABfR A, where very little variation was observed in the pH of the influent, this drop highlights the difficulty in keeping high strength synthetic wastewaters aseptic; even when correct procedures for preservation are followed (Alef, 1995).

The pH of the effluent displays less variation, with pH values in the range 6.4 – 7.5 being observed and the two lowest pH values being seen at times when the pH of the influent was also at its lowest and 11 out of 15 observations being greater than 7.0. In general, effluent pH values were higher than those of the influent as acidic fermentation products were readily broke down in the presence of oxygen by the biofilm. Relatively stable effluent pH values were seen due to the self-regulatory nature of the biological processes taking place in the biofilm.

8.2.4 Ammoniacal nitrogen concentration

Figure 8-4 shows the influent and effluent ammoniacal nitrogen concentrations throughout the dye degradation investigation. As in previous chapters, vertical lines are used to indicate the beginning of each experimental run.

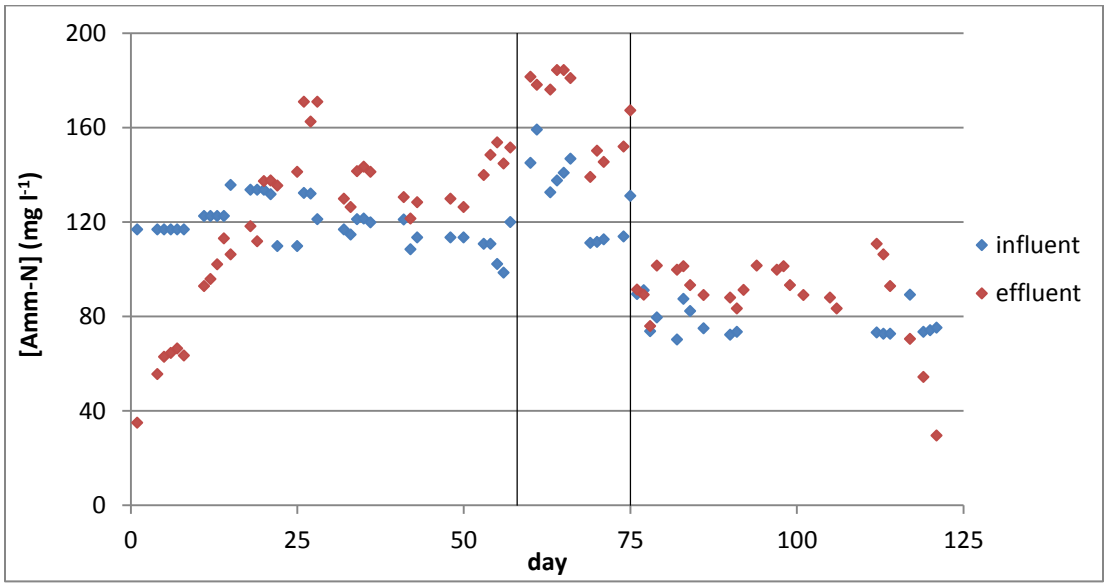

Figure 8-4: Ammoniacal concentrations throughout dye investigation

With hindsight, the use of peptone as a source of ammoniacal nitrogen was a poor choice. Peptone contains approximately 40% nitrogen by weight and is commonly included in mineral media recipes for experimental degradation investigations as a source of ammoniacal nitrogen (e.g. Saratale *et al.*, 2009).

However, the hydrolysis of peptone to aqueous ammoniacal nitrogen does not go to completition under the conditions under which the synthetic dye waste was prepared. Instead, the peptone breaks down during the residence in the reactor, and the higher effluent ammoniacal nitrogen concentration can be attributed to this phenomenon (Lieben, 1943).

8.2.5 Nitrate concentration

No significant nitrate concentrations were observed in the effluent throughout the operation of the MABfR. Three possible explanations for this observation are plausible. Lipscomb *et al.* (2008) measured redox potentials during operation of the biological column from which effluent was taken to seed the reactor used in this work. The

researchers found the highest colour removal was achieved at similar redox potentials to those contained in the literature as being ideal for denitrification.

As such, any nitrate that was produced by nitrification in the aerobic zone could feasibly be denitrified in the anoxic zone, leading to the low effluent nitrate concentrations observed throughout the operation of this reactor.

Alternatively, the absence of significant nitrate detected in the bulk phase could be due to insignificant nitrification taking place. Work by He & Bishop (1994) found the presence of AO7 to have an inhibitory effect on nitrification, even when the dye concentration was less than 5 mg l^{-1}, with the activity of AOB being more sensitive to AO7 than NOB.

A third possibility is that the absence of significant nitrate in the effluent could be due to aerobic heterotrophs outcompeting nitrifiers for space and oxygen in the biofilm (Zhang *et al.*, 1995). The influent COD concentrations used in this reactor were in the range 730 - 930 mgCOD l^{-1}. At this COD concentration, the growth rate of aerobic heterotrophs is very rapid, and prevents nitrifying bacteria from establishing themselves in the biofilm, with no associated production of nitrate.

Without the use of complex molecular biological techniques which were not available for use in this project, it is impossible to say which of these possible explanations is valid.

8.2.6 UV/vis spectrometry

A calibration was carried out by preparing a 125 mg l^{-1} stock solution of AO7, which was diluted to give solutions with AO7 concentrations of 62.5 mg l^{-1}, 31.3 mg l^{-1}, 15.6 mg l^{-1}, 20.0 mg l^{-1}, 10.0 mg l^{-1}, 5.0 mg l^{-1} and 2.5 mg l^{-1}. The absorbance spectra of these solutions over the range 400 – 550 nm is shown in Figure 8-5 below.

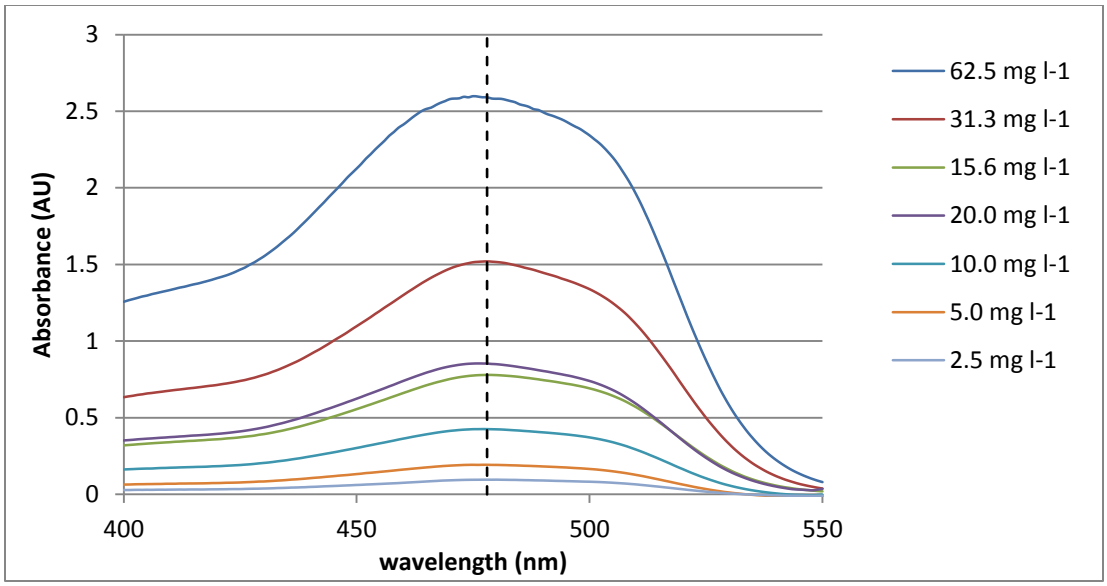

Figure 8-5: Absorbance spectra for standard AO7 solutions

Examination of the data generated by the absorbance spectroscopy reveals that the λ_{max}, the wavelength at which maximum absorbance occurs, is located at a value of 478 nm for the AO7 used in this study. This value is similar to the 480 nm found by Ong *et al.* (Ong *et al.*, 2005) and 483 nm found by Coughlin *et al.* (Coughlin *et al.*, 2002) in AO7 degradation studies.

Using the respective absorbencies of the standard solutions at 478 nm, the calibration curve shown in Figure 8-6 can be drawn.

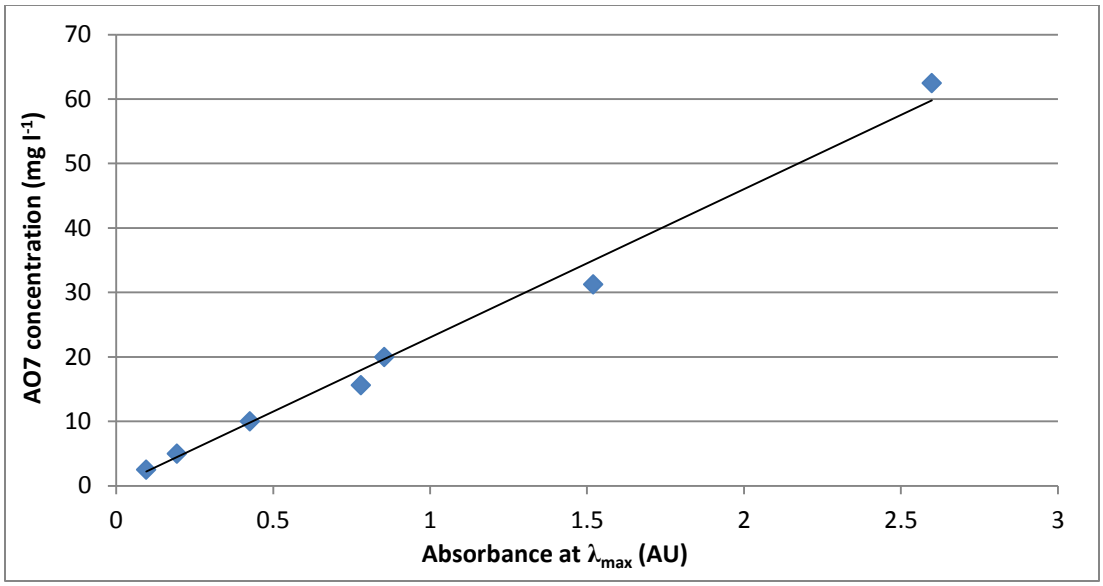

Figure 8-6: Calibration curve for AO7 concentration

Linear regression of the data shown in Figure 8-6 yields the relationship in Equation 8-1, with a correlation fit coefficient of 0.989, which can then be used to relate the AO7 concentration in collected samples to the absorbance of the samples at 478 nm.

$$C_{AO7} = 23.02A_{478} \qquad \textbf{Equation 8-1}$$

Where: C_{AO7} = Acid orange 7 concentration (mg l^{-1})

A_{478} = Absorbance at 478 nm (AU)

When used to calculate influent AO7 concentrations, Equation 8-1 gives the data displayed in Table 8-2.

Table 8-2: Average calculated AO7 concentrations in Runs 1-3 (standard errors shown)

Run	1	2	3
Average calculated $C_{AO7,inf}$	23.0±1.1	24.0±1.8	24.1±0.8

As seen in Table 8-2, the average calculated concentrations in Runs 1-3 are in the range 23.0 - 24.1 mg l^{-1}, despite the influent media containing only 20 mg l^{-1} of AO7. This is

partly due to errors in the preparation of the influent solutions and concentration during the sterilisation procedure, but is also attributable to the presence of Ferric Chloride and Riboflavin in the influent media.

Ferric chloride and riboflavin dissolve in water to give pale yellow coloured solutions. Figure 8-7 shows solutions of these components, at the concentrations used in the influent media in Runs 2 and 3, alongside an AO7 solution for comparison.

Figure 8-7: Solutions of Acid Orange 7 (left), Fe (III) Chloride and Riboflavin (right) at the concentration used in the influent media

As displayed in Figure 8-8, these compounds also absorb light in the same region in which the λ_{max} of AO7 is located. As shown by the red line in Figure 8-8, this gives cumulative absorbance effects, meaning that the apparent AO7 concentration (obtained by calculation using Equation 8-1) is higher than the true value.

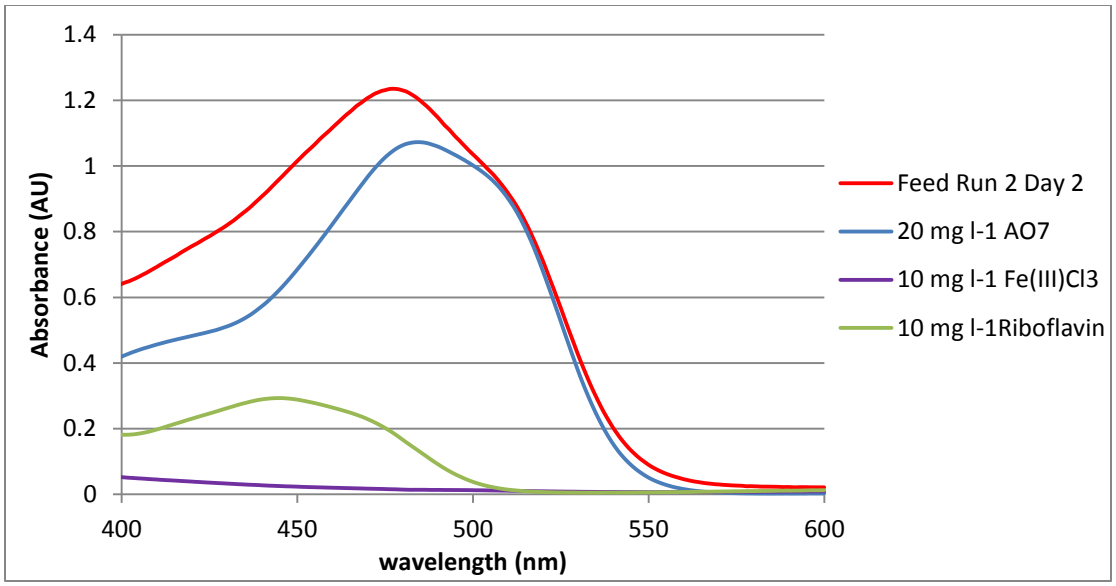

Figure 8-8: Cumulative absorbance effects

This cumulative absorbance effect leads to the overestimation of the dye concentration as exemplified by the data shown in Table 8-2. Although it causes an error in the ascertaining of AO7 concentration, the rate of AO7 removal can still be found using photospectrometry.

In this work, it is assumed that riboflavin acts purely as a redox mediator and that it is not broken down by the action of the biofilm. As such, the absorbance attributable to riboflavin at 478 nm will not differ in influent and effluent samples.

Although iron plays a key role in microbial life and as such will be taken up by the biofilm (Madigan & Martinko, 2006), it is only present in the influent media in trace amounts. At the concentration used, it does not give a visibly coloured solution (Figure 8-7) and gives an absorbance of only 0.015 AU at 478 nm. As such, the contribution of $Fe(III)Cl_3$ can be considered negligible.

As such, the changes in AO7 concentration can be considered reliable and used to calculate AO7 removal rates.

8.2.6.1 λ_{max} shift

Also visible in Figure 8-8 is a decrease in the wavelength at which maximum absorbance is observed. This phenomenon can be attributed to two factors.

Firstly, as previously stated, riboflavin is a yellow solution (Figure 8-7), with a λ_{max} of approximately 450 nm (green line in Figure 8-8). As also seen in Figure 8-8, Riboflavin also gives significant absorbance light in the range 450 – 475 nm, giving increased absorbance over this range and contributing to the shift in λ_{max} of the feed solution.

A shift in the λ_{max} of azo dyes was also observed by Hanna (2005), in work using dolomite for removal of dyes from wastewater via adsorption. The author attributed this shift to the change of pH that occurred when wastewater was brought into contact with the basic dolomite, with associated changing in structure of the dye alternating the electron density around the chromophore. It is possible a similar effect was observed here as the dye was partially broken and conditions in the reactor changed.

8.3 Colour removal

The fractional colour removal in Runs 1 – 3 is shown in Figure 8-9.

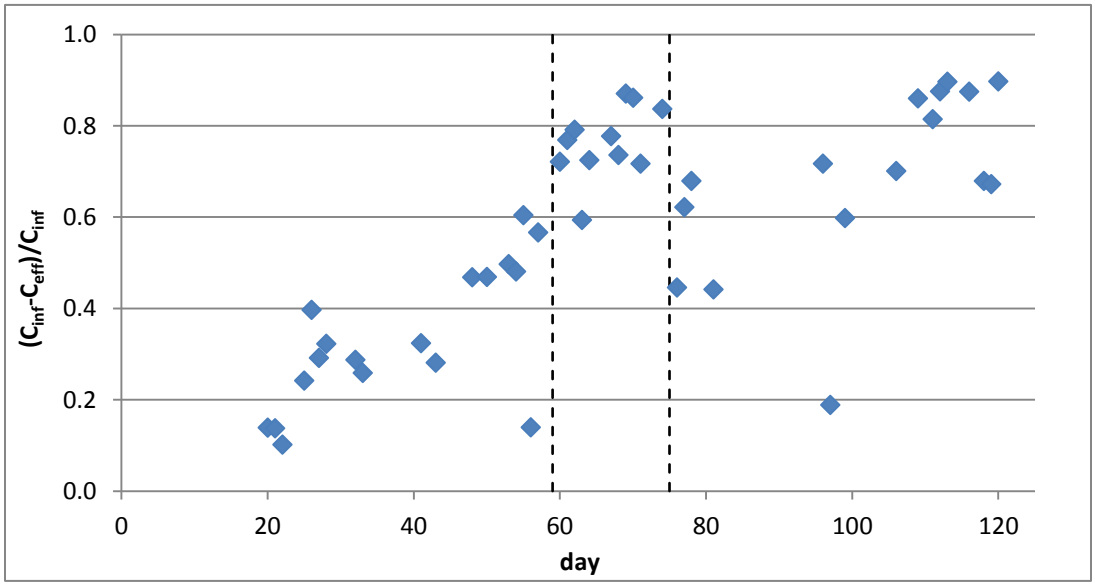

Figure 8-9: Colour removal in Runs 1-3

Initially, colour removals were low, with only 15% removal being observed on Day 20, when the first samples were taken for photospectrometric analysis. From this point, the colour removal follows a general upwards trend as the slow growing anoxic bacteria which are responsible for cleavage of the azo bond increase in numbers, reaching a maximum of 0.87 fractional removal on day 69.

A drop in colour removal is seen around day 75, which coincides with the reduction in the TOD of the influent media. The drop in TOD of the influent media will have had an effect on the position of the anoxic zone. As a result, the bacteria which exploited the niche for cleavage of the azo bond during Runs 1 and 2 no longer experience anoxic conditions and the colour removal rate drops off.

After this drop, the colour removal increases again, with a maximum observed removal of 0.90 on days 113 and 120. This recovery can be attributed to the azo bond cleaving bacteria exploiting the new location of the anoxic zone in significant numbers.

8.3.1 AO7 Removal rate

After using median analysis to eliminate rogue data points, the obtained average AO7 removal rates are shown in Table 8-3 on a mass/membrane area basis, mass/reactor volume basis and moles/reactor volume basis.

Table 8-3: AO7 removal rates in Runs 1-3

Run	r_{AO7} (g $m^{-2}day^{-1}$)	r_{AO7} (g $m^{-3}day^{-1}$)	r_{AO7} (mmol $m^{-3}day^{-1}$)
1	0.38±0.02	1.57±0.10	4.81±0.30
2	1.01±0.07	4.16±0.30	12.76±0.93
3	0.85±0.05	3.49±0.20	10.70±0.60

Examination of the data in Table 8-3 reveals that the rate of AO7 removal was significantly boosted by the addition of riboflavin to the influent media in Run 2, with the AO7 removal rate 2.6 times higher in Run 2 compared to Run 1. This is consistent with

the findings of Van der Zee *et al*. (2003b), who observed approximately a five-fold reduction in decolourisation time in a batch system.

However, this may be misleading. From examination of Figure 8-9, it could be argued that the colour removal was still increasing, and that stable effluent concentrations had not been reached at the end of Run 1. As such, the average removal rate calculated by median analysis is lower than if the removals at the end of the experimental run was used, and it can not be stated with certainty that the AO7 removal rate was boosted by the addition of riboflavin.

It may be the case that riboflavin, or another effective redox mediator, was already being naturally produced by the biofilm, and that colour removal was therefore not limited by the presence of a redox mediator, but rather limited by the numbers of slow growing, anoxic bacteria, who are responsible for the cleavage of the azo bond. It is for this reason that the obtained removal rate is higher in Run 2, when the biofilm had reached maturity.

This uncertainty could have been avoided by continuing each experimental run until stable values had been obtained, but this was not possible as this work took place at the end of the research phase and was subject to time constraints.

The average removal rate in Run 3 was slightly lower than that obtained in Run 2. As discussed above, this is due to a change in the location of the anoxic zone. This would not had occurred were Run 3 extended in duration as the removals at the end of Run 3 were the highest observed in the investigation.

The obtained removal rates cannot be directly compared with other published removal rates contained in literature, as this is the believed to be the first use of a MABfR to decolourise azo dyes. Instead, the results are compared on to alternative biofilm reactor studies in Table 8-4.

Table 8-4: Comparison of AO7 removal rates in literature

Author	Method	Maximum r_{AO7}
This study	MABfR	4.16 g $m^{-3}day^{-1}$
		12.76 mmol $m^{-3}day^{-1}$
Coughlin *et al.* (2002)	Rotating Drum Biofilm	1296 g $m^{-3}day^{-1}$
Ong *et al*. (2005)	Packed Column Biofilm	4342 mmol $m^{-3}day^{-1}$

On first examination, the AO7 removal rates obtained in this study do not compare favourably with those selected from the published research. The maximum rate of AO7 removal, obtained in Run 2 of the investigation, is three orders of magnitude lower than that reported by both Coughlin *et al*. (2002) using a Rotating Drum Biofilm Reactor, and Ong et al. (2005) using a Packed Column Biofilm reactor.

However, the specific surface area used here is significantly lower than what is possible for a MABfR, being two orders of magnitude lower than that used by Pankhania (1994, 1999). If this specific membrane area, 515 m^2m^{-3}, is used in calculating the removal rate on a volume basis, figures of 522 g $m^{-2}day^{-1}$ and 1490 mmol $m^{-2}day^{-1}$ are obtained and the comparison with published research is much more favourable. Although still approximately 50% lower than the rates contained in the literature, they are promising given the early nature of this use of MABfR technology, and could possibly be increased through optimisation of the process.

8.4 COD removal

The influent and effluent COD concentrations in Runs 1 - 3 are shown in Figure 8-10.

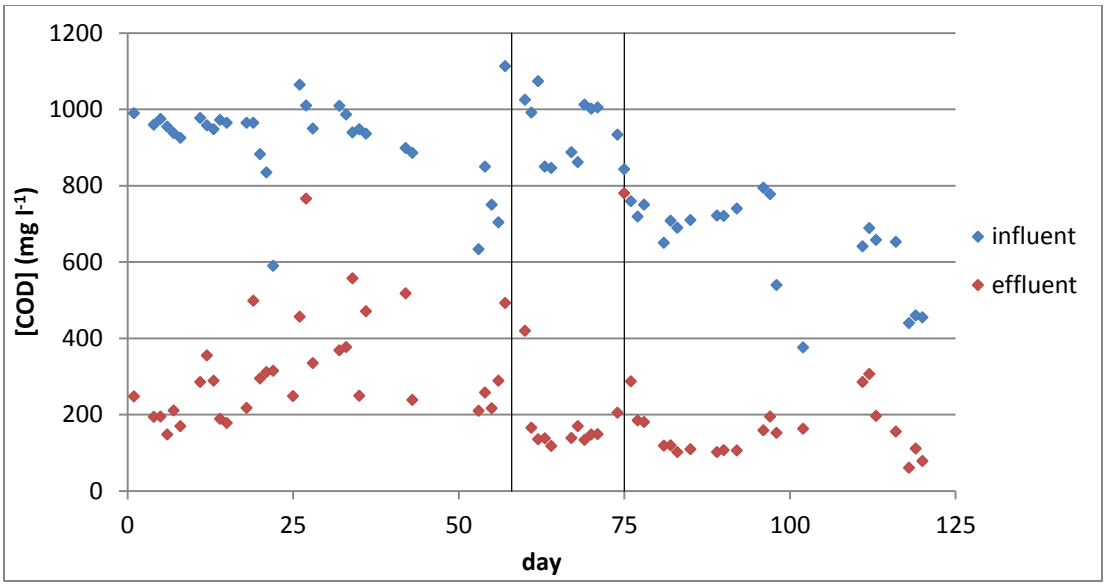

Figure 8-10: Influent and effluent COD concentrations during Runs 1 - 3

There is considerable variation in the influent COD concentration. This is due to the difficulties in keeping high strength synthetic wastewaters aseptic, as discussed previously in relation to the observed variation in the pH of the influent wastewater.

Less variation is seen in effluent concentrations, which are relatively well grouped in the range 100 – 300 mg l^{-1}. Effluent concentrations are more closely grouped in Runs 2 and 3, which can be attributed to the inherent stability of a more mature biofilm.

8.4.1 COD removal rate

The average COD removal rates obtained during the three experimental runs of the dye MABfR is displayed in Table 8-5.

Table 8-5: COD removal rates in Runs 1 - 3

Run	r_{COD} (gCOD $m^{-2}day^{-1}$)
1	29.4±1.4
2	37.9±1.4
3	21.7±1.7

On first examination of the data contained in Table 8-5, the addition of riboflavin in run 2 appears to have boosted COD removal, with the removal rate in Run 2 almost 30% higher than that obtained in Run 1. However, this may also be due to the biofilm reaching maturity during Run 2 and it cannot be concluded that riboflavin boosts COD removal without further experimentation.

In comparison to those reported in the previous chapters, these removal rates are slightly higher (the highest removal rate obtained in Chapter 6 was 21.5±1.7 gCOD $m^{-2}day^{-1}$). This can be partly explained by Monod kinetics, as the COD loadings in this chapter were in the range 28.4 – 46.4 gCOD $m^{-2}day^{-1}$ compared to 23.8 – 42.4 gCOD $m^{-2}day^{-1}$.

Additionally, as discussed in Section 8.2.5 above, the high COD concentrations in this MABfR lead to the rapid growth of aerobic heterotrophs, preventing nitrifiers from establishing themselves in the biofilm. As such, no oxygen is consumed by ammonia oxidation, and all of the oxygen provided to the biofilm is utilized by aerobic heterotrophs, with associated higher COD removal rates (Zhang *et al.*, 1995).

The obtained COD removal rate in Run 3 was lower than that obtained in Run1 and Run 2. There are two possible explanations for this occurring. As observed in the studies with MABfR A, the change in composition of the influent wastewater may have affected the biofilm in such a way as to favour nitrification, and as such, less oxygen was available for COD reduction. The difficulties in achieving complete hydrolysis of the nitrogen source (described in Section 8.2.4) prevented this being qualified by effluent analysis.

Alternatively, as, in order to not disturb the microorganisms responsible for colour removal which are located in the outer layer of the biofilm, the reactor was operated without backwash. As the biofilm density is controlled by the strength of wastewater (Hu *et al.*, 2008), it is possible that the biofilm had grown to a sufficient thickness to act as a barrier to the transfer of oxygen from the membrane into the biofilm and the transfer of substrate into the biofilm.

In a similar way to that described in Chapter 7, and as also observed in pilot trials by Pankhania *et al*. (1999) this mass transfer resistance leads to lower pollutant removal rates, as evidenced here by the observed drop in COD removal rate.

8.5 Worked example

Using the obtained average AO7 removal rate obtained in this study, the membrane area required to treat dyehouse effluent from a local carpet factory can be calculated (Ulster Carpet Mills, Portadown, U.K.).

The factory currently discharges 1800 m^3wk^{-1} of spent azo dye wastewater into the town sewer (Wilkinson 2007), and has an azo dye concentration assumed here to be equivalent in absorbance to the absorbance of a 20 mg l^{-1} of AO7.

There is currently no colour consent placed upon the carpet factory, but it is assumed for the purposes of this calculation to be equivalent to the absorbance of a 5 mg l^{-1} solution of AO7.

Flowrate:

$$Q = 1800\ m^3wk^{-1}$$
$$Q = 257\ m^3day^{-1}$$

Required daily removal (loading basis):

$$L_{AO7,req} = \left(C_{inf} - C_{con}\right) * Q$$
$$L_{AO7,req} = (20 - 5) * 257$$
$$L_{AO7,req} = 3857\ g\ day^{-1}$$

Required membrane area:

$$A_{m,req} = \frac{r_{AO7,req}}{r_{AO7}}$$
$$A_{m,req} = \frac{3857}{1.01}$$
$$A_{m,req} = 3819\ m^2$$

Total membrane area requirement – giving 20% additional allowance:

$$A_{m,req,T} = 1.2 * A_{m,req}$$
$$A_{m,req,T} = 1.2 * 3819$$
$$A_{m,req,T} = 4583\ m^2$$

Using the specific surface area used in this investigation (4.4 m^2m^{-3}), the required membrane area corresponds to a reactor volume of 1040 m^3. This is unfeasibly large, but the specific surface area used in this study is small compared to those reported in literature. Using the highest specific area from literature for a MABfR, reported by Pankhania *et al*. (1999, 1994) as 510 m^2m^{-3}, a reactor volume of 9.0 m^3 is obtained.

However, although the reactor volume may be feasible in scale, the cost of membrane may not be. The membrane unit purchased in order to produce the pilot scale BioSettler system provided 7.2 m^2 of membrane area and cost €1800. At these prices, the required membrane area would cost more than €1M to purchase, and it is unlikely that the use of MABfR would prove the most cost effective solution. Other techniques, like those discussed in Section 8.3.1, are likely to be more financially viable.

8.6 Conclusions

This work has demonstrated that the cleavage of the azo bond, with associated colour reduction, and simultaneous COD removal can take place in the MABfR under controlled conditions – which has not previously been reported in literature.

Although demonstrated in published research using batch studies, the rate of azo dye degradation was not shown to increase following the addition of riboflavin. Although not conclusively shown here, it is believed that this result was seen as availability of riboflavin, or another redox mediator, was not limiting the rate of azo bond cleavage.

COD loading must be matched to inlet pressure, and therefore supply rate of oxygen, in order to achieve stable colour removal. Variations in oxygen demand of the influent wastewater lead to a movement of the anoxic zone, and as the bacteria responsible for

cleavage of the azo bond are slow growing, the decolourising ability of the biofilm is reduced.

Using the removal rates obtained in this work, the membrane area required in order to successfully decolourise from a local dye house was calculated. Although the required membrane area could be accommodated within a reactor size which could feasibly installed at the carpet factory, the costs involved in the purchase of the membrane itself were significant.

For this reason, it is unlikely that the MABfR will prove to be a feasible technology for direct treatment of textile waste. However, given the expense and disposal issues associated with chemical and physical methods, more research is required into biological treatment options involving sequential anoxic and aerobic phases. Rotating Drum Contactors and Packed Bed Reactors are currently suitable candidate technologies.

However, given further development and optimisation of the process, costs of a MABfR could be reduced and removal rates increased to a point where MABfRs can be considered an economically as well as technically viable technique for treatment of azo dye wastewater.

9 Conclusions and Further Work

9.1 Summary of conclusions

The main conclusions that can be drawn from this work are:

Mass Transfer Studies

- The bubble free transfer of oxygen to water using tubular silicone rubber and polyethersulphone membranes was explored. The effect of inlet air pressure, air flowrate and water flowrate was investigated, allowing oxygen flux to be measured and overall mass transfer coefficients to be evaluated.
- Obtained average oxygen fluxes ranged from 0.6 to 2.4 $O_2 m^{-2} h^{-1}$, with higher fluxes being obtained with silicone rubber in all situations. Overall K values were in the range 2.7×10^{-5} to 5.4×10^{-5} ms^{-1}, similar to those observed by other researchers.
- Wilson plots were used to obtain the individual K_L and K_M, allowing relationships to be developed linking K_L to Re, the dimensionless measure of water side turbulence. The obtained empirical relationships were $Sh = 1.99 Re^{1.07} Sc^{0.33}$ for the silicone rubber membrane module and $Sh = 0.96 Re^{1.05} Sc^{0.33}$ for the polyethersulphone module.

Membrane Aeration Biofilm Studies

- Two lab scale MABfRs were designed, built and operated; one treating synthetic secondary municipal WwTW effluent and one treating synthetic dyehouse wastewater.
- For the municipal WwTW reactor, COD, Ammoniacal and Total-Nitrogen were all successfully removed at a variety of inlet air pressures and wastewater compositions, with removal rates as high as 13.8 g $m^{-2} day^{-1}$, 1.92 g $m^{-2} day^{-1}$ and 1.42 g $m^{-2} day^{-1}$ respectively being achieved.
- The results were used to develop a simple model, allowing reactor performance to be predicted outside of the range of wastewater compositions used in this study.

- The dyehouse wastewater reactor was used to successfully decolourise and remove COD from synthetic dyehouse wastewater, with an AO7 removal rate of 1.01 g $m^{-2}day^{-1}$ being obtained. This is believed to be the first time azo dyes have been broken down in a Membrane Aerated Biofilm.

Design and Operation of a pilot scale BioSettler

- Using the information obtained from laboratory studies and best practice from the wastewater treatment industry, a pilot scale BioSettler unit was designed and constructed, combining membrane aerated biofilms and inclined plate settlers into a single innovative technology.
- The unit was operated and monitored at two NIW WwTWs and simultaneous suspended soilds, BOD, Ammoniacal and Total Nitrogen removal was obtained – thus proving the concept of the BioSettler.
- Removal rates up to 33.1 $gm^{-2}day^{-1}$ of BOD and 13.4 $gm^{-2}day^{-1}$ of ammoniacal nitrogen were achieved; higher than those obtained in the lab scale studies.

9.2 Recommendations of further work

In Chapter 6, the effect of C:N ratio on the various biological processes taking place in the biofilm was discussed. A clear relationship was established between the relative amounts of oxygen being consumed by both aerobic heterotrophy and nitrification (and therefore the relative rates of these processes) over the range of C:N ratios used in the synthetics wastewaters used in this process. Expansion of this work to include C:N ratios outside of those found here are required to establish whether the MABfR is a viable technology for the treatment of wastewaters with high C:N ratios, such as those originating from food processing premises contain high amounts of sugar, for example.

No clear relationship between the influent composition and rates of denitrification obtained was established. A reason for this was not found in the literature. This paucity can explained due to the absence of a research driver to explore this issue. In the activated sludge process, it is simple to achieve complete denitrification by recycling

secondary effluent and mixing it with primary effluent. This ensures that the produced nitrate sees high COD concentration which is utilised by denitrifiers. This configuration is not possible in the BioSettler where concentrations of both organic carbon and nitrate are low. Further research is required around this issue to develop a full understanding of denitrification in the MABfR, allowing optimisation of Total Nitrogen removal in the BioSettler.

The pilot scale studies described in Chapter 7 were successful in proving the concept of the BioSettler. BOD, Suspended Solids, Ammoniacal and Total Nitrogen were all successfully and simultaneous treated in the pilot scale unit using 'real' secondary effluent from a municipal WwTW. However, the pilot scale studies also exposed two major limitations of the unit – the removal of settled sludge from the bottom of the unit was not effective, leading to the sludge rising and fouling and causing damage to the membrane arrays, which were not strong enough to bear the weight of the sludge.

The issue with sludge removal is simply one of scale – a larger unit can be fitted with conical hoppers from which sludge can easily be removed by gravity. Membranes with higher tensile strength than the ones used in this work are required to prevent the second issue from arising; either filtration membranes with a larger wall thickness or suitable dense membranes are required. Overcoming these two problems is essential for the BioSettler to establish itself as a wastewater treatment technology.

References

Acrivos, A. & Herbolzheimer, E. (1979), *Enhanced sedimentation in settling tanks with inclined walls;* Journal of Fluid Mechanics 92 435-57.

Ahmadi Motlagh, A.R., Voller, V.R. & Semmens, M.J. (2006), *Advective flow through membrane-aerated biofilms: Modeling results;* Journal of Membrane Science 273 1-2 143-151.

Ahmed, T., Oakley, B.T., Semmens, M.J. & Gulliver, J.S. (1996), *Nonlinear deflection of polypropylene hollow fiber membranes in transverse flow;* Water Research 30 2 431-439.

Ahmed, T. & Semmens, M.J. (1996), *Use of transverse flow hollow fibers for bubbleless membrane aeration;* Water Research 30 2 440-446.

Ahmed, T., Semmens, M.J. & Voss, M.A. (2004), *Oxygen transfer characteristics of hollow-fiber, composite membranes;* Advances in Environmental Research 8 3-4 637-646.

Aleboyeh, A., Olya, M.E. & Aleboyeh, H. (2009), *Oxidative treatment of azo dyes in aqueous solution by potassium permanganate;* Journal of Hazardous Materials 162 2-3 1530-1535.

Alef, K. (1995), *Nutrients, sterilization, aerobic and anaerobic culture techniques* In: Methods in Applied Soil Microbiology and Biochemistry, Academic Press Limited, London.

ASCE (1992), *ASCE Standard - Measurement of Oxygen Transfer in Clean Water, ASCE/EWRI 2-06*, ASCE, Reston, VA, U.S.A.

Baker, R.W., Cussler, E.L., Eykamp, W., Koros, W.J., Riley, R.L. & Strathmann, H. (1991), *Membrane Separation Systems: Recent Developments and Future Directions*, Noyes Data Corporation, Park Ridge, New Jersey, U.S.A.

Bishop, P.L., Zhang, T.C. & Fu, Y.-. (1995), *Effects of biofilm structure, microbial distributions and mass transport on biodegradation processes*, Pergamon Press Inc, Copenhagen, Den.

Bitton, G. (2005), *Wastewater Microbiology*, 3rd edn, John Wiley & Sons, New York, USA.

Boycott, A.E. (1920), *Sedimentation of Blood Corpuscles;* Nature 104 2621 532.

Brindle, K., Stephenson, T. & Semmens, M.J. (1998), *Nitrification and oxygen utilization in a membrane aeration bioreactor;* Journal of Membrane Science 144 1-2 197-209.

Brindle, K. & Stephenson, T. (1996), *Nitrification in a bubbleless oxygen mass transfer membrane bioreactor;* Water Science and Technology 34 9 pt 5 261-267.

British Water (2013), *Code of Practice: Flows and Loads 4 - Sizing Criteria, Treatment Capacity for Sewage Treatment Systems*.

Brown, D. & Labouruer, P. (1983), *The aerobic biodegradability of primary aromatic amines;* Chemosphere 12 249-324.

BSi (2002a), *British Standard BS EN 12255-4:2002, Wastewater treatments plants - Part 4: Primary Settlement*.

BSi (2002b), *British Standard BS EN 12255-6:2002, Wastewater treatments plants - Part 6: Activated sludge processes*.

Casey, E., Glennon, B. & Hamer, G. (2000a), *Biofilm development in a membrane-aerated biofilm reactor: Effect of flow velocity on performance;* Biotechnology and Bioengineering 67 4 476-486.

Casey, E., Glennon, B. & Hamer, G. (2000b), *Biofilm development in a membrane-aerated biofilm reactor: Effect of intra-membrane oxygen pressure on performance;* Bioprocess and Biosystems Engineering 23 5 457-465.

Casey, E., Glennon, B. & Hamer, G. (1999), *Oxygen mass transfer characteristics in a membrane-aerated biofilm reactor;* Journal of Engineering and Applied Science 62 2 183-192.

Chambless, J.D. & Stewart, P.S. (2007), *A Three-Dimensional Computer Model Analysis of Three Hypothetical Biofilm Detachment Mechanisms;* Biotechnology and Bioengineering 97 6 1573-1584.

Clesceri, L.S., Greenberg, A.E. & Eaton, A.D. (1998), *Standard Methods for the Examination of Water and Wastewater*, 20th edn, American Public Health Association, American Water Works Association & Water Environment Federation, Baltimore, MD, U.S.A.

Cook, R.L. & Childress, J.J. (1978), *Performance of Lamella Thickeners in Coal Preparation Plants;* Mining Engineering (Littleton, Colorado) 30 5 566-571.

Côté, P., Bersillon, J. & Huyard, A. (1989), *Bubble-free aeration using membranes: mass transfer analysis;* Journal of Membrane Science 47 1-2 91-106.

Côté, P., Bersillon, J., Huyard, A. & Faup, G. (1988), *Bubble-free aeration using membranes: process analysis;* Journal of the Water Pollution Control Federation 60 11 1986-1992.

Coughlin, M.F., Kinkle, B.K. & Bishop, P.L. (2003), *High performance degradation of azo dye Acid Orange 7 and sulfanilic acid in a laboratory scale reactor after seeding with cultured bacterial strains;* Water Research 37 11 2757-2763.

Coughlin, M.F., Kinkle, B.K. & Bishop, P.L. (2002), *Degradation of acid orange 7 in an aerobic biofilm;* Chemosphere 46 1 11-19.

Coulson, J.M., Richardson, J.F., Backhurst, J.R. & Harker, J.H. (1999a), *Flow in Pipes and Channels* In: Chemical Engineering: Volume 1, 6th edn, Butterworth Heinemann, Oxford.

Coulson, J.M., Richardson, J.F., Backhurst, J.R. & Harker, J.H. (1999b), *Heat Transfer* In: Chemical Engineering: Volume 1, 6th edn, Butterworth Heinemann, Oxford.

Cristovao, R.O., Tavares, A.P.M., Loureiro, J.M., Boaventura, R.A.R. & Macedo, E.A. (2009), *Treatment and kinetic modelling of a simulated dye house effluent by enzymatic catalysis;* Bioresource Technology 100 24 6236-6242.

Cussler, E.L. (1997), *Membranes* In: Diffusion, Mass Transfer in Fluid Systems, 2nd edn, Cambridge University Press, Cambridge, U.K.

Darby, R. (1996), *Compressible flows* In: Chemical Engineering Fluid Mechanics, Marcel Dekker Inc., New York.

DARD & DOE (2010), *Nitrates Action Programme 2011 - 2014 & Phosphorous Regulations*, Northern Ireland Environment Agency, Lisburn, U.K.

Davies, L.C., Pedro, I.S., Novais, J.M. & Martins-Dias, S. (2006), *Aerobic degradation of acid orange 7 in a vertical-flow constructed wetland;* Water Research 40 10 2055-2063.

de Hoxar, D. (2000), *Separator plates put sludge in a spin;* Filtration and Separation 37 8 32-33.

DEFRA (2002), *Sewage Treatment in the UK - UK Implementation of the EC Urban Waste Water Treatment Directive*, DEFRA Publications, London, UK.

Demir, A. (1995), *Determination of settling efficiency and optimum plate angle for plated settling tanks;* Water Research 29 2 611-616.

Dincer, A.R. & Kargi, F. (2000), *Kinetics of sequential nitrification and denitrification processes;* Enzyme and Microbial Technology 27 1-2 37-42.

Dindore, V.Y., Brilman, D.W.F. & Versteeg, G.F. (2005), *Modelling of cross-flow membrane contactors: physical mass transfer processes;* Journal of Membrane Science 251 1-2 209-222.

DOE NI & DARD NI (2004), *Nitrates Directive - Second Consultation Paper: Proposal for the Protection of Northern Ireland's Surface and Groundwaters*.

Doig, S.D., Boam, A.T., Livingston, A.G. & Stuckey, D.C. (1999), *Mass transfer of hydrophobic solutes in solvent swollen silicone rubber membranes;* Journal of Membrane Science 154 1 127-140.

dos Santos, L.M.F. & Livingston, A.G. (1995), *Membrane-attached biofilms for VOC wastewater treatment. II: effect of biofilm thickness on performance;* Biotechnology and Bioengineering 47 1 90-95.

Downing, L.S. & Nerenberg, R. (2008a), *Effect of bulk liquid BOD concentration on activity and microbial community structure of a nitrifying, membrane-aerated biofilm;* Applied Microbiology and Biotechnology 81 1 153-162.

Downing, L.S. & Nerenberg, R. (2008b), *Total nitrogen removal in a hybrid, membrane-aerated activated sludge process;* Water Research 42 14 3697-3708.

Doyle, C. (2011), *Bubblefree membrane aeration using hydrophobic polyestersulphone membranes*, Queen's University, Belfast.

Dreszer, C., Flemming, H.-., Zwijnenburg, A., Kruithof, J.C. & Vrouwenvelder, J.S. (2014), *Impact of biofilm accumulation on transmembrane and feed channel pressure drop: Effects of crossflow velocity, feed spacer and biodegradable nutrient;* Water Research 50 200-211.

Ergas, S.J. & Reuss, A.F. (2001), *Hydrogenotrophic denitrification of drinking water using a hollow fibre membrane bioreactor;* Journal of Water Supply: Research and Technology - AQUA 50 3 161-171.

Essila, N.J., Semmens, M.J. & Voller, V.R. (2000), *Modeling biofilms on gas-permeable supports: Concentration and activity profiles;* Journal of Environmental Engineering 126 3 250-257.

European Council (2000), *Directive 2000/60/EC of the European Parliament and of the Council of 23 October 2000 establishing a framework for Community action in the field of water policy* .

European Council (1991a), *Council Directive 91/271/EEC of 21 May 1991 concerning urban waste-water treatment*.

European Council (1991b), *Council directive 91/676/EEC of 12 December 1991 concerning the protection of waters against pollution caused by nitrates from agricultural sources*.

Fang, Y., Novak, P.J., Hozalski, R.M., Cussler, E.L. & Semmens, M.J. (2004), *Condensation studies in gas permeable membranes;* Journal of Membrane Science 231 1-2 47-55.

Fernandes, A., Morão, A., Magrinho, M., Lopes, A. & Gonçalves, I. (2004), *Electrochemical degradation of C. I. Acid Orange 7;* Dyes and Pigments 61 3 287-296.

Fernandez-Seara, J., Uhia, F.J., Sieres, J. & Campo, A. (2005), *Experimental apparatus for measuring heat transfer coefficients by the Wilson plot method;* European Journal of Physics 26 3 1-11.

Fivelman, Q. (2010), *Stage Two Commerialisation Plan - BioSettler (Confidential)*, IP Pragmatics, London, U.K.

Gerlach, S.A. (1994), *Oxygen conditions improve when the salinity in the baltic sea decreases;* Marine Pollution Bulletin 28 7 413-416.

Gingell, R. & Walker, R. (1971), *Mechanisms of azo reduction by Streptococcus faecalis II, the role of soluble falvins;* Xenobiotics 1 231-239.

Grady, C.P.L., Daigger, G.T. & Lim, H., C. (1999), *Biological Wastewater Treatment*, Second Edition, Revised and Expanded edn, Marcel Dekker, Inc., New York, USA.

Gray, N.F. (2004), *Biology of Wastewater Treatment*, 2nd edn, Imperial College Press, London, U.K.

Green, D.W. & Perry, R.H. (2008), *Section 2: Physical and Chemical Data* In: Perry's Chemical Engineers' Handbook, 8th edn, McGraw-Hill.

Groom,E., Murray,S. and Ferguson,J. The Queen's University of Belfast. (2009), Improvements Relating to Water Treatment PCT/GB2008/004193 .

Hach Company (2007), (June 2007-last update), *DR 2800 Spectrophotometer Procedures Manual*. Available online: http://www.hach.com/fmmimghach?/CODE%3ADOC022.53.00725-200719229|1 [2009, 03/02] .

Hach Company (2001), (August 2001-last update), *sensION Ammonia Gas Combination Electrode*. Available online: http://www.hach.com/fmmimghach?/CODE%3A5192788435%7C1 [2009, 03/02] .

Hanna, J. (2005), *Industrial Wastewater Treatment using Dolomite and Dolomitic Sorbents*, Queen's University Belfast.

Hasar, H., Xia, S., Ahn, C.H. & Rittmann, B.E. (2008), *Simultaneous removal of organic matter and nitrogen compounds by an aerobic/anoxic membrane biofilm reactor;* Water Research, 42 15 4109-4116.

Hazen, A. (1904), *On Sedimentation;* Proceedings of the ASCE 53 45-88.

He, S., Xue, G. & Wang, B. (2009), *Factors affecting simultaneous nitrification and de-nitrification (SND) and its kinetics model in membrane bioreactor;* Journal of Hazardous Materials 168 2-3 704-710.

He, Y. & Bishop, P.L. (1994), *Effect of Acid Orange 7 on nitrification process;* Journal of Environmental Engineering 120 1 108-121.

Healy, M.G. & O'Flynn, C.J. (2011), *The performance of constructed wetlands treating primary, secondary and dairy soiled water in Ireland (a review);* Journal of Environmental Management 92 10 2348-2354.

Hellinga, C., Schellen, A.A.J.C., Mulder, J.W., Van Loosdrecht, M.C.M. & Heijnen, J.J. (1998), *The SHARON process: An innovative method for nitrogen removal from ammonium-rich waste water*, Elsevier Sci Ltd, Kalmir, Sweden.

Hendricks, D.W. (2006), *Sedimentation* In: Water Treatment Unit Processes: Physical and Chemical, CRC Press.

Hendrickson, E.R., Ingram, W.T., Churchill, M.A., Bogan, R.W., Hull, C.H., Faber, H.A., Stone, R. & Nemerow, N.L. (1960), *Solubility of Atmospheric Oxygen in Water, Twenty-ninth Progress Report of the Committee on Sanitary Engineering Research of the Sanitary Engineering Division;* ASCE Proceedings: Journal of the Sanitary Engineering Division41-53.

HMG (2005), *Work at Height Regulations*, U.K.

HMG (2003), *The Water Environment (Water Framework Directive) Regulations (Northern Ireland).*

HMG (1999), *The Water (Northern Ireland) Order 1999*, U.K.

HMG (1995), *The Urban Waste Water Treatment Regulations (Northern Ireland) 1995*, Northern Ireland.

Hu, S., Yang, F., Sun, C., Zhang, J. & Wang, T. (2008), *Simultaneous removal of COD and nitrogen using a novel carbon-membrane aerated biofilm reactor;* Journal of Environmental Sciences 20 2 142-148.

Humpal, G.J. & Chiesa, R. (1990), *Considerations for selection, design, and operation of inclined plate settlers for industrial wastewater treatment;* Proceedings of the Industrial Waste Conference 563.

Hwang, J.H., Cicek, N. & Oleszkiewicz, J.A. (2010), *Achieving biofilm control in a membrane biofilm reactor removing total nitrogen;* Water Research 44 7 2283-2291.

Irwin, S. (21st April 2006), *Final settler concentrations*.

Janelt, G., Bolt, P., Gerbsch, N., Buchholz, R. & Cho, M.-. (1997), *The lamellar settler - a low-cost alternative for separating the micro-alga Chlorella vulgaris from a cultivation broth?* Applied Microbiology and Biotechnology 48 1 6-10.

Kadar, Y. & Siboni, G. (1998), *Optimization of energy economy in the design and operation of wastewater treatment plants*.

Khoyi, M.R. & Yaghmaei, S. (2005), *Simulation of competition between two microorganisms in a biofilm reactor based on different growth models;* Biochemical Engineering Journal, 23 1 63-72.

Komorowska-Kaufman, M., Majcherek, H. & Klaczynski, E. (2006), *Factors affecting the biological nitrogen removal from wastewater;* Process Biochemistry 41 5 1015-1021.

Lackner, S., Terada, A. & Smets, B.F. (2008), *Heterotrophic activity compromises autotrophic nitrogen removal in membrane-aerated biofilms: Results of a modeling study;* Water Research 42 4-5 1102-1112.

Lee, K. & Rittmann, B.E. (2002), *Applying a novel autohydrogenotrophic hollow-fiber membrane biofilm reactor for denitrification of drinking water;* Water Research 36 8 2040-2052.

Lees, H. (1951), *Isolation of the Nitrifying Organisms from Soil;* Nature 167 4244 355-356.

Levine, W.G. (1991), *Metabolism of azo dyes: implication for detoxication and activation.* Drug Metabolism Reviews 23 3-4 253-309.

Li, J., Zhu, L., Xu, Y. & Zhu, B. (2010), *Oxygen transfer characteristics of hydrophilic treated polypropylene hollow fiber membranes for bubbleless aeration;* Journal of Membrane Science 362 1-2 47-57.

Li, T., Liu, J., Bai, R. & Wong, F.S. (2008), *Membrane-aerated biofilm reactor for the treatment of acetonitrile wastewater;* Environmental Science and Technology 42 6 2099-2104.

Lieben, F. (1943), *On the hydrolysis of proteins and peptones at high temperatures and on the catalytic effect of metal ions on the rate of hydrolysis;* The Journal of Biological Chemistry 151 1 117-121.

Lipscomb, D., Larkin, M., Irvine, H. & Allen, C. (2008), *BIOCOL process for remediation of dye house wastewaters*.

Livingston, A.G., Arcangeli, J., Boam, A.T., Zhang, S., Marangon, M. & Freitas dos Santos, L.M. (1998), *Extractive membrane bioreactors for detoxification of chemical industry wastes: Process development;* Journal of Membrane Science 151 1 29-44.

Mace, G.R. & Laks, R. (1978), *Developments in Gravity Sedimentation;* Chemical Engineering Progress 74 7 77-83.

Madigan, M.T. & Martinko, J.M. (2006), *Microbial Ecology* In: Brock Biology of Microorganisms, 11th Edition edn, Pearson Education, Inc., Upper Saddle River, New Jersey.

Manser, R., Gujer, W. & Siegrist, H. (2006), *Decay processes of nitrifying bacteria in biological wastewater treatment systems;* Water Research 40 12 2416-2426.

Masschelein, W.J. (1992), *Lamellar and Turbular Assisted Settling Processes* In: Unit Processes in Drinking Water Treatment, CRC Press, Boca Raton, Florida, U.S.A.

Matsumoto, S., Terada, A. & Tsuneda, S. (2007), *Modeling of membrane-aerated biofilm: Effects of C/N ratio, biofilm thickness and surface loading of oxygen on feasibility of simultaneous nitrification and denitrification;* Biochemical Engineering Journal, 37 1 98-107.

McCarty, P.L. (1975), *Stoichiometry of Biological Reactions;* Progress in Water Technology 7 1 157-172.

Meng, Q., Yang, F., Liu, L. & Meng, F. (2008), *Effects of COD/N ratio and DO concentration on simultaneous nitrification and denitrifcation in an airlift internal circulation membrane bioreactor;* Journal of Environmental Sciences 20 8 933-939.

Metcalf & Eddy, I. (2003), *Wastewater engineering : treatment and reuse*, 4th edn, McGraw-Hill, Boston, London.

Metso Minerals (2006), , *Inclined Plate Settlers*. Available online: http://www.metsominerals.com/inetMinerals/MaTobox7.nsf/DocsByID/909127C821746DDE41256B41004D7B71/$File/Inclined_Plate_Settler.pdf [2008, 04/04] .

Monroe, D. (2007), *Looking for Chinks in the Armor of Bacterial Biofilms;* Journal of the Public Library of Science: Biology.

Morgenroth, E. (2008), *Biofilm Reactors* In: Biological Wastewater Treatment: Principles, Modeling, and Design, IWA Publishing, London, U.K.

NI Water (2013), , *About Us: Facts and Figures*. Available online: http://www.niwater.com/facts-and-figures/ [2014, April 22nd] .

NIEA (2014), *Regulation of Water Utility Sector Discharges 2012*, Northern Ireland Environment Agency, Lisburn, U.K.

NIEA (2009), *North Eastern River Basin Management Plan Summary*, Northern Ireland Environment Agency, Lisburn, U.K.

OECD (1984), *OECD Guidelines for testing chemicals: 209 "Activated Sludge, Respiration Inhibition Test"*.

O'Neill, R., Ahmad, M.N., Vanoye, L. & Aiouache, F. (2009), *Kinetics of aqueous phase dehydration of xylose into furfural catalyzed by ZSM-5 zeolite;* Industrial and Engineering Chemistry Research 48 9 4300-4306.

Ong, S., Toorisaka, E., Hirata, M. & Hano, T. (2005), *Decolorization of azo dye (Orange II) in a sequential UASB-SBR system;* Separation and Purification Technology 42 3 297-302.

Pandey, A., Singh, P. & Iyengar, L. (2007), *Bacterial decolorization and degradation of azo dyes;* International Biodeterioration and Biodegradation 59 2 73-84.

Pankhania, M., Brindle, K. & Stephenson, T. (1999), *Membrane aeration bioreactors for wastewater treatment: completely mixed and plug-flow operation;* Chemical Engineering Journal 73 2 131-136.

Pankhania, M., Stephenson, T. & Semmens, M.J. (1994), *Hollow fibre bioreactor for wastewater treatment using bubbleless membrane aeration;* Water research 28 10 2233-2236.

Parkson (2010), , *Lamella EcoFlow Inclined Plate Settler*. Available online: http://www.parkson.com/sites/default/files/documents/document-lamella-ecoflow-brochure-482.pdf [2014, April 6th] .

Paul, E.L., Atiemo-Obeng, V. & Kresta, S.M. (2004), *Handbook of Industrial Mixing: Science and Practice*, Wiley Interscience, Hoboken, NJ, U.S.A.

Pavasant, P., Freitas dos Santos, L.M., Pistikopoulos, E.N. & Livingston, A.G. (1996), *Prediction of optimal biofilm thickness for membrane-attached biofilms growing in an extractive membrane bioreactor;* Biotechnology and Bioengineering 52 3 373-386.

Pearce, C.I., Christie, R., Boothman, C., Von Canstein, H., Guthrie, J.T. & Lloyd, J.R. (2006), *Reactive azo dye reduction by Shewanella strain J18 143;* Biotechnology and Bioengineering 95 4 692-703.

Peng, L., Chen, X., Xu, Y., Liu, Y., Gao, S. & Ni, B. (2015), *Biodegradation of pharmaceuticals in membrane aerated biofilm reactor for autotrophic nitrogen removal: A model-based evaluation;* Journal of Membrane Science 494 39-47.

Picard, C., Logette, S., Schrotter, J.C., Aimar, P. & Remigy, J.C. (2012), *Mass transfer in a membrane aerated biofilm;* Water research 46 15 4761-4769.

Ponder, E. (1925), *On Sedimentation and Rouleaux Formation;* Quarterly Journal of Experimental Physiology 15 235-252.

Probstein, R.F. & Hicks, R.E. (1978), *Lamella Settlers: A New Operating Mode for Hign Performance;* Industrial Water Engineering 15 1 6-8.

Radcliff, R. & Zarnadze, A. (2004), *Application of Membrane Technology to the Production of Drinking Water;* Water Conditioning and Purification 46 8 23-25.

Robb, W.L. (1968), *Thin silicone membranes - their permeation properties and some applications;* Annals of the New York Academy of Science 146 1 119-137.

Rogers, G.F.C. & Mayhew, Y.R. (1994), *Thermodynamic and Transport Properties of Fluids (S.I. Units).*

Rubino, V. (1996), *Caught in the crossfire: wastewater plant retrofit;* Pollution Engineering 28 6 72-75.

Saleh, A.M. & Hamoda, M.F. (1999), *Upgrading of secondary clarifiers by inclined plate settlers;* Water Science and Technology 40 7 141-149.

Salem, A.I., Okoth, G. & Thöming, J. (2011), *An approach to improve the separation of solid–liquid suspensions in inclined plate settlers: CFD simulation and experimental validation;* Water Research 45 11 3541-3549.

Saratale, R.G., Saratale, G.D., Kalyani, D.C., Chang, J.S. & Govindwar, S.P. (2009), *Enhanced decolorization and biodegradation of textile azo dye Scarlet R by using developed microbial consortium-GR;* Bioresource Technology 100 9 2493-2500.

Sarkar, S., Kamilya, D. & Mal, B.C. (2007), *Effect of geometric and process variables on the performance of inclined plate settlers in treating aquacultural waste;* Water Research 41 5 993-1000.

Satoh, H., Ono, H., Rulin, B., Kamo, J., Okabe, S. & Fukushi, K. (2004), *Macroscale and microscale analyses of nitrification and denitrification in biofilms attached on membrane aerated biofilm reactors;* Water Research 38 6 1633-1641.

Schneider, M., Reymond, F., Marison, I.W. & von Stockar, U. (1995), *Bubble-free oxygenation by means of hydrophobic porous membranes;* Enzyme and Microbial Technology 17 9 839.

Schöner, P., Plucinski, P., Nitsch, W. & Daiminger, U. (1998), *Mass transfer in the shell side of cross flow hollow fiber modules;* Chemical Engineering Science 53 13 2319-2326.

Semmens, M.J., Dahm, K., Shanahan, J. & Christianson, A. (2003), *COD and nitrogen removal by biofilms growing on gas permeable membranes;* Water Research 37 18 4343-4350.

Shah, D.B. & Coulman, G.A. (1978), *Kinetics of Nitrification and Denitrification Reactions;* Biotechnology and Bioengineering 20 1 43-72.

Shanahan, J.W. & Semmens, M.J. (2006), *Influence of a nitrifying biofilm on local oxygen fluxes across a micro-porous flat sheet membrane;* Journal of Membrane Science 277 1-2 65-74.

Shanahan, J.W. & Semmens, M.J. (2004), *Multipopulation model of membrane-aerated biofilms;* Environmental Science and Technology 38 11 3176-3183.

Shaw, C.B., Carliell, C.M. & Wheatley, A.D. (2002), *Anaerobic/aerobic treatment of coloured textile effluents using sequencing batch reactors;* Water Research 36 8 1993-2001.

Smyth, B. (2011), *Pumping Energy Requirements*.

Smyth, B., Crilly, A. & McDowell, K. (2013), *Water efficiency as a means of reducing carbon emissions in Northern Ireland (NI) water;* Journal of Water Supply: Research and Technology - AQUA 62 8 525-533.

Sponza, D.T. & Isik, M. (2002), *Ultimate azo dye degradation in anaerobic/aerobic sequential processes*, IWA Publishing.

Stephenson, T., Judd, S., Jefferson, B. & Brindle, K. (2000), *Membrane Bioreactors for Wastewater Treatment*, First Edition edn, IWA Publishing, London.

Steube, T. (2009), *Manual for MOLSEP cartridge FS10 and FE10*, Microdyn-Nadir, Weisbaden, Germany.

Stewart, R. (2014), *Nutrient consent in NI as enforced by NIEA*.

Tan, N.C.G., Borger, A., Slender, P., Svitelskaya, A.V., Lettinga, G. & Field, J.A. (2000), *Degradation of azo dye Mordant Yellow 10 in a sequential anaerobic bioaugmented aerobic bioreactor;* Water Science and Technology 45 337-344.

Tchobanoglous, G. & Burton, F.L. (1991a), *Biological Unit Processes* In: Wastewater Engineering: Treatment, Disposal and Reuse, 3rd edn, McGraw-Hill, New York, U.S.A.

Tchobanoglous, G. & Burton, F.L. (1991b), *Metcalf & Eddy's Wastewater Engineering: Treatment, Disposal, Reuse,* 3rd edn, McGraw-Hill, Singapore.

Tchobanoglous, G., Burton, F.L. & Stensel, H.D. (2004), *Physical Unit Operations* In: Wastewater Engineering: Treatment and Reuse, Fourth edn, McGraw Hill, Singapore.

Terada, A., Hibiya, K., Nagai, J., Tsuneda, S. & Hirata, A. (2003), *Nitrogen removal characteristics and biofilm analysis of a membrane-aerated biofilm reactor applicable to high-strength nitrogenous wastewater treatment;* Journal of Bioscience and Bioengineering 95 2 170-178.

Thumheer, T., Koehler, T., Cook, A.M. & Leisinger, T. (1986), *Orthanilic acid and analogs as carbon sources for bacteria: groth physiology and enzymatic desulphonation;* Journal of General Microbiology 132 1215-1220.

Timberlake, D.L., Strand, S.E. & Williamson, K.J. (1988), *Combined aerobic heterotrophic oxidation, nitrification and denitrification in a permeable-support biofilm;* Water Research 22 12 1513-1517.

Tsushima, I., Ogasawara, Y., Shimokawa, M., Kindaichi, T. & Okabe, S. (2007), *Development of a super high-rate Anammox reactor and in situ analysis of biofilm structure and function;* Water Science and Technology 55 8 9-17.

US EPA (2012), *Summaries of Water Pollution Reporting Categories (adapted from Document no. EPA 841-R-12-104),* US EPA.

Van Der Zee, F. P., Bisschops, I.A.E., Blanchard, V.G., Bouwman, R.H.M., Lettinga, G. & Field, J.A. (2003a), *The contribution of biotic and abiotic processes during azo dye reduction in anaerobic sludge;* Water Research 37 13 3098-3109.

Van Der Zee, F. P., Bisschops, I.A.E., Lettinga, G. & Field, J.A. (2003b), *Activated carbon as an electron acceptor and redox mediator during the anaerobic biotransformation of azo dyes;* Environmental Science and Technology 37 2 402-408.

Van Der Zee, F.P. & Villaverde, S. (2005), *Combined anaerobic-aerobic treatment of azo dyes - A short review of bioreactor studies;* Water Research 39 8 1425-1440.

Venkatesh, G. & Brattebo, H. (2011), *Energy consumption, costs and environmental impacts for urban water cycle services: Case study of Oslo (Norway);* Energy 36 2 792-800.

Vladisavljevic, G.T. (1999), *Use of polysulfone hollow fibers for bubbleless membrane oxygenation/deoxygenation of water;* Separation and Purification Technology 17 1 1-10.

Walker, G.M., Hansen, L., Hanna, J.-. & Allen, S.J. (2003), *Kinetics of a reactive dye adsorption onto dolomitic sorbents;* Water Research 37 9 2081-2089.

Walter, B., Haase, C. & Rabiger, N. (2005), *Combined nitrification/denitrification in a membrane reactor;* Water Research 39 13 2781-2788.

Wang, J., Liu, G., Lu, H., Jin, R., Zhou, J. & Lei, T. (2012), *Biodegradation of Acid Orange 7 and its auto-oxidative decolorization product in membrane-aerated biofilm reactor;* International Biodeterioration & Biodegradation 67 73-77.

Wenk, S.E. (1990), *The theory, design and experience of Lamella Gravity Settlers in the phosphate industry;* Fertilizer Research 25 139-143.

Wilkinson, R. (2007), *Effluent concentrations at Ulster Carpets Mills (personal communication - email).*

Yamagiwa, K. & Ohkawa, A. (1994), *Simultaneous Organic Carbon Removal and Nitrification by Biofilm formed on Oxygen Enrichment Membrane;* Journal of Chemical Engineering of Japan 27 5 638-643.

Yang, M. & Cussler, E.L. (1986), *Designing Hollow Fiber Contactors;* AICHE Journal 32 11 1910-1916.

Yasuda, H. & Lamaze, C.E. (1972), *Transfer of gas to dissolved oxygen in water via poroous and nonporous polymer membranes;* Journal of Applied Polymer Science 16 595-601.

Zhang, T.C., Fu, Y. & Bishop, P.L. (1995), *Competition for substrate and space in biofilms;* Water Environment Research 67 6 992-1003.

Zhang, H. & Cloud, A. (2006), *The permeability characteristics of silicone rubber*, Soc. for the Advancement of Material and Process Engineering, Covina, CA 91724-3748, United States.

Zheng, J., Dai, Z., Wong, F. & Xu, Z. (2005), *Shell side mass transfer in a transverse flow hollow fiber membrane contactor;* Journal of Membrane Science 261 1-2 114-120.

Zhu, I.X. (2008), *Effect of Oxygen Partial Pressure and COD Loading on Biofilm Performance in a Membrane Aerated Bioreactor*, University of Toronto, Toronto, Ontario, Canada.

Appendices

A1 Results summaries – Mass Transfer Studies

A1.1 Saturation coefficients for use in Equation 3-2

Inlet pressure (barg)		Silicone Rubber	Polyethersulphone
0.2	a	16.03	15.24
	b_1	-0.36	-0.41
	b_2	1.81×10^{-3}	5.62×10^{-3}
	b_3	36.1×10^{-6}	-53.7×10^{-6}
0.25	a	16.12	14.56
	b_1	-0.53	-0.33
	b_2	12.0×10^{-3}	2.91×10^{-3}
	b_3	-0.13×10^{-3}	-3.32×10^{-6}
0.4	a	16.33	15.71
	b_1	-0.46	-0.49
	b_2	8.77×10^{-3}	10.4×10^{-3}
	b_3	-81.0×10^{-6}	-0.12×10^{-3}
0.5	a	16.61	15.03
	b_1	-0.37	-0.33
	b_2	2.80×10^{-3}	1.53×10^{-3}
	b_3	17.3×10^{-6}	24.0×10^{-6}
0.8	a	17.80	15.08
	b_1	-0.48	-0.27
	b_2	8.00×10^{-3}	-0.25×10^{-3}
	b_3	-60.1×10^{-6}	36.2×10^{-6}
1.0	a	22.15	15.62
	b_1	-0.55	-0.29
	b_2	3.30×10^{-3}	-1.46×10^{-3}
	b_3	5.21×10^{-6}	99.0×10^{-6}
2.0	a	27.40	
	b_1	-1.11	
	b_2	33.9×10^{-3}	
	b_3	-0.40×10^{-3}	

A1.2 Observed oxygen flux

Numbers in red type correspond to experiments where the regression coefficient in the plot of of $\ln\left(\frac{C^*-C_t}{C^*}\right)$ versus t is poor (<0.98). These experiments are omitted from the calculation of the displayed averages.

A1.2.1 Effect of air side flowrate

Silicone rubber

Inlet Flowrate (lpm)		0.6	1	2	3	4	5
$gO_2m^{-2}h^{-1}$	J_1	1.49	1.38	1.55	1.41	1.53	1.38
	J_2	1.50	1.43	1.28	1.47	1.51	1.43
	J_3	1.45	1.45	1.46	1.52	1.45	1.43
	Average	1.48	1.42	1.43	1.47	1.50	1.41

Polyethersulphone

Inlet Flowrate (lpm)		0.6	1	2	3	4	5
$gO_2m^{-2}h^{-1}$	J_1	0.59	0.58	0.53	0.55	0.56	0.54
	J_2	0.55	0.51	0.49	0.56	0.55	0.55
	J_3	0.50	0.51	0.56	0.55	0.53	0.53
	J_4	0.53	0.53				0.52
	Average	0.56	0.52	0.53	0.55	0.55	0.53

Effect of inlet air pressure

Silicone rubber

Pressure (barg)		0.2	0.25	0.4	0.5	0.8	1	2
Flowrate (lpm)		5	4	2.5	2	1.25	1	0.5
$gO_2m^{-2}h^{-1}$	J_1	1.29	1.25	1.38	1.46	1.61	1.84	2.43
	J_2	1.18	1.23	1.41	1.49	1.64	1.71	2.42
	J_3	1.25	1.22	1.53	1.46	1.57	1.69	2.38
	J_4			1.40				
	average	1.24	1.23	1.44	1.47	1.61	1.75	2.41

Polyethersulphone

Pressure (barg)		0.2	0.25	0.4	0.5	0.8	1
Flowrate (lpm)		5	4	2.5	2	1.25	1
$gO_2m^{-2}h^{-1}$	J_1	0.71	0.73	0.66	0.75	0.71	0.75
	J_2	0.71	0.74	0.74	0.75	0.78	0.79
	J_3	0.67	0.74	0.78	0.78	0.76	0.79
	J_4						
	J_5						
	average	0.70	0.74	0.72	0.76	0.75	0.78

A1.2.2 Effect of water side flowrate

Silicone rubber

Flowrate (ml min^{-1})		157.5	210.0	262.5	315.0	367.5	472.5	555.0
$gO_2m^{-2}h^{-1}$	J_1	0.97	0.97	1.06	1.14	1.19	1.06	1.13
	J_2	0.90	0.95	1.06	1.10	1.15	1.14	1.25
	J_3	0.94	0.80	1.05	1.11	1.11	1.14	1.31
	J_4		0.92			1.10		1.31
	J_5					1.14	1.26	1.27
	average	0.94	0.95	1.06	1.12	1.12	1.15	1.25

Polyethersulphone

Flowrate (ml min^{-1})		157.5	210.0	262.5	315.0	367.5	420.0	472.5
$gO_2m^{-2}h^{-1}$	J_1	0.50	0.50	0.51	0.49	0.57	0.61	0.56
	J_2	0.42	0.48	0.39	0.56	0.61	0.50	0.51
	J_3	0.44	0.40	0.52	0.45	0.44	0.42	0.46
	J_4	0.40	0.43	0.46	0.47	0.49	0.57	0.47
	J_5		0.45	0.44		0.47	0.50	0.47
	average	0.44	0.45	0.46	0.49	0.52	0.52	0.49

A2 Biofilm Reactor Studies MABfR A - Results summaries

A2.1 Inlet pressure studies (Chapter 5)

A2.1.1 COD

Influent

Inlet Pressure (barg)	1.0	1.1	1.2	1.3	1.4	1.6	2.0
Observation	Influent COD (mg l^{-1})						
1	72	69	68	72	75	76	71
2	68	74	70	70	73	70	72
3	70	76	76	72	72	76	72
4	64	70	73	72	72	73	73
5	78	71	68	71	72	72	72
Average	70	72	71	71	73	73	72
Standard Error	2.3	1.3	1.5	0.4	0.6	1.2	0.3

Effluent

Inlet Pressure (barg)	1.0	1.1	1.2	1.3	1.4	1.6	2.0
Observation	Effluent COD (mg l^{-1})						
1	40	30	41	27	31	18	14
2	28	28	42	31	39	24	17
3	24	28	27	28	27	26	18
4	21	28	24	30	27	22	14
5	34	23	25	31	24	29	16
Average	29	27	32	29	30	24	16
Standard Error	3.43	1.17	3.99	0.81	2.60	1.85	0.80

A2.1.2 Ammoniacal Nitrogen

Influent

Inlet Pressure (barg)	1.0	1.1	1.2	1.3	1.4	1.6	2.0
Observation	Influent Ammonical Nitrogen (mg l^{-1})						
1	9.87	9.35	9.56	9.52	9.77	9.62	9.84
2	9.62	9.27	9.07	9.51	9.88	9.72	9.78
3	9.77	9.14	9.45	9.48	9.76	9.6	9.6
4	9.56	9.35	9.46	9.65	9.9	9.77	9.21
5	9.77	9.45	9.45	9.62	9.77	9.6	9.03
Average	9.72	9.31	9.40	9.56	9.82	8.07	9.49
Standard Error	0.06	0.05	0.08	0.03	0.03	1.75	0.16

Effluent

Inlet Pressure (barg)	1.0	1.1	1.2	1.3	1.4	1.6	2.0
Observation	Effluent Ammonical Nitrogen (mg l^{-1})						
1	6.85	3.11	3.06	3.53	3.57	3.97	2.54
2	4.49	3.21	2.91	3.51	3.81	4.42	2.25
3	3.92	3.35	2.31	2.92	3.85	4	2.04
4	5.82	3.52	3.21	3.31	4.43	3.77	2.29
5	5.07	3.01	5.43	2.84	4.42	3.83	2.04
Average	5.23	3.24	3.38	3.22	4.02	4.00	2.23
Standard Error	0.51	0.09	0.53	0.15	0.17	0.11	0.09

A2.1.3 Nitrate Nitrogen

Influent

Inlet Pressure (barg)	1.0	1.1	1.2	1.3	1.4	1.6	2.0
Observation	Influent Nitrate Nitrogen (mg l^{-1})						
1	<0.1	<0.1	<0.1	<0.1	<0.1	<0.1	<0.1
2	<0.1	<0.1	<0.1	<0.1	<0.1	<0.1	<0.1
3	<0.1	<0.1	<0.1	<0.1	<0.1	<0.1	<0.1
4	<0.1	<0.1	<0.1	<0.1	<0.1	<0.1	<0.1
5	<0.1	<0.1	<0.1	<0.1	<0.1	<0.1	<0.1

Effluent

Inlet Pressure (barg)	1.0	1.1	1.2	1.3	1.4	1.6	2.0
Observation	Effluent Nitrate Nitrogen (mg l^{-1})						
1	3.6	3.6	6.0	5.1	3.7	3.2	4.0
2	5.0	4.1	5.4	4.9	4.5	3.7	4.6
3	5.2	3.6	4.4	5.3	3.6	3.6	4.5
4	2.4	4.8	5.1	5.0	3.4	3.9	4.6
5	4.4	4.5	5.4	5.2	3.6	3.5	4.5
Average	4.1	4.1	5.3	5.1	3.8	3.6	4.4
Standard Error	0.5	0.2	0.3	0.1	0.2	0.1	0.1

A2.2 Pollutant loading studies (Chapter 6)

Run 8

Observation	Amm-N inf mg l^{-1}	Amm-N eff mg l^{-1}	COD inf mg l^{-1}	COD eff mg l^{-1}	Nit-N inf mg l^{-1}	Nit-N eff mg l^{-1}
1	11.17	6.95	78	57	<0.1	1.5
2	12.3	7.08	60	21	<0.1	1.0
3	9.12	6.14	62	27	<0.1	1.5
4	11.99	6.28	63	18	<0.1	2.9
5	11.04	5.79	81	53	<0.1	1.5
6	12.33	5.57	61	19	<0.1	1.1
7	11.19	7.01	68	1	<0.1	3.8
8	12.24	6.55	76	11	<0.1	2.0
9	13.03	6.31	76	35	<0.1	1.5
10	13.03	6.34	76	38	<0.1	1.5
11	10.86	5.93	53	4	<0.1	1.5
12	10.86	5.55	53	14	<0.1	2.0
13	10.66	5.36	65	21	<0.1	0.9
14	8.13	5.52	54	20	<0.1	0.9
15	9.77	5.24	54	15	<0.1	1.6
16	10.74	4.86	60	30	<0.1	0.7
17	13.12	6.41	74	1	<0.1	2.4
18	12.56	7.8	65	7	<0.1	0.4
19	12.39	6.13	52	36	<0.1	0.7
20	12.16	8.22	80	38	<0.1	0.6
21	12.16	7.93	52	32	<0.1	3.1
22	12.16	8.21	63	52	<0.1	1.5
23	12.3	6.07	63	48	<0.1	0.8
24	13.12	7.62	58	42	<0.1	0.7
25	12.3	6.62	71	31	<0.1	1.7
26	11.83	6.28	72	32	<0.1	0.6
27	12.27	6.3	72	27	<0.1	0.7
28	12.27	6.18	71	34	<0.1	1.6
29	12.68	6.15	72	33	<0.1	0.5

Run 9

Observation	Amm-N inf mg l^{-1}	Amm-N eff mg l^{-1}	COD inf mg l^{-1}	COD eff mg l^{-1}	Nit-N inf mg l^{-1}	Nit-N eff mg l^{-1}
1	10.3	6.25	67	12	5.5	6.8
2	10.3	5.66	58	10	5.8	8.4
3	10.62	6.22	70	46	6.0	8.1
4	9.91	5.45	71	20	4.9	8.6
5	9.51	4.92	81	44	6.0	7.9
6	9.38	5.58	66	35	6.0	5.6
7	10.59	4.99	77	37	5.4	5.0
8	10.16	5.4	76	39	4.5	5.4

Run 10

Observation	Amm-N inf mg l^{-1}	Amm-N eff mg l^{-1}	COD inf mg l^{-1}	COD eff mg l^{-1}	Nit-N inf mg l^{-1}	Nit-N eff mg l^{-1}
1	7.26	3.7	63	23	5.4	7.5
2	7.18	3.8	75	50	5.0	6.4
3	7.14	3.42	73	39	4.9	7.2
4	7.08	3.52	63	30	4.6	7.9
5	7.11	3.7	75	50	6.5	4.8
6	7.2	3.52	77	52	0.0	7.1

Run 11

Observation	Amm-N inf mg l^{-1}	Amm-N eff mg l^{-1}	COD inf mg l^{-1}	COD eff mg l^{-1}	Nit-N inf mg l^{-1}	Nit-N eff mg l^{-1}
1	8.4	3.14	122	35	4.8	7.8
2	8.33	3.49	119	55	5	7.6
3	8.18	3.96	113	62	5.1	7.4
4	8.59	4.39	113	58	5.3	6.8
5	8.81	4.49	127	77	5	8
6	7.78	3.81	117	65	5.9	7.5
7	7.48	2.98	108	40	5.1	10.2
8	8.49	3.22	115	52	5.4	9.8
9	6.62	3.45	116	77	5.3	8.6
10	7.45	3.71	115	60	4.8	8
11	8.38	4.37	117	17	5.2	7
12	9.08	3.94	126	61	4.6	5.9
13	7.82	3.56	106	83	5.8	7
14	7.65	3.61	125	62	5.9	6.9
15	8.05	3.41	120	77	5.4	6.7

Run 12

Observation	Amm-N inf mg l^{-1}	Amm-N eff mg l^{-1}	COD inf mg l^{-1}	COD eff mg l^{-1}	Nit-N inf mg l^{-1}	Nit-N eff mg l^{-1}
1	7.13	3.8	62	43	4.5	7.3
2	5.79	1.858	81	29	5.2	6.2
3	6.92	5.09	78	38	6.3	6.7
4	7.71	4.07	69	37	6.6	10.1
5	7.67	2.92	66	10	5.9	10.5
6	8.1	0.1059	67	14	5.1	5.1
7	7.96	0.1091	62	8	5.1	4.9
8	9.46	2.42	66	9	5.3	5.3
9	8.25	3.87	67	37	4.1	12.6
10	6.89	1.742	77	65	4.8	0.4
11	5.02	1.986	67	6	6.1	12.4
12	8.57	1.986	74	43	6.1	10.0
13	8.28	4.16	66	6	6.1	8.0
14	8.38	4.8	80	48	4.9	5.4
15	9.28	4.38	66	32	6	6.9
16	9.44	1.094	70	49	5.8	4.2
17	9.86	0.292	62	21	6.6	5.7
18	8.95	6.37	66	15	5.4	8.7
19	8.88	2.51	65	17	5	4.9

A3 Pilot plant studies

A3.1 Tank dimensions

Plate packs

number of plate packs	N	2			
number of plates in pack	n_p	11			
plate spacing	ω_p	0.11	m		
plate thickness	p_t	0.01	m		
plate angle	α	55	°	0.960	radians
length of plates	l_p	1	m		
breath of plates	b_p	0.5	m		
area of plates	A_p	0.5	m^2	$A_p = l_p b_p$	
length of plate packs	l_{pp}	1.10	m	$l_{pp} = (n_p - 1)\omega_p$	
total settling area	A_T	5.74	m^2	$A_T = N(n_p - 1)A_p Cos\ \alpha$	
total settling volume	V_{ST}	0.818	m^3	$V_{ST} = N(n_p - 1)(\omega_p - p_t)l_p b_p Sin\alpha$	
total plate pack volume	V_{pp}	0.90	m^3	$V_{pp} = N(n_p - 1)\omega_p l_p b_p Sin\ \alpha$	
specific settling area (volume)		3.97	m^2m^{-3}		
specific settling area (footprint)		2.86	m^2m^{-2}		

Sludge collection zone

sludge collection angle	θ	20	°	0.35	radians
height of sludge zone	h_{sz}	0.40	m		

volume of sludge zone	V_{sz}	0.26	m^3	$V_{sz} = \frac{1}{2} h_{sz} l_{pp} b_{iz}$

Inlet zone

feed channel breadth	b_f	0.2	m	$b_f = 0.2 N b_p$
inlet zone breadth	b_{iz}	1.2	m	$b_{iz} = N b_p + b_f$
volume of inlet zone	V_{iz}	0.28	m^3	$V_{iz} = \frac{1}{2} l_p h_{pp} b_{iz} Sin(90 - \alpha)$

Tank dimensions

height of platepack	h_{pp}	0.82	m	$h_{pp} = l_p Sin\,\alpha$
length of platepack	l_{pp}	1.10	m	$l_{pp} = (n-1)\omega_p$
height of sludgezone	h_{sz}	0.40	m	$h_{sz} = l_{pp} Tan\ \theta$
total tank volume	V_T	1.45	m^3	$V_T = V_{iz} + V_{pp} + V_{sz}$
footprint	A_f	2.01	m^2	$A_f = b_{iz}(l_{pp} + l_p Sin\,(90 - \alpha))$
minimum height of tank	h_{min}	1.22	m	
minimum breadth of tank	b_{min}	1.2	m	

A3.2 CAD diagrams

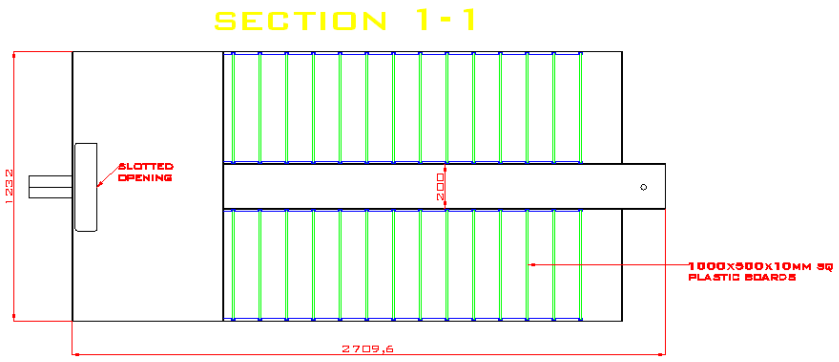

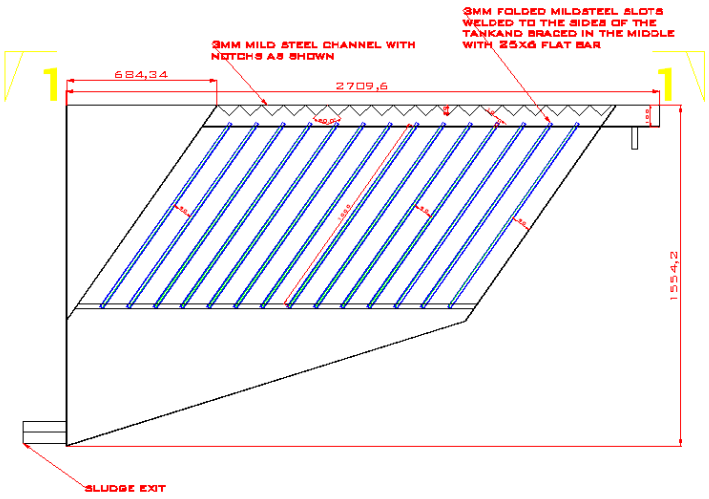

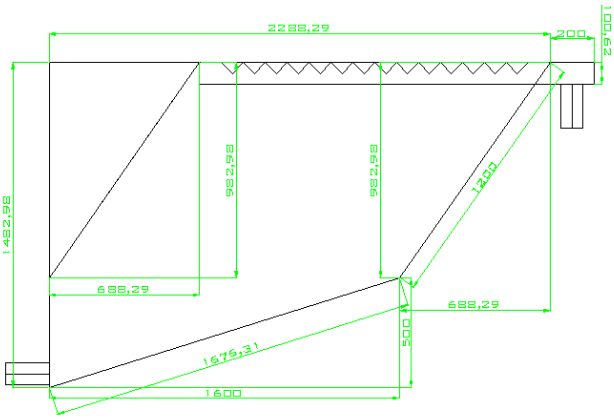

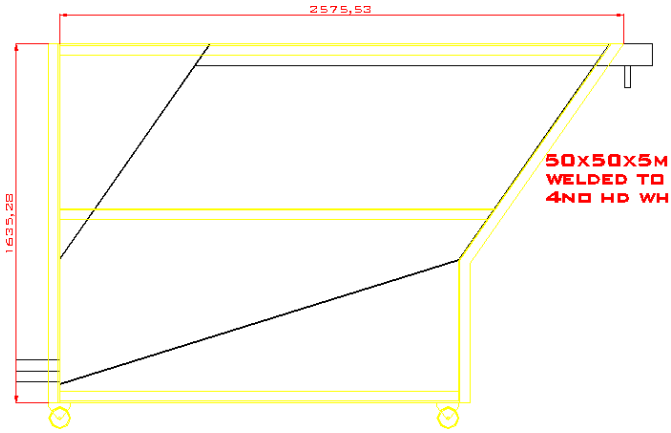

50X50X5MM ANGLE SURROUND WELDED TO THE 3MM TANK, WITH 4NO HD WHEELS

SECTION 2-2

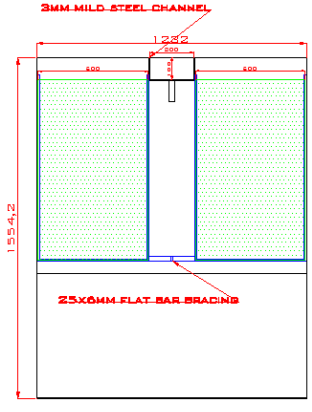

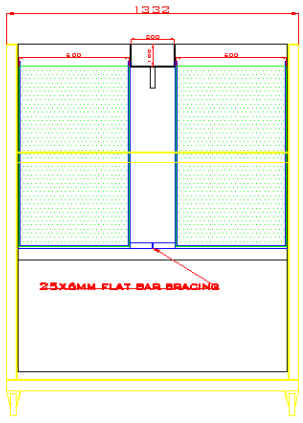

A3.3 Pilot Plant Studies – sample analysis

		Raw data - plant effluent							Raw data - BioSettler effluent						
Day	flowrate l day^{-1}	COD mg l^{-1}	BOD mg l^{-1}	Amm -N mg l^{-1}	Nit-N mg l^{-1}	SS mg l^{-1}	pH	Tot-N mg l^{-1}	COD mg l^{-1}	BOD mg l^{-1}	Amm -N mg l^{-1}	Nit-N mg l^{-1}	SS mg l^{-1}	pH	Tot-N mg l^{-1}
1	4077														
2	4077														
3	4077														
4	4077														
5	4077														
6	4077	563		55.7	0.9	70.9	7.47	56.6	483		45.5	0.7	92.5	7.56	46.2
7	4077	443	101	48	0.4	79	7.57	48.4	463	99	46.2	1	78	7.6	47.2
8	4077	261		40.7	0.6	54	7.7	41.3	187		30.7	1.3	38	7.72	32.0
9	4077	358		44	0.6	68	7.65	44.6	285		31.7	0.5	44	7.61	32.2
10	4077														
11	4077														
12	4077														
13	4077	205		22	0.3	41	7.38	22.3	182		22.2	1.1	38	7.19	23.3
14	4077	236	51.2	22.8	0.3	39	7.34	23.1	189	37.4	27.5	0.2	31	7.5	27.7
15	4077	122		25.5	2.4	33	7.68	27.9	111		24.4	0.8	23	7.66	25.2
16	4077	148		22.2	1.3	27	7.36	23.5	129		26.8	1.1	18	7.7	27.9
17	4077	316		51.2	0.9	51	7.64	52.1	154		28.4	0.9	38	7.69	29.3
18	4077	537		58.5	0.7	94	7.71	59.2	283		37.9	1.3	62	7.69	39.2

19	4077	347		44.3	0.1	88		44.4	325		35.6	6.8	88		42.4
20	4077	278	83	33.6	0.1	89		33.7	128	49	18.11	6.8	62		24.9
21	4077	173		27.9	0.9	25	7.57	28.8	129		26.4	1.1	30	7.48	27.5
22	4077	197		32.6	1.2	49	7.54	33.8	142		27.5	1.1	29	7.53	28.6
23	4077	248		30.3	0.9	57	7.49	31.2	170		33.7	0.8	37	7.59	34.5
24	4077	264		30.7	0.9	58	7.42	31.6	251		31.8	0.6	61	7.49	32.4
25	4077	324		33	1	84	7.32	34.0	290		31.4	0.8	61	7.48	32.2
26	4077	309		43	0.7	66	7.36	43.7	235		41.8	0.5	65	7.54	42.3
27	4077	156		34.5	0.7	59	7.56	35.2	173		30.4	0.6	59	7.44	31.0
28	4077	132	51	22.8	2.4	43	7.21	25.2	158	62	29	0.7	53	7.59	29.7
29	4077	188		30	0.4	36	7.73	30.4	208		28.8	0.3	49	7.71	29.1
30	4077	222		31.3	1.3	23	7.77	32.6	264		29.2	0.2	39	7.74	29.4
31	4077	163		23.7	0.7	29	7.59	24.4	204		29.6	0.3	38	7.74	29.9
32	4077	178		23.8	2	27	7.65	25.8	214		25.8	0.5	42	7.78	26.3
33	4077	160		34.8	2.1	12	7.54	36.9	164		35.6	0.6	44	7.58	36.2
34	4077	172		34	4	14	7.56	38.0	148		34.8	0.4	52	7.64	35.2
35	4077	171		31.9	9.1	6	7.69	41.0	150		37.4	1.1	9	7.68	38.5
36	4077	158		33.6	1.3	37	7.82	34.9	297		23.6	1.2	391	7.41	24.8
37	4077	234		27.9	1.7	19	7.82	29.6	196		26.7	0.9	104	7.67	27.6
38	4077	309		36.3	1.1	58	7.69	37.4	154		28.1	0.6	38	7.71	28.7
39	4077	244		29.9	1.1	69	7.78	31.0	207		40.2	0.5	36	7.59	40.7
40	4077	103		10.42	2.3	24	7.18	12.7	105		11.3	0.9	36	7.64	12.2
41	4077	234		14.22	11.9	17	7.14	26.1	127		25.4	1.4	38	7.46	26.8
42	4077	116	4.1	19.19	14.1	27	7.3	33.3	79	10.8	18.2	2.6	20	7.32	20.8

A4 Biofilm Reactor Studies MABfR B - Results summaries

Run 1

Observation	Amm-N inf mg l^{-1}	Amm-N eff mg l^{-1}	COD inf mg l^{-1}	COD eff mg l^{-1}
1	116.9	35	990	248
2	116.9	55.6	960	194
3	116.9	63	975	195
4	116.9	64.6	955	148
5	116.9	66.5	938	211
6	116.9	63.5	925	170
7	122.7	92.9	977	286
8	122.7	95.9	958	355
9	122.7	102.1	948	289
10	122.7	113.2	972	189
11	135.8	106.4	965	178
12	133.7	118.3	965	218
13	133.7	111.9	965	499
14	133.7	137.4	883	295
15	131.8	137.7	835	312
16	109.9	135.5	590	315
17	109.9	141.3	-	249
18	132.4	171	1065	457
19	132.1	162.6	1010	766
20	121.3	171	950	335
21	116.9	130	1009	369
22	114.8	126.5	987	377
23	121.3	141.6	940	557
24	121.6	143.5	948	250
25	119.9	141.3	936	471
26	121.1	130.6	-	-
27	108.6	121.6	899	518
28	113.5	128.5	886	239
29	113.5	130	-	-
30	113.5	126.5	-	-
31	110.9	140	634	210
32	110.9	148.6	850	258
33	102.3	153.8	750	217
34	98.6	144.9	704	289
35	120	151.6	1113	493

Run 2

Observation	Amm-N inf mg l^{-1}	Amm-N eff mg l^{-1}	COD inf mg l^{-1}	COD eff mg l^{-1}
1	145.2	181.6	1025	420
2	159.2	178.2	992	166
3	-	-	1074	136
4	132.7	176.2	850	138
5	137.7	184.5	847	118
6	140.9	184.5	888	139
7	146.9	181.1	862	170
8	111.2	139.2	1013	134
9	111.7	150.3	1002	148
10	112.7	145.5	1005	149
11	113.9	152.1	934	205
12	131.2	167.32	843	780

Run 3

Observation	Amm-N inf mg l^{-1}	Amm-N eff mg l^{-1}	COD inf mg l^{-1}	COD eff mg l^{-1}
1	89.5	91.4	759	287
2	91.2	89.3	719	185
3	73.8	76	750	181
4	79.6	101.6	650	119
5	70.3	99.8	708	120
6	87.5	101.4	690	102
7	82.4	93.3	710	110
8	75	89.1	722	102
9	72.4	88.1	721	107
10	73.5	83.4	740	106
11	73.3	91.34	795	159
12	72.8	101.6	778	195
13	72.8	99.8	540	152
14	89.3	101.4	376	163
15	73.5	93.3	641	286
16	74.3	89.1	689	307
17	75.3	88.1	658	197

A5 Dissemination

Conferences

Murray, S., Allen, S.J. & Groom, E. (2008), *Use of Membrane Aerated Biofilm Reactors for Upgrading of Municipal Wastewater Treatment Works (Presentation)*, IWA, Nanyang Technological University, Singapore.

Murray, S., Moroney, N., Allen, S.J. & Groom, R.E. (2008), *Treatment of Azo Dye Waste Using a Membrane Aerated Biofilm Reactor (Poster Presentation)*, Canadian Society for Chemical Engineering, Ottawa, Canada.

Murray, S. & Groom, E. (2010), *The BioSettler^{TM}: pilot-scale demonstration of a novel wastewater treatment technology (Presentation and Conference Paper)*, Aqua Enviro, Royal Armouries, Leeds, U.K.

Patent

Groom, E., Murray, S. & Ferguson, J. The Queen's University of Belfast, U.K. (2011), *Improvements relating to water treatment*; US 2011000805, EP2222608, CN101896434